Syntheses and Coordination Studies of [9]aneN_3 Substituted with Increasing Numbers of 2-Hydroxyethyl Pendant Arms

Steffen Phillip Creaser B.Sc. (Hons)

A thesis submitted for the degree of

Doctor of Philosophy

in

The University of Adelaide

Faculty of Science

December 1999

THE UNIVERSITY OF ADELAIDE

TABLE OF CONTENTS

Chapter 2. Syntheses of Hydroxyethyl Functionalised [9]aneN$_3$ Ligands

Chapter 3. Equilibrium Studies

Chapter 4. Kinetic Studies of 4-Nitrophenyl Acetate Hydrolysis

Chapter 5. Syntheses Towards the Isolation of a Zinc Finger Model

Chapter 6. Experimental

ABSTRACT

This thesis describes the syntheses of three 1,4,7-triazacyclononane ([9]aneN$_3$) macrocyclic ligands functionalised with increasing numbers of 2-hydroxyethyl pendant arms. The facile synthesis of a novel di-protected [9]aneN$_3$ derivative that provides a simple route to single 2-hydroxyalkyl triaza macrocycles through reaction with epoxides is also described.

The effect of the 2-hydroxyethyl pendant arms on the acid/base and metal binding properties of each ligand were investigated by aqueous potentiometric titrations and by molecular modelling studies using *ab initio* calculations. The pendant arms were found to have both a positive and negative effect on amine basicity depending on the number of attached pendant arms and the level of amine protonation. The inductive withdrawing nature of the hydroxyethyl groups serves to lower the basicity of the amine donors, however, the pendant arm may also raise the pK_a value by directing the oxygen lone pairs towards the ring centre and increase the electron density within the donor cavity. *Ab initio* calculations of the triply protonated one- and two-arm ligands show that the hydroxyethyl arms may also stabilise the protonation process by forming intramolecular hydrogen bonds with ammonium protons.

The stability constants, K, of the [9]aneN$_3$ ligands with one and two 2-hydroxyethyl pendant arms with Zn^{II} and Cd^{II} ion in aqueous solution have been determined. Comparison between the stability constants of [9]aneN$_3$ and the one-, two- and three-arm derivatives with Zn^{II} and Cd^{II} reveal that the 2-hydroxyethyl pendant arms may either lower or raise the overall complex stability. The one-arm ligand complexes were found to be less stable than complexes with [9]aneN$_3$. This is probably due to the combined effects of steric strain caused by the formation of a five-membered chelate and the inductive withdrawing nature of the pendant arm. When a second and third pendant arm was attached to [9]aneN$_3$ a step-wise increase in stability was observed.

Each ligand was found to bind Zn^{II} ion with greater affinity than Cd^{II} ion. Complementary *ab initio* calculations have shown the smaller Zn^{II} ion to be better accommodated in the binding cavity of each functionalised ligand. Metal-ligand bond distances were consistently shorter in the Zn^{II} models and the Zn^{II} ion was shown to sit deeper

in the donor cavity. Depending on the number of pendant arms and degree of solvation, the metal ions were found to exist in either distorted tetrahedral, trigonal bipyramidal or trigonal prismatic environments.

The Zn^{II} complex of the single 2-hydroxyethyl arm ligand was investigated for esterase activity as a potential enzyme mimic. The rate constant of 4-nitrophenyl acetate hydrolysis by the Zn^{II} complex at pH 9.2 in aqueous solution, however, was found to be lower than that of the reaction of 4-nitrophenyl acetate and the uncomplexed ligand. The low rate suggests that the Zn^{II} complex is unable to coordinate the carbonyl group of 4-nitrophenyl acetate as required for ester activation. The reduced rate constant of the Zn^{II} complex compared with that of the uncomplexed ligand suggests a bimolecular reaction involving nucleophilic attack of 4-nitrophenyl acetate by the coordinated ring amine groups.

As part of an ongoing project, preliminary synthetic studies have been performed to establish an effective synthetic route towards the isolation of a simple Class 1 zinc finger model based on the [9]aneN_3 macrocycle. By attaching a single pendant arm of varying length and complexity to the Zn^{II} complex of [9]aneN_3, it is envisaged that an extended chelate ring will form at the Zn^{II} centre and effectively mimic the loop structure of a zinc finger motif. An important precursor to a potential zinc finger model has been isolated in low yield although further modification of the synthetic procedure is necessary.

STATEMENT

This thesis contains no material which has been accepted for the award of any other degree or diploma in any university or other tertiary institution and, to the best of my knowledge and belief, contains no material previously published or written by another person, except where due reference has been made in the text of the thesis.

I give consent to this thesis, when deposited in the University Library, being made available for loan and photocopying.

Steffen Creaser

December, 1999.

ACKNOWLEDGEMENTS

I would like to extend my sincere gratitude to my two supervisors Professor Stephen Lincoln and Dr. Simon Pyke for assisting me throughout my Ph.D. experience and providing me with both support and independence in my research.

I must also thank my parents who have provided me with constant support and encouragement throughout my education. I wish to gratefully acknowledge the assistance of my mother Dr. Inge Creaser for proof reading this thesis and helping me in my transition from organic chemistry to inorganic/coordination chemistry.

I also wish to thank all the members of the Lincoln group and members of Lab 1 and 2 for their assistance throughout the past three and a half years. The assistance of the technical staff in the Chemistry Department is also greatly appreciated. I must also thank Dr. Paul Wabnitz, Dr. John Valente and Dr.'s Daniela Caiazza and Lou Rendina for their friendship.

The financial assistance of an Australian Post-graduate Award from the Australian Research Council is gratefully acknowledged.

ABBREVIATIONS AND SYMBOLS

The following abbreviations and symbols have been used in the text.

Å	Ångström (10^{-10} metres)
Ab	Antibody
A	Absorbance
AP	Alkaline phosphatase
ATP	Adenosine triphosphate
BisBoc-[9]aneN_3	*N,N'*-Bis(*tert*-butyloxycarbonyl)-1,4,7-triazacyclononane
Boc	*tert*-Butoxycarbonyl
Boc-ON	2-(*tert*-butoxycarbonyloxyimino)-2-phenylacetonitrile
Bhec[9]	*N,N'*-Bis(2-hydroxyethyl)-1,4,7-triazacyclononane
bp	Boiling point
br	Broad
calcd.	Calculated
conc.	Concentrated
X^2	Chi squared
C	Coulombs
CA	Carbonic anhydrase
C_q	Quaternary carbon
COSY	Correlation spectroscopy
CP	Carboxypeptidase
δ	Chemical shift
d	Doublet or day
DCC	1,3-dicyclohexylcarbodiimide
deg.	Degree(s)
DMF	*N,N*-Dimethylformamide
DMSO	Dimethyl sulfoxide
DNA	Deoxyribonucleic acid

E	Potential energy (Hartrees)
E	Observed electrode potential (mV)
E_o	Standard electrode potential (mV)
ECP	Effective core potential
EI	Electron impact
emf	Electromotive force (volts)
Et_3N	Triethylamine
exp.	Experiment
F	Faraday's constant (C mol^{-1})
FAB	Fast atom bombardment
Fmoc	9-Fluorenylmethoxycarbonyl
Fmoc-Cl	9-Fluorenylmethyl chloroformate
h	Hour(s)
H	Hamiltonian operator
HSAB	Hard-Soft Acid-Base
Hec[9]	*N*-(2-hydroxyethyl)-1,4,7-triazacyclononane
HMBC	Heteronuclear multiple bond correlation
HMQC	Heteronuclear multiple quantum coherence
HSQC	Heteronuclear single quantum coherence
Hz	Hertz (s^{-1})
I	Ionic strength
J	Coupling constant
K	Degree(s) Kelvin
K	Stability constant
K_a	Acid dissociation constant
k_o	Spontaneous rate constant (s^{-1})
k_{obs}	Observed rate constant (s^{-1})
k_{NA}	Specific rate constant (s^{-1} mol^{-1} dm^3)
K_w	Equilibrium constant for the self ionisation of water
KHphthalate	Potassium hydrogen phthalate

L	Ligand
Lg	Leaving group
Lit.	Literature
ln	Logarithm to base e
Ln	Lanthanide ion
log	Logarithm (base 10)
LSI	Liquid spray ionisation
ν_{max}	Maximum infrared absorbance (cm^{-1})
min	minute(s)
m	Multiplet
M	unspecified metal
M^+	Molecular ion
M^{II}	Unspecified divalent metal ion
MHz	Megahertz ($10^6\ s^{-1}$)
mm Hg	1 mm Hg = 101325 kg m^{-1} s^{-2}
mp	melting point
m/z	mass to charge ratio
NA	4-Nitrophenyl acetate
NOE	Nuclear Overhauser enhancement
N_q	Quaternary nitrogen
NMR	Nuclear magnetic resonance (spectroscopy)
PET	Photo-induced electron transfer
Pg	Protecting group
pH	$-\log_{10}[H^+]$
pK_a	$-\log_{10}[K_a]$
pK_w	$-\log_{10}[K_w]$
pm	Picometre (10^{-8} metres)
ppm	Parts per million
q	Quartet
quint	Quintet

R	Gas constant (J K^{-1} mol^{-1})
R_f	Relative retention with regard to solvent on a TLC plate
RNA	Ribonucleic acid
s	Singlet
sec.	Second(s)
t	Triplet
T	Temperature (K)
TCTA	*N*,*N*',*N*"-Triacetate-1,4,7-triazacyclononane
TLC	Thin layer chromatography
TFA	Trifluoroacetic acid
Tosyl chloride	*p*-Toluenesulfonyl chloride
[9]aneN_3	1,4,7-Triazacyclononane
Thec[9]	*N*,*N*',*N*"-Tris(2-hydroxyethyl)-1,4,7-triazacyclononane
ϕ	Twist angle
UV	Ultraviolet
Ψ	Wavefunction
Z	Benzylcarbonyl
Z-ON	2-(Benzyloxycarbonyloxyimino)-2-phenylacetonitrile

Chapter 1.

1.1. Introduction

In recent decades, the coordination chemistry of polyaza macrocyclic ligands has attracted a great deal of attention from both biological and inorganic chemists and remains a highly investigated field of chemistry. The ability of *N*-functionalised derivatives of 1,4,7-triazacyclononane ([9]aneN$_3$) to coordinate metal ions and form complexes of substantial thermodynamic stability has made them important tools in both preparative inorganic chemistry and bioinorganic research.

Polyaza macrocyclic ligands comprise a large family of polydentate ligands that incorporate nitrogen donor atoms attached to a cyclic backbone. Work in this thesis is concerned with the [9]aneN$_3$ ligand system, which contains three nitrogen atoms separated by three ethylene bridges. It had once been an expensive and difficult ligand to prepare, however, the high yielding preparative method of Richman and Atkins[1,2] has since allowed extensive research into its chemical and physical properties.

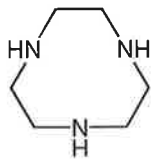

[9]aneN$_3$

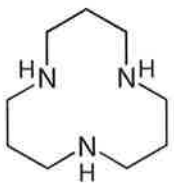

[12]aneN$_3$

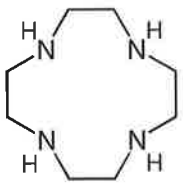

[12]aneN$_4$

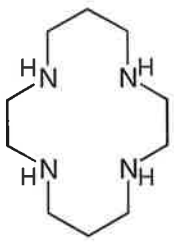

[14]aneN$_4$

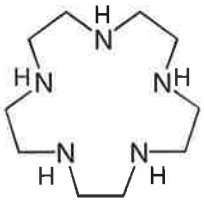

[15]aneN$_5$

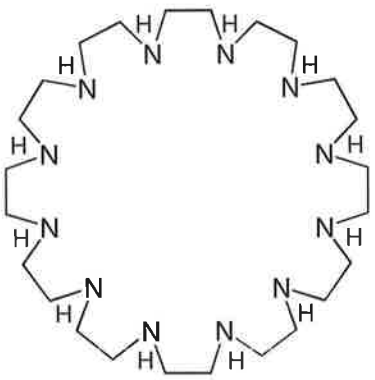

[36]aneN$_{12}$

Figure 1. Some typical polyaza macrocycles.

The number of aza macrocyclic ligands is substantial. Subtle variations of the macrocyclic structure may dramatically alter the steric and electronic properties of the ligand and produce many new metal complexes with unique properties. The polydentate cyclic structure bestows a high degree of kinetic and thermodynamic stability to metal ion complexes and considerable attention has focussed on the spectral and structural properties and the kinetic and thermodynamic aspects of their metal complexes.

Such extensive investigation has led to the design of many exciting new metal complexes with diverse and highly specific functions which have found utility in areas such as cation recognition, photoelectric and luminescence chemistry, molecular recognition, symmetric synthesis and catalysis.

1.2. The Macrocycle Effect

Many aza macrocyclic ligands display enhanced thermodynamic stability of their metal ion complexes compared with their open chain analogues. The effect that cyclisation has on the binding affinity of the metal ion complexes is referred to as the "macrocycle effect". First introduced in 1969 by Cabbiness and Margerum[3], the term "macrocycle effect" was used to explain the enhanced stability of a Cu^{II} complex formed from a tetra-aza macrocyclic ligand compared with the complex formed with its open chain analogue. Although the stability of the macrocyclic complex was expected to increase with a greater number of chelate rings, as defined by the "chelate effect",[4] the additional stability was far greater than expected solely from the presence of an additional chelate ring. Since then, the enhanced stability of macrocyclic complexes has become well established where the "macrocycle effect" is explained through a Gibbs energy term by the metathetic reaction 1.1,

$$ML^{n+}_{noncyclic} + L_{cyclic} \longrightarrow ML^{n+}_{cyclic} + L_{noncyclic} \qquad (1.1)$$

Unlike the chelate effect, which is essentially an entropy effect, the macrocyclic effect has both enthalpic and entropic origins and considerable attention has gone into separating the two components. Early investigations into the origin of the macrocyclic effect were

contradictory with some authors attributing the extra stability wholly to entropy[5,6,7,8,9,10,11] or wholly to enthalpy[12,13,14,15,16,17] terms, however, it has become more widely acknowledged that both components are important contributors.[18,19,20,21,22]

The favourable entropy contribution to the macrocycle effect is a result of the rigid and pre-organised structure of the macrocyclic ligand.[23,24] Compared with its non-cyclic counter part, the macrocyclic ligand requires less organisation of its donor atoms when coordinating a metal centre and hence does not lose configurational entropy to the same extent. A flexible open chain ligand must undergo considerable geometric rearrangement or "organisation" to accommodate a metal ion and will consequently generate a negative entropy component.

The enhanced stability of the macrocyclic complex may also be explained in terms of enthalpy, the magnitude of which depends on either favourable ligand desolvation enthalpy or configurational enthalpy of the macrocycle. The macrocyclic ligand tends to be less solvated than its linear counterpart as the compact cyclic arrangement of the ligand physically prevents the donor atoms from hydrogen bonding with the same number of water molecules as in the open chain form. As a consequence, less energy is usually required for desolvation of the ligand in order for metal binding to occur. The ring system also provides a favourable configurational enthalpy component, as the donor atoms are pre-orientated in favourable positions for metal binding. The non-cyclic ligand must expend more energy to arrange itself around the metal ion to achieve complexation and hence is enthalpicly less stable than the macrocyclic complex. The magnitude of configurational enthalpy depends on both the matching of the ring cavity to the metal ion size and the stereochemical preference of the metal ion.

The enhanced stability of macrocycle complexes is also due to their enhanced kinetic inertness with respect to formation and decomplexation of the complex in aqueous solutions. In an open chain complex, decomplexation may occur by successive displacement of the donor atoms by solvent molecules at the metal centre. This begins at one end of the molecule and proceeds in a step-wise manner along the length of the chain. In the presence of acid the dissociated nitrogen atoms are quickly protonated and unable to complex the metal ion. This mechanism, however, is disfavoured with a cyclic ligand because there is no "free end".

Decomplexation is more complicated and involves sequential substitution of the metal ion in the coordination site by solvent molecules, which weaken and finally break the metal-ligand coordination bonds. This mechanistic restraint on dissociation substantially increases the stability of the ligand complex.[25,26]

1.3. Acid-Base Properties of [9]aneN$_3$

Ring closure in polyaza ligands also leads to considerable differences in the acid/base properties of the donor atoms compared with the open chain analogues.[27] In small macrocycles such as [9]aneN$_3$, the cyclic arrangement generally leads to an enhancement of the first protonation constant of the amine nitrogens. The basicity of the first amine nitrogen of [9]aneN$_3$ (pK_{a1} = 10.42)[28] is considerably higher than in its linear counterpart diethylenetriamine, (pK_{a1} = 9.70).[29,30] This difference is explained by the pre-orientation of the donor nitrogens. The cyclic ring structure directs the non-bonding electron pairs of each nitrogen atom towards the centre of the ring. This creates an area of high electron density that facilitates protonation of the first nitrogen. This stabilisation is observed in the crystal structure of protonated Me$_3$[9]aneN$_3$ where the added proton is shown to hydrogen bond with the two other nitrogen donors, Figure 2.

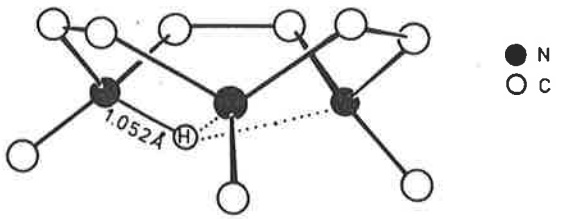

Figure 2. The x-ray crystal structure of the cation [Me$_3$[9]aneN$_3$]-H$^+$.[32]

The degree of stabilisation by the neighbouring donors in the linear molecule, diethylenetriamine, is significantly lower as more free energy is expended arranging the nitrogen donor atoms in a favourable cradle position.

The ring structure also causes a significant difference in the value of the second pK_a compared with the linear molecule. Successive protonation of the ring nitrogens of [9]aneN$_3$

is less favourable and leads to a much lower pK_a. The closely situated ammonium nitrogens in the ring cause significant electrostatic repulsion and consequently the second nitrogen of [9]aneN$_3$ is much less basic (pK_{a1} = 10.42, pK_{a2} = 6.82).[28] In the case of diethylenetriamine, however, repulsion between the two ammonium nitrogens is minimised as they are situated at opposite ends of the linear molecule. As a consequence, the second nitrogen of diethylenetriamine is only slightly less basic than the first (pK_{a1} = 9.70, pK_{a2} = 8.98).[29,30]

Protonation of the third nitrogen in [9]aneN$_3$ is highly disfavoured due to the large electrostatic repulsion caused by three closely situated ammonium ions. The third pK_a of [9]aneN$_3$ remains too low to be measured. Successive protonation of diethylenetriamine is also unfavourable, however, the linear structure is still able to reduce the extent of repulsion between the charged ammonium ions and a third, yet significantly lower, protonation constant is measured (pK_{a3} = 4.24).[29,30]

1.4. Functionalised Macrocyclic Ligands

The attachment of functionalised pendant arms to [9]aneN$_3$ has given rise to a diverse range of metal coordinating ligands with seemingly unlimited applications. One of the earliest examples of functionalised 1,4,7-triazacyclononanes was *N,N',N''*-triacetato-1,4,7-triazacyclononane (**TCTA**) which is formed by treating [9]aneN$_3$ with sodium bromoacetate in aqueous solution.[31] Such tri-substituted [9]aneN$_3$ derivatives are potentially hexadentate, having an N$_3$O$_3$ donor set, able to surround a metal ion with octahedral or trigonal prismatic geometry.[32] The metal complex of (**TCTA**) exhibits a three-fold axis of symmetry containing three five-membered chelate rings, (-M-N-C-C-N-), Figure 3.

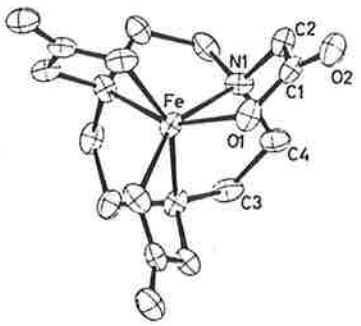

Figure 3. The structure of [Fe^{II}(**TCTA**)](δ isomer).[33]

This favourable "cage" geometry confers high thermodynamic stability making it an excellent chelator of metal ions. The increased stability is provided by the coordinating pendant arms that allow a more rapid entry of the metal ion into the macrocycle cavity than is possible with the unfunctionalised macrocycle.[34] The mechanism of complexation is thought to involve the initial capture of the metal ion by the pendant arms followed by transfer to the macrocycle cavity, Scheme 1, although binding directly to the triaza face is also possible.[35,36,37]

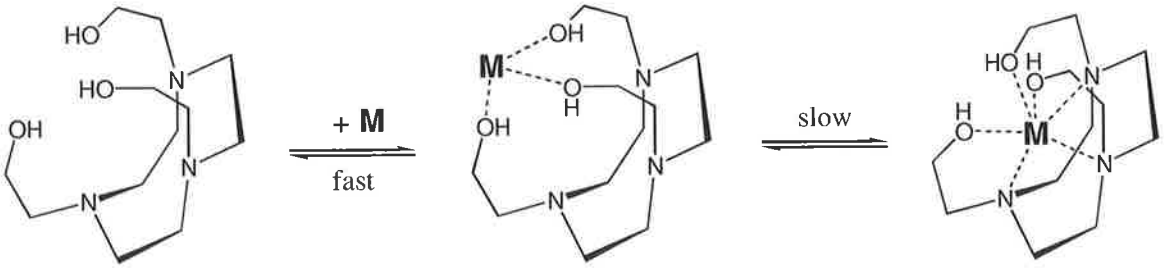

Scheme 1

The entry of metal ions into the cavities of pendant arm macrocycles is also faster due to a decreased incidence of *N*-inversion which often occurs following initial metal binding of unfunctionalised macrocyclic ligands.[38,39,40]

Once the metal ion has bound within the ligand cavity, the complex may be considered chiral, as the macrocyclic base may adopt either a Δ (δδδ) or Λ (λλλ) conformation of the five-membered chelate rings, depending on which face of the ligand the metal atom binds.[32]

In the Δ isomer, the three pendant arms are observed to twist in a clockwise direction (Figure 3), while the pendant arms of the Λ isomer twist in an anti-clockwise direction. Interconversion between the two enantiomers proceeds through both a ring inversion and rearrangement of the pendant arms upon release and recapture of the metal ion.

The extent to which the pendant arms rotate around each metal ion depends on the size of the bound ion, and is referred to as the twist angle. The twist angle, ϕ, is defined as the rotation of the plane of the coordinating oxygen atoms compared with the plane of the ring nitrogens, Figure 4. It is 30° in a regular octahedron and 0° in a trigonal prism.

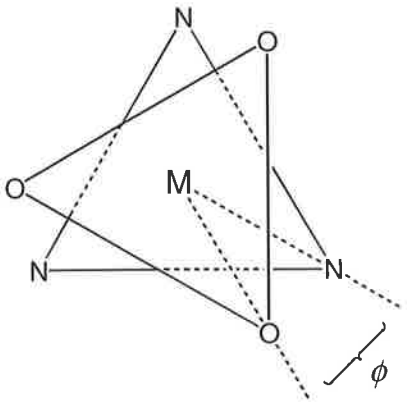

Figure 4

1.5. Attachment of Pendant Arms to [9]aneN$_3$

The three reactive nitrogen atoms of [9]aneN$_3$ allow a range of potential functionalised derivatives to be synthesised. Alkylation of either one, two or all three nitrogen atoms may lead to a seemingly endless array of ligands possessing divergent steric and electronic properties that offer unique coordination environments. By far the largest class of functionalised ligands are those with three identical pendant arms. Derivatives with less than three pendant arms are also common but generally require more subtle synthetic pathways. As a consequence, there are far fewer one- and two-arm derivatives compared with the large range of fully substituted ligands.

The isolation of fully substituted aza macrocycles is synthetically quite simple. The attachment of three identical pendant arms to [9]aneN$_3$ is usually achieved by reaction with three equivalents of either a methylating agent or halo-alkylating agent. Treatment of [9]aneN$_3$ with formaldehyde and acetic acid selectively methylates all three secondary nitrogens without producing quaternised ammonium nitrogens, Scheme 2a.[41]

Functionalisation of [9]aneN$_3$ with α-bromo-carbonyl agents such as sodium bromoacetate[42,33] or 2-bromoacetamide[43] is a very efficient method of producing ligands with hexadentate coordinating environments, Scheme 2b. Another highly efficient method of attaching functionalised pendant arms to [9]aneN$_3$ is by reaction with strained alkylating agents such as ethylene oxide,[44,45] episulfide[46] and aziridines[47]. Such reactions proceed through nucleophilic attack by the macrocycle nitrogens to release the steric strain of the

three-membered ring. The *N*-functionalisation of aza macrocycles by reaction with substituted epoxides, Scheme 2c, is an area of considerable synthetic activity and has led to the formation of an impressive array of metal complexes.[45,48,49,50,51,52,53]

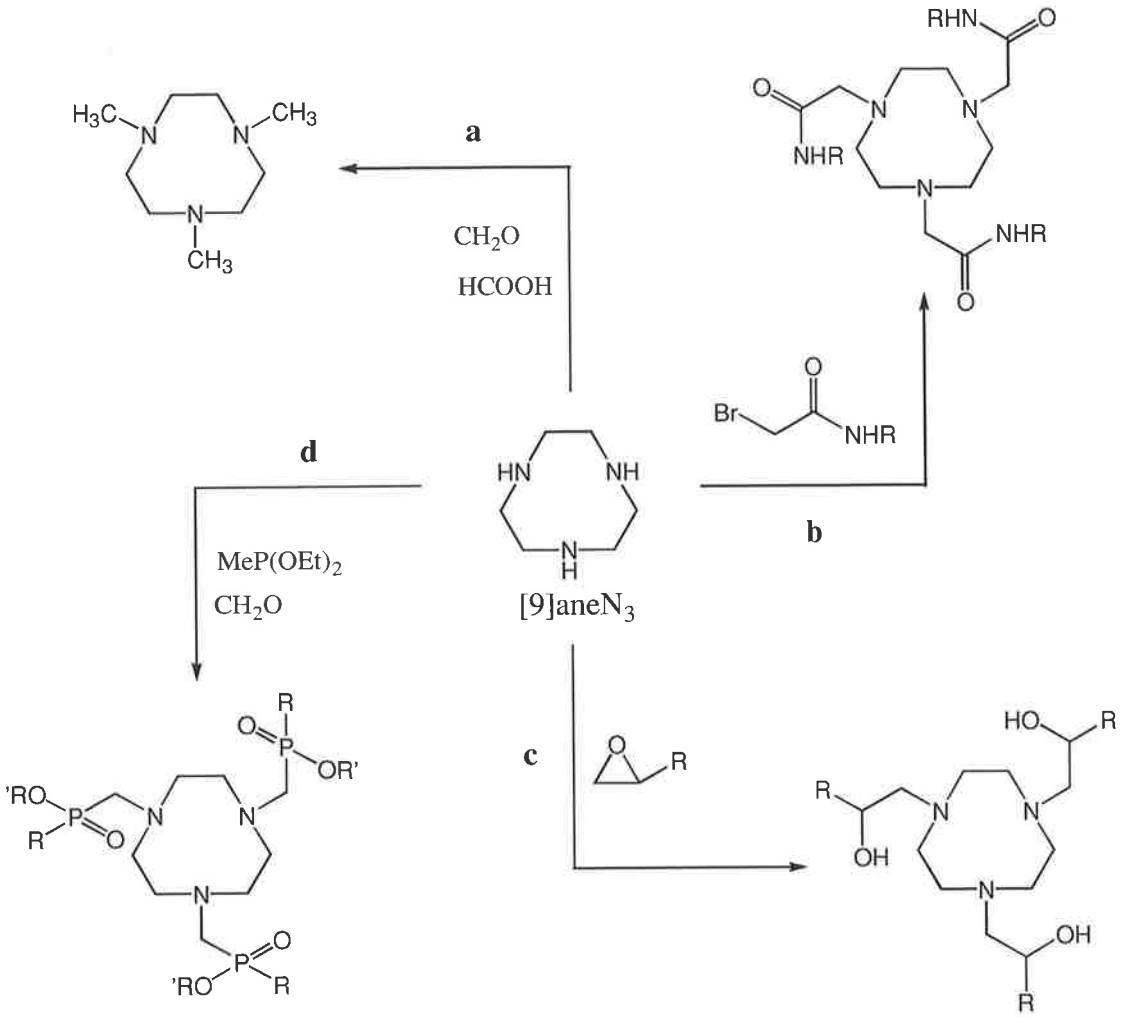

Scheme 2. Some examples of tri-alkylated [9]aneN_3 derivatives.

Phosphorylation of [9]aneN_3 provides an alternative range of ligands containing phosphyl groups, Scheme 2d,[54] whilst other functional moieties such as bipyridylmethyl[55] and imidazolylmethyl[56] may also be attached.

Alkylation of less than the total number of nitrogens of aza macrocycles is synthetically more challenging. Although there are isolated examples of mono and di-substituted [9]aneN_3 derivatives formed by direct alkylation,[57,58,59,60,61,62] treatment of aza macrocycles with either one or two equivalents of alkylating agent generally leads to a complex mixture of products. Separation of the alkylated species is difficult and often requires further derivatisation[63] or metal complexation.[64]

The most effective method of achieving selective alkylation is through the use of protecting groups or by altering the functionality of selected nitrogen groups prior to alkylation. Protection of [9]aneN$_3$ with *N*-tosyl groups is one method. Both mono- and di-tosylates of [9]aneN$_3$ can be isolated by successive hydrolysis of the *N*-tosyl groups of tri-tosylated [9]aneN$_3$.[65,66] An alternative method, developed by Bulkowski, involves the use of selectively protected diethylenetriamine during macrocycle formation, Scheme 3. The di-tosylated species **1** is obtained when the benzyl protecting group is later removed with potassium *tert*-butoxide.[67]

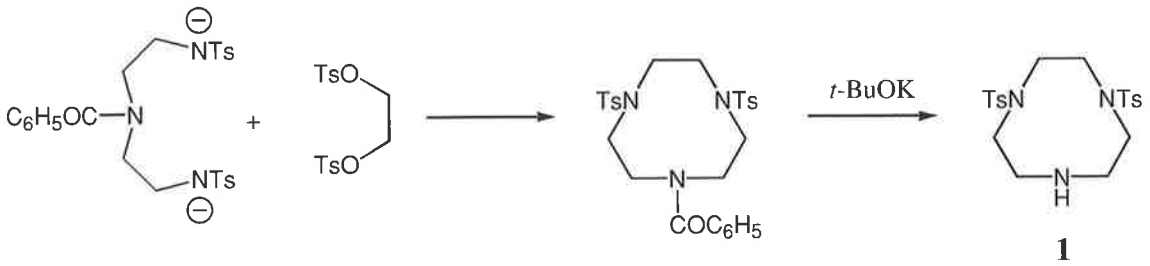

Scheme 3

The use of *N*-tosyl protecting groups in [9]aneN$_3$ chemistry has remained limited, however, primarily due to the difficulty associated with removing them. Hydrolysis of the *N*-tosyl groups is usually achieved with concentrated sulfuric acid at 120°C, which makes them unsuitable for use with acid sensitive functional groups.

Sherry has developed a general method of synthesising a wide range of mono- and di-substituted [9]aneN$_3$ derivatives using carbamate protecting groups.[68] Reaction of [9]aneN$_3$ with two equivalents of 2-(*tert*-butoxycarbonyloxyimino)-2-phenylacetonitrile, Boc-ON, was found to give the di-protected species **2**, Scheme 4, in high yield. Mono-protection of [9]aneN$_3$ was subsequently achieved by treating **2** with *N*-(benzyloxycarbonyloxy)succinimide, Z-ON, followed by acidic hydrolysis of the Boc functional groups to give the benzylcarbonyl species **3**.

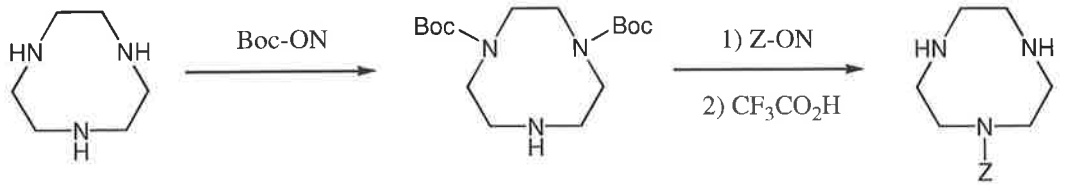

2 **3**

Di-protected **Mono-protected**

Scheme 4

The advantage of carbamate protecting groups lies in the ease of removal. The Boc (tBuCO$_2$) groups are easily hydrolysed at room temperature with trifluoroacetic acid while the Z ($PhCH_2CO_2$) groups may be hydrolysed with hydrobromic acid or by hydrogenolysis. In terms of di-protection, however, the tosylate **1** and carbamate species **2** share a similar limitation. The bulky protecting groups decrease the reactivity of the third amine donor towards ordinary alkylating agents. Such di-protected species are usually unsuitable for reaction with epoxides and generally require activated alkylating agents such as organo-triflates or acyl-bromide compounds.

A commonly employed method of mono-alkylating the slightly larger aza macrocycle, [12]aneN$_3$, involves masking the functionality of two of the nitrogen atoms as internal amide groups. The high dilution reaction of 1,5,9-triazanonane and diethyl malonate gives the di-amide **4**, Scheme 5.[69,70] The reduced nucleophilicity of the amide nitrogens allows selective alkylation at the single amine nitrogen. The amide groups are then reduced with borane to give the mono-alkylated species **5**.[71]

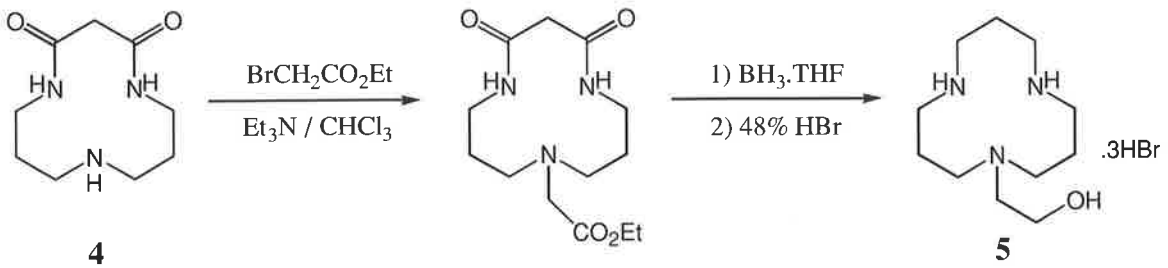

4 **5**

Scheme 5

This method of protection has been used for a range of aza macrocycles,[69,72,73] however, a similarly protected [9]aneN$_3$ derivative has yet to be isolated.

By far the most popular method of achieving mono alkylation of [9]aneN$_3$ is through the use of the tri-cyclic macrocycle **6**, Scheme 6. First isolated by Atkins,[74] the bridged macrocycle **6** is neatly synthesised from [9]aneN$_3$ by condensation with dimethylformamide dimethylacetal, Scheme 6a.[75,76,77]

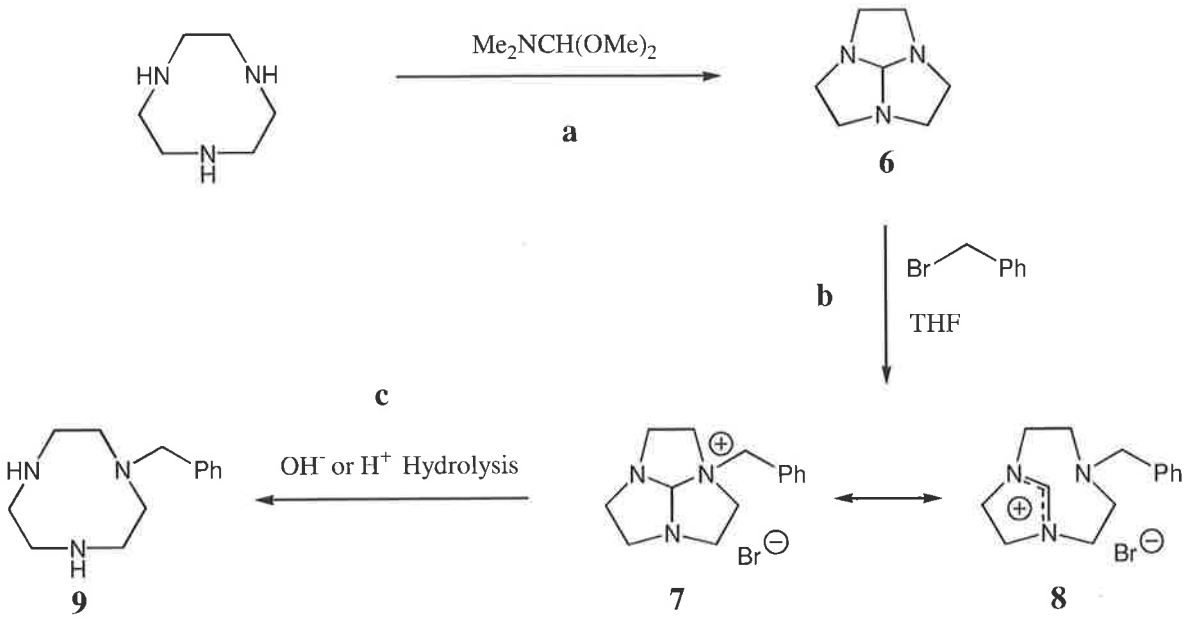

Scheme 6

Reaction of the bridged macrocycle **6** with a bromo-alkylating agent produces a cationic intermediate that precipitates from solution when the reaction is performed in a polar aprotic solvent. Both the precipitation process and reduced reactivity of the cationic intermediate prevent further alkylation of the nitrogen atoms. The reactivity of the intermediate is substantially lower than that of the bridged macrocycle **6** due to contributions from two amidinium canonical forms, **7** and **8**, where the cationic charge is distributed over all three nitrogens[78], Scheme 6b. Hydrolysis of the intermediate species under acidic or basic conditions cleaves the bridging carbon to give the mono-alkylated derivative **9,** Scheme 6c.[79]

This method is especially useful for creating bis-macrocyclic ligands where two macrocycles are linked by a bridging alkyl group. Reaction of the bridged macrocycle **6** with a single equivalent of an alkyl bromide will afford a mono-substituted macrocycle, Scheme 7a, however, when half an equivalent of a di-bromo alkylating agent is used, a bis-macrocyclic species is produced, Scheme 7b. This method has led to a large array of mono-alkylated[79,80,81,78,82,83] and bridged bis-macrocyclic[84,85,86,87,88] aza macrocycle derivatives.

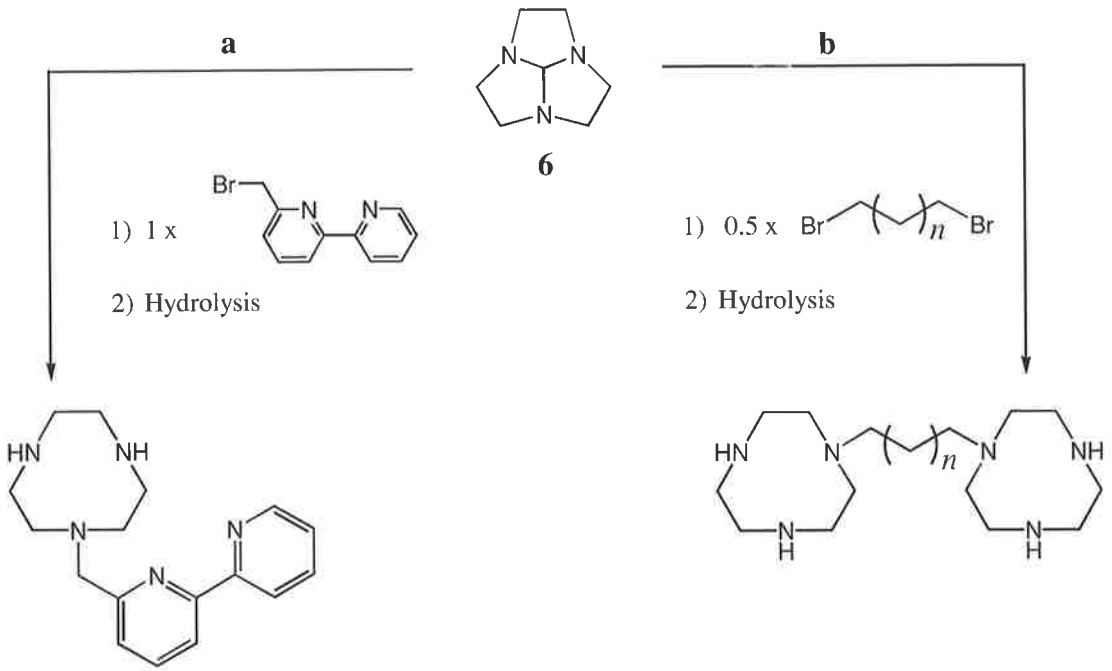

Scheme 7

1.6. Application of *N*-functionalised [9]aneN$_3$ Ligands

The attachment of ligating pendant arms to [9]aneN$_3$ has given rise to a vast range of new metal ligating systems with diverse chemical properties. Many substituted aza macrocycles can be designed to selectively bind specific metal ions on the basis of charge and ion size.

Mg^{II} plays a pivotal role in intracellular events such as adenosine triphosphate (ATP) hydrolysis. To successfully monitor the levels of free, ionised Mg^{II} in functioning tissue, it is important to design ligand systems that discriminate over other divalent alkaline earth ions such as Ca^{II} which plays an important role as an intracellular second messenger.[89] The tris-methylpropyl ligand **10** in Figure 5, is more than 500 times more selective for Mg^{II} than for Ca^{II} in CD_3CN. The small size of the ligand cavity allows it to saturate the first coordination sphere of Mg^{II} more effectively than the larger Ca^{II} ion and is potentially useful in monitoring Mg^{II} levels in blood plasma.[90]

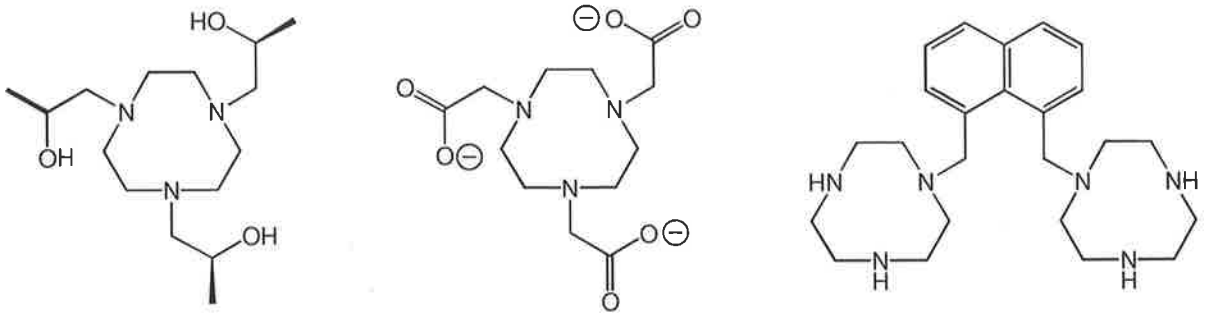

10 **11** **12**

Figure 5

The tris-acetato ligand **11** is one of numerous tri-alkylated [9]aneN$_3$ ligands[91,92] that act as highly selective catalysts for olefin epoxidation when complexed with Mn^{II}. In the presence of H_2O_2, the [Mn^{II}-**11**] complex can epoxidise a large range of olefins in methanol and acetone with as much as 99% stereoretention, Scheme 8.[92]

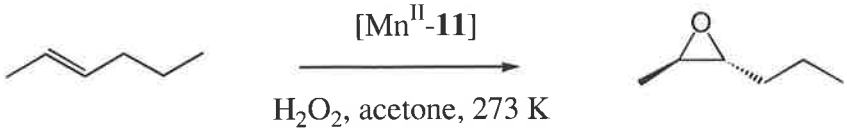

Scheme 8

The preparation of bis-macrocyclic ligands has also attracted considerable attention as they provide useful binucleating model systems[65,66] for studying metalloproteins that are known to or presumed to contain bridged metal cores at their active centres. The resulting complexes have also been used to develop new catalytic reagents with biological activity. The binuclear Cu^{II} complex of ligand **12** in Figure 5 shows strong resemblance in activity to a range of phosphoesterases such as RNase H and 3',5'-exonuclease that actively hydrolyse RNA.[93] The two Cu^{II} centres are able to cooperatively bind a single phosphate diester group from RNA that is then hydrolysed by a bound Cu^{II}-OH$^-$ anion, Scheme 9. The binuclear Cu^{II} complex of **12** is about 500 times more reactive per metal centre than the [Cu^{II}-[9]aneN$_3$] complex.

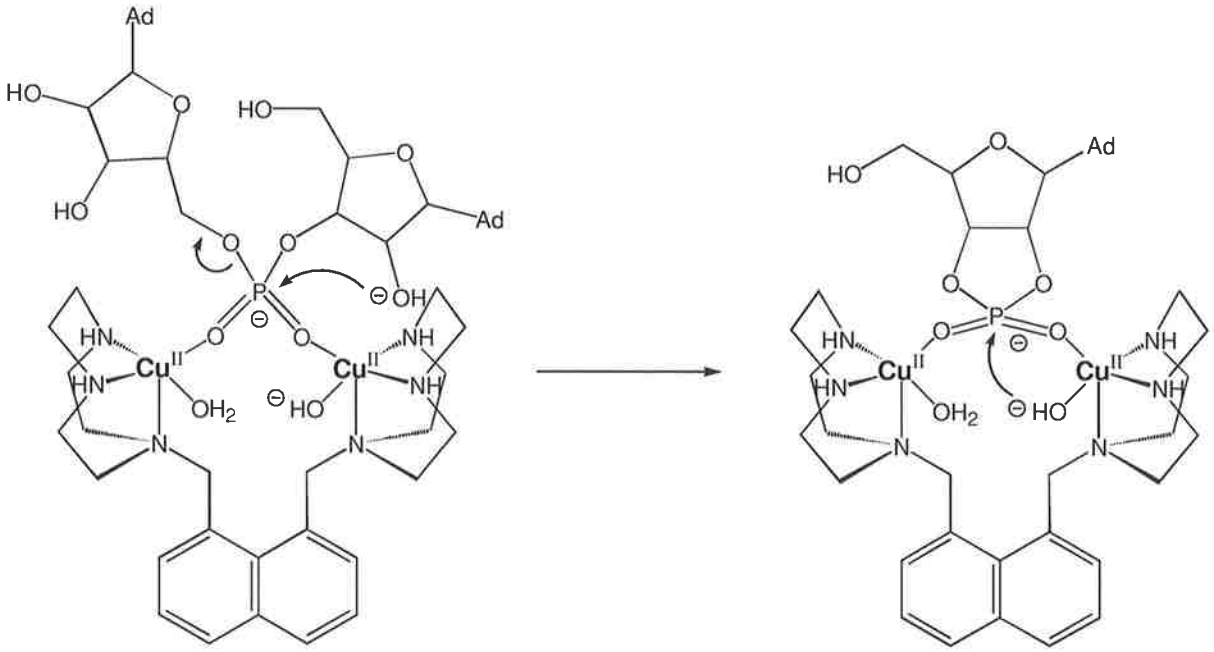

Scheme 9

1.6.1. Cation Recognition

An exciting area of coordination chemistry involves the use of macrocycle ligands in the recognition of cations in solution. Using fluorescence imaging spectroscopy, ions may be detected with fluorescent sensors derived from crown ethers or polyaza macrocycles.

The fluorescent sensor is known as a fluoroionophore and consists of a cation receptor or ionophore that contains an electron donor, D, (e.g. amino group) that is linked by a saturated bridge (e.g. $-CH_2-$) to a fluorescent molecule or fluorophore, Figure 6.[94] Upon excitation of the fluorophore, photo-induced electron transfer (PET)[95] from the donor, D, to the acceptor, A, causes a quenching of fluorescence. In a cation free situation, fluorescence is essentially "switched off" by the PET process, Figure 6a. However, when a cation is added to from a complex, the electrons of the donor, D, are attracted towards the cation and the electron transfer to the fluorophore is reduced. This causes a marked enhancement of fluorescence without causing a spectral shift, Figure 6b.[94]

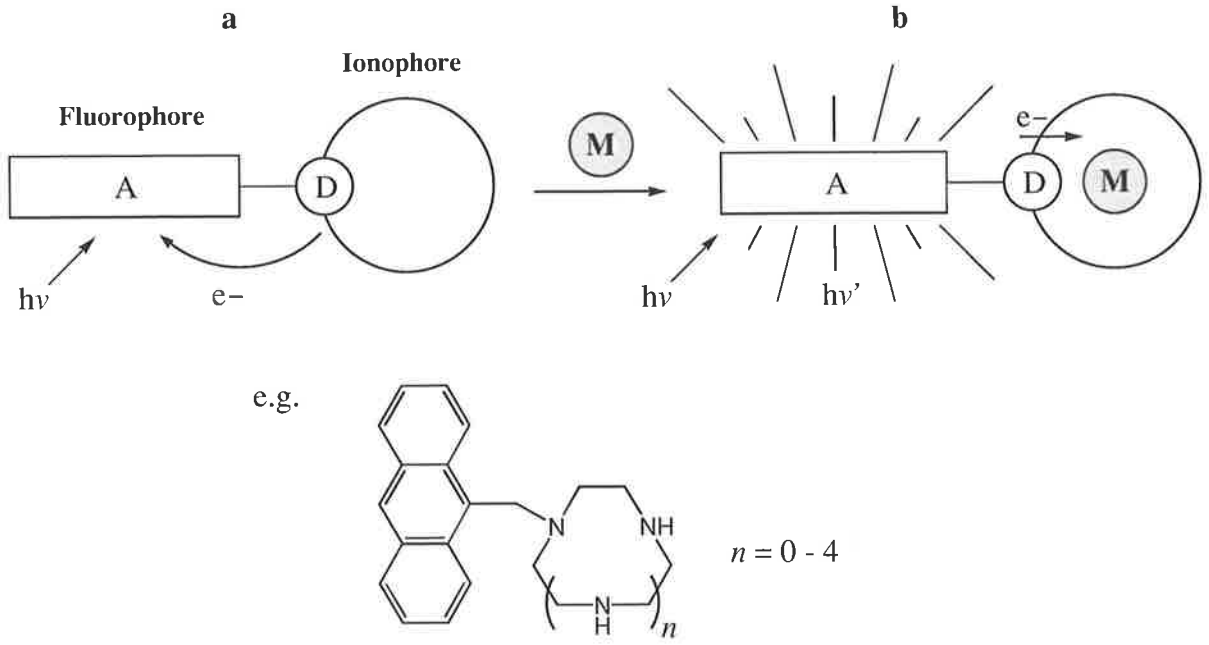

Figure 6.

Different cations will give unique fluorescent signatures when bound by a specific fluoroionophore. The selectivity and efficiency of binding will depend on both ligand design and characteristics of the cation such as its ionic radius, charge, coordination number and hardness.

Considerable attention has also been paid to the development of fluorescent pH indicators.[96,97] Protonation of the amine donors in an uncomplexed system raises the oxidation potential of the ionophore and suppresses the PET process, consequently fluorescence becomes the dominant decay channel of the excited fluorophore and the sensor becomes "switched on". Increasingly sophisticated systems are under development for real-space monitoring of pH gradients at the molecular level. Sensors with hydrophobic tails that are able to anchor into detergent micelles may possibly be used to give depth dependent pH measurements and allow spatial mapping of pH at the surface of biological membranes.[94]

1.6.2. Luminescent Probes

Another important area of research involving aza macrocycles is luminescence chemistry of lanthanide complexes.[98,99] Traditionally, interest in lanthanides has focussed on their use as

shift reagents in NMR spectroscopy due to the ability of Eu^{III} and Yb^{III} to greatly increase the chemical shifts of ligand complexes, and as relaxation agents that decrease the relaxation times of nearby nuclei through dipolar interactions. The latter property has been exploited in magnetic resonance imaging where Gd^{III} is used as an *in vivo* contrast agent.[100] Lanthanide luminescence has also attracted considerable attention, and current interest has centred on the development of solution-state luminescent probes for use in immunological assays.

A luminescent probe consists of a chromophore linked to a ligand which complexes the lanthanide ion, Ln. In an efficient model, excitation by a conventional light source causes a transfer of energy from the chromophore to the complexed ion, Figure 7.[98] The lanthanide ion, Ln, then becomes excited to the emissive state and intense luminescence results.

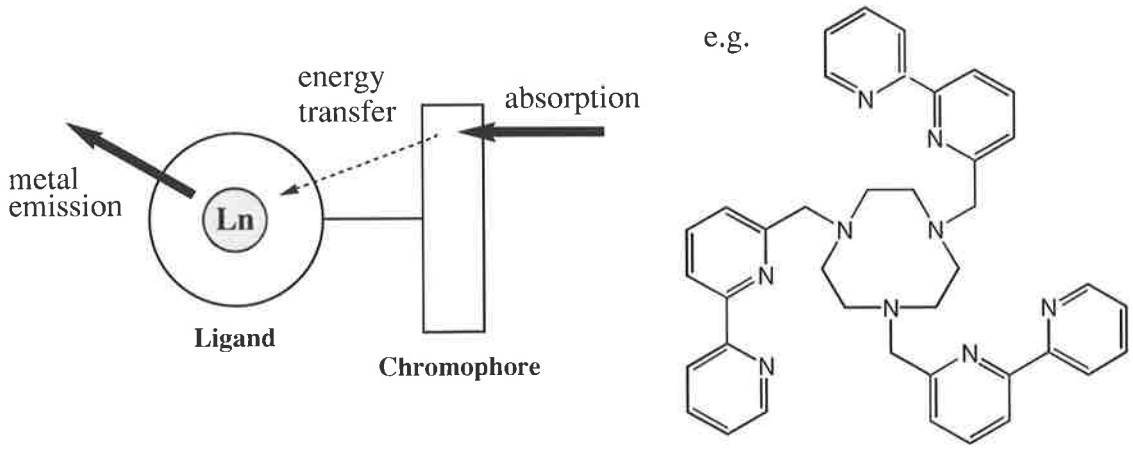

Figure 7

The ability of polydentate macrocyclic ligands to bind metal ions with high thermodynamic stability has also proved helpful in cancer research. Monoclonal antibodies conjugated to β or γ-emitting radioisotopes are increasingly used in medicine to locate human breast and colorectal cancers. For this technique to work, it is essential that the radioisotope (e.g. ^{111}In, $t_{1/2}$ = 2.83 days) remains attached to the antibody for an extended period of time. Aza macrocycles functionalised with acetato pendant arms are ideal carriers for antibody, Ab, probes, Figure 8. The tri-positive indium ion forms an electrically neutral complex that is less sensitive to acid-catalysed dissociation. The slow rate of dissociation ensures that the radiolabel remains secured for several days allowing a longer detection time.[101,102,103,104]

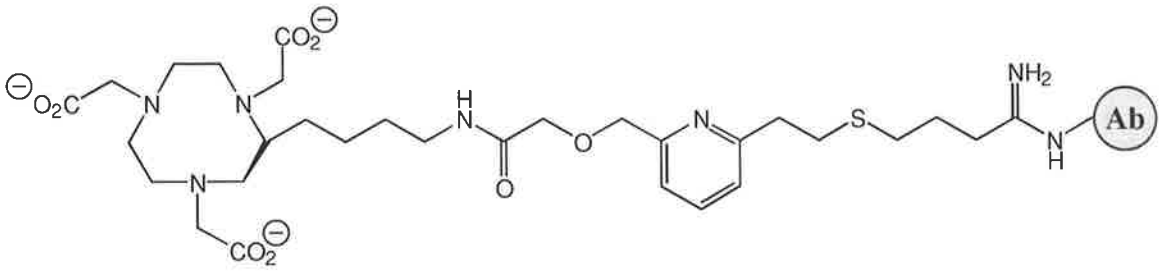

Figure 8

This technique is also used for time-resolved luminescent assays using lanthanide complexes. Amplified DNA obtained from cervical smears can be tested for human papillomavirus with a Eu^{III} complex labeled antibody, Ab. Such luminescent probes offer a safe alternative to isotopic labeling and allow highly specific, quantitative detection of infectious and genetic diseases.[105]

1.7. Designing Enzyme Mimics

Macrocyclic polyamines have found wide application in the design of bioinorganic model systems of nuclease and peptidase metalloproteins.[106,107,108,109] The large size and complexity of many enzyme systems often restrict detailed analysis of their catalytic and spectroscopic properties. The trend has been to design and synthesise low molecular weight model systems that mimic the active sites of metalloproteins.[110,111] The aza macrocycles are particularly suited to this area of research as they allow systematic structural modification and offer high kinetic and thermodynamic stability that allows easy determination of their protonation and metal binding constants at low pH. [109]

A large area of research has focused on the design of models for metalloenzymes associated with hydrolysis and hydration of biological molecules. Interestingly, such hydrolytic enzymes almost exclusively contain Zn^{II} at the active centre. Examples of Zn^{II} containing metalloenzymes include carbonic anhydrase,[112,113] alkaline phosphatase,[114,115] carboxypeptidase,[116,117,118] alcohol dehydrogenase[119,120] and many DNA and RNA polymerases.[121,122] In most cases the acidic Zn^{II} ion is closely situated near a carboxy, imidazole or alcohol group which acts concertedly with Zn^{II} to generate a nucleophile (e.g. RO^-, HO^-, or H^-) to attack electrophilic centres of carbonyl and phosphate groups.

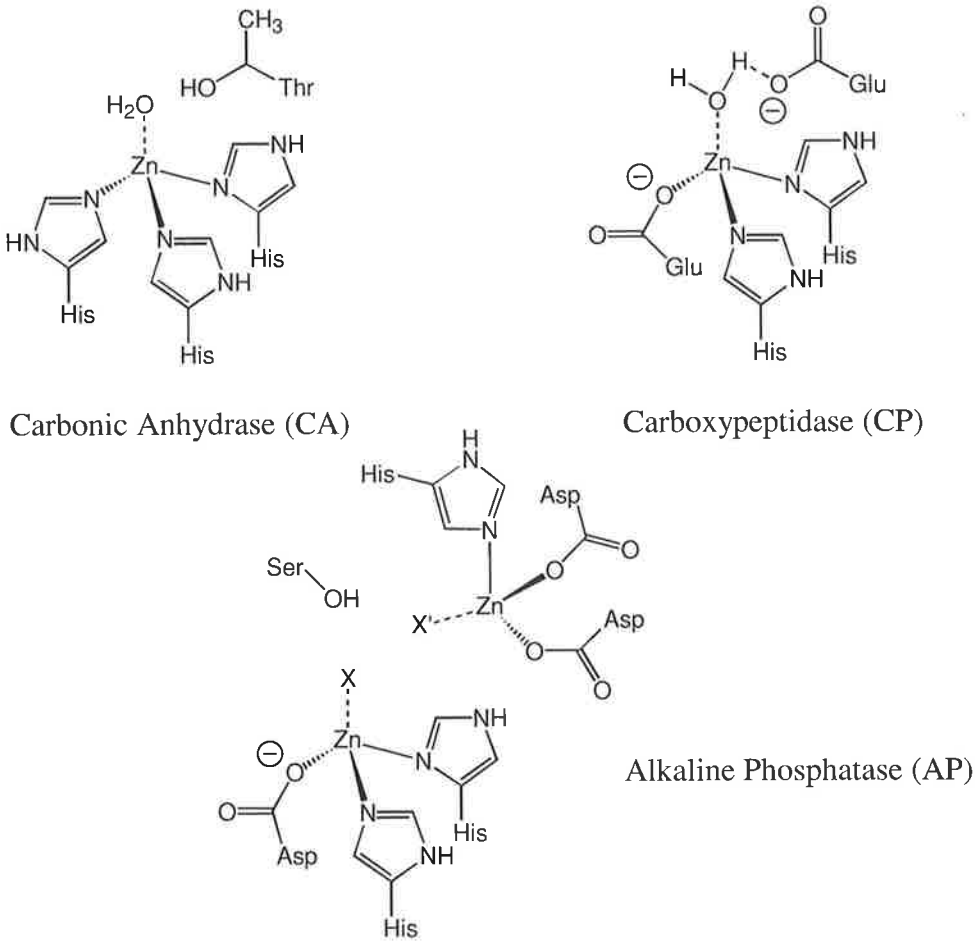

Figure 9. Examples of the active centres of some hydrolytic enzymes that contain Zn^{II}.

Interest by Kimura in the activity of Zn^{II} containing metalloenzymes has led to the development of numerous enzyme mimics based on the [12]aneN$_3$ ligand. When investigating the Zn^{II}-[12]aneN$_3$ complex, Kimura found the large cavity size rendered the Zn^{II} ion surprisingly acidic, generating a Zn^{II}-OH^- species with a pK_a of 7.3, almost identical to that of carbonic anhydrase, CA, Scheme 10.[123]

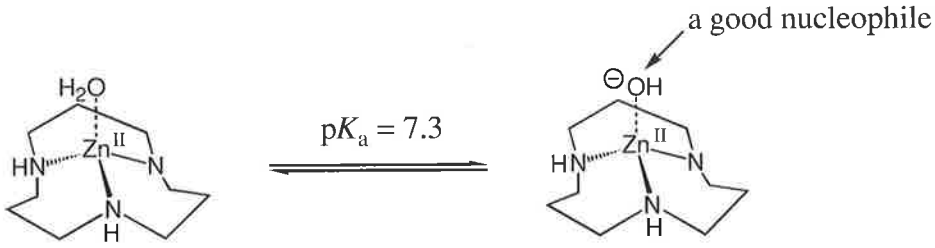

[Zn^{II}-[12]aneN$_3$]

a CA model

Scheme 10

The complex was in fact an excellent model for CA, displaying near identical binding affinities for a range of substrates.

Another Zn^{II} containing enzyme of interest to Kimura was alkaline phosphatase, AP, a phosphomonoesterase that hydrolyses phosphate monoesters at alkaline pH. Alkaline phosphatase belongs to a group of metalloenzymes known as serine proteases where a nucleophilic serine alkoxide anion initiates the substrate hydrolysis and the Zn^{II}-OH^- acts as the secondary nucleophile. Initial attack by the deprotonated serine (Ser_{102}) gives a transient phosphoseryl intermediate **13**, Scheme 11, which is then attacked by an adjacent Zn^{II}-OH^- species which completes the hydrolysis and releases the serine (Ser_{102}) alkoxide to give **14**. Release of the phosphate group and attachment of a new substrate then completes the cycle.[71]

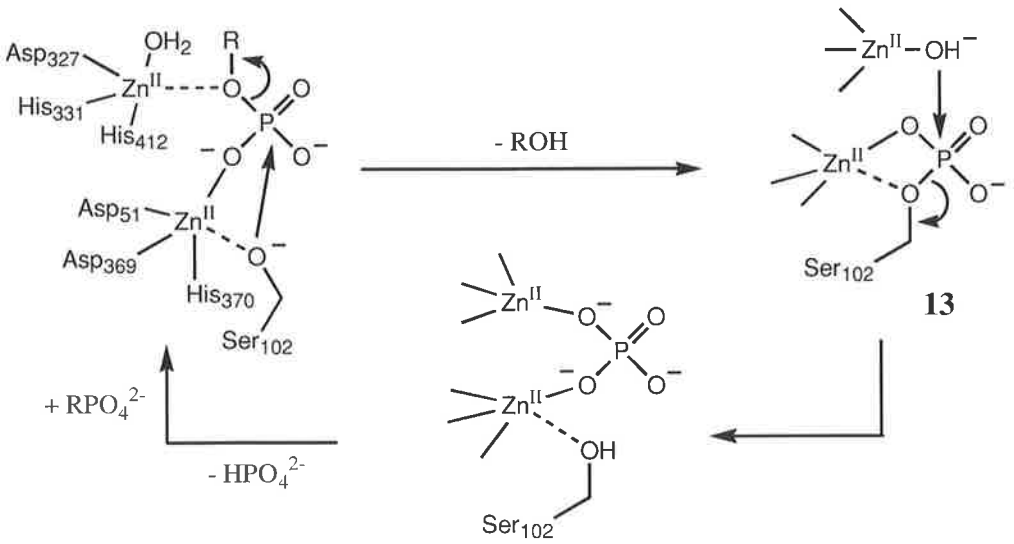

Scheme 11. The catalytic cycle of alkaline phosphatase (AP).

To model the activity of alkaline phosphatase, Kimura placed a single hydroxyethyl arm on [12]aneN_3 in the hope that the hydroxyl group, under the influence of the trapped Zn^{II} ion, would generate a strong nucleophile, Scheme 12.[71]

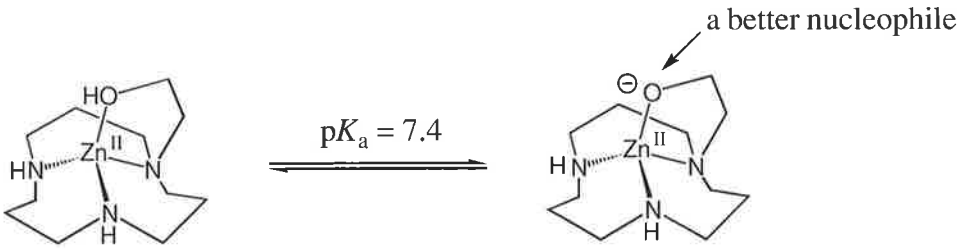

[Zn^{II}-**15**]

an AP model

Scheme 12

The alkoxide anion was found to be four times more reactive towards 4-nitrophenyl acetate hydrolysis than the Zn^{II}-OH^- species of [Zn^{II}-[12]aneN_3].

The greater reactivity of the alkoxide anion may be due to a lower degree of solvation of the nucleophile, which facilitates attack at the electrophilic centre of the substrate. Hydrolysis of 4-nitrophenyl acetate by the [Zn^{II}-**15**] complex is thought to proceed by the mechanism illustrated in Scheme 13.[71]

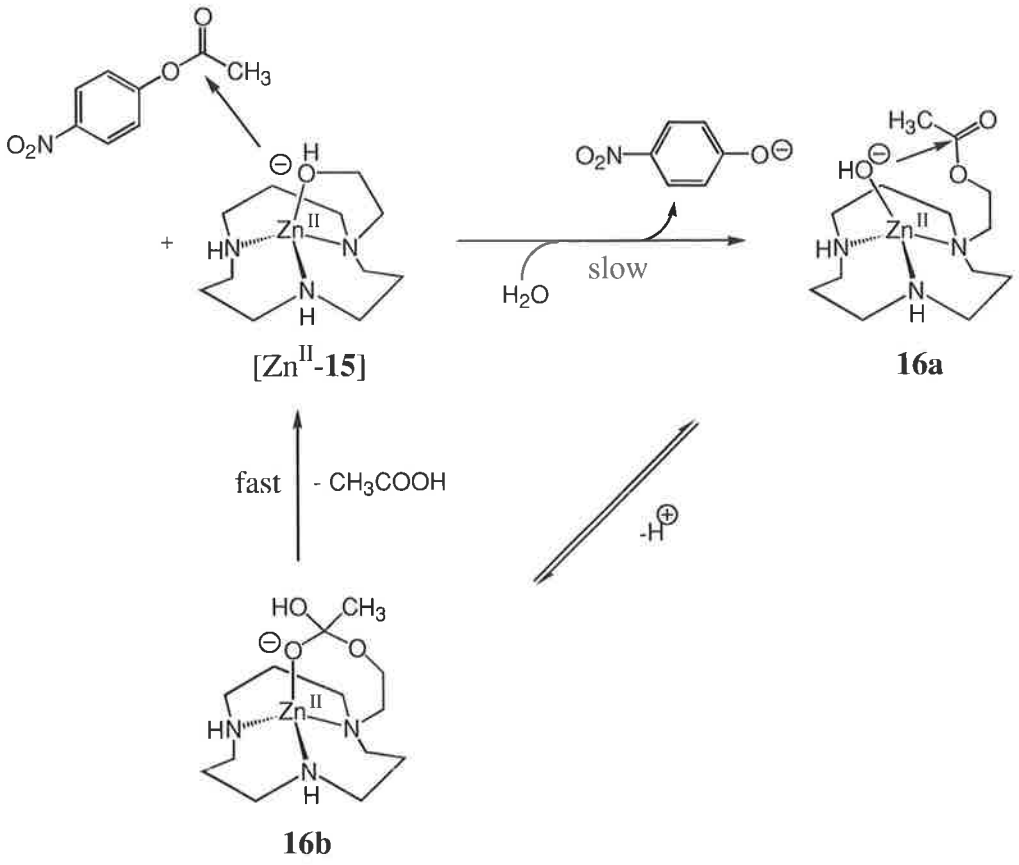

[Zn^{II}-**15**]

16a

16b

Scheme 13

Initial attack of the substrate by the alkoxide anion of [Zn^{II}-**15**] releases the 4-nitrophenolate. In accordance with a serine protease, a Zn^{II} bound water molecule then attacks the ester carbonyl group of complex **16a** to give the transient structure **16b** that rapidly decomposes to give the free metal complex and the cycle continues, Scheme 13.

Kimura's proposed mechanism, however, is rather ambiguous as the precise interaction between the substrate and the metal complex remains unclear. Hydrolysis of the ester group may occur through two distinct mechanistic pathways as shown in Figure 14. In mechanism **A**, the Zn^{II}-OH^- species of the macrocyclic complex makes a direct nucleophilic attack at the carbonyl centre of the ester group, Scheme 14. This mechanism relies on simple collision between the two reactants in solution. Alternatively, the hydrolysis reaction may proceed through mechanism **B** where the ester group is first coordinated to Zn^{II} ion. The coordinatively unsaturated Zn^{II} ion allows the possibility for the carbonyl oxygen atom to interact with the metal centre. The polarised carbonyl group would then be more susceptible to attack by either the alkoxide anion or a free hydroxyl anion.

A **B**

Scheme 14

The aim of the work described in Chapter 4 of this thesis is to further investigate the hydrolysis mechanism using analogous ligands derived from the slightly smaller [9]aneN_3 macrocycle in the hope that new information concerning the precise interaction between the ligand complex and 4-nitrophenyl acetate may be obtained.

1.8. Molecular Modelling

Throughout this thesis molecular modelling has been used in conjunction with experimental observations to provide information on molecular structure and chemical properties of certain ligands and their metal complexes.

There are two broad areas of computational chemistry that should be considered before a molecule is to be modelled.[124] The first area is molecular mechanics, which may be viewed as force field models. Molecular mechanics calculations are based on interactions amongst atoms and do not explicitly consider the electrons in a molecular system. Electronic effects are approximated through parametrisation which makes the calculations fast and computationally less expensive. This method is especially useful when modelling very large systems to obtain a fast geometrical estimation. There are however, disadvantages to molecular mechanics. The force fields are parametrised for only a limited class of molecules and are not suitable for all molecular systems. Also, the disregard of electrons means that molecular mechanics fail to achieve good results in systems where electronic effects predominate.

The second area of computational chemistry is electronic structure methods. These differ from molecular mechanics in that they employ the theory of quantum mechanics rather than classical physics as the basis for their computation. Quantum mechanics involves solving the Schrödinger equation (1.2) to obtain the energy and other related properties of the molecule.

$$\mathbf{H}\Psi = E\Psi \qquad (1.2)$$

Where **H** is the Hamiltonian operator,

E is the energy of the system,

and Ψ is a wavefunction of the positions and momenta of all particles.

Exact solutions to the Schrödinger equation are computationally practical for only the smallest systems such as the hydrogen atom. Electronic structure methods, however, use mathematical approximations to solve the Schrödinger equation and subsequently may be used over a large range of molecules.

Of the two major classes of electronic structure methods, namely semi-empirical and *ab initio* methods, the latter offers higher quality predictions for a broad range of systems. Semi-empirical methods use parameters derived from experimental data but *ab initio* calculations are based solely on the laws of quantum mechanics.

Computational models in this thesis have been obtained by *ab initio* calculations using the Gaussian 94[125] suite of programmes. Gaussian 94 achieves optimisation of the molecular potential energy by varying the molecular geometry of the species of interest. Geometry optimisations are achieved by predicting equilibrium structures of the molecular system and then determining which direction on its potential energy surface will lead to a lowering of energy, Figure 10. An optimisation is usually complete when forces in the molecule are minimised, corresponding to a minimum or a "well" in the potential energy surface. At such a point, motion in any direction leads to an increase in energy. A geometry optimisation may fall into a local minimum which is the lowest point in some limited region of the potential energy surface but not necessarily the lowest possible energy. A global minimum on the other hand is the lowest energy anywhere on the potential surface. When a geometry optimisation is obtained it is important to test whether it represents a local or global minimum. This is normally achieved by using different input structures of the same molecule to encourage an alternate pathway along the potential energy surface. In relatively simple molecules a global minimum can normally be established when varying input structures all converge to the same minimum.

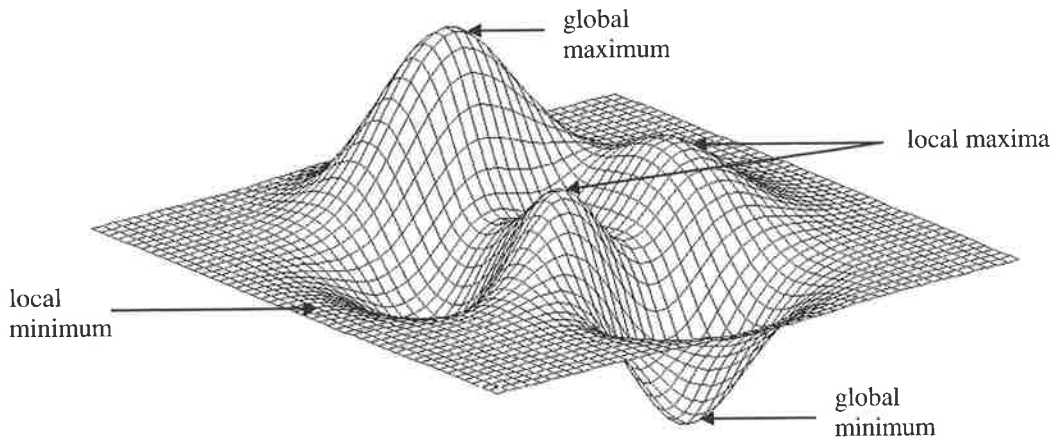

Figure 10. A potential energy surface.

Calculations in this thesis have been performed at the Hartree-Fock level of theory using one of three alternate basis sets, namely 6-31G(*), LanL2DZ or LanL2MB.[126] A basis set is used to approximate the orbitals in a given system by assigning a defined set of mathematical functions to each atom. The degree of accuracy of these approximations is largely related to

the size of the basis set and the relevance of the basis functions to the electronic requirements of the system being modelled. Larger basis sets impose fewer restrictions on the location of electrons in space and achieve more accurate approximations of the molecular orbitals. The disadvantage, however, is that very large basis sets are computationally more expensive and may often take considerable time to reach a solution. When choosing a basis set, the computational chemist must consider both the level of accuracy offered by the basis set and its practicality in terms of computational time.

In this thesis, relatively small molecules with less than 10 atoms, excluding hydrogen atoms, have been minimised with the 6-31G(*) basis set. This is a polarised basis set that adds orbitals with angular momentum to the description of each atom and is commonly used for calculations involving up to medium sized molecules.

Molecules involving heavier atoms beyond the third row, such as Zn^{II} and Cd^{II}-ligand complexes, have been minimised with the LanL2DZ basis set. This basis set is slightly more economical than the 6-31G(*) basis set. Electrons close to the nucleus of heavy atoms are considered collectively using effective core potential (ECP) approximations while valence electrons are treated separately.

Very large molecules with more than 20 atoms have been minimised with the LanL2MB basis set which offers more rapid and less accurate approximations. It imposes fixed-size atomic orbitals for atoms in the first row and uses ECP for atoms beyond the third row. This basis set is extremely useful for providing fast structural information for very large systems that do not require precise global energy minimisations.

1.9. Zinc Fingers

One of the most intriguing and until recently, poorly understood areas in biological science has been the control of gene activation in multicellular organisms. Every cell in an embryo contains the same genetic information, however, some cells differentiate to become skin cells, some bone marrow and others neurons. The fates of individual cells are controlled by the activation of different segments or combinations of genes in the developing embryo. For a gene to be activated, several proteins known as transcription factors must first bind to the

DNA promoter. This association represents an "on switch" and only then can a ribosome transcribe the DNA template into a translatable RNA message from which the cellular proteins are synthesised. By activating different combinations of promoters, a relatively small number of transcription factors are able to activate a large array of genes essential for embryo development.[127]

Exactly how such transcription factors recognises a specific docking site on a promoter remained one of nature's most elusive questions. The solution to selective gene activation, however, now lies in the discovery of small projections on transcription factors known as zinc fingers that are perfectly suited to DNA recognition.[127,128,129,130]

1.9.1. Discovery of Zinc Fingers

The pioneering steps in zinc finger discovery came in 1980 with the isolation of a transcription factor called TFIIIA from the frog *Xenopus laevis*. TFIIIA is one of three transcription factors required to activate the gene responsible for producing 5S RNA.[131] The transcription factor was rather unusual in that it was found to bind to a relatively long patch of DNA of 45 base pairs. Other similarly sized transcription factors normally bind to tracts of DNA no longer than 15 base pairs.

Insight into the structure of TFIIIA arose during the isolation of the TFIIIA-5S RNA complex from frog ovaries. The method of isolation was known to exclude certain metal ions and initial attempts proved disappointing as the isolation procedure had removed Zn^{II} that held the complex together. After modification of the extraction procedure to avoid potential Zn^{II} chelators, a good supply of the complex was isolated. The TFIIIA-5S RNA was found to contain an unusually high number of Zn^{II} ions. Enzyme digestion was then used to chop TFIIIA into smaller pieces. Interestingly, the digestion process was found to stop at fragments of three-kilodalton units that resisted further attack. The results suggested a remarkable repeating structure within TFIIIA where a string of tandem three-kilodalton units, each containing 30 amino acids per segment, were folded around a single Zn^{II} ion to form a tightly compacted domain. Each segment was found to contain a conserved pair of cysteine amino acids and a pair of histidine amino acids in virtually identical positions which, when folded, would coordinate a Zn^{II} ion. Each domain was separated by a chain of approximately five

amino acids and were later termed zinc fingers as they are used to "clasp" the DNA double helix, Figure 11.

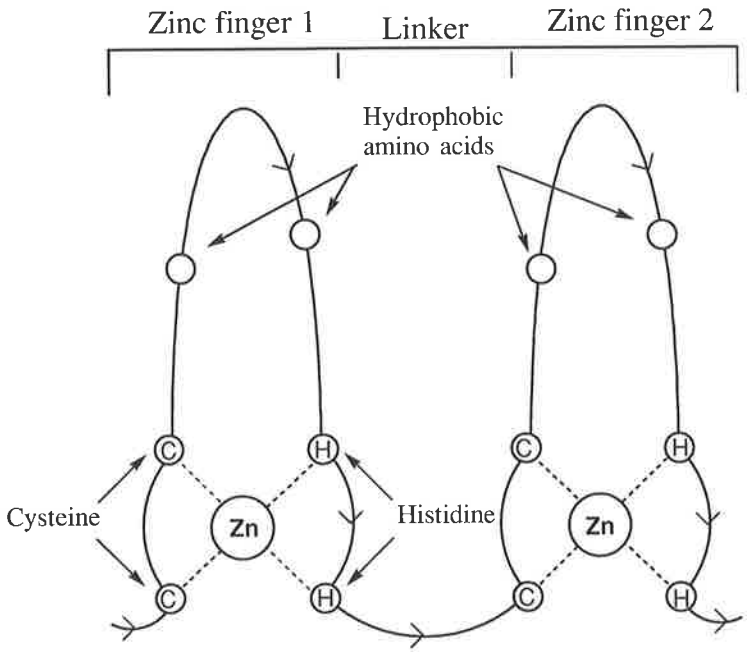

Figure 11. A classic zinc finger mini-domain.

The method with which zinc fingers are able to recognise specific DNA sequences was predominantly established by Berg and Wright who were able to solve the three dimensional structure of the zinc finger module through a combination of theoretical techniques and NMR spectroscopy.[132] The left half of the domain consists of two beta strands folded back on one another to form a beta sheet while the right half twists into an alpha-helix, Figure 12. The two cysteine residues reside at the bottom of the beta sheet and the two histidine residues are located at the bottom of the alpha-helix. The zinc ion is coordinated at the base of the domain by the four amino acid residues that essentially pin the structure together, Figure 12A. In addition to the cysteine and histidine amino acids, each finger also contains three conserved hydrophobic amino acids in virtually identical positions. These residues are thought to assist folding of the strands and maintain the three-dimensional shape of the finger by creating a hydrophobic interior, Figure 12B.

Since the discovering of the transcription factor TFIIIA, hundreds of transcription factors containing zinc fingers have now been identified. The enormous range of DNA-binding motifs has since been subdivided into three classes based on the nature of the zinc coordination motif.

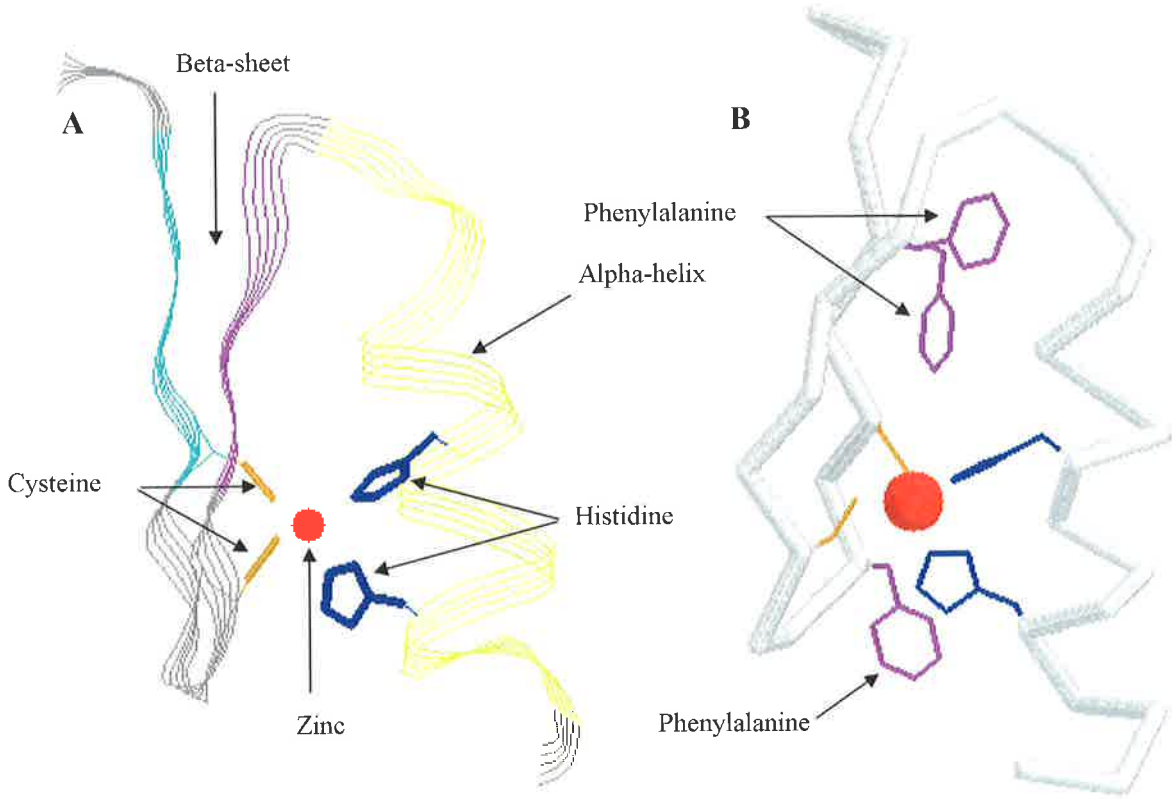

Figure 12. NMR structures of TF SW15 showing beta-sheet (cyan and magenta) and alpha helix (yellow) secondary structure (**A**), and the hydrophobic interior created by phenylalanine residues (magenta) (**B**).[133]

1.9.2. Classes of Zinc Fingers[133]

The most common class of zinc finger, known as Class 1, contains the classic structure of an approximately 30 residue motif that coordinates a single Zn^{II} ion through two cysteine and two histidine residues, Figure 12. There are more than 200 example of Class 1 zinc fingers which are believed to be encoded by 1% of the human chromosome.

The exact nature of DNA recognition by a Class 1 zinc finger was revealed in 1991 by x-ray crystallography of the complex formed between the DNA-binding domain of the mouse transcription factor Zif268 and its DNA target.[134] The co-crystal structure showed the Zif268 zinc fingers binding as monomers in the major groove, making base-specific contacts on only one strand of DNA. The fingers were shown to curl around almost one turn of the DNA helix in a screw-like motion at approximately 96° to one another, Figure 13.

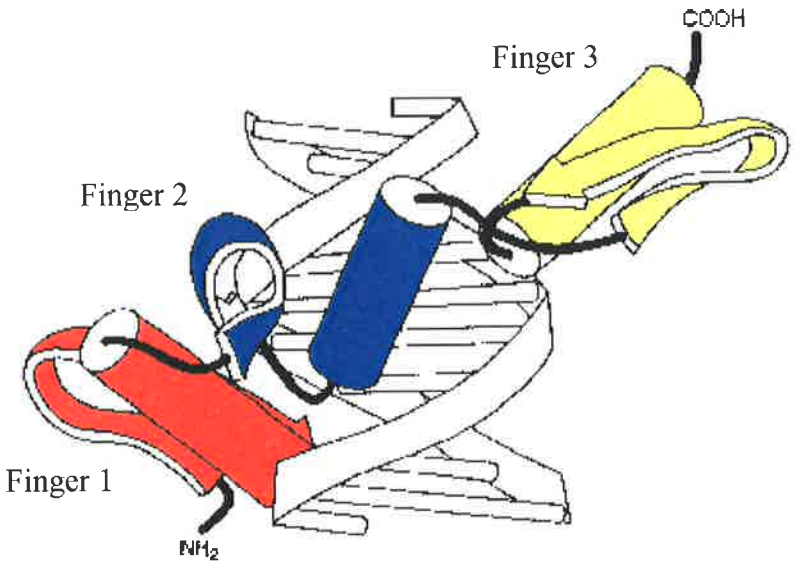

Figure 13. X-ray crystal structure of the mouse Zif268 protein/DNA complex.[134]

It was revealed that each finger made contact with successive three-base-pair sites on the single strand of DNA by residues at the N-terminal end of each alpha-helix. Additional non-specific interactions are also made between the alpha-helix and beta-sheets with phosphate groups in the DNA back bone or "rungs".

The second class of zinc fingers are found in the steroid hormone receptor proteins such as the oestrogen and glucocorticoid receptors. Structurally, the Class 2 zinc fingers contain an approximately 70 residue motif consisting of two loop-helix elements each containing one Zn^{II} ion coordinated by four cysteine residues, Figure 14(A-B). The N-terminal helix (shown in green) lies in the major groove and is responsible for DNA recognition while the C-terminal helix (red) is packed behind at right angles.[135,136]

Unlike the Class 1 zinc fingers, which act as independent structural units, the zinc fingers of nuclear receptors fold together as dimers to form a unified globular domain that recognises the two half sites on DNA. The DNA binding site is known as a palindrome as it contains two identical sequences that run in opposite directions. For the dimer to bind to the palindromic binding site two criteria must be met. Firstly, the N-terminal loop helix in each dimer must be specific for the binding site in the major groove and secondly the length between the two dimerised units must match the distance between the two binding sites, Figure 15.[137]

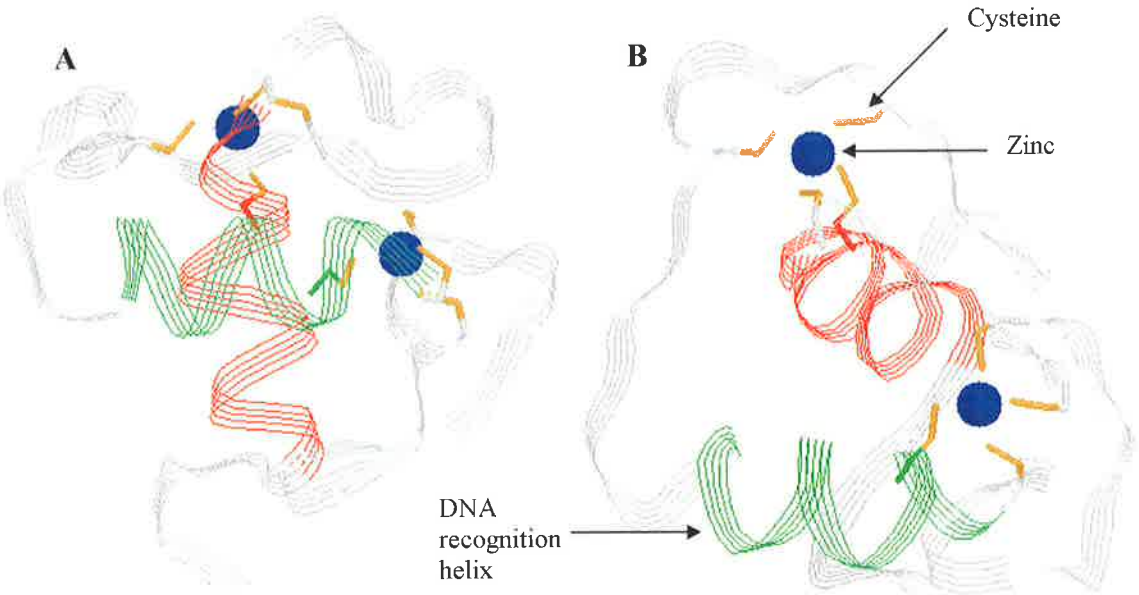

Figure 14. A three-dimensional structure of the DNA binding domain of the glucocorticoid receptor as seen from the major groove of DNA (**A**) and as seen from above (**B**).

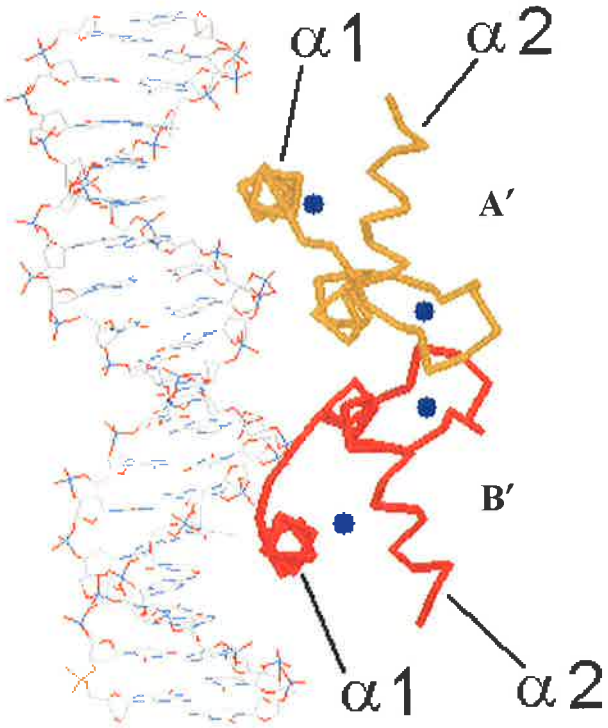

Figure 15. A view of the complex formed between the DNA-binding domains of two glucocorticoid receptor molecules, A′ and B′, and their palindromic DNA recognition sequence.

An insufficient intake of Zn^{II} in the diet can lead to symptoms such as delayed sexual development. In the absence of Zn^{II}, the oestrogen and androgen receptors are unable to fold properly and consequently cannot activate the appropriate genes for hormone production.

The final class of zinc fingers is found exclusively in fungal transcriptional activators. Each Class 3 motif contains an approximately 65 residue motif with two Zn^{II} ions coordinated by six cysteine residues. They are similar to the Class 2 zinc fingers in that each protein binds as a dimer to a palindromic recognition site. The motif is divided into a recognition module which contains the metal binding domain and a dimerisation domain separated by a linker region, Figure 16A. Each recognition module consists of two short alpha-helices (shown in red and cyan) that are followed by an extended strand. Correct juxtaposition of these elements is ensured by the coordination of the two Zn^{II} ions. The dimerisation domain (shown in green) consists of an amphipathic alpha-helix (hydrophobic on one side and polar on the other) which associates with the dimerisation domain of a second dimer protein, Figure 16B.

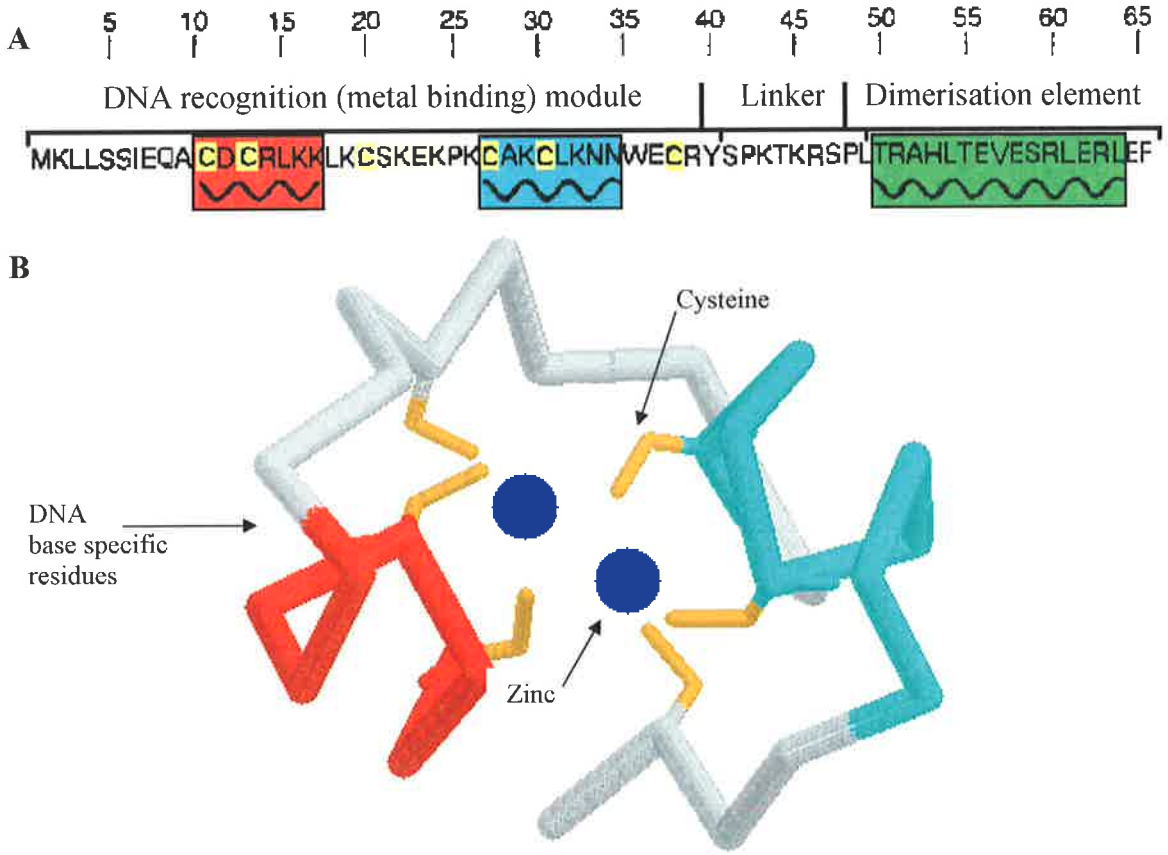

Figure 16. The DNA-binding domain of the yeast Gal4 protein (**A**) and the three dimensional structure of the DNA recognition module (**B**).[133]

In the short period since the discovery of the classic zinc finger protein TFIIIA, an enormous amount of knowledge about the structure and recognition process of zinc fingers has been established. Such insight into gene activation has immense medical potential. Preliminary work[138,139,140,141,142] in the modification of zinc finger proteins may someday lead to the design of tailor made, zinc finger, DNA binding proteins. Such designed proteins could be powerful therapeutic tools, enabling researchers to control specific genes in the body responsible for cancer production or even suppressed immune development.

1.10. Work Presented in this Thesis

This thesis is a starting point towards the isolation of a novel set of zinc finger models. The principal objective of this thesis was to establish some groundwork in the design and synthesis of a basic zinc finger model based on a [9]aneN$_3$ macrocycle ligand.

In order to design a macrocyclic model system, whether it be a catalytic enzyme or protein mimic, it is important to have a firm understanding of the intrinsic acid/base and coordination properties of the ligand system. As a consequence, the preliminary objective of this work was to design and synthesise three derivatives of [9]aneN$_3$ with increasing numbers of hydroxyethyl pendant arms and compare their acid/base properties and coordination ability with Zn^{II} and Cd^{II}. There has been substantial research into the coordination chemistry of either one, two or three arm functionalised ligands, however, there remains no direct comparison between same macrocyclic ligands with different numbers of pendant arms. The acid/base properties and stability constants of each system are expected to differ in each case and comparison between each ligand will help identify the effect that each arm plays on the overall electronic and coordination ability of each system.

A further interest lies in resolving the ambiguous mechanism of ester hydrolysis by Kimura's [Zn^{II}-**15**] complex, where the Zn^{II}-OH^- species may act as either a direct nucleophile or where the ester carbonyl group must first coordinate to the metal centre prior to hydrolysis. The Zn^{II} complexes of the three [9]aneN$_3$ ligands with increasing numbers of pendant arms are possible models for Kimura's system where the Zn^{II} ion is coordinated to varying degrees of saturation. The one- and two-arm ligand complexes may be considered

coordinatively unsaturated and allow the possibility for the carbonyl group of 4-nitrophenyl acetate to coordinate to the Zn^{II} ion. The Zn^{II} ion in the three arm complex is, however, already saturated by a N3O3 donor set and would discourage any interaction. Comparison between the rate constants of each complex against 4-nitrophenyl acetate hydrolysis may possibly help to differentiate between the two mechanisms and will be discussed in further detail in Chapter 4.

The prevailing interest in this thesis lies in the development of a simple model system of a zinc finger binding motif. There is an ongoing interest in our group to design numerous microscale models of a Class 1 zinc finger using the [9]aneN_3 macrocycle as the primary coordinating unit. By attaching a single pendant arm of varying length and complexity, it is envisaged that it will loop back to form an extended chelate ring at the Zn^{II} centre and effectively mimic the loop structure of a zinc finger motif.

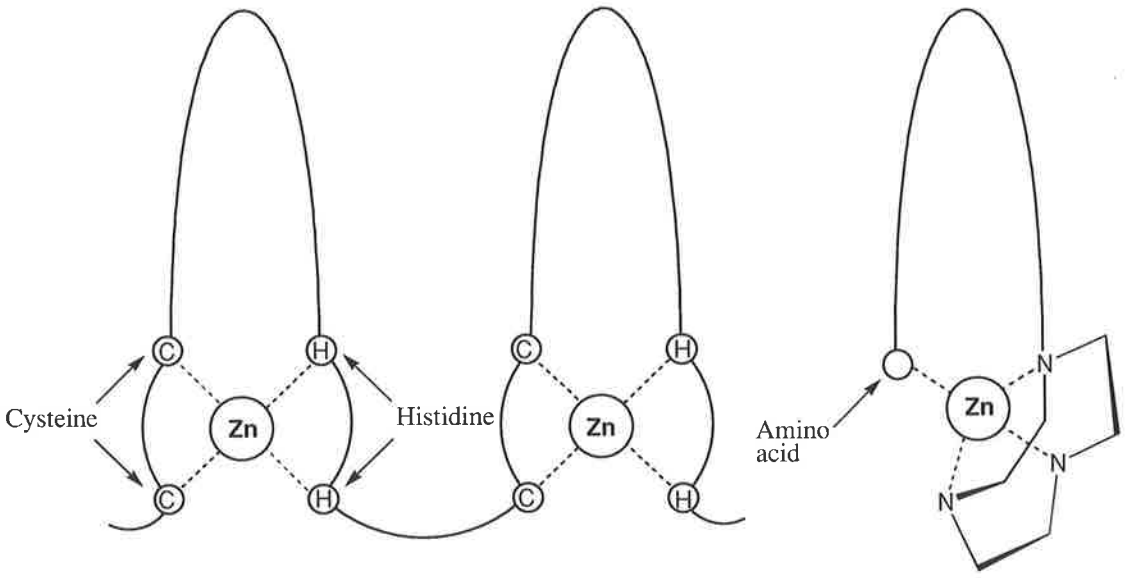

Figure 17

As part of an ongoing project, the final aim of this work was to establish some initial synthetic strategies towards the design of a zinc finger model.

Chapter 2. Syntheses of Hydroxyethyl Functionalised [9]aneN$_3$ Ligands

2.1. Introduction

In order to investigate and hopefully further elucidate the mechanism of ester hydrolysis by Kimura's [Zn^{II}-**15**] complex, Scheme 15, variations of the ligand, based on the smaller [9]aneN$_3$ macrocycle, will be used as model systems.

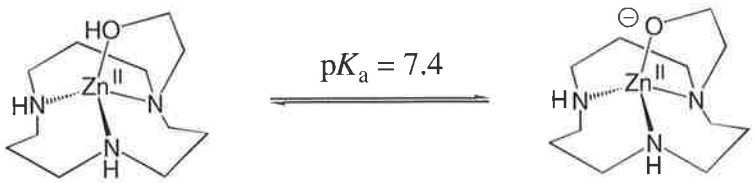

[Zn^{II}-**15**]

Scheme 15

The three target ligands have been named hec[9] **17**, bhec[9] **18** and thec[9] **19** and represent the one-, two- and three-pendant arm ligands, respectively, Figure 18. The nomenclature for each ligand stems from the parent name describing the one arm ligand, hydroxy-ethyl-cyclononane, (i.e. hec) and the number of atoms in the macrocyclic ring (i.e. 9). The two and three arm ligands are differentiated by the prefix bis- and tris- and assume the names, bhec[9] and thec[9], respectively.

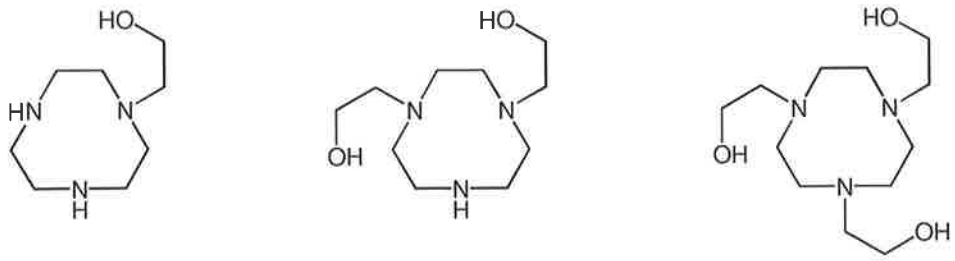

hec[9] **17**

bhec[9] **18**

thec[9] **19**

Figure 18

Whereas Kimura examined the basicity and metal binding stability of only the single pendant arm ligand,[71] physical measurements were performed on all three ligands to determine their spectroscopic, protonation and stability constants. Having established the protonation constant

and metal binding constants with Zn^{II} and Cd^{II}, investigations into their potential coordination environments were made using *ab initio* calculations.

Although the activity of each ligand with Zn^{II} was the prior concern, the interaction of each ligand with Cd^{II} was also a major interest. Cd^{II} may be viewed as an opposing metal element to Zn^{II}. Whereas Zn^{II} is a biologically essential element,[143] fundamental to the activity of metalloenzymes such as alkaline phosphatase, Cd^{II} is biologically devastating. It is an extremely toxic heavy metal that deactivates metalloenzymes in the body by competitively binding with metal ions at the active sites. A further reason for using Cd^{II} lies in its unique NMR properties. The predominant aim of this project is to synthesise a potential zinc finger model where a long pendant arm is looped back onto a coordinated Zn^{II} centre. In order to prove that a loop structure has been established, it is important to determine when the pendant arm has coordinated the metal centre. Apart from through space interactions (i.e. NOE) within the loop structure, interaction between the pendant arm and a Cd^{II} metal centre may also prove helpful. ^{111}Cd (spin = ½) has a relative abundance of 12.75% and will couple with both the ring protons and the primary pendant arm protons. If the pendant arm does coordinate the Cd^{II} centre, $^{3}J_{H,Cd}$ coupling will produce satellites in the ^{1}H NMR spectrum and differentiate between a system where the pendant arm remains uncoordinated.

2.2. Synthesis of 1,4,7-Triazacyclononane, [9]aneN$_3$

The three target ligands derive their structure from the [9]aneN$_3$ macrocycle. Although structurally simple, the synthesis of [9]aneN$_3$ is lengthy, involving initial functionalisation of linear starting material followed by 1:1 condensation of the reactant components to achieve ring formation. The macrocycle was synthesised from acyclic material by modification of standard literature procedures.[2,144,145]

The initial step towards the synthesis of [9]aneN$_3$ involved the tosylation of diethylenetriamine and ethanediol. Diethylenetriamine was treated with three equivalents of tosyl chloride in the presence of triethylamine to give the tri-tosylated amine **20** as long thin needles in 90% yield, Scheme 16a. Similarly, ethanediol was reacted with two equivalents of tosyl chloride under similar conditions to give the di-tosylated species **21** as a white crystalline compound in 91% yield, Scheme 16b.

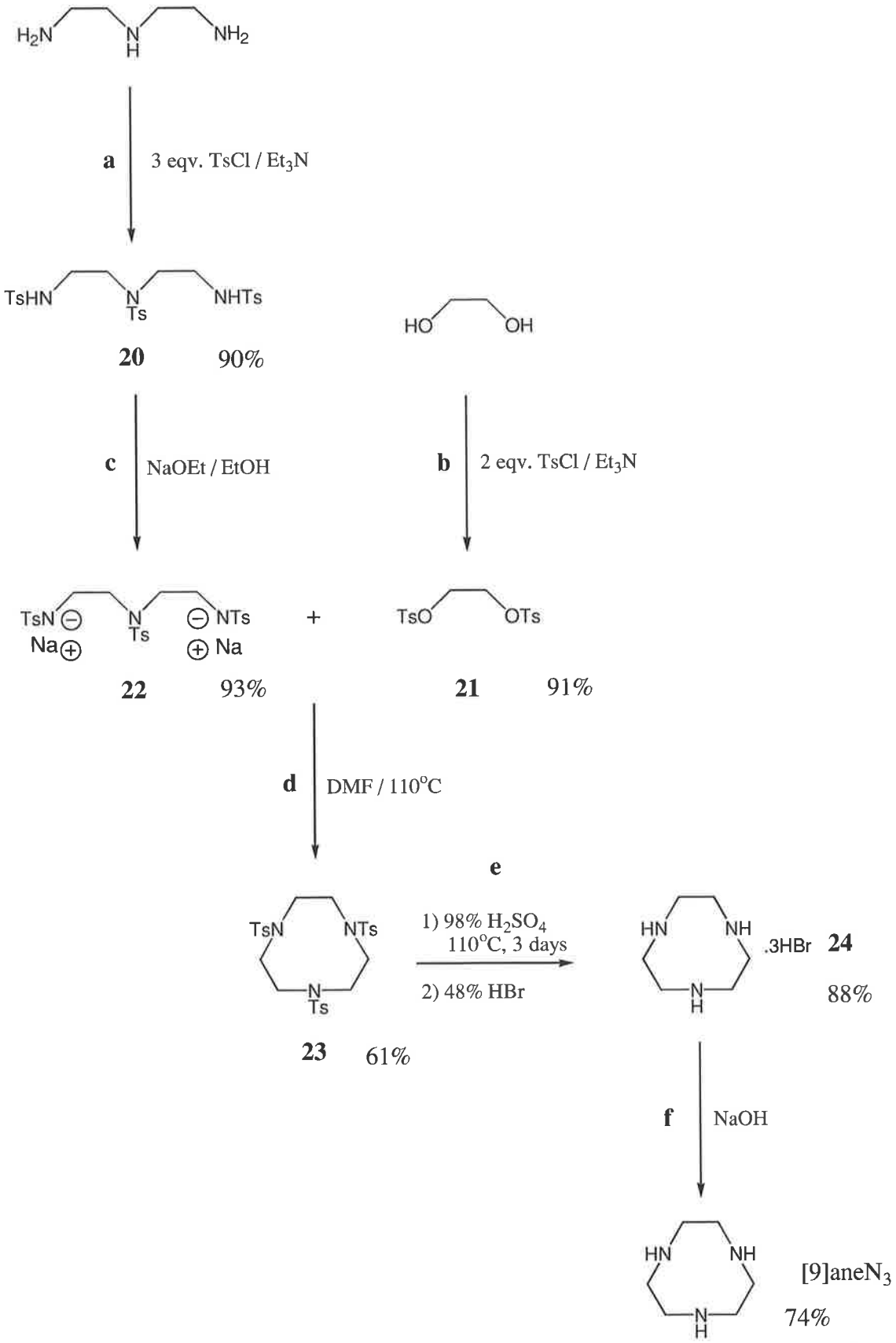
H2N
N
H
NH2
a
3 eqv. TsCl / Et3N
TsHN
N
Ts
NHTs
20
90%
HO
OH
c
NaOEt / EtOH
b
2 eqv. TsCl / Et3N
TsN
N
Ts
NTs
Na
Na
22
93%
+
TsO
OTs
21
91%
d
DMF / 110°C
e
TsN
NTs
N
Ts
23
61%
1) 98% H2SO4
110°C, 3 days
2) 48% HBr
HN
NH
N
H
.3HBr
24
88%
f
NaOH
HN
NH
N
H
[9]aneN3
74%

Scheme 16

Each compound was characterised by the appearance of aromatic benzyl and aromatic methyl resonances in the ^{13}C NMR spectra and sharp melting points that compared favourably with literature values.[144,145] To facilitate coupling of the two substrates, compound **20** was converted to the activated di-sodium salt **22** by treatment with sodium ethoxide in dry ethanol. Filtration and prolonged desiccation of the product under high vacuum at approximately 80°C gave **22** as a white hygroscopic powder in 93% yield, Scheme 16c. The insolubility of the disodium salt **22** in deuterium oxide (D_2O) or deuterated chloroform ($CDCl_3$) precluded it from NMR analysis, however, an elevated melting point 294°C distinguished it from the protonated species **20** which had a melting point of 173°C.

Formation of the macrocyclic ring was achieved by 1:1 condensation of **22** and **21**. The two reactants were mixed in dry dimethylformamide (DMF) for 12 hours at 80°C to afford the tri-tosylated macrocycle **23** as a white solid that was recrystallised from acetone in good yield, Scheme 16d. The ^{13}C NMR spectrum of **23** revealed a highly symmetrical compound displaying a single ring carbon resonance at δ 51.9 parts per million (ppm) and the appropriate aromatic resonances of the *N*-tosyl groups. The identity of the cyclic species was further confirmed by FAB mass spectrometry of **23**, which displayed a base peak at *m/z* 592.

Having isolating the tosylated macrocycle **23**, it was necessary to remove the *N*-tosyl groups. Treatment of **23** with 98% sulfuric acid at 110°C gave [9]aneN_3 as a hygroscopic sulfonic acid salt. This was isolated as a brown solid and immediately converted to the more stable trihydrobromide salt **24** by acidification with 48% hydrobromic acid, Scheme 16e. The product was characterised as an off-white, water-soluble powder with a melting point of 269-277°C that compared favourably with the literature value of 277-278°C. Removal of the *N*-tosyl groups resulted in a substantial loss in molecular mass displaying a base peak at *m/z* 130 by FAB mass spectrometry. The ^{13}C NMR spectrum of **24** in D_2O revealed only a single resonance at δ 44.5 ppm corresponding to the six identical ethylene ring carbons.

The free amine was finally obtained by treating **24** with aqueous sodium hydroxide until pH 9 followed by benzene extraction using a Dean-Stark apparatus. In this way, [9]aneN_3 was isolated as a white amorphous solid in an overall yield of 33%, Scheme 16f. The sample was deemed to be of high purity, displaying a single carbon resonance in the ^{13}C NMR spectrum and a melting point of 42-46°C.

2.3. Syntheses and Design of Pendant Arm Derivatives of [9]aneN$_3$

2.3.1. Synthesis of Trishydroxyethyl-1,4,7-triazacyclononane, Thec[9]

Attachment of the three hydroxyethyl pendant arms to [9]aneN$_3$ was achieved by reaction of the macrocycle with three equivalents of ethylene oxide in ethanol, Scheme 17.[45] Extreme care was taken when handling the alkylating agent due to its high toxicity and volatility. All measurements of ethylene oxide were performed using chilled glassware and the [9]aneN$_3$ solution was cooled to 0°C before adding the reagent. The reaction mixture was allowed to stir in a tightly stoppered flask for three days at room temperature. In this way, the three arm ligand, thec[9] **19**, was isolated as a viscous oil in quantitative yield.

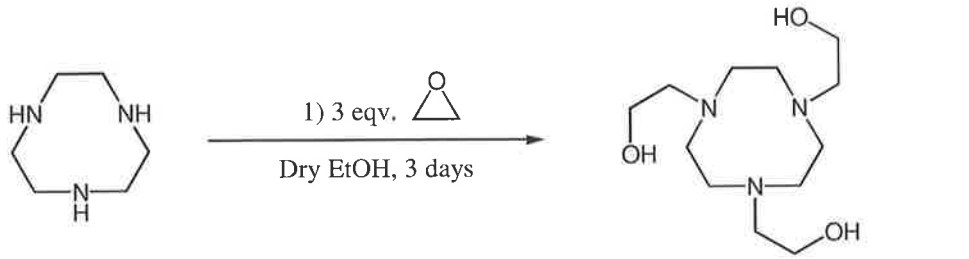

19 100%

Scheme 17

The compound was considered spectroscopically pure displaying only three resonances in the ^{13}C NMR spectrum. In addition to a single ring resonance at δ 53.1 ppm, two resonances at δ 59.3 and δ 60.0 ppm were also observed corresponding to the three identical *N*-ethylene and three identical *O*-ethylene arm carbons, respectively. In addition, the mass spectrum of **19** also showed a base peak at *m/z* 261 confirming the attachment of three hydroxyethyl pendant arms.

Although this method represents a high yielding approach to **19**, it offers little avenue for purification of the product if the need arises. Due to the extreme polarity and low volatility of **19**, the product could not be purified by either column chromatography or distillation. When an excess of ethylene oxide was used in the alkylation procedure, some additional low intensity peaks were often observed in the ethylene region of the ^{13}C NMR spectrum. Although the identity of these signals is unclear they may be caused by over-alkylation of the

tertiary nitrogen atoms. Apart from further derivatisation or metal complexation, the only available method of separating the impurities from **19** is to acidify the ligand with 48% hydrobromic acid and attempt to recrystallise the solid hydrobromide salt. When an impure sample of **19** was obtained, the product was acidified to give a brittle crystalline solid, however, this failed to recrystallise in isopropanol. On each occasion a precipitate was obtained which was shown to carry the impurity by ^{13}C NMR analysis.

An alternative method by Hancock[44,45] involves synthesising **19** as a mono-hydrobromide salt rather than as the free ligand. This approach gives the product as a crystalline solid that can be more easily purified by recrystallisation. Following this procedure, [9]aneN$_3$.3HBr **24** was reacted with two equivalents of sodium ethoxide in ethanol to give [9]aneN$_3$ as the mono-hydrobromide salt **25** which was then treated *in situ* with three equivalents of ethylene oxide and allowed to stir for three days at room temperature, Scheme 18(a-b). This method afforded a white solid that was recrystallised from isopropanol to give thec[9] as white crystals in 63%. Spectroscopic analysis of the product in D_2O confirmed the identity of the product, however, the melting point of 154°C was considerably higher than that quoted by Hancock[44] at 102°C. Elemental analysis of the crystals revealed the product to be thec[9].NaBr **26** rather than the mono-hydrobromide salt, Scheme 18b.

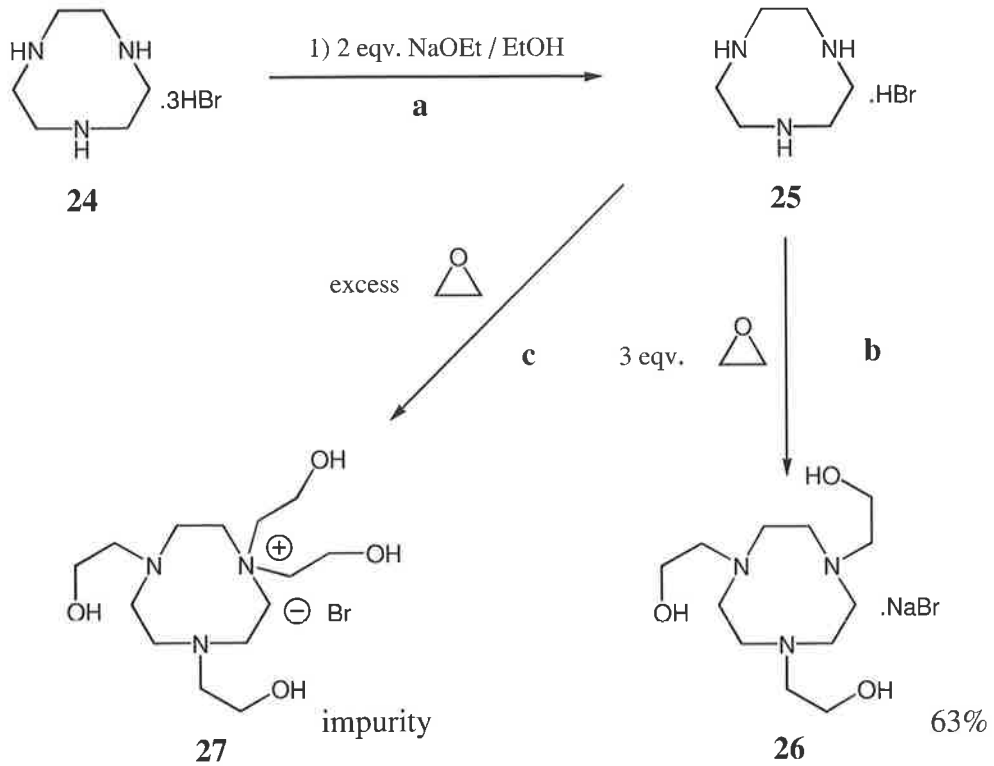

Scheme 18

Although this procedure offers the advantage of isolating thec[9] as a crystalline solid, the presence of the bromide anion also increases the risk of over alkylation of the tertiary nitrogens. When an excess of ethylene oxide was used, a substantial amount of the tetrakis species **27** was formed in addition to **26**, in some instances giving 1:1 ratio by ^{13}C NMR analysis, Scheme 18c. The two products were separated by repeated fractional recrystallisation in isopropanol and **27** was isolated as white crystals with a melting point of 120°C. Its identity as the four-arm species was confirmed by elemental analysis and NMR spectroscopy, which revealed a symmetrical structure showing three ring carbon resonances and four arm carbon resonances.

Compound **27** is interesting in that it contains four potential ligating pendant arms and is an extension of the one-, two- and three-arm ligand series. Although the quaternary nitrogen is unable to participate in coordination of a metal ion, the four oxygen atoms and two remaining nitrogen atoms may provide a stable coordinating environment. To examine the coordination potential of **27**, without having to perform potentiometric titrations, the Zn^{II} complex was modelled by *ab initio* calculations using the Gaussian 94 programme,[125] Figure 19.

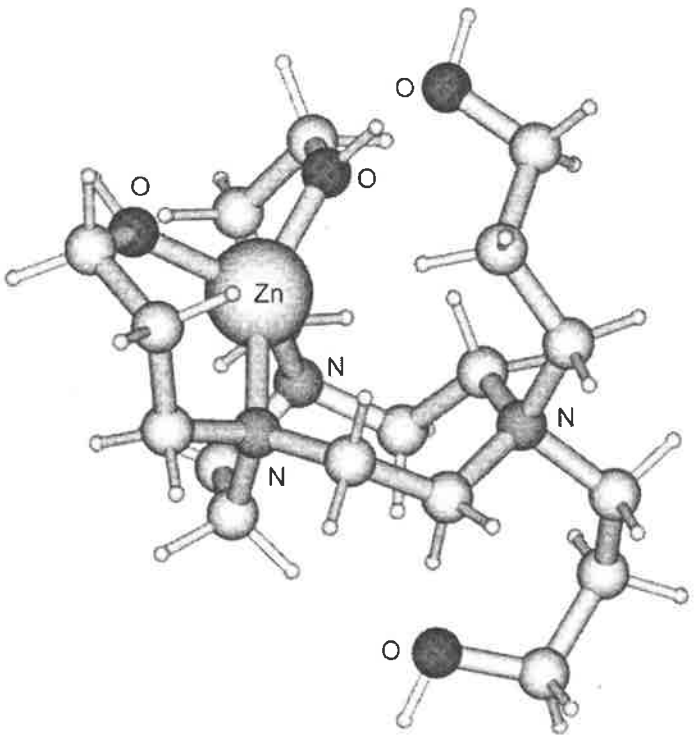

Figure 19. Energy-minimised structure of [Zn^{II}-**27**] determined through Gaussian 94 using the LanL2DZ basis set.

The minimised structure of the [Zn^{II}-**27**] complex shows the Zn^{II} ion coordinated by two tertiary nitrogens and two oxygen atoms of their pendant arms. The quaternary nitrogen is seen to repel the metal ion at such a distance that neither of its pendant arms are able to make contact with the Zn^{II} ion. One pendant arm lies above the plane of the macrocyclic ring while the other lies below. Although four donor atoms coordinate the Zn^{II} ion, the stability of the complex is expected to be low as there are only two coordinating nitrogen donors. With regard to the Hard-Soft Acid-Base (HSAB) classification,[146,147,148] Zn^{II} is considered a borderline hard-soft Lewis acid and Cd^{II} a soft Lewis acid. Both metal ions tend to bind more strongly to soft bases such as amine nitrogen. Oxygen is a relatively hard base and shows greater affinity for hard metal ions such as the alkali earth metals. A complex in which all three nitrogen atoms are able to coordinate the Zn^{II} ion is much more desirable as it provides a greater degree of stability.

2.3.2. Synthesis of Bishydroxyethyl-1,4,7-triazacyclononane, Bhec[9]

The alkylation of less than the total number of amine nitrogens of [9]aneN_3 is inherently more difficult. When [9]aneN_3 is reacted with less than three equivalents of alkylating agent a complex mixture of alkylated products generally occurs. Generally, these products cannot be separated by chromatography and often require further derivatisation or metal complexation to separate the reaction products.[64,63]

Selective alkylation of unprotected [9]aneN_3 has been achieved using either a large excess of [9]aneN_3[61] or large alkylating groups that prevent over alkylation on steric grounds.[68] Selective alkylation of [9]aneN_3 with less than three equivalents of ethylene oxide is particularly difficult as the small pendant arms provide little steric influence. The pendant arms may actually encourage further alkylation by hydrogen bonding with other ethylene oxide molecules.

Another possible technique is to perform the alkylation reaction at reduced pH so as to lower the reactivity of the amine donors and improve the chance of correct stoichiometric interaction between the macrocycle and the alkylating agent. This method was tested as a possible pathway to synthesise the two-arm ligand, bhec[9]. [9]aneN_3.3HBr **24** was treated

with two equivalents of sodium ethoxide in dry ethanol to generate the mono-hydrobromide species. The mono-protonated [9]aneN$_3$ was then reacted *in situ* with two equivalents of ethylene oxide and left to stir for three days at room temperature. This gave a viscous oil that was further acidified with 48% hydrobromic acid and recrystallised from ethanol to give the desired product **18** as white needles in a 37% yield, Scheme 19.

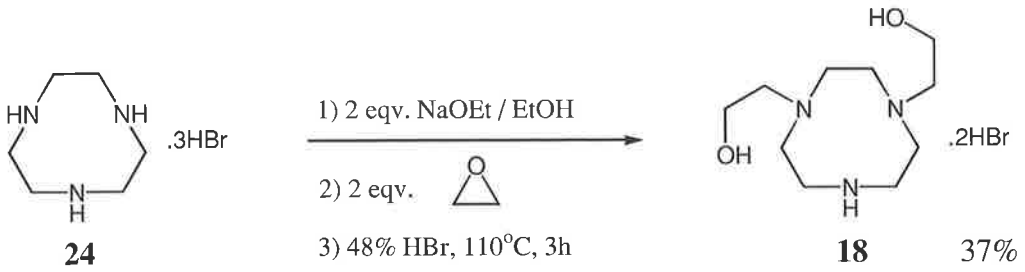

24 **18** 37%

Scheme 19

The two arm ligand was distinguished from [9]aneN$_3$ and thec[9] by its two-fold symmetry, displaying three ring carbons resonances and two pendant arm resonances in the ^{13}C NMR spectrum. Elemental analysis also identified the product as the dihydrobromide salt with a melting point of 155°C.

Although this procedure initially proved successful, subsequent attempts to isolate **18** failed. Attempts to repeat the reaction consistently gave a complex mixture of products and all attempts to purify the products by recrystallisation proved ineffective. Reactions requiring stoichiometric amounts of ethylene oxide are difficult to perform. The extreme volatility of ethylene oxide (bp 10°C) makes it extremely difficult to measure, especially when performing small-scale reactions. Generally, a slight excess of ethylene oxide is often required to compensate for evaporation while handling the reagent. The inability to repeat the initial reaction is most probably due to inaccurate measurement of the alkylating agent.

An alternative approach towards isolating di-substituted [9]aneN$_3$ involves protecting one of the nitrogen atoms prior to alkylation. This method is more complicated, primarily due to the difficulty associated with attaching a single protecting group on [9]aneN$_3$. The earliest method of mono-protection involved the removal of two *N*-tosyl groups from tri-tosylated [9]aneN$_3$,[65] however, hydrolysis of the *N*-tosyl groups requires very harsh acidic conditions.

An alternative method involves hydrolysis of the bridged macrocycle **6**, which ring opens to give the mono-protected formamide species **28** as shown in Scheme 20. This method

gives a suitable protected [9]aneN$_3$ species that will react readily with alkylating agents and is easily deprotected under acidic or basic hydrolysis conditions.[149]

To generate the mono-protected species **28**, it was necessary to first synthesise the bridged macrocycle **6**. Reaction of [9]aneN$_3$ with neat *N,N*-dimethylformamide dimethyl acetal at 85°C gave an amber coloured oil that was purified by Kugelrohr distillation to give **6** as a colourless oil in 95% yield, Scheme 20a. The ^{13}C NMR spectrum of **6** displayed a three-fold symmetry showing a single resonance at δ 51.8 ppm for the six ethylene carbons and a resonance at δ 104 ppm for the central bridge carbon.

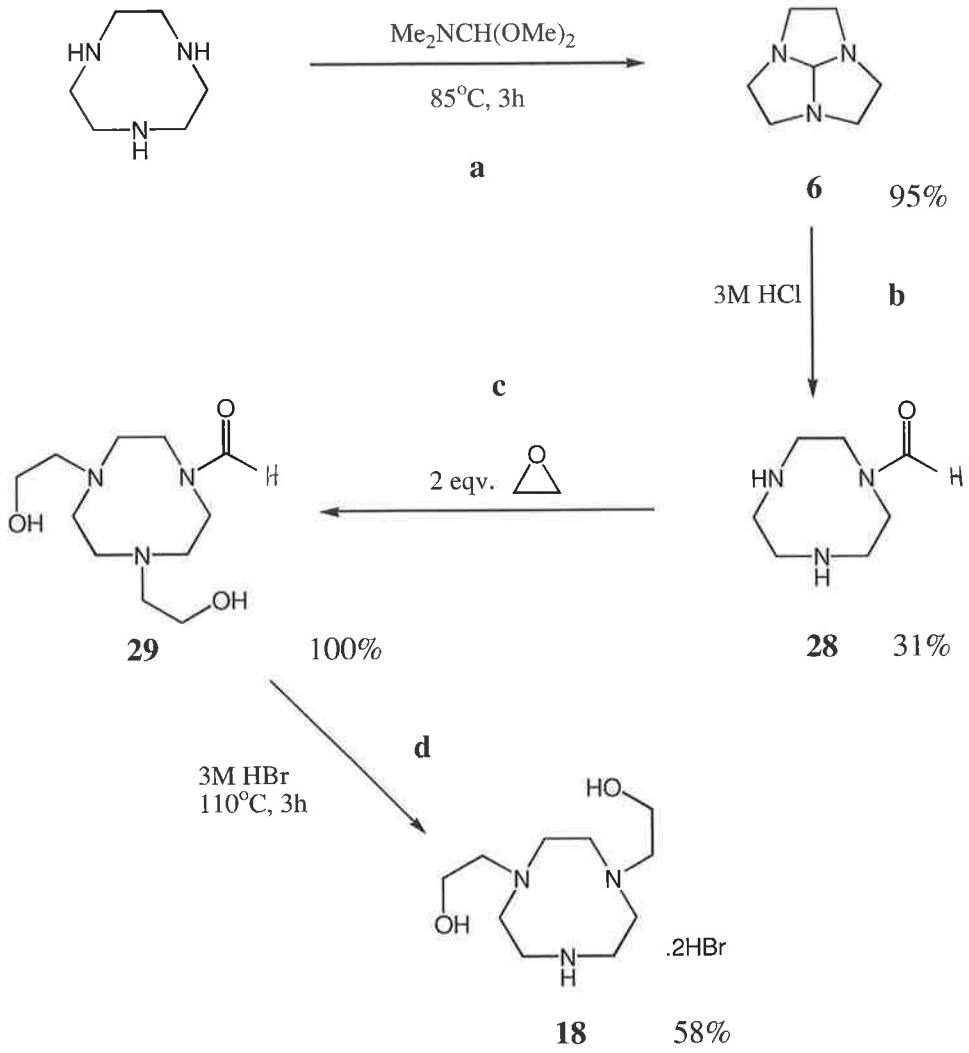

Scheme 20

Conversion of the bridged macrocycle **6** to the mono-formamide **28** was achieved by stirring the compound in aqueous 3M hydrochloric acid for 12 hours at room temperature. The pH of the reaction mixture was then adjusted with sodium hydroxide to pH 9 and the mono-formamide **28** was successively extracted into dichloromethane. Purification of the product by flash chromatography gave **28** as a white amorphous solid in 31% yield. The formamide species **28** was characterised by a loss of symmetry exhibiting six ring carbon resonances and a single carbonyl resonance in the ^{13}C NMR spectrum. The low yield was primarily due to the high water solubility of **28**, which made it difficult to extract from the aqueous reaction mixture. The extraction process was helped somewhat by saturating the aqueous solution with sodium chloride before extracting with dichloromethane. Benzene extraction using a Dean-Stark apparatus was not appropriate in this situation as the refluxing conditions caused the formamide group to hydrolyse in the basic medium and give [9]aneN_3.

Attachment of the two hydroxyethyl arms to the mono-formamide species was achieved by reacting **28** with two equivalents of ethylene oxide in ethanol over three days. This gave the di-alkylated species **29** in quantitative yield as a viscous oil, Scheme 20c. Due to a lack of symmetry in **29**, ten ethylene carbon resonances were observed in the ^{13}C NMR spectrum corresponding to six ring and four pendant arm carbons. Identification of each NMR resonance was achieved by a combination of correlation spectroscopy (COSY), heteronuclear single quantum coherence (HSQC) and heteronuclear multiple bond correlation (HMBC) spectral analyses. The HSQC spectrum of **29** is shown in Figure 20. Symmetry within **29** is prevented by the presence of the asymmetric formamide functional group. The proton and oxygen atoms of the formamide group lie in the same plane as the ring and create unique environments on either side of the functional group. As a consequence, there is no symmetry within the molecule and each proton and carbon atom displays a unique NMR resonance. This is most clearly shown in the HSQC spectrum where the two pendant arms are seen to be nonequivalent, each displaying two triplet resonances in the ^{1}H NMR portion and two unique carbon resonances in the ^{13}C NMR portion, Figure 20.

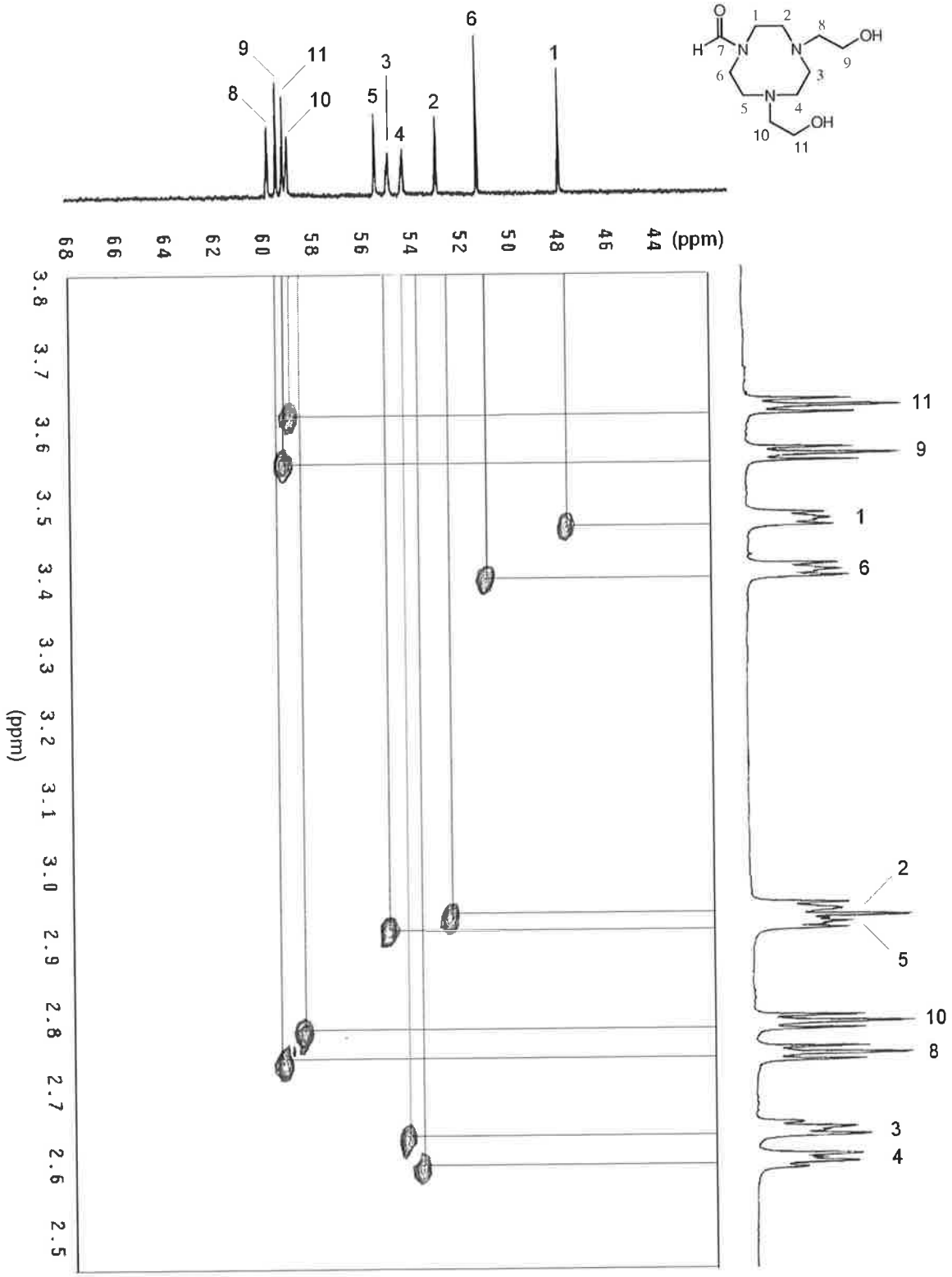

Figure 20. The 600 MHz heteronuclear single quantum coherence (HSQC) spectrum of **29** in $CDCl_3$ showing the ethylene resonances.

The two-arm ligand was finally generated by hydrolysing the formamide group of **29** with 3M hydrobromic acid under refluxing conditions. Recrystallisation of the product from ethanol then gave the di-alkylated species **18** as light brown needles in 58% yield, Scheme 20d.

The product was deemed identical to that obtained from direct alkylation of [9]aneN_3 (Scheme 19, page 41), possessing an identical melting point and exhibiting similar NMR spectra. Although the overall yield from [9]aneN_3 was only 17%, this method was the more reliable.

2.3.3. Synthesis of Hydroxyethyl-1,4,7-triazacyclononane, Hec[9]

Recently, a general synthesis of [9]aneN_3 substituted by hydroxyethyl pendant arms at two of the nitrogens was published.[79] Although there are isolated examples of [9]aneN_3 substituted with only one hydroxyethyl pendant arm,[82,61] there remains no general synthetic method for attaching a range of single hydroxyalkyl pendant arms to [9]aneN_3.

The most successful method of attaching mono-pendant arms to [9]aneN_3 has involved reaction of the bridged macrocycle **6** with acyl bromides followed by hydrolysis under acidic or basic reflux conditions, Scheme 6, page 11. It was initially envisaged that this method could be used to generate [9]aneN_3 substituted with a single acetic acid group, which could then be reduced using borane-tetrahydrofuran to give the hydroxyethyl derivative, hec[9] **17**, Scheme 21.

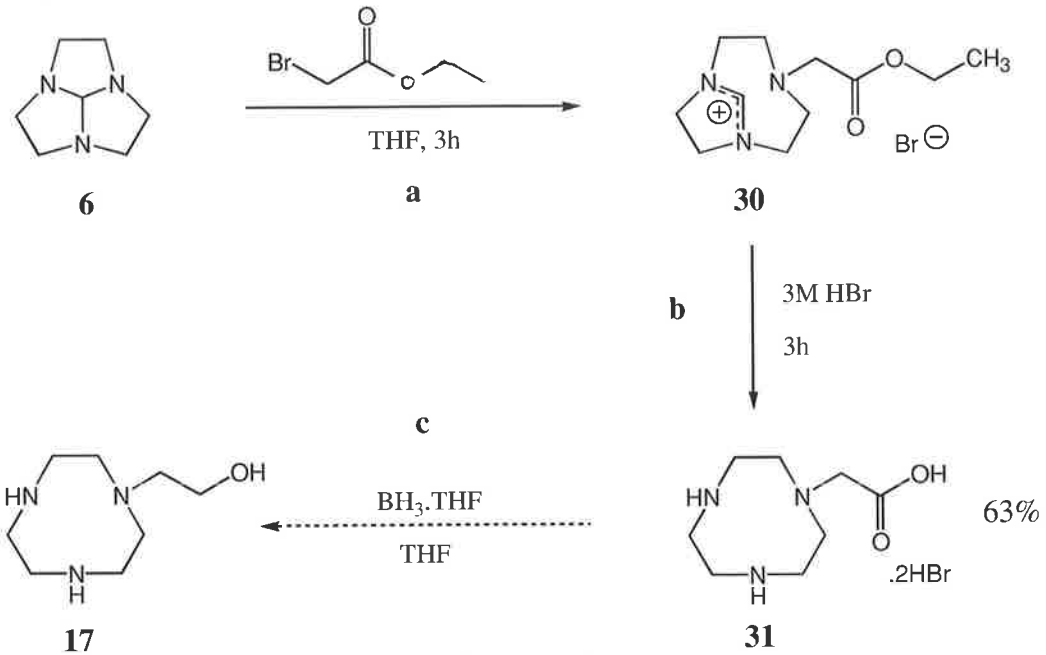

Scheme 21

In an attempt to generate the acid functionalised species, the bridged macrocycle **6** was reacted with ethyl bromoacetate in THF. Upon adding the bromo-alkylating agent, a white precipitate was generated instantaneously corresponding to the intermediate **30**, Scheme 21a. After stirring for three hours the precipitate was collected and hydrolysed with aqueous 3M hydrobromic acid. The product was then recrystallised from water and ethanol to afford **31** as white crystals in 63% yield, Scheme 21b. The product was characterised by the appearance of four ethylene carbon resonances and a single carbonyl resonance in the ^{13}C NMR spectrum, and a carbonyl absorbance at 1718 cm^{-1} in the infrared spectrum. An elemental analysis showed it to be the dihydrobromide salt.

Despite obtaining the carboxylic acid **31** in good yield, the subsequent reduction step proved more difficult. Isolation of the neutral species and its application in the reduction reaction was complicated by the zwitterion nature of the molecule. Anion exchange chromatography proved unsuitable for generating the neutral form of **31** as the carboxylate anion would adhere to the column. Regeneration of the column with aqueous sodium hydroxide released the ligand, but it was then converted to the anionic form **32**. Conversion to the neutral form therefore required the addition of sodium hydroxide to the dihydrobromide salt until pH 9 followed by removal of water by benzene extraction. An additional problem was encountered in that the presence of both acid and amine functionality in the ligand allows contributions from two zwitterion species, which greatly decreased its solubility in THF, Scheme 22.

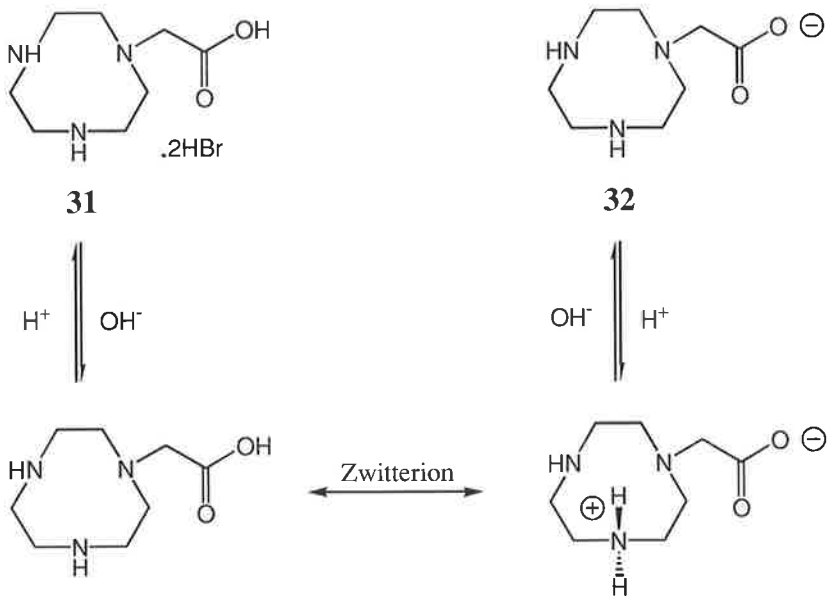

Scheme 22

Since polar-aprotic solvents do support charged species, the neutralised ligand proved insoluble in both THF and ether and was consequently unsuitable for reduction with borane-tetrahydrofuran.

An alternative method of synthesising hec[9] is by the direct alkylation of the bridged macrocycle **6** with bromoethanol. Schröder had previously attempted this reaction without success citing complications due to loss of HBr from bromoethanol under the basic conditions.[82] As a result, the bromoethanol was protected as a benzyl ether before reacting with **6**. Following acid hydrolysis and removal of the benzyl group by hydrogenolysis, the single arm species **17** was isolated as the free ligand.[82] Schröder's explanation, however, for the failed reaction between the bridged macrocycle **6** and bromoethanol seems unconvincing. It seems more likely that the alcohol group would increase the solubility of the charged intermediate and reduce the amount of precipitation.

To clarify the situation, the reaction was repeated using THF instead of ether. After adding bromoethanol to **6**, the reaction mixture was allowed to stir for seven days at room temperature. Removal of the solvent gave a sticky viscous oil, which was then refluxed in water to hydrolyse the bridging ring. The product was passed through an anion exchange column to remove hydrogenbromide and the mono-alkylated formyl derivative **33** was isolated in 57% yield, Scheme 23a.

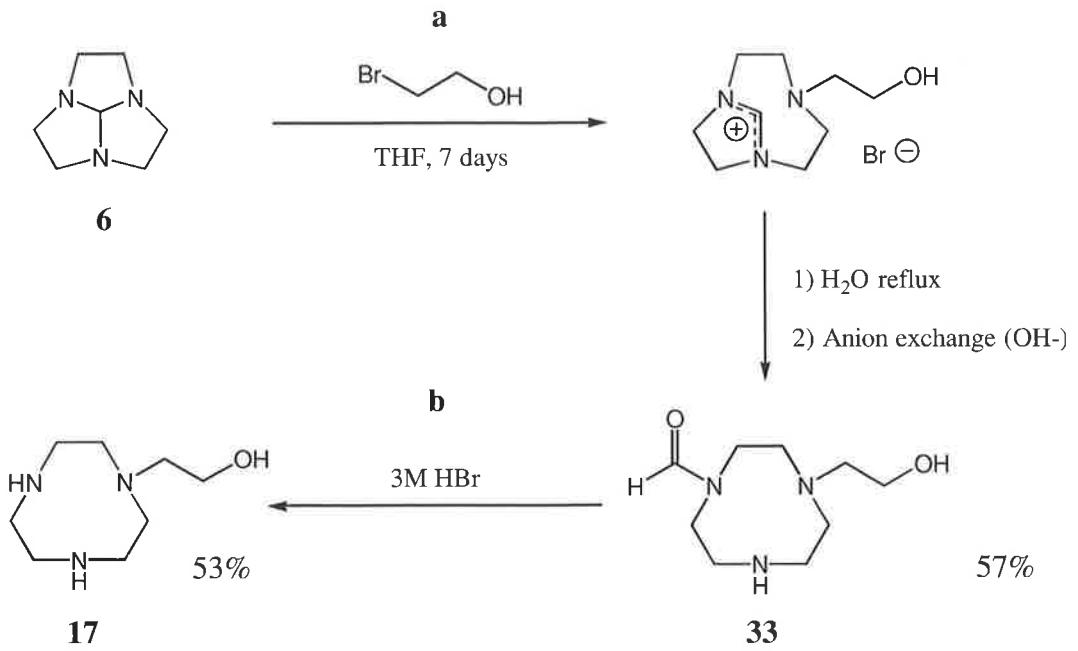

Scheme 23

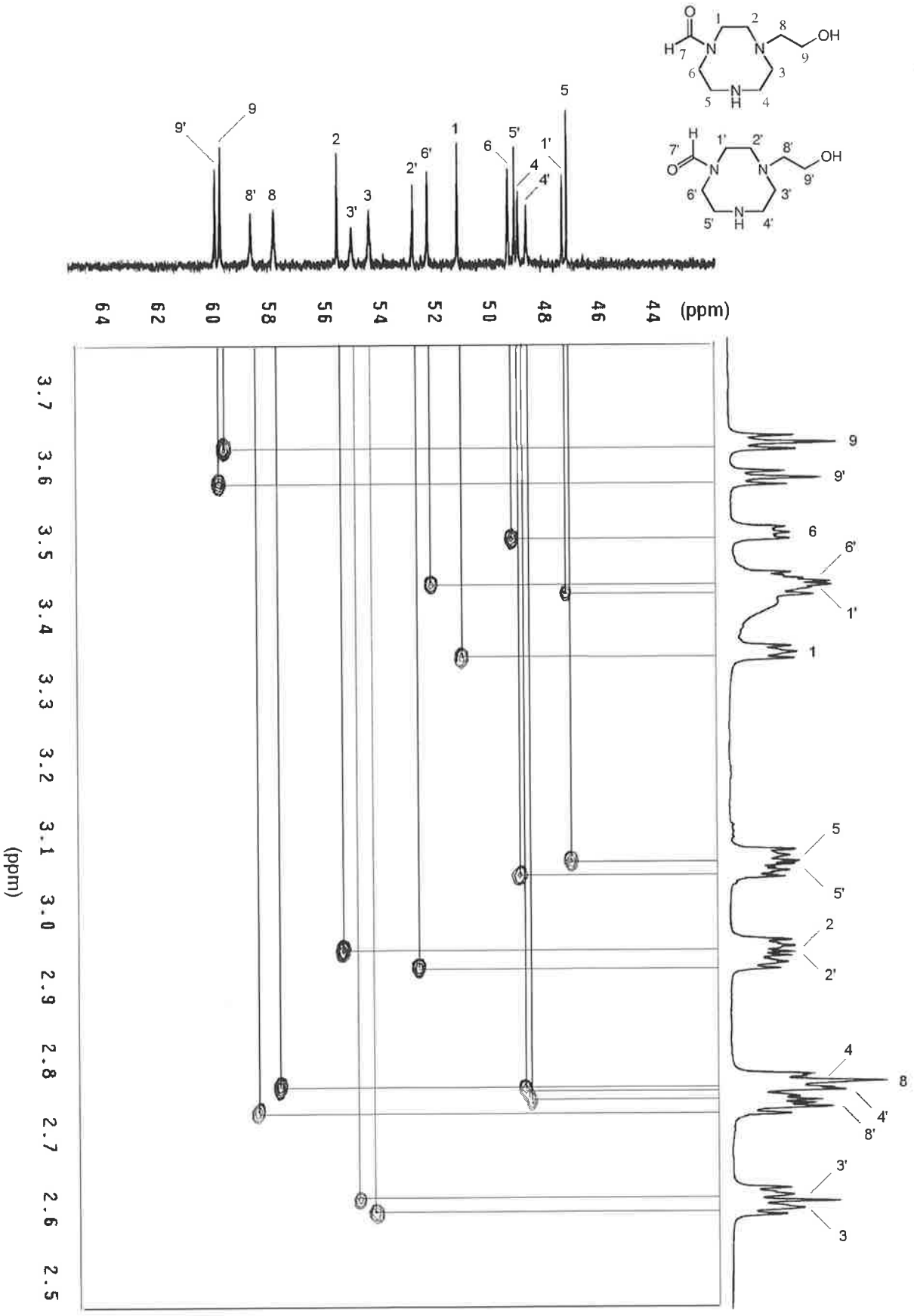

Figure 21. 600 MHz heteronuclear single quantum coherence (HSQC) spectrum of **33** in $CDCl_3$ showing the ethylene resonances.

Analysis of **33** by NMR spectroscopy revealed complex spectra with a large number of resonances. The ^{13}C NMR spectrum of **33** in $CDCl_3$ exhibits 16 aliphatic (12 ring and four arm) and two carbonyl resonances while the ^{1}H NMR spectrum showed a doubling of the expected number of proton resonances. The *O*-ethylene arm carbon is split into two unique resonances and clearly gives two unique triplets at δ 3.58 and δ 3.63 ppm in the ^{1}H NMR spectrum, Figure 21. This number of observed resonances is consistent with **33** existing in two unique isomeric forms. Restricted rotation about the C-N formamide bond causes the two isomers to interconvert slowly on the NMR time scale. As a consequence, each isomer displays a unique set of resonances in the NMR spectra.

The single arm ligand, hec[9], was formed by hydrolysing the formamide group from **33** with 3M hydrobromic acid. Recrystallisation of the product from water and ethanol gave hec[9] **17** as light brown crystals in 53% yield, Scheme 23b. The ^{13}C NMR spectrum of **17** was consistent with the literature values of the free ligand, displaying three ring carbon resonances and two smaller arm carbon resonances in the ^{13}C NMR spectrum. The identity of **17** was further confirmed by high-resolution mass spectrometry and an accurate elemental analysis that showed the product to exist as the dihydrobromide salt.

Although this method was an effective pathway to the isolation of hec[9], the yield was rather poor and it does not represent a general method for producing other single arm derivatives. In order to synthesise other hydroxyalkyl derivatives of hec[9], modified bromo-alcohol agents are needed. This becomes increasingly complicated when chiral substituents with specific stereochemistry are required.

An efficient method of attaching a range of hydroxyalkyl pendant arms to [9]aneN_3 is through reaction with substituted epoxides. This has led to a large range of tri-substituted ligands, but there remains no general synthetic method for attaching a single hydroxyalkyl arm to [9]aneN_3 using epoxides. To successfully mono-alkylate [9]aneN_3 with epoxides, a suitably di-protected [9]aneN_3 intermediate was needed. Existing protection methods involve either selective detosylation[65,66] or the use of bulky carbamate groups[68] that decrease the reactivity of the third amine donor towards ordinary alkylation. Reaction of bis-Boc protected [9]aneN_3 **2** with ethylene oxide in both ethanol and DMF over several days led to no significant reaction as detected by TLC analysis, Scheme 24a. Such di-protected species are

usually unsuitable for reaction with epoxides and generally require activated alkylating agents such as organo-triflates or acyl-bromide compounds. The reaction of epoxide and the bridged macrocycle **6**, as a pathway to mono-alkylated [9]aneN$_3$, is also inappropriate with the reaction in ethanol giving a mixture of products as shown by TLC and NMR analyses, Scheme 24b.

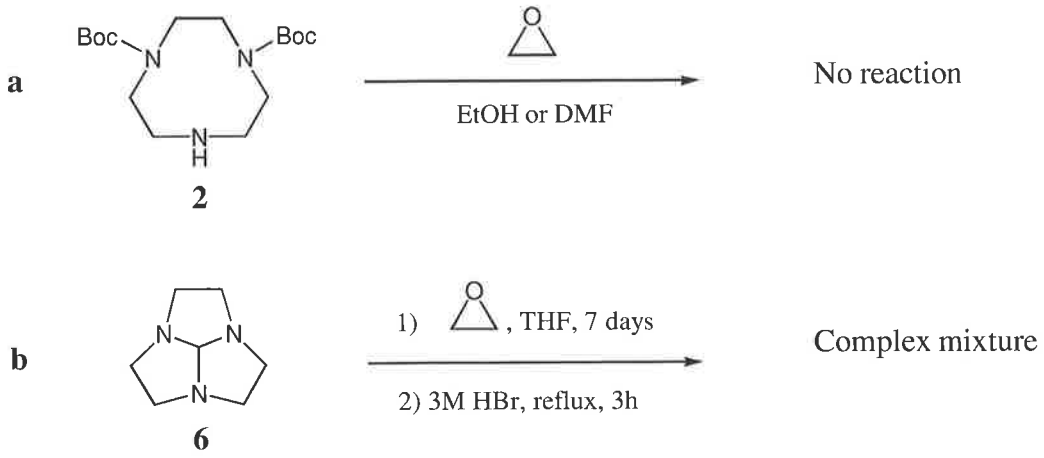

Scheme 24

A more efficient di-protected species would require smaller protecting groups, which would impose less steric influence over the third amine donor. One possible intermediate is the diamide **34** where two of the nitrogens are protected as internal amide groups, Scheme 25. The reduced reactivity of the two amide nitrogen groups over the single amine donor, would allow preferential alkylation at only one nitrogen atom. The amide functional groups could later be reduced with borane-tetrahydrofuran to afford the mono-alkylated product.

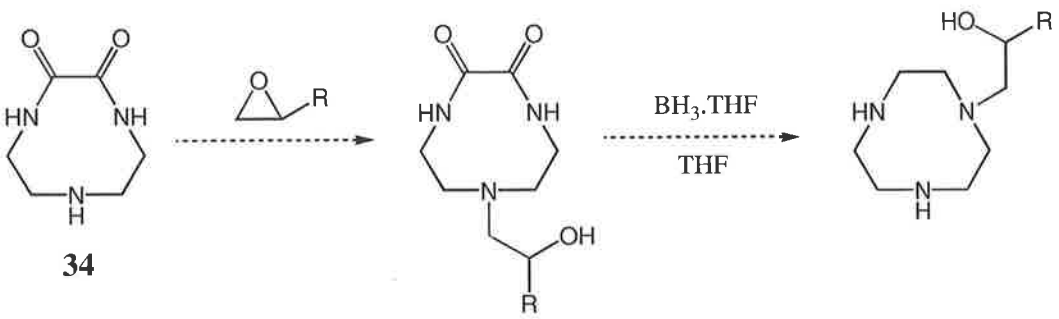

Scheme 25

This method of protection has been used successfully for larger aza macrocycles to produce a range of selectively alkylated products.[71] Introduction of the amide functional groups into larger macrocycle ligands is usually achieved during the ring cyclisation step under high dilution reaction conditions.

Synthesis of the di-amide species **34** was attempted by reacting oxalyl chloride and diethylenetriamine together under high dilution conditions in dichloromethane. The reaction proved extremely vigorous generating hydrochloride gas and producing an instant precipitate of polymeric material, Scheme 26a. The oxalyl chloride proved too reactive, providing little discrimination between the formation of cyclic material and linear polymer.

In a second attempt, oxalyl chloride was exchanged with the less reactive diethyl oxalate. The two reactants were combined under high dilution conditions into refluxing ethanol and allowed to reflux for five days, Scheme 26b.

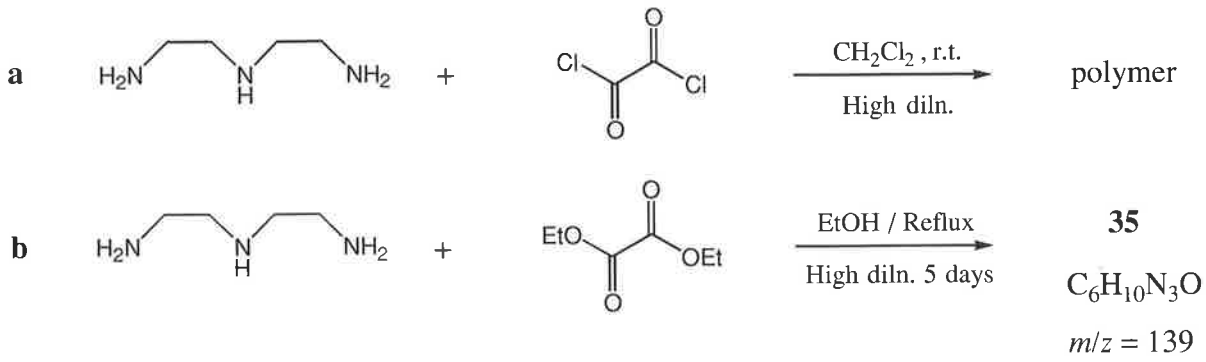

Scheme 26

A small amount of polymeric material was still produced, giving an insoluble white material, but to a much lesser degree than experienced with oxalyl chloride. The polymeric material was filtered from the reaction mixture and the filtrate reduced in volume and purified by flash column chromatography to give a white crystalline solid, **35**, in 44% yield.

The identity of **35**, however, remained unclear as its physical and spectral properties were inconsistent with those expected for diamide **34**. Rather than displaying one carbonyl absorbance in the infrared spectrum, the product displayed two absorbances at 1680 and 1620 cm^{-1}, which suggested the presence of both a carbonyl and an alkene group in the molecule. Furthermore, the mass spectrum revealed a base peak at *m/z* 139, which was 18 mass units below that of the diamide **34**. Also, the elemental analysis suggested a product that

differed from **34** by the loss of a water molecule. The identity of the product was finally established by x-ray crystallography to be the bicyclic ring species **35**, Figure 22.

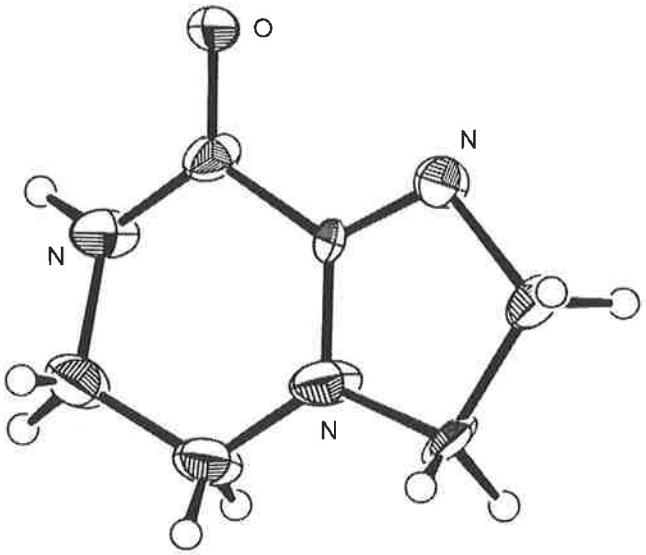

Figure 22. X-ray crystal structure of **35**.

It became evident that the diamide species **34** had undergone further intramolecular cyclisation to form **35**. Under the refluxing conditions, the nine-membered diamide species had preferentially transformed to the thermodynamically more stable five- and six-membered bicyclic ring system by the loss of water, Scheme 27.

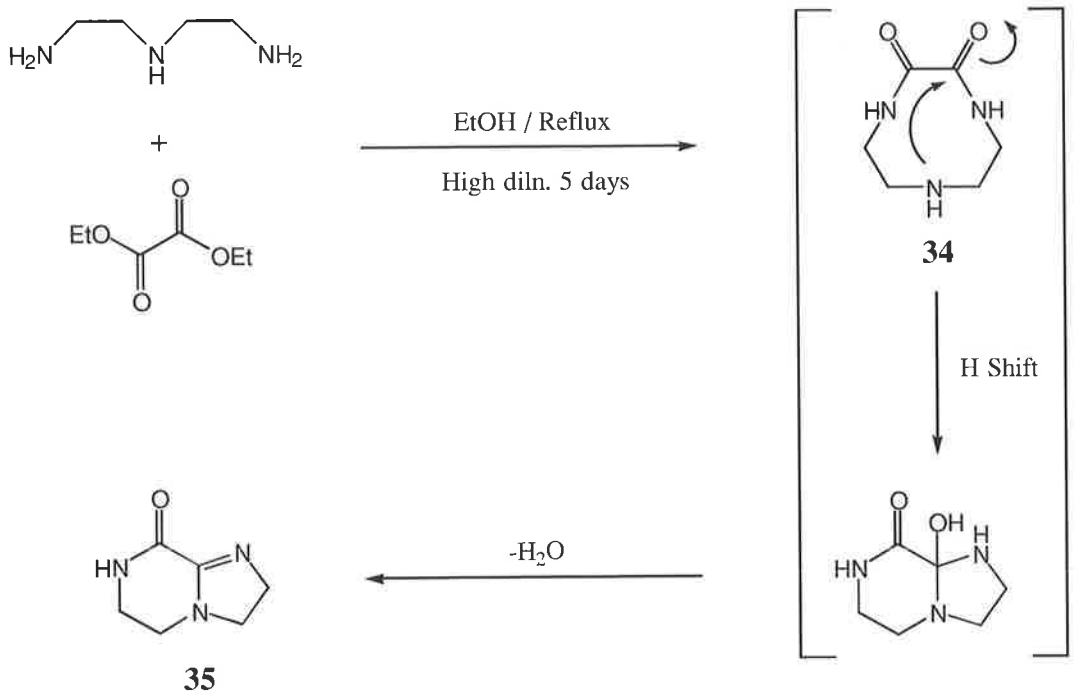

Scheme 27

The bicyclic species **35** has previously been reported in the patent literature as a ligand to selectively complex precious metals and precipitate them from an aqueous solution.[150] Unfortunately, the product was unsuitable for the alkylation procedure and further attempts to isolate the diamide species **34** were abandoned.

Having failed to introduce internal amide functional groups to [9]aneN$_3$, attention was then shifted to the introduction of external amide groups. As mentioned previously, most functional groups used to di-protect [9]aneN$_3$ tend to lower the reactivity of the third amine donor on steric grounds. It was therefore imperative that the amide functional groups remained relatively small. The reaction of the bridged macrocycle **6** with acyl bromides is a common method of achieving mono-alkylation of [9]aneN$_3$. Similarly, this method could also be used to attach a single amide protecting group to [9]aneN$_3$ by reacting it with acetyl bromide. If the charged intermediate were then subjected to aqueous hydrolysis, ring opening would introduce a formamide group to the second ring nitrogen, and give [9]aneN$_3$ substituted with two potential protecting groups.

In an attempt to synthesise such a di-protected species, the bridged macrocycle **6** was treated with one equivalent of acetyl bromide in THF. The charged intermediate **36** instantly precipitated as a white solid, which was collected and hydrolysed in refluxing water. The product was neutralised by anion exchange chromatography and the novel di-protected species **37** was obtained as a white solid in 89% yield, Scheme 28.

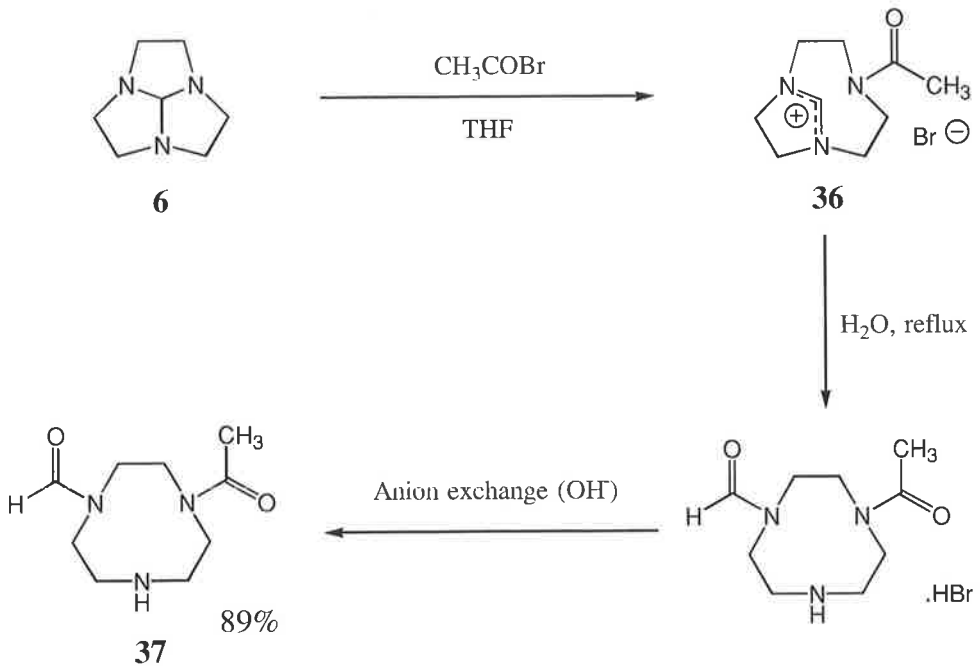

6 **36** **37**

Scheme 28

Although high resolution mass spectrometry of **37** and a single spot observed by TLC inferred a single compound, the NMR spectra of **37** were extremely complex suggesting the presence of numerous isomeric forms. The ^{13}C NMR spectrum of **37** in $CDCl_3$ showed 21 aliphatic resonances (three methyl, 18 ring), three formyl C=O resonances and three acetamide resonances as the major spectral components, Figure 23. The ^{1}H NMR spectrum, on the other hand, revealed three major methyl singlets and three major formyl singlets. Additional fourth methyl and fourth formyl singlets were also observed but were considerably lower in intensity. This number of observed resonances in both the ^{13}C and ^{1}H NMR spectra was consistent with **37** existing as three major and one minor isomeric form.

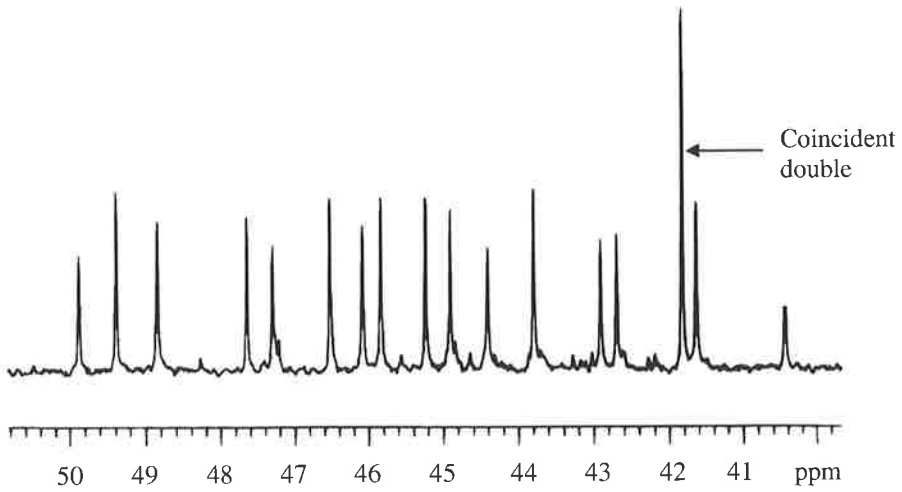

Figure 23. The 75.47 MHz ^{13}C NMR spectrum of **37** in $CDCl_3$ showing 17 major macrocyclic ring resonances. The resonance at δ 46.4 represents two coincidental signals and resolves into two separate resonances in $(CD_3)_2SO$. The base line resonances, which increase slightly in intensity in $(CD_3)_2SO$, arise from a fourth, less stable isomer.

Restricted rotation about the two C-N amide bonds cause **37** to exist in numerous isomeric forms which interconvert slowly on the NMR time scale.[151,149] Rotation about each amide group of **37** allows the possibility of four configurational isomers, where the amide oxygen atoms are directed in either a clockwise direction (**37a**), an anti-clockwise direction (**37b**), away from each other (**37c**) or towards one another (**37d**) as shown in Figure 24. Each isomer represents a unique configuration and would give individual resonances in the NMR spectra.

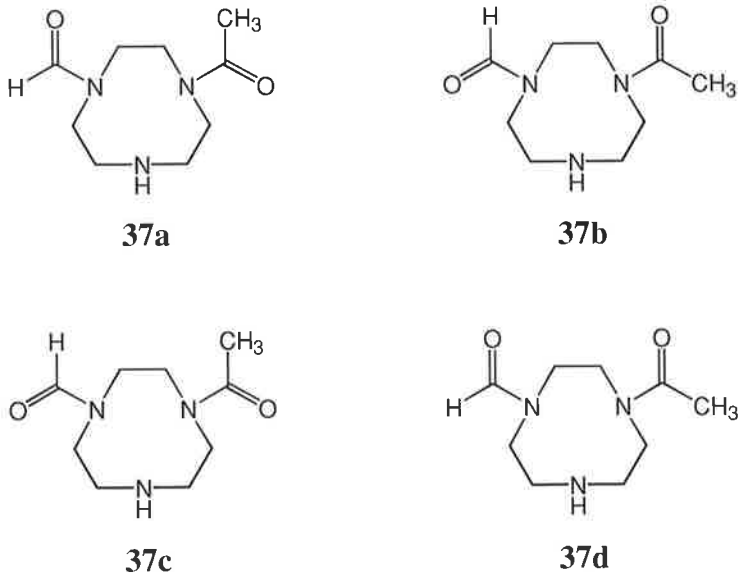

37a **37b**

37c **37d**

Figure 24. The four possible configurational isomers of **37** due to C-N amide bond rotation.

In an attempt to gain some insight into the relative stabilities of each isomer and to establish why only three predominate in the NMR spectra, *ab initio* calculations were performed on each isomer. An input structure representing each configuration was minimised using the Gaussian 94 programme[125] with the LanL2DZ basis set and the final selected geometries where then further minimised with the 6-31G(*) basis set. The aim of this exercise was to obtain the global minimised structures of each isomer and compare their relative energies. This task, however, soon became very large as it was found that, in addition to configurational isomerism, rotation of individual ring atoms contributed to a great number of possible molecular geometries, each leading to a local energy minimum on the potential energy surface.

To obtain an optimised structure for each isomer, numerous input structures with altered ring geometries were minimised to obtain the lowest possible geometry within each of the four isomer groups. Each input structure gave a unique energy minimum and a total of 18 geometries were minimised in an attempt to locate the four global minima, Figure 25. The lowest energy geometry within each of the four isomer groups was then selected and minimised further with the 6-31G(*) basis set to obtain the final minimum energy values. This approach was taken to reduce the overall computational time as minimisations with the 6-31G(*) basis set are computationally more expensive.

37a - Oxygen groups directed in a clockwise direction.

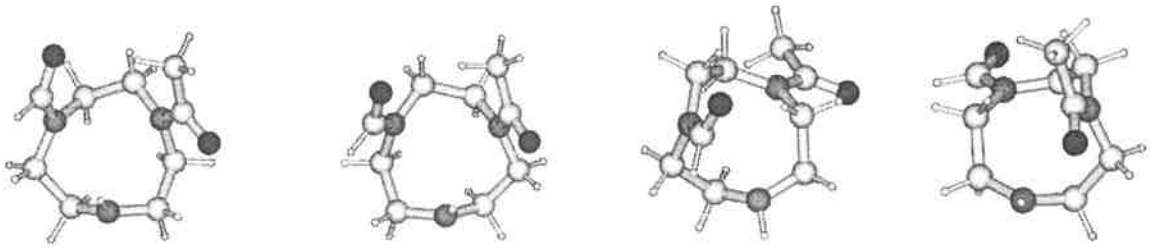

E = -663.575538 〈 E = -663.570057 〈 E = -663.568781 〈 E = -663.566602

37b - Oxygen groups directed in an anti-clockwise direction.

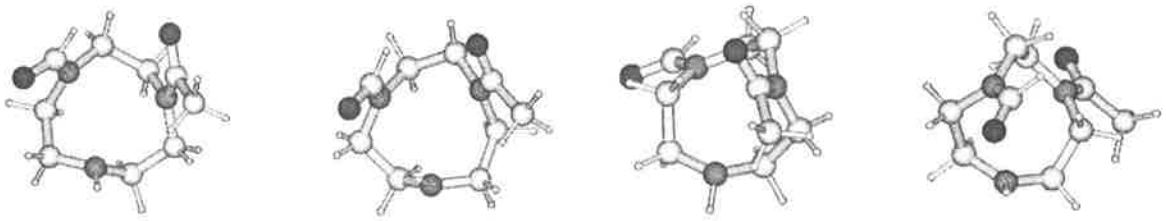

E = -663.576652 〈 E = -663.569361 〈 E = -663.567335 〈 E = -663.567048

37c - Oxygen atoms directed outward, away from each other.

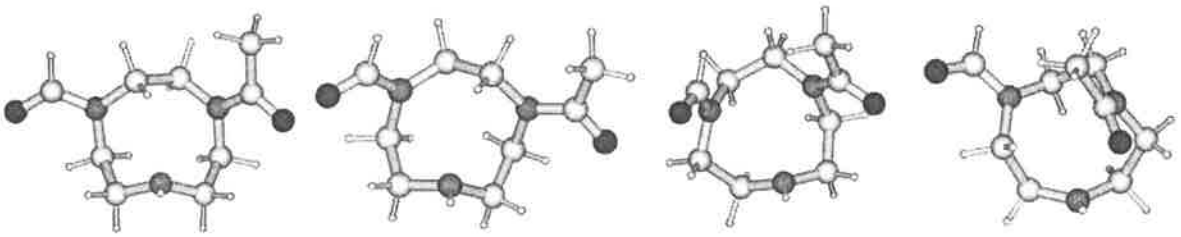

E = -663.572326 〈 E = -663.571111 〈 E = -663.569252 〈 E = -663.567982

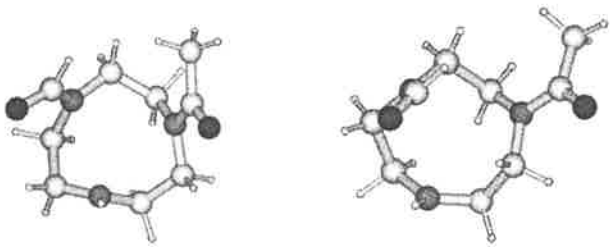

〈 E = -663.567583 〈 E = -663.567466

37d - Oxygen groups directed inward, towards each other.

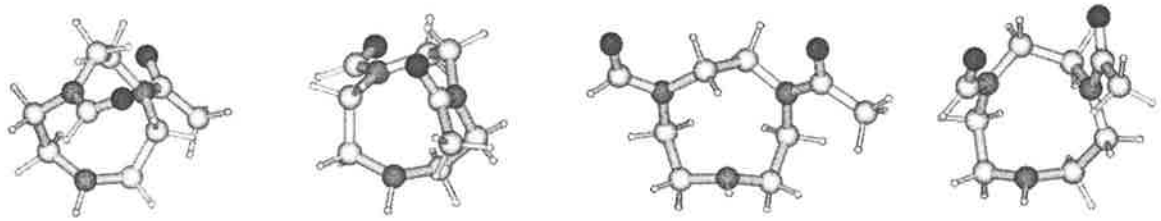

E = -663.569185 〈 E = -663.568724 〈 E = -663.568030 〈 E = -663.566974

Figure 25. Optimised geometries of **37** determined by Gaussian 94 using the LanL2DZ basis set. Energies are shown below each structure and are quoted in Hartrees.

The final minimised structures suggest the lowest energy conformations of each isomer to be those shown in Figure 26 where the energies of **37a**, **37b**, **37c** and **37d** are -663.783743, -663.783645, -663.779449 and -663.775964 Hartrees respectively in the gas phase (1 Hartree = 2625.5 kJ mol^{-1}). The isomers **37a** and **37b**, where the amide dipoles are aligned, represent the most stable configurations. The least stable isomer is **37d** where the oxygen atoms of each amide group are orientated towards one another. Due to the large number of local energy minima within each isomer group, it is uncertain whether these geometries represent true global minima for each isomer. Further modelling, however, was deemed unnecessary as the differences in potential energy between each new geometry within a group were becoming increasing small and considered negligible compared with the relative energy differences between each isomer group.

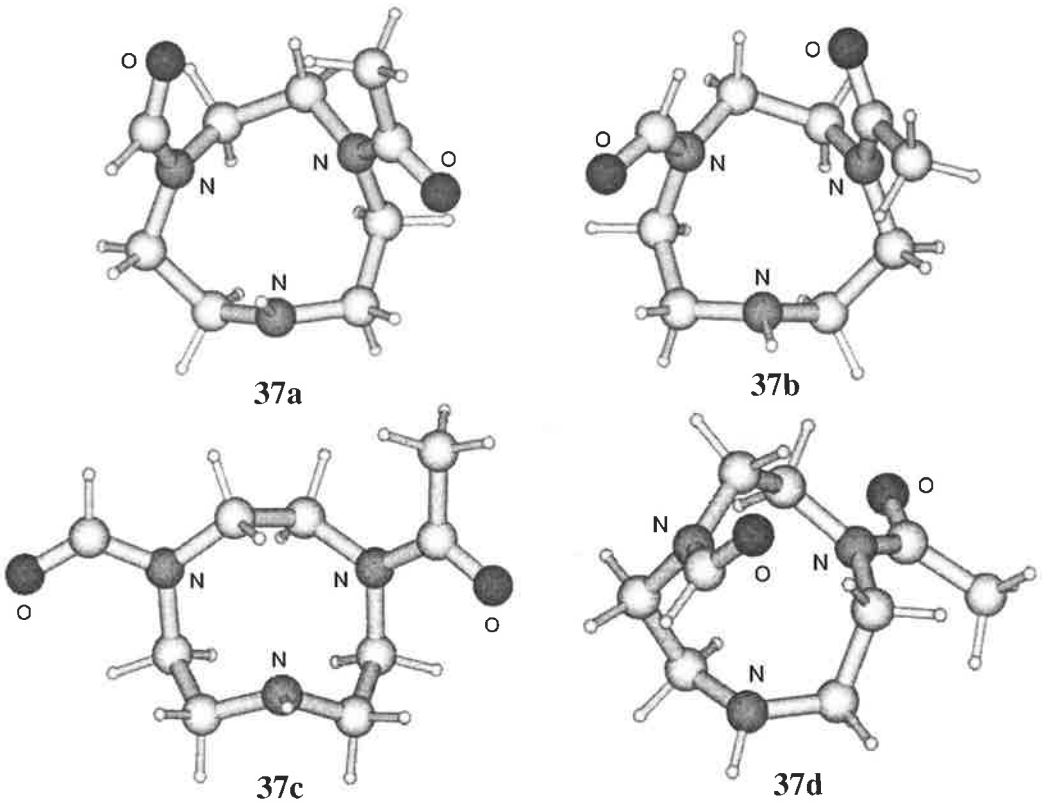

Figure 26. The four most stable isomers of **37** obtained from *ab initio* calculations.

While these calculations generate the probable isomeric structures in the gas phase, they are not necessarily a guide to the relative stabilities in solution. It is known that tertiary amides form intermolecular dipole-dipole aggregates in solution, which may account for the qualitatively similar populations of the three dominant isomers in the NMR spectra.[151]

In an attempt to synthesise mono-alkylated [9]aneN$_3$, the di-protected species **37** was treated with ethylene oxide over three days using the standard procedure. This gave a viscous oil with a reduced R_f value on alumina gel TLC compared with **37**. Analysis of the product by NMR spectroscopy revealed extremely complex spectra. In addition to the ring carbon resonances there was a multitude of new resonances representing the arm carbons for each configurational isomer. The large number of resonances, all with varying intensities, prevented a concise interpretation of the spectra, however, high resolution mass spectrometry suggested the alkylated product had been formed.

Due to the complexity of the NMR spectra, the product could not be fully identified. It was therefore necessary to proceed with the deprotection step and analyse the final product. The alkylated product was treated with aqueous 3M hydrobromic acid under refluxing conditions for three hours to give a light brown solid. This was then recrystallised from water and ethanol to give the dihydrobromide salt of hec[9] **17** as small crystals in an overall yield of 75% from **37**, Scheme 29a. The spectral and physical data for **17** were identical to those obtained from the previous methods. This procedure, however, offered the highest yield of mono-alkylated product and gave good reproducibility.

The reaction procedure was repeated using (-)-propylene oxide and (+)-glycidol to test the generality of **37** with substituted epoxides. Reaction of **37** with both epoxides under the same conditions gave the two novel single arm species **38** and **39** in 74% and 82 % yield, respectively, Scheme 29b-c. The methyl substituted ligand **38** was distinguished from hec[9] by the presence of the methyl carbon resonances at δ 22.5 ppm in the ^{13}C NMR spectrum and a clearly defined doublet (d) at δ 1.14 ppm in the ^{1}H NMR spectrum. The di-alcohol ligand **39** was identified by the two hydroxy carbon resonances at δ 66.2 and δ 70.9 ppm for the primary and secondary alcohol carbons, respectively, and a highly distinctive dddd resonance at δ 3.97 in the ^{1}H NMR for the proton adjacent to the secondary alcohol group.

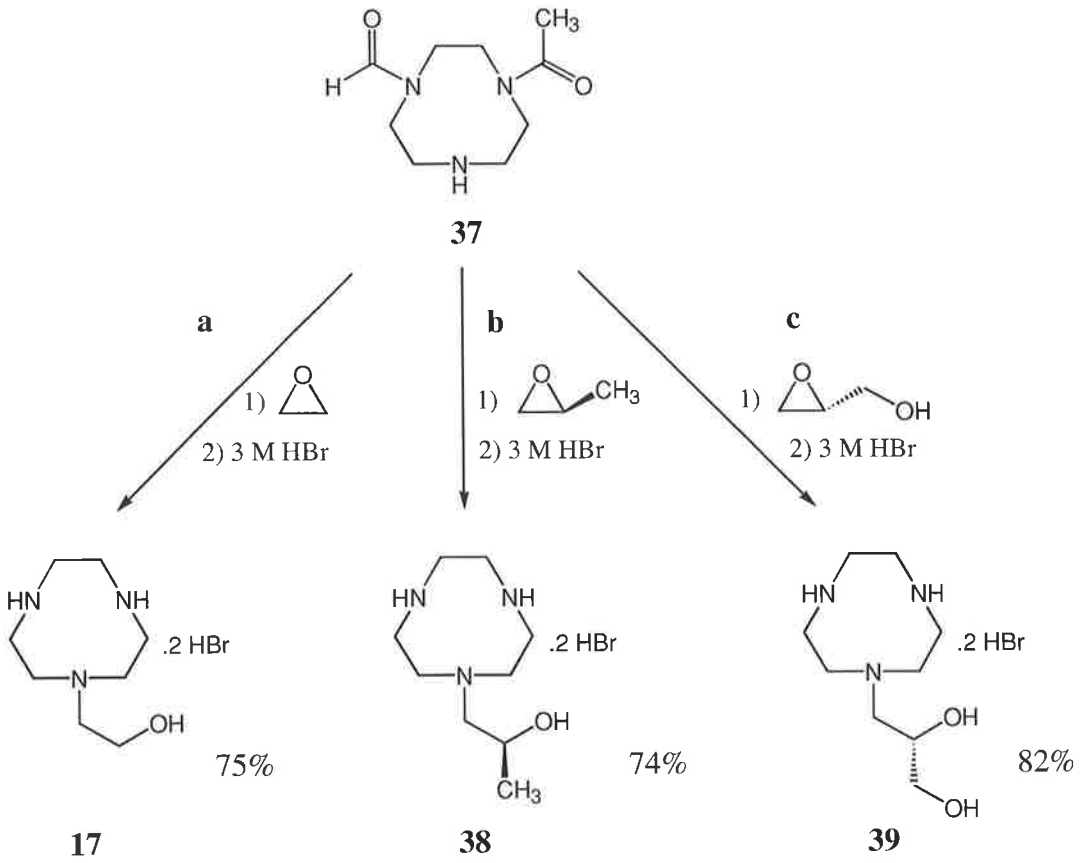

Scheme 29

This represents the first general method for producing mono-functionalised [9]aneN$_3$ derivatives with small hydroxyalkyl pendant arms. Apart from allowing selective mono-alkylation of [9]aneN$_3$, it also allows the opportunity to attach stereospecific functional groups by simply using enantiometrically pure substituted epoxides.

2.4. Summary

The three target ligands, hec[9], bhec[9] and thec[9], representing [9]aneN$_3$ substituted with one, two and three pendant arms, respectively, have been successfully isolated using various synthetic procedures. The macrocyclic ligand [9]aneN$_3$ was synthesised in six steps in 33% yield through modification of literature procedures.[2,144,145] Functionalisation of [9]aneN$_3$ with hydroxyethyl pendant arms was generally achieved with ethylene oxide with a suitable

macrocyclic derivative and the three target ligands were isolated in moderate to good yield from [9]aneN$_3$.

The three-arm ligand, thec[9], was synthesised by two different literature methods.[44,45] Direct alkylation of [9]aneN$_3$ with ethylene oxide over three days gave thec[9] as the free ligand in quantitative yield, Scheme 17. Thec[9] was also isolated as a sodium bromide complex in 63% yield by initial reaction of [9]aneN$_3$.3HBr with sodium ethoxide followed by *in situ* reaction with ethylene oxide. When an excess of ethylene oxide was used, over alkylation gave the tetrakis compound **27** as an impurity, Scheme 18.

The novel two-arm ligand, bhec[9], was synthesised in two different ways. The first method involved treatment of [9]aneN$_3$.3HBr with sodium ethoxide followed by *in situ* reaction with ethylene oxide. Following acidification with hydrobromic acid, bhec[9] was isolated as the dihydrobromide salt in 37% yield, Scheme 19. The second method involved a four-step synthesis whereby [9]aneN$_3$ was first converted to the bridged macrocycle **6** and then hydrolysed to give the mono-protected formamide species **28**. Reaction of **28** with ethylene oxide followed by acid hydrolysis of the formamide functional group then gave bhec[9] as the dihydrobromide salt in 17% overall yield from [9]aneN$_3$, Scheme 20.

Despite testing numerous unsuccessful methods, two unique synthetic procedures for isolating the one-arm ligand, hec[9], have been established. In the first instance, [9]aneN$_3$ was converted to the bridged macrocycle **6** and treated with bromoethanol in THF for one week. Following acid hydrolysis, hec[9] was isolated as the dihydrobromide salt in 29% overall yield, Scheme 23. An alternative method has also been devised whereby the bridged macrocycle **6** is converted to the novel di-protected species **37** by reaction with acetyl bromide in THF followed by aqueous hydrolysis, Scheme 28. Treatment of **37** with ethylene oxide followed by acid hydrolysis then gave hec[9] as the dihydrobromide salt in 61% yield from [9]aneN$_3$. Similarly, two other single arm derivative **38** and **39** were isolated in 63% and 71% yields, respectively, using the substituted epoxides propylene oxide and glycidol, Scheme 29. This method represents the first general procedure for attaching a range of single hydroxyalkyl arms to [9]aneN$_3$.

Chapter 3. Equilibrium Studies

3.1. Introduction

The acid-base properties and metal binding affinities of macrocyclic ligands provide essential information about their coordination abilities and their effectiveness in various chemical and biochemical environments. Such information is generally gained by measuring the equilibrium constants of the ligand system in an appropriate chemical environment. An equilibrium constant is a quotient involving the concentrations or activities of the reacting species in solution at equilibrium. Its value is directly related to the Gibbs free energies of both products and reactants in their standard states and hence is a measure of the reactivities of the reactants and products.[152]

An aza macrocyclic ligand can be considered a polyprotic base in aqueous solution and will exist as an equilibrium mixture of its free and protonated forms. The protonation constant, K_a, of this equilibrium is represented in equation 3.1,

$$H_{n-1}\mathbf{L} + H^+ \rightleftharpoons H_n\mathbf{L}^+ \qquad K_{an} = \frac{[H_n\mathbf{L}^+]}{[H_{n-1}\mathbf{L}][H^+]} \qquad (3.1)$$

where **L** is the macrocyclic ligand.

The pK_a is determined from the negative log of the protonation constant,

$$pK_{an} = -\log K_{an} \qquad (3.2)$$

When the ligand coordinates a metal ion, equilibrium is established between the free ligand, the metal ion and the resulting complex. The stability constant, K, of this association is represented in equation 3.3,

$$M^{n+} + L \rightleftharpoons M^{n+}L \qquad K = \frac{[M^{n+}L]}{[L][M^{n+}]} \qquad (3.3)$$

where M is the metal ion and ML is the complex.

The pK_a represents a quantitative measure of the basicity of the donor atoms within the ligand while the stability constant is a measure of a ligand's affinity for a metal ion in solution.

3.1.1. Methods of Determining Equilibrium Constants

There are many well-established methods for determining the equilibrium constants of polyaza macrocyclic ligands and their metal complexes. Some typical methods include potentiometry,[153,154,28,155,156,157] polarography,[158,5,8,9,11,159] nuclear magnetic resonance spectroscopy (NMR),[160,161,162] and ultraviolet spectroscopy.[163,164,165,166,167] Any technique that can determine the concentration of one species in solution can be used to calculate the concentration of all the remaining equilibrium species. The technique chosen for this study is potentiometry as it represents the most conventional method of determining equilibrium constants of polyaza macrocycles. Potentiometry involves the use of a highly accurate glass electrode that measures the change in hydrogen ion concentration during the titration of well defined acidic ligand solutions with a standard base in the absence and presence of a known concentration of metal ion.

Because the concentration of ionic solutes in solution parallels their activity, potentiometric titrations are performed at a constant ionic strength using a supporting electrolyte such as sodium nitrate ($NaNO_3$). The non-reacting electrolyte is usually present at a concentration approximately 100 times greater than the ionic species under investigation. Maintaining a constant ionic strength has the advantage that concentration quantities determined by potentiometry can be compared with quantities measured by other techniques such as absorbance spectroscopy.[152]

Potentiometry has its limitations. It has a general working range between pH 2-12 and is ideal for equilibrium systems where the degree of complex formation is sensitive to pH changes in this range. However, for systems where complex formation is complete at very

low pH or where equilibria occur above pH 12, other alternative methods such as electronic absorption spectrophotometry and NMR spectroscopy can be employed. These techniques are especially useful as they also provide microscopic information about the sites of protonation or metal coordination and can be used to follow pH dependent reactions.

In instances where the ligand is weakly basic and shows little or no affinity for hydrogen ions, substitution methods may be used. This involves the displacement of a metal ion from the ligand by another metal that has comparable affinity for the ligand.[168] The equilibrium reaction can be followed spectrophotometrically if the displaced metal ion or the new complex causes a considerable change in absorbance.[169]

An extension of this method is ligand-ligand displacement whereby a ligand-metal complex is converted to a more stable complex by another ligand that displays greater affinity for the metal ion. This method can be followed potentiometrically where the extent of conversion is measured by the amount of base needed to neutralise hydrogen ions displaced from the second ligand as it binds the metal ion.[170,171] A second metal ion that coordinates the displaced ligand but not the secondary ligand is also needed to help drive the equilibrium forward. The equilibrium between each species is represented in equation 3.4,

$$\mathbf{ML} + \mathrm{H}_n\mathbf{L}' + \mathrm{M}' \rightleftharpoons \mathbf{ML}' + \mathrm{M}'\mathbf{L} + n\mathrm{H} \qquad (3.4)$$

where **L** and **L′** are the opposing ligands and M′ is the secondary metal ion.

In order to calculate the stability constant of the complex under investigation, **ML**, the stability constants of the other two complexes, **ML′** and M′**L**, must already be known.

3.2. Acid Dissociation Constants of Hec[9], Bhec[9] and Thec[9]

3.2.1. Potentiometric Titrations

The pK_a's of the three pendant arm ligands hec[9] **17**, bhec[9] **18** and thec[9] **19** were determined by potentiometric titration[152] of aqueous solutions of protonated ligand against sodium hydroxide using a pH electrode to measure the change in electric potential (mV) with increased volume. The ligand solutions contained five equivalents of perchloric acid to ensure complete protonation of the macrocycle amine donors. The standard electrode potential (E_o) of the electrode and the ionisation constant of water (pK_w) for the titration were initially determined by titrating the sodium hydroxide base against perchloric acid. Titration of each ligand then gave a titration curve (Figure 27) that was fitted against a theoretical model generated by the programme Superquad[172] using the previously determined E_o and pK_w values.

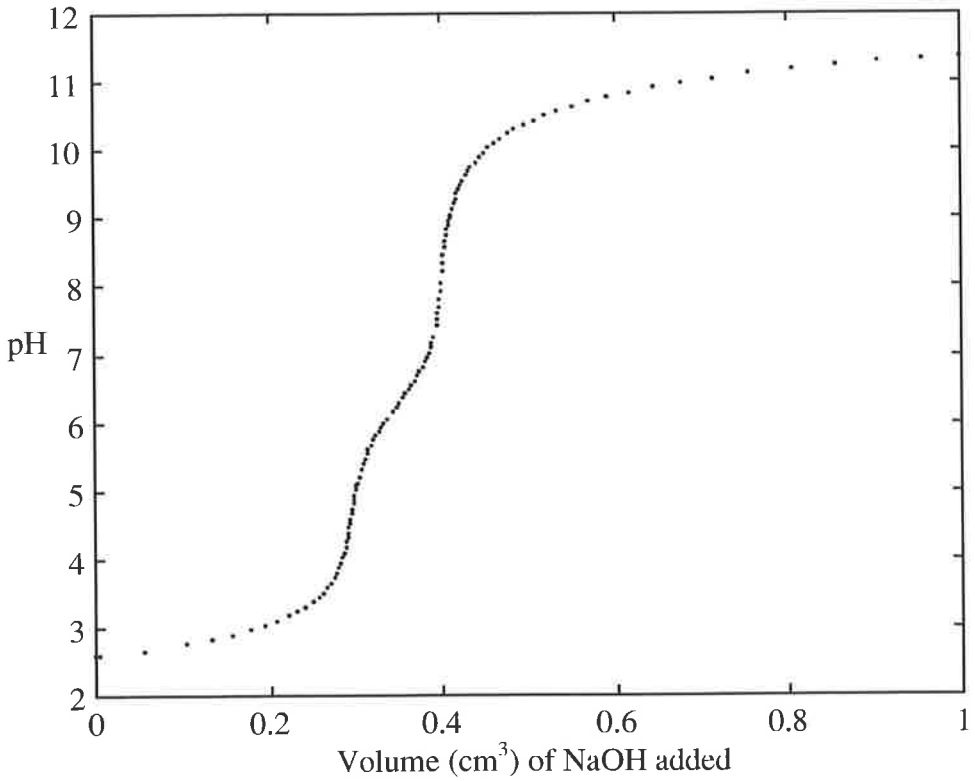

Figure 27. A typical titration curve of acidified ligand (10 cm^3) against NaOH at 298.2 (± 0.2) K. [hec[9]] = 0.001 mol dm^{-3}, [H^+] = 0.005 mol dm^{-3}, [NaOH] = 0.100 mol dm^{-3}, I = 0.10 ($NaNO_3$).

In the initial acidic solution, the three basic nitrogen donor groups of each ligand are fully protonated and are gradually deprotonated during titration with sodium hydroxide. The equilibrium amongst the deprotonated species may be represented as follows,

$$H_3\mathbf{L} \rightleftharpoons H_2\mathbf{L} + H^+ \qquad K_{a3} = \frac{[H_2\mathbf{L}][H^+]}{[H_3\mathbf{L}]} \qquad (3.5)$$

$$H_2\mathbf{L} \rightleftharpoons H\mathbf{L} + H^+ \qquad K_{a2} = \frac{[H\mathbf{L}][H^+]}{[H_2\mathbf{L}]} \qquad (3.6)$$

$$H\mathbf{L} \rightleftharpoons \mathbf{L} + H^+ \qquad K_{a1} = \frac{[\mathbf{L}][H^+]}{[H\mathbf{L}]} \qquad (3.7)$$

Where K_{a1}, K_{a2} and K_{a3} are the equilibrium constants and **L** is the triaza macrocyclic ligand.

It should be noted that the glass electrode measures the activity of the hydrogen ion, a_{H+}, but this usually approximates to its concentration, $[H^+]$.

The pK_a of each nitrogen donor was determined from the negative log of the equilibrium constant, K_a,

$$pK_{a1} = -\log K_{a1} \qquad (3.8)$$

$$pK_{a2} = -\log K_{a2} \qquad (3.9)$$

and

$$pK_{a3} = -\log K_{a3} \qquad (3.10)$$

Each ligand was titrated in triplicate and typical titration curves for thec[9] **19**, bhec[9] **18** and hec[9] **17** are shown in Figure 28. The pK_a values determined from the titration data are shown in Table 1 and include the pK_a values of [9]aneN$_3$ for comparison.

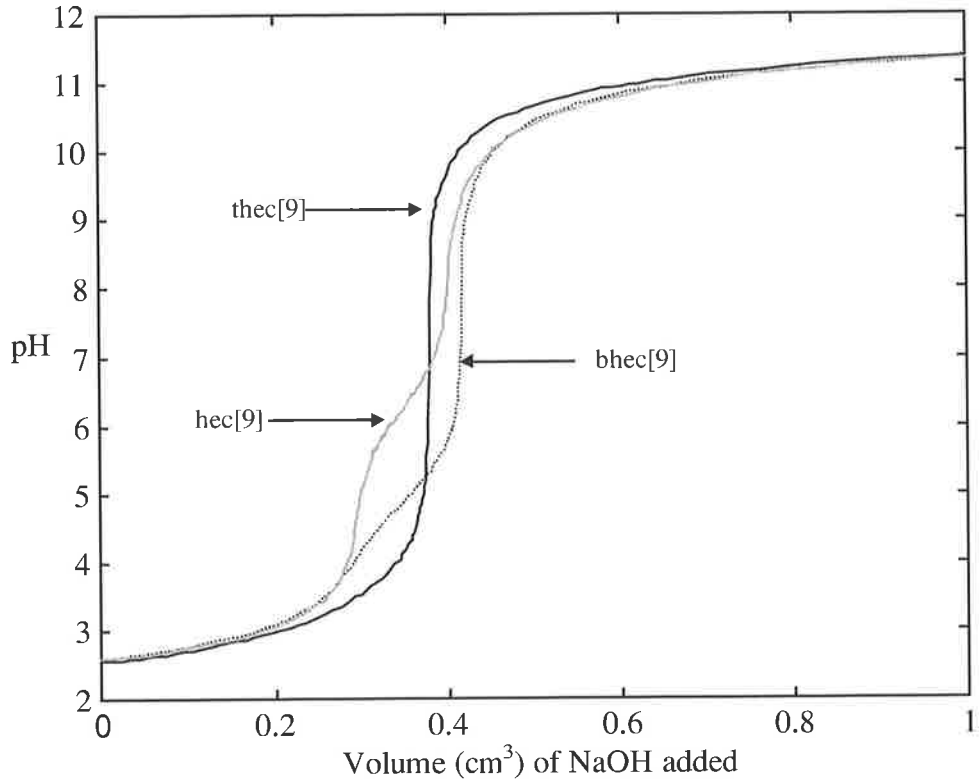

Figure 28. Typical titration curves of acidified ligand thec[9] **19**, bhec[9] **18** and hec[9] **17** against NaOH at 298.2 (± 0.2) K. [Ligand] = 0.001 mol dm^{-3}, $[H^+]$ = 0.005 mol dm^{-3}, [NaOH] = 0.100 mol dm^{-3}, I = 0.10 ($NaNO_3$).

The pK_a's of [9]aneN_3 and the pendant arm analogues, hec[9] **17**, bhec[9] **18** and thec[9] **19,** differ significantly in value. The hydroxyethyl pendant arms have a pronounced effect on the pK_a's of each amine donor and the difference in value of each protonation constant can be visualised in Figure 29.

When considering the first protonation constant, pK_{a1}, of each ligand, there is an unusual trend in the value of each protonation constant as the number of pendant arms increases. The first ligand in the series is [9]aneN_3 (pK_{a1} = 10.42)[28], which has no pendant arms. When a single hydroxyethyl arm is attached to the macrocyclic ligand, as represented by hec[9] (pK_{a1} = 10.24), the protonation constant decreases. However, when a second pendant arm is attached, bhec[9] (pK_{a1} = 11.02), the protonation constant is seen to rise and the addition of a third arm, thec[9] (pK_{a1} = 11.50), leads to an even greater increase in basicity.

Table 1. pK_a values of four [9]aneN_3 macrocyclic ligands determined by aqueous potentiometric titrations at 298 (± 0.2) K, I = 0.1 mol dm^{-3} ($NaNO_3$).

Ligand	pK_{a1}	pK_{a2}	pK_{a3}
[9]aneN_3	10.42[a]	6.82[a]	-
hec[9] **17**	10.24 (± 0.02)[b]	6.17 (± 0.02)[b]	1.97 (± 0.05)[b]
bhec[9] **18**	11.02 (± 0.05)[b]	4.97 (± 0.07[b]	2.25 (± 0.14)[b]
thec[9] **19**	11.50 (± 0.01)[b] 11.52 (± 0.04)[c]	3.79 (± 0.06)[b] 3.42 (± 0.02)[c]	- -

[a]Ref.[28], [b]This work, [c]Ref.[44]

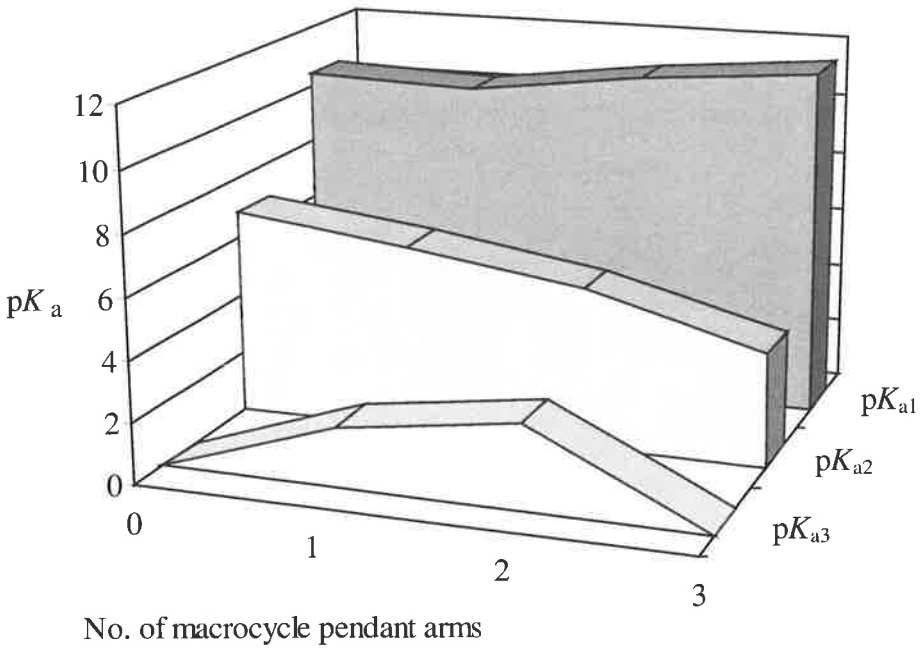

Figure 29. A comparison of the pK_a's of four [9]aneN_3 macrocyclic ligands with increasing numbers of hydroxyethyl pendant arms.

The difference in value of the pK_a's between each ligand can be explained by the dual stabilising and destabilising nature of the hydroxyethyl pendant arms. The hypothetical geometries of each ligand at varying degrees of protonation are shown in Figure 30 as a guide to explaining the dual effect the pendant arms have on amine basicity. The reduced protonation constant of hec[9] **17** compared with that of [9]aneN$_3$ is caused by the inductive withdrawing nature of the hydroxyethyl arm. This serves to lower the concentration of electrons in the nitrogen donor, which in turn, lowers its affinity towards protonation. As a consequence, the nitrogen donor is less basic than in [9]aneN$_3$ and displays a reduced protonation constant, Figure 30(c1).

When a second hydroxyethyl arm is attached to [9]aneN$_3$, in the case of bhec[9] **18**, the effect is quite different. Attachment of a second arm causes a substantial increase in the value of the first protonation constant compared with [9]aneN$_3$ and hec[9]. Despite the inductive withdrawing nature of the two pendant arms, the presence of an additional arm leads to a marked increase in amine basicity. The hydroxyethyl arms of bhec[9] may also assist protonation by directing the non-bonding electron pairs of each oxygen atom towards the centre of the macrocyclic ring. This has the effect of raising the electron density within the ring cavity and increases the ligand's affinity towards protonation, Figure 30(d1). This stabilisation process in bhec[9] appears to be absent in hec[9], as indicated by the reduced protonation constant. It is possible that the ring of hec[9] becomes slightly distorted upon protonation, such that the pendant arm is directed away from the ring centre. In this case, the pendant arm oxygen is unable to direct its lone pair electrons towards the ring centre and consequently is unable to stabilise the protonation process, Figure 30(c1).

The addition of a third pendant arm, in the case of thec[9], leads to an even greater increase in amine basicity. The presence of a third pendant arm oxygen raises the electron density in the macrocycle cavity even higher than in bhec[9], and subsequently thec[9] displays the greatest protonation constant of all four ligands, Figure 30(e1).

The effect of the hydroxyethyl arms on the value of the second pK_a is quite different. As previously mentioned, the second pK_a of [9]aneN$_3$ is considerably lower than the first due to electrostatic repulsion between the two closely situated ammonium ions. The value of the second pK_a, however, falls even further as the nitrogen donors are functionalised with

increasing numbers of hydroxyethyl pendant arms. There is a step-wise decline in amine basicity from [9]aneN$_3$ (pK_{a2} = 6.82) to hec[9] (pK_{a2} = 6.17) to bhec[9] (pK_{a2} = 4.97) and to thec[9] (pK_{a2} = 3.79), Figure 29. When the ligands are doubly protonated it appears that the pendant arms offer no stabilising effect and only serve to lower amine basicity due to their inductive withdrawing nature. The addition of a second proton may further distort the macrocycle ring so that the pendant arms in each ligand are directed away from the ring cavity. In this case, the oxygen atoms are unable to contribute their lone pairs to the protonation process and only serve to withdraw electrons from the nitrogen donors, Figure 30 (c2), (d2) & (e2).

Comparison between the third pK_a of each ligand reveals a very different trend again. Unlike the open chain ligand, diethylenetriamine (pK_{a3} = 4.25), its cyclic analogue [9]aneN$_3$ does not display a third protonation constant in aqueous solution. The close proximity of the three nitrogen atoms makes protonation of all three donors highly unfavourable and, consequently, its third pK_a is too low to be measured. Interestingly, however, when the amine nitrogens are functionalised with one and two pendant arms, measurable third pK_a's are observed. There is a step-wise increase in basicity from [9]aneN$_3$ to hec[9] (pK_{a3} = 1.97) and bhec[9] (pK_{a3} = 2.25) with the addition of each arm. When a third arm is added, however, the value of the third protonation constant again falls to a value too low to be measured. The existence of a third protonation constant for both hec[9] **17** and bhec[9] **18** suggests some form of stabilisation of the triply protonated aza ring. When hec[9] **17** is triply protonated, it is possible that ring distortion causes the pendant arm oxygen to be more closely positioned to an ammonium proton on the opposite face of the ring where it may form a weak intramolecular hydrogen bond. This would have the effect of stabilising the protonation process and raising the value of the protonation constant, Figure 30(c3). When two pendant arms are added to the macrocycle, there is a greater incidence of hydrogen bond interaction and the protonation constant is raised slightly higher, Figure 30(d3).

a

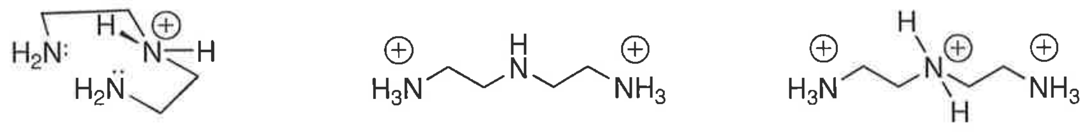

1 pK_1 = 9.70 **2** pK_2 = 8.98 **3** pK_3 = 4.25

b

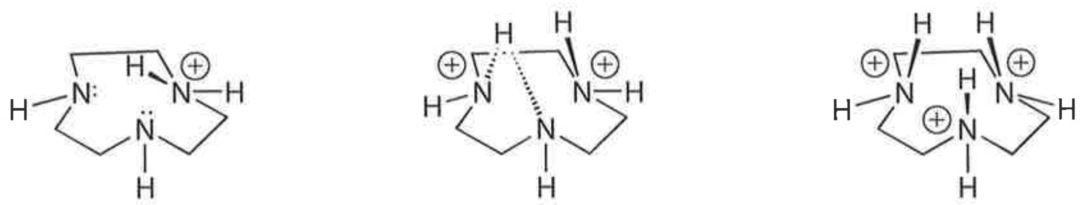

1 pK_{a1} = 10.42 **2** pK_{a2} = 6.82 **3** pK_{a3} = not measurable

c

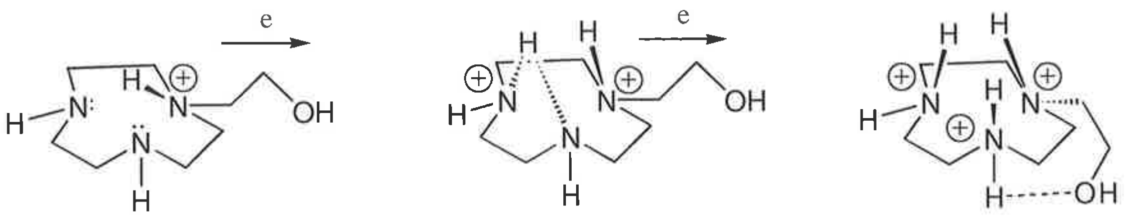

1 pK_{a1} = 10.24 **2** pK_{a2} = 6.17 **3** pK_{a3} = 1.97

d

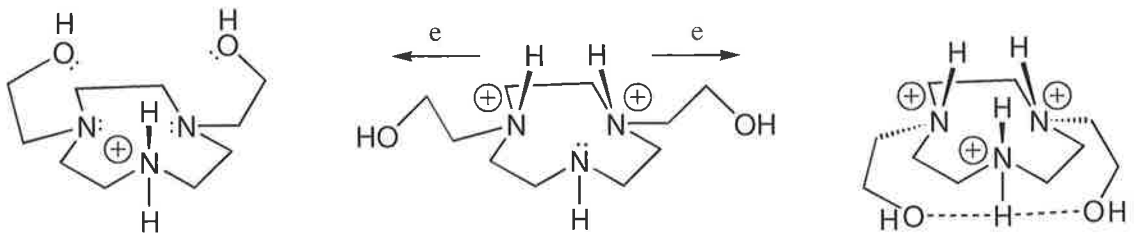

1 pK_{a1} = 11.02 **2** pK_{a2} = 4.97 **3** pK_{a3} = 2.25

e

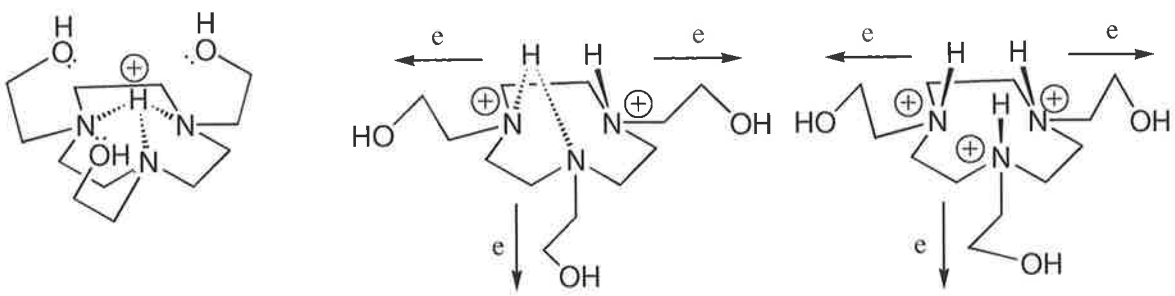

1 pK_{a1} = 11.5 **2** pK_{a2} = 3.8 **3** pK_{a3} = not measurable

Figure 30. A comparison of the pK_a's of five triaza ligands and their hypothetical geometries in solution. The arrows indicate the inductive withdrawal of electrons from the amine donors.

The absence of a third protonation constant in thec[9] suggests that no hydrogen bond interactions occur. It could be reasoned that, in the three-arm species, there is no favourably positioned ammonium proton for the pendant arm oxygen atoms to interact with. As a consequence there is no stabilisation through hydrogen bonding and the protonation constant remains too low to be measured, Figure 30(e3).

In an effort to understand the true nature of the stabilisation process that exists in the triply protonated hec[9] and bhec[9] systems, and why it is absent in the thec[9] system, each ligand was modelled, in its triply protonated form, using the Gaussian94 programme[125] with the LanL2DZ basis set. Although the minimised structures represent the ligand geometries in the gas phase and do not consider solvent effects, they are helpful guides to the structures in solution and are shown in Figure 31. The modelled geometries of the triply protonated hec[9] and bhec[9] systems both reveal intramolecular hydrogen bond interactions. The minimised structure of hec[9]-H_3 **40** clearly shows the hydroxyethyl pendant arm forming a hydrogen bond with an ammonium hydrogen at a distance of 265 picometres (pm), Figure 31. It is noteworthy that the hydroxyl group does not interact with the ammonium proton on the pendant arm nitrogen atom but on the adjacent nitrogen atom. The bond lengths do not allow an internal five-membered hydrogen bond ring, which is why no stabilisation is present in the singly protonated hec[9] system. The hydrogen bond interaction seen in the triply protonated system, however, would help stabilise the highly energetic hec[9]-H_3 **40** species and raise the value of the third pK_a to a measurable level.

A similar intramolecular hydrogen bond is seen in the minimised structure of bhec[9]-H_3 **41**. Both pendant arms are twisted in a clockwise direction towards adjacent ammonium protons, but only one of the hydroxyl groups is able to form a hydrogen bond at a slightly longer distance of 303 pm. Interestingly, the hydrogen bond is formed with the ammonium proton on the unfunctionalised nitrogen atom. The other hydroxyl group is directed towards the ammonium proton on its right hand side but does not form a hydrogen bond. The slightly higher protonation constant of bhec[9] (pK_{a3} = 2.8) compared with that of hec[9] (pK_{a3} = 1.97) had initially raised the idea that two stabilising hydrogen bonds might be present in the two arm system, but the minimised structure of **41** suggests that only one hydrogen bond occurs.

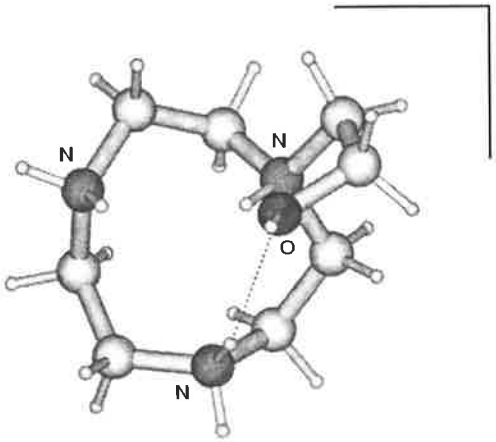

hec[9]-H_3 **40**

pK_{a3} = 2.0

O-H_N Bond length =

265.103 pm

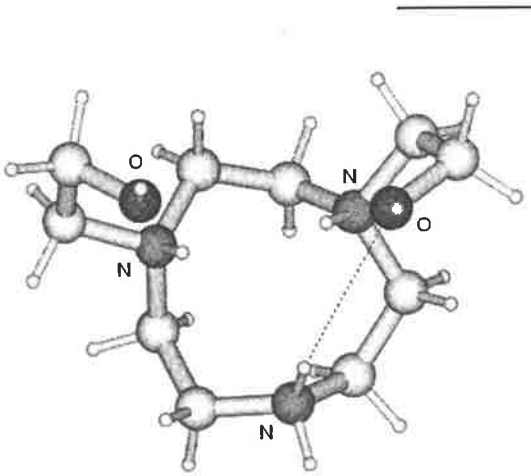

bhec[9]-H_3 **41**

pK_{a3} = 2.8

O-H_N Bond length =

302.855 pm

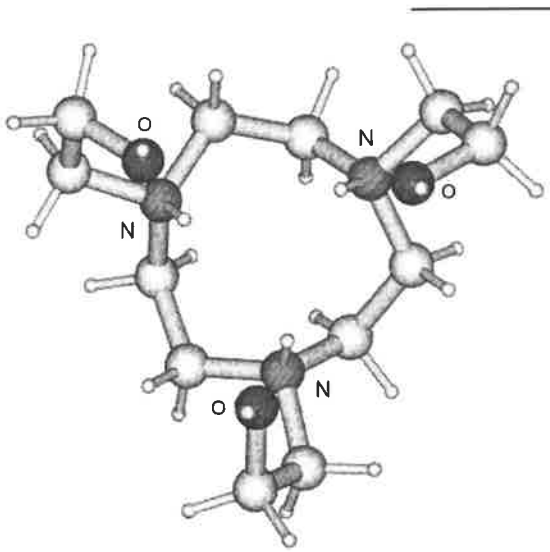

thec[9]-H_3 **42**

pK_{a3} = not measurable

O-H_N distance =

385.698 pm

Figure 31. Global energy-minimised structures of hec[9]-H_3 **40**, bhec[9]-H_3 **41** and thec[9]-H_3 **42** determined by Gaussian 94 using the LanL2DZ basis set. Hydrogen bonds are shown as broken lines. The globalised minimum energies for **40**, **41** and **42** are –552.755837, -705.678259 and –858.595999 Hartrees, respectively.

In a dynamic situation, however, this interaction would occur more frequently when there are two arms present, which may account for the raised protonation constant in the bhec[9] system.

The minimised structure of thec[9]-H_3 **42** shows no intramolecular hydrogen bonding. The three hydroxyethyl arms are seen to twist in a clockwise direction, where the oxygen atoms are directed towards adjacent ammonium protons but do not form hydrogen bonds. In both the hec[9]-H_3 **40** and bhec[9]-H_3 **41** systems, the hydrogen bond is made between a pendant arm oxygen atom and an ammonium proton on an unfunctionalised nitrogen atom. In the case of thec[9]-H_3 **42**, however, there are no unfunctionalised nitrogen atoms and, subsequently, no hydrogen bond interactions occur. It is possible that the pendant arm oxygen atoms are prevented from interacting with the adjacent ammonium protons because of electron repulsion between the neighbouring oxygen atoms. Only where there is no adjacent oxygen atom can the pendant arm oxygen get close enough to form a hydrogen bond with the ammonium proton.

The gas phase models are not accurate representations of the ligand geometries in solution where significant hydrogen bonding between the amine and hydroxyl groups and water is anticipated. However, the minimised structures of **40**, **41** and **42** show good correlation with the aqueous titration results and support the notion that the pendant arms are able to stabilise the third protonation process by forming weak hydrogen bonds in the hec[9] and bhec[9] systems.

3.3. Metal Complexes of Hec[9], Bhec[9] and Thec[9] with Zn^{II} and Cd^{II}

3.3.1. Stability Constants of Hec[9] and Bhec[9] with Zn^{II} and Cd^{II}

The stability constants for the Zn^{II} and Cd^{II} complexes of hec[9] **17** and bhec[9] **18** were determined by potentiometric titration of an aqueous solution containing an equal amount of protonated ligand and metal ion against sodium hydroxide. By using the previously established pK_a values, the stability constants of the metal complexes were determined by the difference in binding affinity of the donor atoms for the metal ions over the protons. A typical titration curve of a ligand-metal solution is shown in Figure 32.

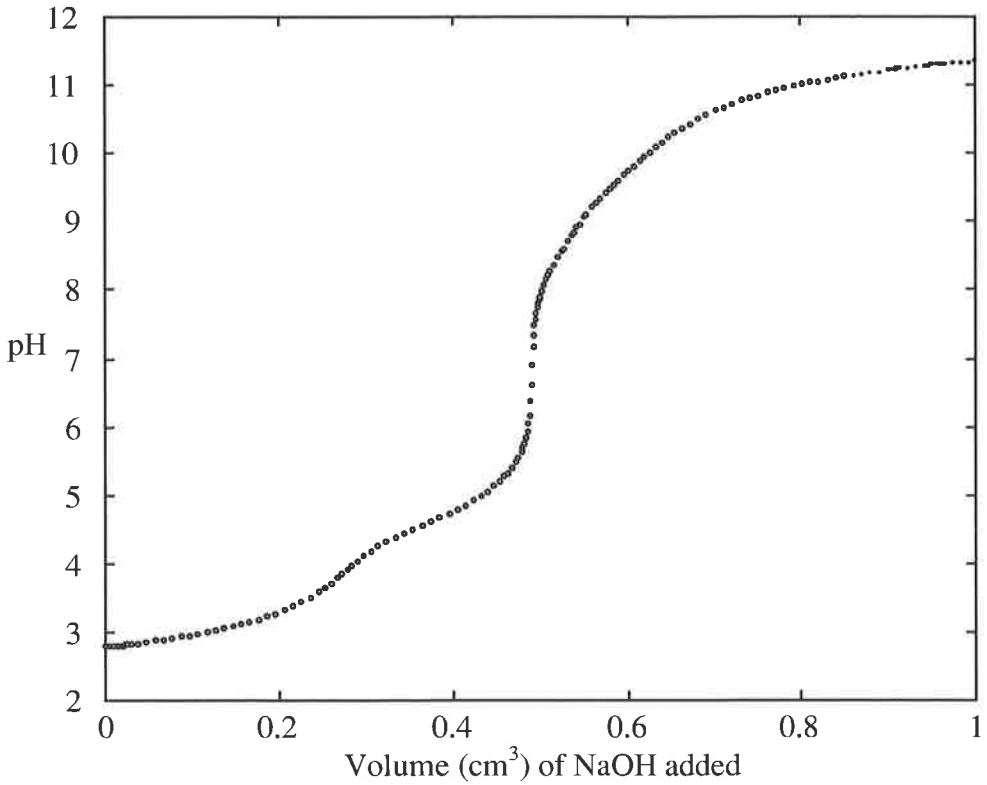

Figure 32. A typical titration curve of acidified ligand (10 cm^3) and M^{II} ion (1:1) against NaOH at 298.2 (± 0.2) K. [hec[9]] = 0.001 mol dm^{-3}, [$ZnSO_4$] = 0.001 mol dm^{-3}, [H^+] = 0.005 mol dm^{-3}, [NaOH] = 0.100 mol dm^{-3}, I = 0.10 ($NaNO_3$).

The association of free ligand and metal ion to form a single complex is represented in equation 3.11,

$$M^{II} + \mathbf{L} \rightleftharpoons M^{II}\mathbf{L} \qquad K(M^{II}\mathbf{L}) = \frac{[M^{II}\mathbf{L}]}{[\mathbf{L}][M^{II}]} \qquad (3.11)$$

Where $K(M^{II}\mathbf{L})$ is the stability constant, M^{II} = Zn^{II} or Cd^{II}, and **L** = macrocyclic ligands hec[9] or bhec[9].

Due to the borderline hard acid nature of Zn^{II}, a pendant arm hydroxyl group coordinated to the Zn^{II} centre will become appreciably polarised and may generate a Zn^{II}-bound hydroxide or alkoxide anion where the protonation constant for the acidic proton is given as,

$$Zn^{II} + \mathbf{L} \rightleftharpoons Zn^{II}H_{-1}\mathbf{L} + H^{+} \qquad K(Zn^{II}H_{-1}\mathbf{L}) = \frac{[Zn^{II}H_{-1}\mathbf{L}][H^{+}]}{[Zn^{II}][\mathbf{L}]} \qquad (3.12)$$

where H_{-1} refers to the removed proton.

The protonation constant K_a is calculated by dividing equation (3.12) by equation (3.11)

$$K_a = \frac{K(Zn^{II}H_{-1}\mathbf{L})}{K(Zn^{II}\mathbf{L})} \qquad (3.13)$$

$$= \frac{[Zn^{II}H_{-1}\mathbf{L}][H^{+}]}{[Zn^{II}][\mathbf{L}]} \times \frac{[Zn^{II}][\mathbf{L}]}{[Zn^{II}\mathbf{L}]} \qquad (3.14)$$

$$= \frac{[Zn^{II}H_{-1}\mathbf{L}][H^{+}]}{[Zn^{II}\mathbf{L}]} \qquad (3.15)$$

and finally $pK_a = -\log K_a \qquad (3.16)$

$$= \log\left[\frac{[Zn^{II}\mathbf{L}]}{[Zn^{II}H_{-1}\mathbf{L}][H^{+}]}\right] \qquad (3.17)$$

The combined titration curves of hec[9] **17** and its metal complexes with Zn^{II} and Cd^{II} are shown in Figure 34a (page 78) and the combined titration curves of bhec[9] **18** and its metal complexes with Zn^{II} and Cd^{II} are shown in Figure 34b. The stability constants and pK_a's of the metal complexes are given in Table 2 and include the literature values of [9]aneN_3 and thec[9] **19** for comparison. It should be noted that no precipitation was noticed during the course of the titrations.

Examination of the stability constants in Table 2, show the binding affinities of each ligand to be directly related to both the size of the metal ion and the number of coordinating pendant arms. When comparing the stability constants of each ligand with either Zn^{II} or Cd^{II}, there is a noticeable preference for Zn^{II} coordination. Each ligand displays a stability constant with Zn^{II} ion that is approximately 1.7 log$K$ units higher than with Cd^{II} ion. The macrocyclic

cavity is more suited to the smaller Zn^{II} ion that has an ionic radius of 74 pm. The Cd^{II} ion has a larger ionic radius of 96 pm and is less well accommodated by the macrocyclic ring. The Cd^{II} ion causes additional strain within the complex and lowers the overall stability. The stronger affinity towards Zn^{II} is also noticed when comparing the titration curves of each complex with Zn^{II} and Cd^{II}, Figure 34, page 78. Both the Zn^{II} and Cd^{II} complexes of each ligand show significant shifts to the right hand side of the titration curve of acidified ligand but the shift is more pronounced with the Zn^{II} complex.

The effect that each pendant arm has on the binding affinity of each ligand is best appreciated when comparing the stability constants of each ligand series, with increasing numbers of pendant arms, with one metal ion. The first ligand complex in the Zn^{II} series is [Zn^{II}-[9]aneN_3] (log$K$ = 11.62). When a single hydroxyethyl arm is attached to the macrocyclic ligand, as represented by [Zn^{II}-**17**] (log$K$ = 10.45), there is a substantial decrease in value of the stability constant. However, when a second pendant arm is attached, [Zn^{II}-**18**] (log$K$ = 11.32), the stability constant is seen to rise and the addition of a third arm, [Zn^{II}-**19**] (log$K$ = 12.07), leads to an even greater increase in stability, Figure 33.

The attachment of hydroxyethyl arms to amines generally leads to a lowering of stability in metal complexes compared with analogues without hydroxyethyl arms.[173,174,175] The hydroxyethyl pendant arm may lower the stability constant in two ways. Firstly, the inductive withdrawing nature of the hydroxyethyl arm serves to lower the basicity of the amine and secondly, it forms a five-membered chelate ring with the metal ion, which imposes a high degree of steric strain in the complex compared with the [9]aneN_3 analogue.

Interestingly, when a second and third hydroxyethyl arm are attached to the [9]aneN_3 macrocycle, there is a step-wise increase in stability such that the stability constant of [Zn^{II}-**19**] is approximately 0.4 log$K$ units higher than in [Zn^{II}-[9]aneN_3]. Although the pendant arms have a negative effect on the thermodynamic stability of the bound metal ion, they may enhance the kinetic stability of the metal complex by affecting the rate of complex formation and decomplexation. The hydroxyethyl arms assist the metallation reaction by providing points of contact outside the macrocyclic ring for the incoming metal ion.[37]

Table 2. Comparison between the stability constants and pK_a's of four [9]aneN$_3$ macrocyclic ligand-metal complexes with Zn^{II} (ionic radius 74 pm) and Cd^{II} (ionic radius 97 pm).[a]

Complex	No. of pendant arms	log$K$(Cd^{II})	log$K$(Zn^{II})	pK_a(Zn^{II})
[M^{II}-[9]aneN$_3$]	0	9.5[b]	11.62[c]	-
[M^{II}-**17**]	1	8.74 (± 0.02)[d]	10.45 (± 0.05)[d]	8.87 (± 0.11)[d]
[M^{II}-**18**]	2	9.79 (± 0.02)[d]	11.32 (± 0.02)[d]	8.50 (± 0.03)[d]
[M^{II}-**19**]	3	10.59[e]	12.07[f]	-

[a] Ionic radii of 6-coordinate metal ion, [b] Ref.[31], [c] Ref.[176], [d] This work, [e] Ref.[45], [f] Ref.[44]

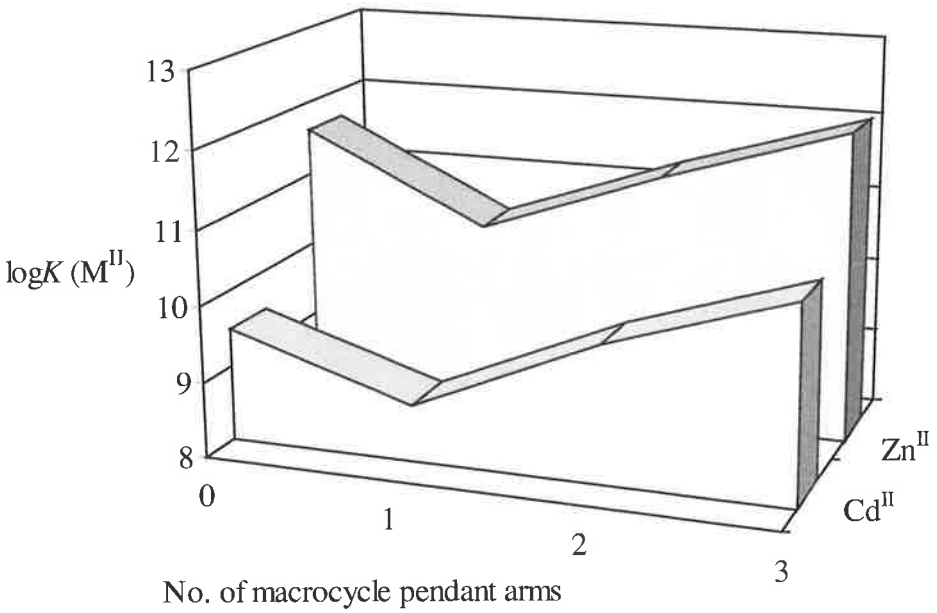

Figure 33. A comparison of the stability constants (log$K$'s) of four [9]aneN$_3$ macrocyclic ligands with increasing numbers of hydroxyethyl pendant arms.

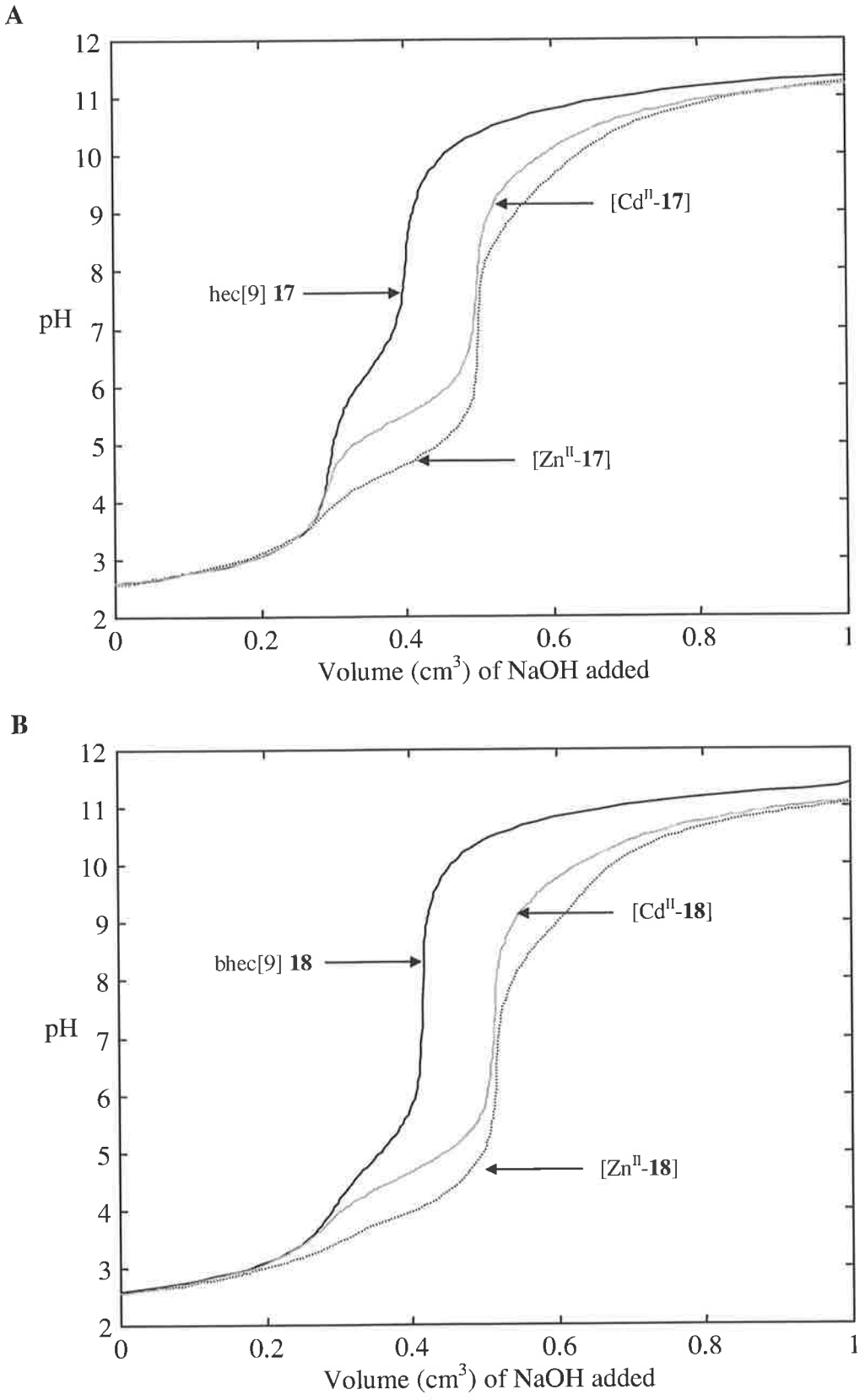

Figure 34. Typical titration curves of acidified hec[9] (**A**) and bhec[9] (**B**) in the absence and presence of Zn^{II} and Cd^{II} against NaOH at 298.2 (± 0.2) K. [Ligand] =0.001 mol dm^{-3}, [$ZnSO_4$] = 0.001 mol dm^{-3}, [$CdSO_4$] = 0.001 mol dm^{-3}, [H^+] = 0.005 mol dm^{-3}, [NaOH] = 0.100 mol dm^{-3}, I = 0.10 ($NaNO_3$).

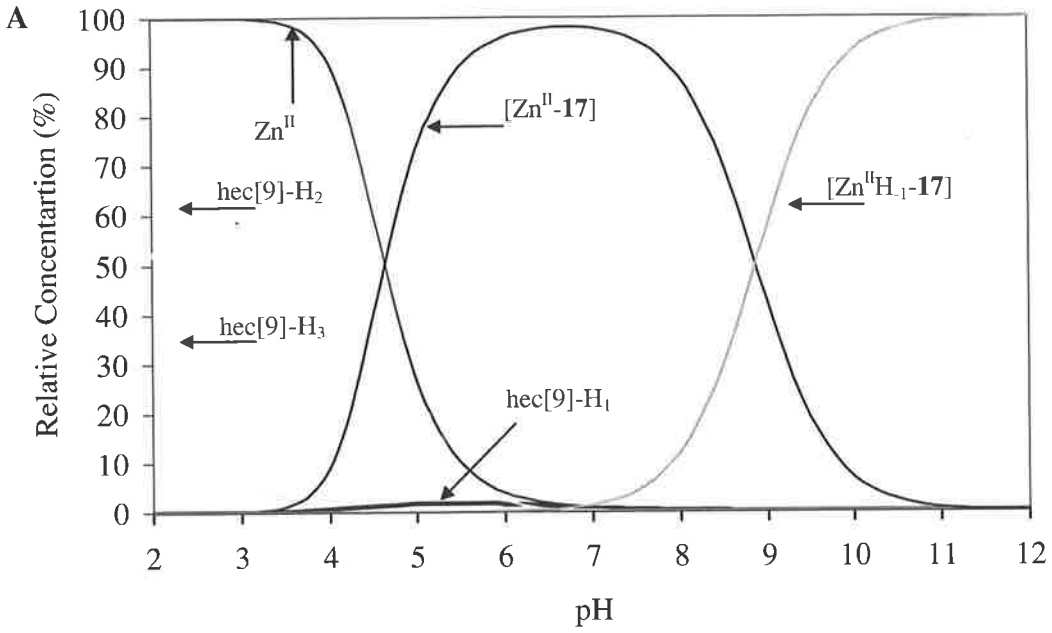

Species	hec[9]-H_3	hec[9]-H_2	hec[9]-H_1	Zn^{II}	$[Zn^{II}$-**17**]	$[Zn^{II}H_{-1}$-**17**]
Max (%)	48.3	95.9	1.77	100	98.1	99.9
at pH	2	3.6	5.4	2	6.6	12

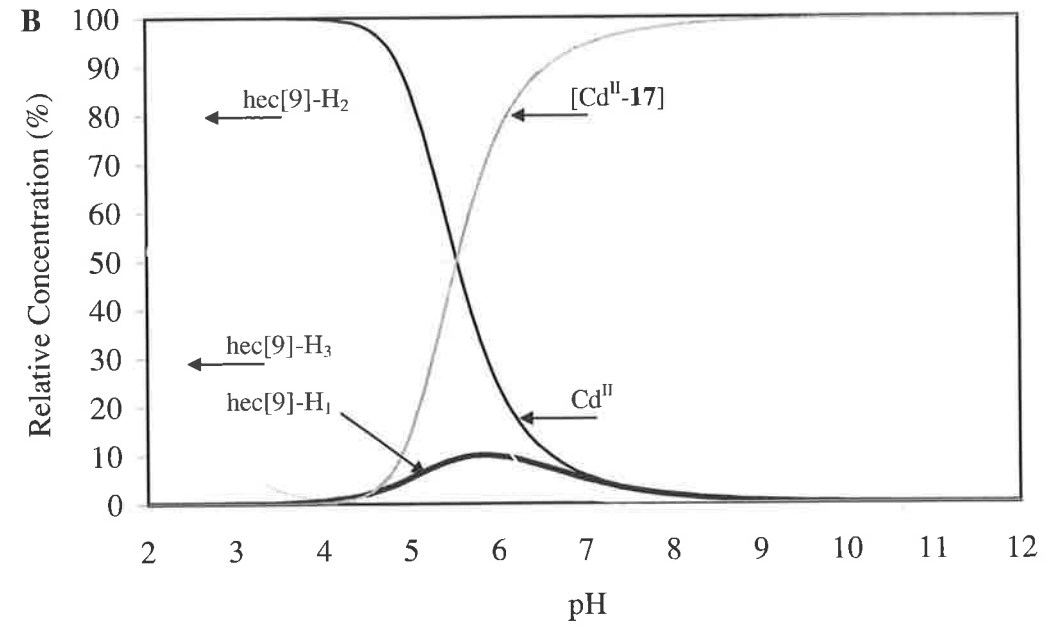

Species	hec[9]-H_3	hec[9]-H_2	hec[9]-H_1	Cd^{II}	$[Cd^{II}$-**17**]
Max (%)	48.3	98.2	10.0	100	99.9
at pH	2	4.0	5.8	2	12

Figure 35. Species distribution diagrams of hec[9] (0.001 mol dm^{-3}) with Zn^{II} (0.001 mol dm^{-3}) (**A**) and with Cd^{II} (0.001 mol dm^{-3}) (**B**) as a function of pH at 298 K, I = 0.10 ($NaNO_3$).

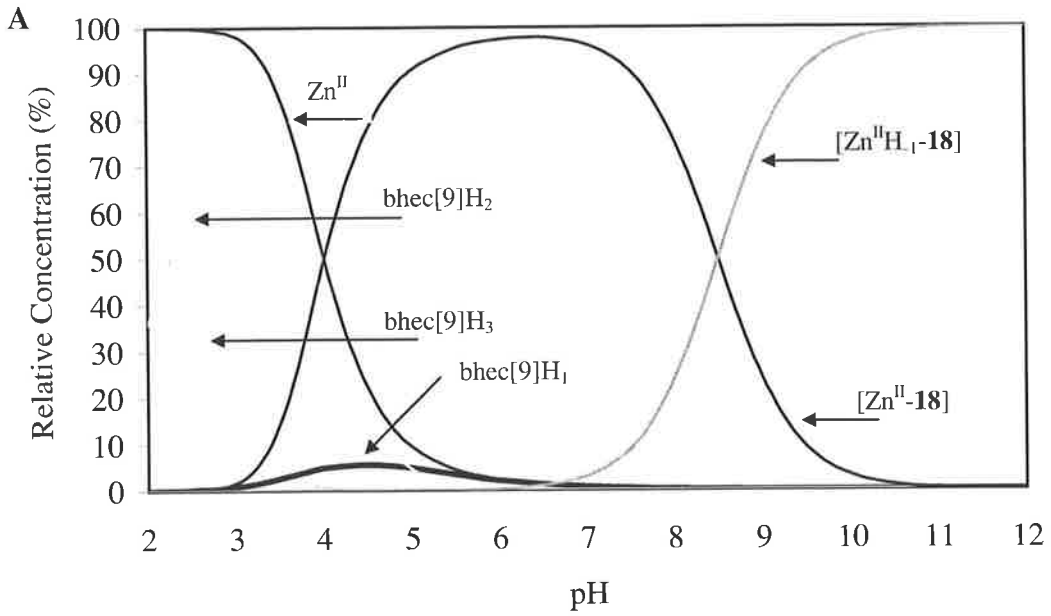

Species	bhec[9]-H_3	bhec[9]-H_2	bhec[9]-H_1	Zn^{II}	[Zn^{II}-**18**]	[$Zn^{II}H_{-1}$-**18**]
Max (%)	64.0	84.7	5.57	100	97.8	100
at pH	2	3.3	4.4	2	6.4	12

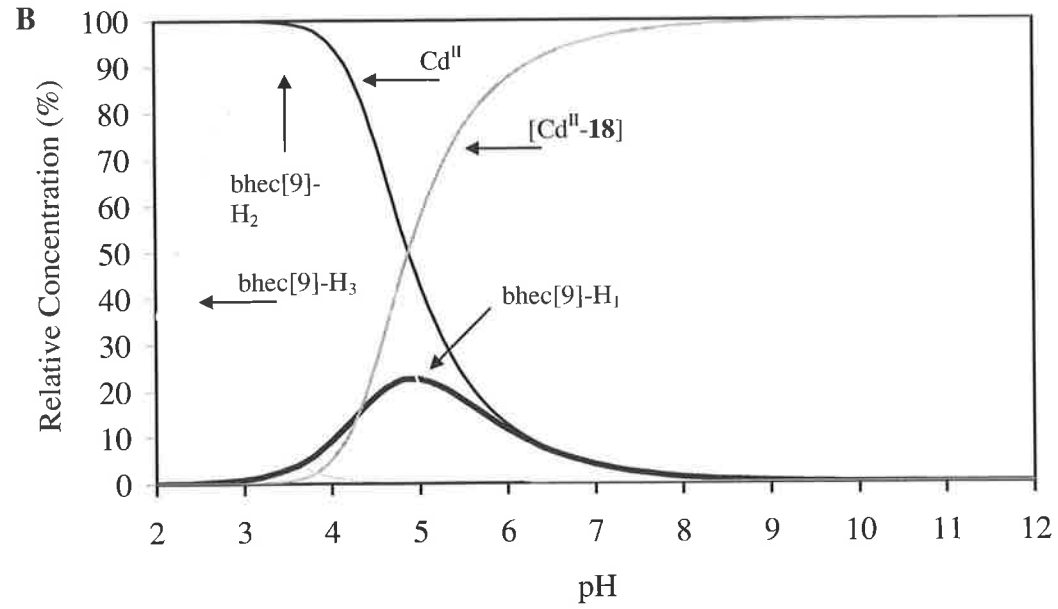

Species	bhec[9]-H_3	bhec[9]-H_2	bhec[9]-H_1	Cd^{II}	[Cd^{II}-**18**]
Max (%)	64.0	91.0	22.5	100	100
at pH	2	3.6	5.0	2	12

Figure 36. Species distribution diagrams of bhec[9] (0.001 mol dm^{-3}) with Zn^{II} (0.001 mol dm^{-3}) (**A**) and with Cd^{II} (0.001 mol dm^{-3}) (**B**) as a function of pH at 298 K, I = 0.10 ($NaNO_3$).

The captured metal ion may then be transferred into the macrocyclic cavity for more rapid complexation, Scheme 1, page 6. Aza macrocycles generally display slow rates of metal incorporation due to the slow rate of reaction between the metal ion and the protonated forms of the ligand. This is due to electrostatic repulsion between the metal ion and the protonated ligand. The hydroxyethyl pendant arms, however, provide an initial coordination site for the metal ion outside the cavity where repulsion with the ammonium protons is less severe and transfer of the metal ion to the ring cavity then becomes more rapid.

The coordination of the metal ion by the pendant arms also decreases the rate of decomplexation. The pendant arms surround the metal ion in a favourable cage geometry that prevents rapid release from the macrocyclic cavity. Both of these effects contribute to greater kinetic inertness, which in turn increases the overall stability of the complex. The effect is more pronounced as the number of coordinating pendant arms increases.

The two-arm [Zn^{II}-**18**] system (log$K$ = 11.32) was found to be more stable than the one-arm [Zn^{II}-**17**] system (log$K$ = 10.45) but less stable than [Zn^{II}-[[9]aneN_3] (log$K$ = 11.62). The additional pendant arm facilitates metal complexation and raises the value of the stability constant compared with the one arm ligand. However, the two pendant arms also inductively withdraw electrons from the donor nitrogens and impart greater steric strain by way of chelate ring formation. This negative effect lowers the value of the stability constant compared with that of the [9]aneN_3 complex. When three arms are attached, in the case of [Zn^{II}-**19**] (log$K$ = 12.07), the stability constant was found to be higher than the [9]aneN_3 complex. Although the additional arm creates a third chelate ring that might cause greater steric strain, the three pendant arms allow more efficient incorporation of the metal ion into the ring cavity and act to slow its release.

Examination of the stability constants of each Cd^{II} complex reveals a similar trend. As the number of hydroxyethyl arms increases there is an initial drop in stability from [Cd^{II}-[9]aneN_3] (log$K$ = 9.5), to [Cd^{II}-**17**] (log$K$ = 8.74), followed by a stepwise increase in stability to [Cd^{II}-**18**] (log$K$ = 9.79) and to [Cd^{II}-**19**] (log$K$ = 10.59), Figure 33. There is however, a noticeable difference between the Zn^{II} and Cd^{II} series. The two- and three-arm Cd^{II} complexes display a much greater increase in stability from the [9]aneN_3 complex compared with the Zn^{II} series where the three-arm ligand complex is only slightly more stable than the [9]aneN_3

complex. This difference cannot be interpreted as a stronger affinity of the pendant arms for Cd^{II} as the hard oxygen donors would be expected to bind the soft Cd^{II} less favourably than the borderline hard Zn^{II} ion. Rather, the difference between the two series reflects the weaker complexation of the larger Cd^{II} ion by the unfunctionalised [9]aneN_3 macrocycle. When complexed by [9]aneN_3, the Cd^{II} ion remains highly exposed to the surrounding environment as the macrocycle binds to only a small face of the metal ion. It should be noted that transition metals do not sit within the ring of [9]aneN_3 but form complexes where the metal ion sits above the nitrogen plane. When a single arm is added to [9]aneN_3, the stability again decreases due to the steric strain and reduced basicity, however when a second and third pendant arm are attached, the Cd^{II} ion becomes better accommodated and is surrounded to a greater extent. This greatly reduces the degree of metal solvation and slows the rate of decomplexation. The effect of the pendant arms is actually very similar in both the Zn^{II} and Cd^{II} complexes. Figure 33 shows an almost parallel increase in stability between the Zn^{II} and Cd^{II} complexes with the attachment of a second and third pendant arm.

Finally, some comment should be made on the degree of pendant arm stabilisation. The amount of stabilisation that is provided by the hydroxyethyl arms is rather meagre compared with the stability that is already provided by the macrocyclic ring. The smaller stabilising effect of the pendant arms can be explained both in terms of base hardness and the steric strain. Amine nitrogen atoms represent soft or polarisable bases and prefer to bind soft acids such as the transition metal ions by covalent interactions. Amine nitrogen atoms show strong affinity for borderline hard-soft Zn^{II} ions and soft Cd^{II} ions. Oxygen on the other hand is considered a hard or nonpolarisable base, and favours strong ionic bonding with hard acids with high positive charge and small size such as the alkali earth metals. Soft acids and bases can associate more closely and achieve better overlap of their wave functions used for covalent bonding. A hard base such as oxygen will, however, mismatch with a soft acid, resulting in poor covalency and weak ionic bonding. This is reflected in the small enhancement of stability provided by the pendant arm oxygen atoms in both the Zn^{II} or Cd^{II} complexes.

Each hydroxyethyl arm forms a five-membered chelate ring by coordinating with the metal centre. As previously mentioned, chelate ring formation imposes greater steric strain

within the metal-ligand complex compared with the unfunctionalised system. Although each additional arm encapsulates the metal ion to a greater extent, the steric strain of the pendant arm chelate rings serves to lower the stability of the complex. Both the hard-base nature of the oxygen atoms and the steric strain caused by chelate ring formation contribute to a low stabilising effect.

Both the one-arm [Zn^{II}-**17**] complex (pK_a = 8.87) and the two-arm [Zn^{II}-**18**] complex (pK_a = 8.50) display measurable pK_a's corresponding to either a Zn^{II} bound alcohol group or water molecule. Interestingly, a similar pK_a is not observed for the three-arm [Zn^{II}-**19**] complex. The exact reason for this is unclear although there are two possible explanations. Firstly, it could be that the Zn^{II} ion is simply rendered less acidic within the six-coordinate environment of thec[9] and the Zn^{II} bound alcohol group is polarised to a lesser extent, or alternatively, it could be that the pK_a's measured in the hec[9] and bhec[9] systems are actually due to Zn^{II} bound water molecules rather than pendant arm alcohol groups. In the thec[9] system, the Zn^{II} ion is coordinatively saturated by the six donor atoms and water cannot bind.

3.3.2. Comparison Between [Zn^{II}-17] and [Zn^{II}-15]

The [Zn^{II}-**17**] complex was synthesised to further investigate the activity of Kimura's alkaline phosphatase model, [Zn^{II}-**15**]. The ligands are similar, in that they display three step-wise pK_a's, but their Zn^{II}-complexes show significant differences in metal binding stability and in the acidity of the coordinated alcohol or water molecule, Table 3.

The three pK_a's of hec[9] **17** are all lower than the corresponding values for **15**, inferring that hec[9] is the less basic ligand. The high value of the first protonation constant of **15** (pK_{a1} = 11.7) compared with hec[9] (pK_{a1} = 10.24) reflects the greater flexibility of the [12]aneN_3 ligand. Protonation is made more facile as the nitrogen donors can adopt more favourable positions to stabilise the ammonium proton. Similarly, the greater flexibility and larger size of the ring help to lower the electrostatic repulsion between ammonium ions when a second and third proton are added. This is quite different to hec[9], where the third protonation process is probably stabilised by hydrogen bonding between an ammonium proton and the pendant arm oxygen atom.

Table 3. Comparison of the pK_a's of hec[9] and **15** and the Zn^{II} complexation constants of [Zn^{II}-**17**] and [Zn^{II}-**15**].

Ligand	pK_{a1}	pK_{a2}	pK_{a3}	log$K$(Zn^{II})	pK_a (Zn^{II})
hec[9][a]	10.24	6.17	1.97	10.45	8.87
15[b]	11.7	6.92	2.2	7.6	7.4

[a] This work, [b] Ref.[71]

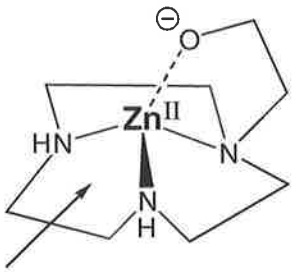

5 membered chelate ring

[Zn^{II}-**17**]

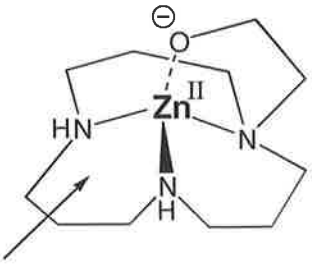

6 membered chelate ring

[Zn^{II}-**15**]

Figure 37

The two ligands display significantly different binding affinities for Zn^{II}. The stability constant of the [Zn^{II}-**17**] complex is approximately 2.7 log$K$ units greater than that of [Zn^{II}-**15**]. The hec[9] ligand forms three five-membered chelate rings upon metal complexation, excluding the pendant arm chelate ring, while the larger [12]aneN_3 based ligand **15**, creates three six-membered chelate rings, Figure 37. The formation of five-membered chelate rings is more favourable as it imposes less steric strain in the molecule and bestows greater stability.

The most important property of the [Zn^{II}-**17**] complex, in terms of modelling the catalytic activity of [Zn^{II}-**15**], is the protonation constant of the Zn^{II} bound alcohol or water molecule. The OH group of [Zn^{II}-**15**] deprotonates with a pK_a value of 7.4 at 25°C to give a Zn^{II}- RO^- species (R = H or alkyl) which is thought to closely resemble the nucleophilic serine hydroxyl group at the active centre of alkaline phosphatase.[71] The OH group of hec[9]-

Zn^{II}, however, displays a much higher pK_a of 8.87 and consequently does not represent a good model for alkaline phosphatase. At pH 7.4, less than 3% of the [Zn^{II}-**17**] complex exits as the deprotonated species, as determined by the species distribution diagram in Figure 35A.

3.4. Structural Studies of the Metal Complexes of Hec[9], Bhec[9] and Thec[9] with Zn^{II} and Cd^{II}

Having established the relative stabilities of each ligand with Zn^{II} and Cd^{II} in aqueous solution, molecular modelling calculations were performed on each ligand in the absence and presence of Zn^{II} and Cd^{II} to examine the coordination structures of each system. *Ab initio* calculations using the Gaussian 94 programme[125] are especially useful for studying metal-ligand interactions as they provide valuable information on the precise stereochemistry of the coordinated metal ion and the suitability of the ligand to successfully accommodate different metal ions. The stability of a metal-ligand complex can often be gauged by the level of strain imposed on the ligand system as it coordinates the metal ion. The molecular models provide a visual reference with precise bond lengths and angles that are useful in determining the quality of host-guest accommodation and provide complementary information to stability measurements derived from potentiometric titrations.

The models generated by *ab initio* calculations are not true representations of the ligand structures in solution but rather their geometries in the gas phase. In this regard, the models are not accurate as they do not consider solvent effects but they are reasonable guides to the solution state structure.

When modelling the macrocyclic ligand complexes there are two possible structures to consider. Each system may exist in one of two enantiomeric forms depending on which face of the ligand the metal ion binds. In the Λ or $\lambda\lambda\lambda$ isomer of a hexadentate system the three pendant arms are seen to rotate in an anti-clockwise direction when viewed from the pendant arm side of the complex, while in the Δ or $\delta\delta\delta$ isomer the pendant arms rotate in a clockwise direction, Figure 38. Interconversion between the two enantiomers in solution involves the release of the metal ion and a complete ring inversion whereupon the metal is recaptured on the opposite face of the ligand. Both enantiomers posses identical potential energies and

represent two unique global energy minima on the potential energy surface. To maintain consistency, all minimisations have been performed on the Λ enantiomer of each ligand and the metal complexes and all calculations were performed using the LanL2DZ basis set.

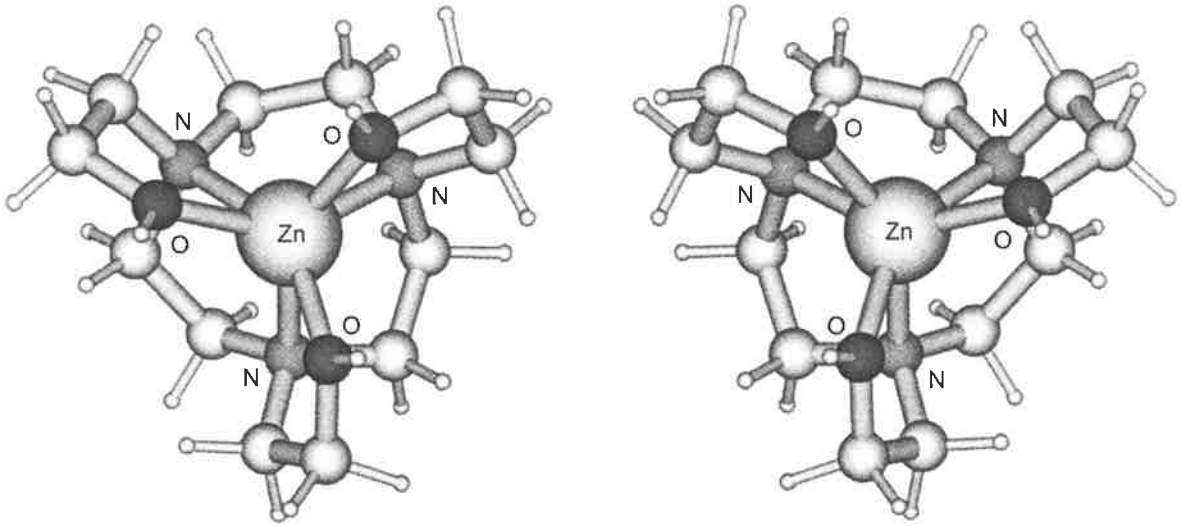

Λ Δ

Figure 38. The Λ (λλλ) and Δ (δδδ) enantiomers of [Zn^{II}-**19**] generated by Gaussian 94 using the LanL2DZ basis set.

3.4.1. *Ab initio* Calculations of Thec[9], [Zn^{II}-19] and [Cd^{II}-19]

The minimised structures of Λ thec[9] **19** and its metal complexes with Zn^{II} and Cd^{II} are shown in figure 39. The free ligand displays a C_3 axis of symmetry were each hydroxyethyl pendant arm is orientated in an anti-clockwise direction when viewed from the pendant arm side of the triangular triaza plane. The pendant arm oxygen atoms sit outside the circumference of the macrocyclic ring and render the two carbons in each macrocyclic ethylene linkage nonequivalent, Figure 39. When viewed from the side of the molecule, the pendant arms are seen to extend above the macrocyclic ring creating a basket-like structure where the three oxygen atoms form a triangular plane that lies parallel to the triangular plane of the triaza ring, Figure 39.

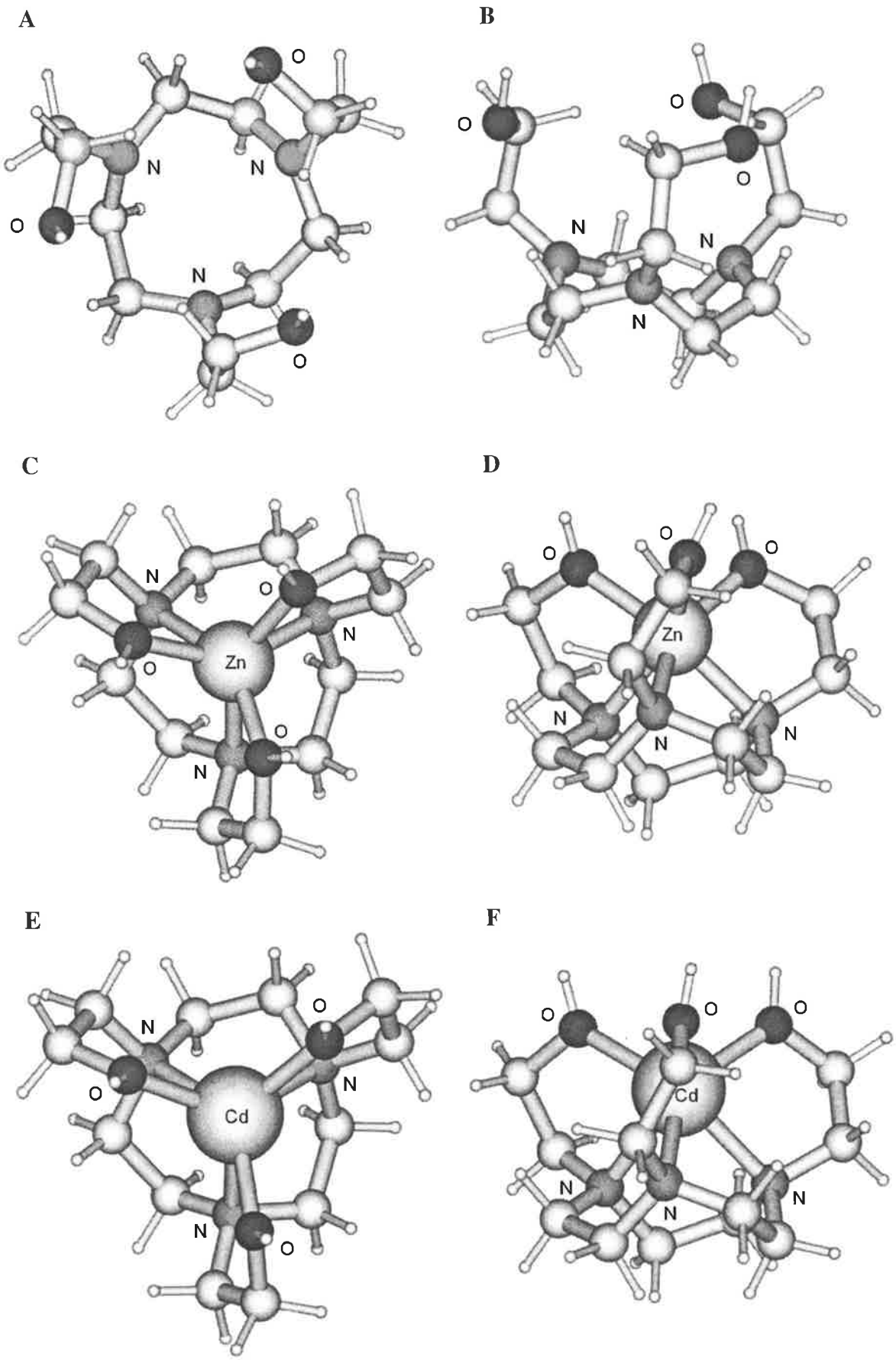

Figure 39. Global energy minimised structures of Λ thec[9] (**A** and **B**), [Zn^{II}-**19**] (**C** and **D**) and [Cd^{II}-**19**] (**E** and **F**) determined by Gaussian 94 using the LanL2DZ basis set.

Table 4. Parameters derived from molecular orbital calculations using the Gaussian 94 LanL2DZ basis set.

Distance (pm)	thec[9]	[Zn^{II}-**19**]	[Cd^{II}-**19**]	Δ Zn^{II}-Cd^{II}
O-O	469.930	305.403	347.350	41.947
N-N	311.420	289.860	297.437	7.577
O-N	315.257	270.560	282.327	11.767
M^{II}-O	-	213.160	229.513	16.353
M^{II}-N	-	220.913	239.587	18.674
M^{II}-O plane	-	119.780	111.630	-8.150
M^{II}-N plane	-	144.210	167.070	22.860
O-H	95.230	95.383	95.447	0.064
O-H adj.	485.067	346.696	381.883	35.187
Angle ϕ (deg.)				
Twist angle	32.749	12.653	9.203	-3.450
O-M^{II}-N angle	-	77.105	73.968	-3.137

The globalised minimum energies for thec[9] and its Zn^{II} and Cd^{II} ion complexes are -857.718353, -920.971923 and -903.974829 Hartrees, respectively (1 Hartree = 2625.5 kJ mol^{-1}).

The triangular oxygen plane is approximately 66% larger than the triangular nitrogen plane where the calculated O-O and N-N distances are 469 and 311 pm, respectively. The calculated twist angle (ϕ), delineated by the skew of the triangular oxygen and nitrogen planes when viewed down the C_3 axis, is 32.7°. Other selected interatomic distances and angles appear in Table 4.

When Zn^{II} or Cd^{II} are added to thec[9], the ligand surrounds the metal ions in a six-coordinate environment between the three amine and three oxygen donor atoms, Figure 39(C-F). The minimised structures of [Zn^{II}-**19**] and [Cd^{II}-**19**] both display distorted trigonal prismatic geometries where the twist angles between the nitrogen and oxygen planes are 12.7° and 9.3°, respectively. The smaller twist angle observed with Cd^{II} reflects the larger size of the metal ion. The Cd^{II} ion (ionic radius = 97 pm) causes an expansion of the donor cage in comparison with Zn^{II} (ionic radius = 74 pm) which fits more neatly in the macrocyclic cavity. The respective O-O and N-N bond distances in the Cd^{II} complex are 41.9 and 7.6 pm longer than those in the Zn^{II} complex are. Similarly, the M^{II}-O and M^{II}-N bond distances are also longer in the Cd^{II} complex. An increase in the M^{II}-N plane distance of 22.9 pm and a decrease in the M^{II}-O plane distance of 11.8 pm in the Cd^{II} complex with respect to the Zn^{II} complex, indicates that the larger Cd^{II} ion is poorly accommodated by thec[9] and causes greater steric strain within the ligand.

These results complement the stability measurements from the potentiometric titrations that showed [Cd^{II}-**19**] to be much less stable than [Zn^{II}-**19**]. The smaller Zn^{II} ion creates less strain within the ligand and allows better overlap of the metal and donor orbitals.

3.4.2. *Ab initio* Calculations of Bhec[9], [Zn^{II}-18] and [Cd^{II}-18]

The minimised structures of Λ bhec[9] **18** and its Zn^{II} and Cd^{II} complexes are presented in Figure 40. The global minimised structure of bhec[9] shows no axis of symmetry. Although, the two hydroxyethyl pendant arms are twisted slightly in an anti-clockwise direction, the hydroxyl groups are orientated towards each other and interact through a weak[177] hydrogen bond. The amine proton of the unsubstituted nitrogen atom is directed towards the centre of the macrocyclic ring and its lone-pair electrons face outward.

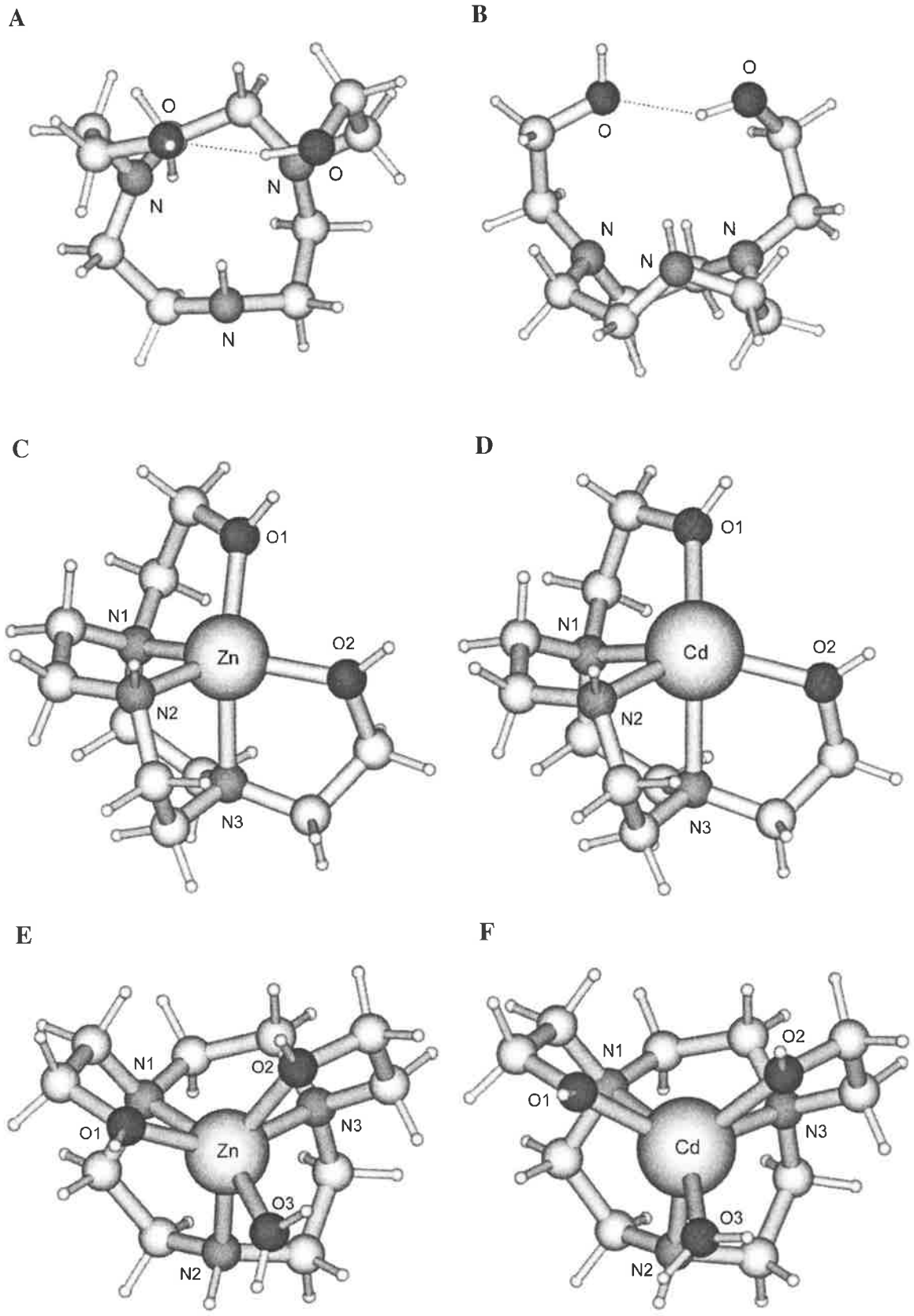

Figure 40. Global energy-minimised structures of Λ bhec[9] (**A** and **B**), [Zn^{II}-**18**] (**C**), [Cd^{II}-**18**] (**D**), [$Zn^{II}H_2O$-**18**] (**E**) and [$Cd^{II}H_2O$-**18**] (**F**) determined by Gaussian 94 using the LanL2DZ basis set. Hydrogen bonds are shown as broken lines.

Table 5. Bond distances and angles for [M^{II}-**18**] complexes with Zn^{II} and Cd^{II} (**A**) and with $Zn^{II}H_2O$ and $Cd^{II}H_2O$ (**B**) derived from molecular orbital calculations using the Gaussian 94 LanL2DZ basis set.

A

Distance (pm)	Zn^{II}	Cd^{II}	ΔM^{II}
M^{II}-O1	208.454	225.235	16.781
M^{II}-O2	206.388	224.032	17.644
M^{II}-N1	214.455	234.458	20.003
M^{II}-N2	211.339	230.392	19.053
M^{II}-N3	217.811	236.637	18.826
Angle ϕ (deg)			
O1-M^{II}-N3 (apical)	148.581	140.509	-8.07
N1-M^{II}-N2 (basal)	85.676	79.235	-6.44
N2-M^{II}-O2 (basal)	128.311	130.917	2.606
O2-M^{II}-N1 (basal)	140.570	133.927	-6.643
Total basal angle	354.557	344.079	-10.478

B

Distance (pm)	$Zn^{II}H_2O$	$Cd^{II}H_2O$	Δ ($M^{II}H_2O$)
M^{II}-O1	211.821	229.297	17.466
M^{II}-O2	218.103	231.719	13.616
M^{II}-O3	217.815	234.121	16.306
M^{II}-N1	221.722	240.637	18.915
M^{II}-N2	218.890	236.606	17.716
M^{II}-N3	220.573	239.846	19.273
Angle ϕ (deg)			
Twist angle O1	11.935	9.326	-2.609
Twist angle O2	14.375	10.303	-4.072

The globalised minimum energies for the [M^{II}-**18**] complexes with Zn^{II}, Cd^{II}, Zn^{II}-H_2O and Cd^{II}-H_2O are, -768.061006, -751.061632, -844.110194 and -827.116340 Hartrees, respectively (1 Hartree = 2617.13 kJ mol^{-1}).

Since bhec[9] has only two pendant arms, the addition of M^{II} produces a coordinatively unsaturated metal complex. The metal ions in both the Zn^{II} and Cd^{II} complexes are surrounded in a distorted trigonal bipyramidal environment by the three ring nitrogen atoms and the two pendant arm oxygen atoms, Figure 40(C-D). The Zn^{II} ion lies predominately in the basal plane defined by the N1, N2 and O2 atoms with a total basal angle of 354.6° for N1-Zn^{II}-N2, N2-Zn^{II}-O2 and O2-Zn^{II}-N1. The calculated apical angle defined by O1- Zn^{II}-N3 is bent at 148.6°. The apical N-M^{II} and O-M^{II} distances in both complexes are slightly longer than the corresponding distances in the basal plane. Other selected interatomic bond distances and angles appear in Table 5.

The larger size of Cd^{II} causes an increase in the O-O, O-M^{II}, M^{II}-N and N-N distances compared with Zn^{II} and further distorts the trigonal bipyramidal structure. The Cd^{II} ion is less well accommodated by the ligand and lies slightly above the basal plane towards the apical oxygen. This reduces the total basal angle to 344.1° and causes a greater bend in the apex so that the apical angle is reduced to 140.5°.

As the [M^{II}-**18**] complexes are coordinatively unsaturated, it is possible that a water molecule may coordinate to the metal ion and occupy the sixth coordination site. In such an event, the metal would become surrounded in a six-coordinate environment similar to that observed with thec[9]. The [M^{II}-**18**] complexes were further minimised with a single water molecule to investigate the change in geometry. The minimised structures of [$Zn^{II}H_2O$-**18**] and [$Cd^{II}H_2O$-**18**] both display distorted trigonal prismatic geometries where the pendant arms are rotated in an anti-clockwise direction, Figure 40(E-F). The O1 and O2 pendant arm oxygen atoms are twisted at slightly different angles to the triangular nitrogen plane so that their calculated twist angles (ϕ) are 11.9° and 14.4° with Zn^{II}, respectively, and 9.3° and 10.3° with Cd^{II}, respectively.

Both the five-coordinate and aquated six-coordinate geometries of [M^{II}-**18**] are possible in an aqueous environment and could exist in equilibrium. It can be argued, however, that the five-coordinate geometry represents the dominant configuration as the two-arm ligand is geometrically preorientated to coordinate the metal ion in a trigonal bipyramidal environment. Conversion to six-coordinate configuration may be less favourable as it involves additional organisation of the donor atoms.

3.4.3. *Ab initio* Calculations of Hec[9], [Zn^{II}-17] and [Cd^{II}-17]

The third ligand system to be investigated was the one arm ligand hec[9] **17**. The minimised structure of hec[9] is shown in Figure 41(A-B). The single pendant arm is orientated above the macrocyclic ring so that the oxygen atom is positioned almost in the centre of the triangular nitrogen plane. The amine protons of the two unsubstituted nitrogen atoms are directed towards the centre of the ring and interact with the pendant arm oxygen atom through weak[177] hydrogen bonds.

In both the Zn^{II} and Cd^{II} complexes, the metal ion is surrounded in a distorted tetrahedral environment by the three ring nitrogen atoms and the single pendant arm oxygen atom, Figure 41(C-D). The Zn^{II} ion lies predominately in the basal plane defined by the N1, N2 and O1 atoms with a total basal angle of 358.8° for N1-Zn^{II}-N2, N2-Zn^{II}-O1 and O1-Zn^{II}-N1. The apex is defined by M^{II}-N3 and its bond length is slightly longer than the corresponding M^{II}-N bonds in the basal plane. Other interatomic bond distances and angles appear in Table 6.

The addition of Cd^{II} again causes an increase in the O-M^{II} and M^{II}-N bond distances compared with Zn^{II}. The larger Cd^{II} ion is less well accommodated by hec[9] and causes greater distortion of the tetrahedral environment. The metal ion is projected above the basal plane away from the apex nitrogen and reduces the total basal angle to only 349.1°. The tetrahedral structures of the Zn^{II} and Cd^{II} complexes reveal a large open face that could allow further coordination by a water molecule in an aqueous environment. To investigate what effect this would have on the coordination structure, the [M^{II}-**17**] complexes were further minimised with an added water molecule.

The minimised structures of [$Zn^{II}H_2O$-**17**] and [$Cd^{II}H_2O$-**17**] both display distorted trigonal bipyramidal geometries where the water molecule resides at the apex defined by O2-M^{II}-N3, Figure 41(E-F). In the Zn^{II} complex, the metal ion is raised slightly higher in the basal plane away from the apical nitrogen compared with the tetrahedral structure. As a consequence, the total basal angle is reduced from 358.8° in the four coordinate structure to 353.9° in the five coordinate structure.

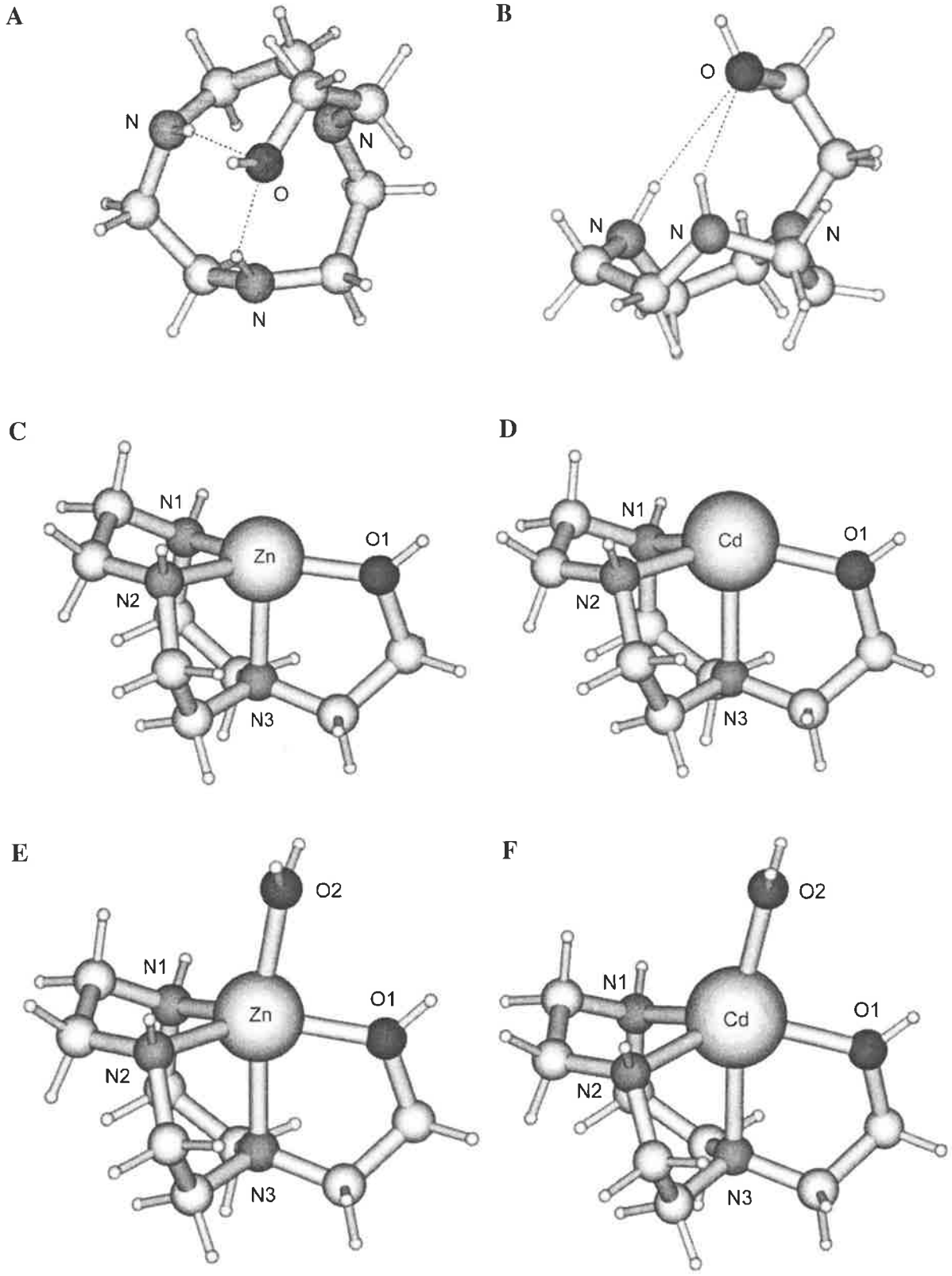

Figure 41. Global energy-minimised structure of Λ hec[9] (**A** and **B**), [Zn^{II}-**17**] (**C**), [Cd^{II}-**17**] (**D**), [$Zn^{II}H_2O$-**17**] (**E**) and [$Cd^{II}H_2O$-**17**] (**F**) determined by Gaussian 94 using the LanL2DZ basis set. Hydrogen bonds are shown as broken lines.

Table 6. Bond distances and angles for [M^{II}-**17**] complexes with Zn^{II}, Cd^{II}, $Zn^{II}H_2O$ and $Cd^{II}H_2O$ derived from molecular orbital calculations using the Gaussian 94 LanL2DZ basis set.

Distance (pm)	Zn^{II}	Cd^{II}	ΔM^{II}	$Zn^{II}H_2O$	$Cd^{II}H_2O$	$\Delta (M^{II}H_2O)$
M^{II}-O1	198.925	218.393	19.468	205.255	224.710	019.455
M^{II}-O2	-	-	-	213.761	229.279	015.518
M^{II}-N1	207.487	227.537	20.005	212.021	231.506	19.485
M^{II}-N2	207.134	227.036	19.902	212.510	231.845	19.335
M^{II}-N3	209.712	231.109	21.397	218.562	237.625	19.063
M^{II}-(NNO plane)	11.86	39.86	28.00	28.19	52.12	23.93
Angle ϕ (deg)						
O2-M^{II}-N3 (apical)	-	-	-	169.976	167.363	-2.613
N1-M^{II}-N2 (basal)	88.313	81.052	-7.261	86.068	79.352	-6.716
N2-M^{II}-O1 (basal)	137.209	136.223	-0.986	137.601	135.153	-2.448
O1-M^{II}-N1 (basal)	133.324	131.827	-1.497	130.218	127.901	-2.317
Total basal angle	358.846	349.102	-9.744	353.887	342.406	-11.481

The globalised minimum energies for the [M^{II}-**17**] complexes with Zn^{II}, Cd^{II}, Zn^{II}-H_2O and Cd^{II}-H_2O are -615.136975, -598.138655, -691.203483 and -674.206542 Hartrees, respectively (1 Hartree = 2617.13 kJ mol^{-1}).

The calculated apical angle defined by O2- Zn^{II}-N3 is bent at 170.0° while the apical Zn^{II}-O and Zn^{II}-N bond distances are again slightly longer than the corresponding basal bond distances.

The five-coordinate Cd^{II} complex displays a similar coordination environment. The Cd^{II} ion is raised further from the basal plane in comparison with the tetrahedral structure such that the total basal angle is reduced from 349.1° in the four-coordinate structure to 342.4° in the five-coordinate structure. The apical angle is bent only slightly more than in the corresponding Zn^{II} complex with an apical angle of 167.4°.

The apical angles of both the five-coordinate [M^{II}-**17**] complexes are significantly greater than the apical angles observed in the corresponding five-coordinate [M^{II}-**18**] complexes. The apices of the [M^{II}-**17**] complexes are defined by N-M^{II}-OH_2 where the oxygen atom belongs to a coordinated water molecule. The apices of the [M^{II}-**18**] complexes, however, contain a pendant arm oxygen atom that is more rigidly constrained. The pendant arm linkage imposes more steric strain and causes greater distortion from an ideal trigonal bipyramidal geometry. As a consequence, the apical angles of the Zn^{II} and Cd^{II} complexes of bhec[9] are 21.4° and 26.9° less, respectively, than the apical angles in the corresponding five-coordinate hec[9] complexes.

The trigonal bipyramidal geometry of the [$M^{II}H_2O$-**17**] allows the possibility of two configurational isomers. The first isomer **43** has an apex defined by the N-M^{II}-OH_2 where the oxygen atom belongs to a Zn^{II}-bound water molecule and the nitrogen atom belongs to the substituted ring nitrogen. This structure is essentially symmetric where the plane of symmetry runs co-planar to the pendant arm chelate ring, Figure 42.

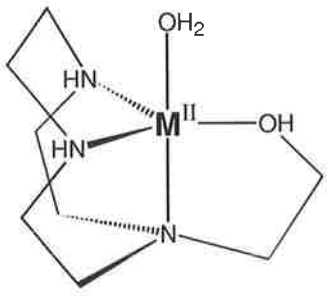

43

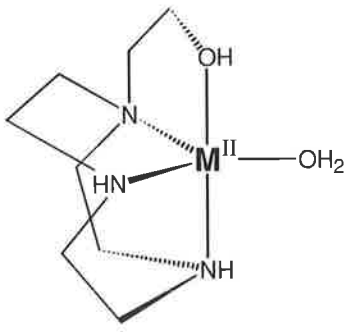

44

Figure 42

The second isomer **44** has an N-M^{II}-O apex where the oxygen atom belongs to the pendant arm hydroxyl group and the nitrogen belongs to an unsubstituted ring nitrogen. In this structure the coordinated water molecule resides in the basal plane and there is a total lack of symmetry. Both isomers of the [$Zn^{II}H_2O$-**17**] complex were minimised in an attempt to identify the most stable configuration. Surprisingly, both input structures converged to give **43** as the global minimum. This result suggests that the unsymmetrical isomer **44** is considerably less stable, possibly due to the increased strain on the apex by the restrictive pendant arm bridge.

The addition of a second water molecule to the [$M^{II}H_2O$-**17**] complex results in a six-coordinate trigonal prismatic geometry, Figure 43. The pendant alcohol and two water molecules form an irregular triangular oxygen plane that is skewed in an anti-clockwise direction from the nitrogen plane. The pendant arm oxygen has a twist angle (ϕ) of 15.2° in the Zn^{II} complex and 12.1° in the Cd^{II} complex, both of which are slightly larger than the twist angles observed in the six-coordinate bhec[9] and thec[9] complexes. The interatomic bond distances appear in Table 7.

In solution, the [M^{II}-**17**] complex may interconvert between each of the three possible coordination structures, namely tetrahedral, trigonal bipyramidal and trigonal prismatic. The tetrahedral geometry that is formed when hec[9] first binds the metal ion may easily convert to the five-coordinated trigonal bipyramidal geometry by addition of a single water molecule. This conversion causes very little disruption or additional organisation of the ligand atoms and it can be argued that the five-coordinate structure would dominate in an aqueous environment. Conversion to the six-coordinate structure is also possible, although additional energy is needed to reorientate the donor atoms to accommodate the extra water molecule. It is therefore reasonable to assume that the five-coordinate geometry represents the major contributor to the structure of [M^{II}-**17**] in solution. Support for a five coordinate structure is provided by the x-ray crystal structure of Kimura's [Zn^{II}-**15**] complex, which displays a dimeric structure containing two trigonal bipyramidal geometries.[71]

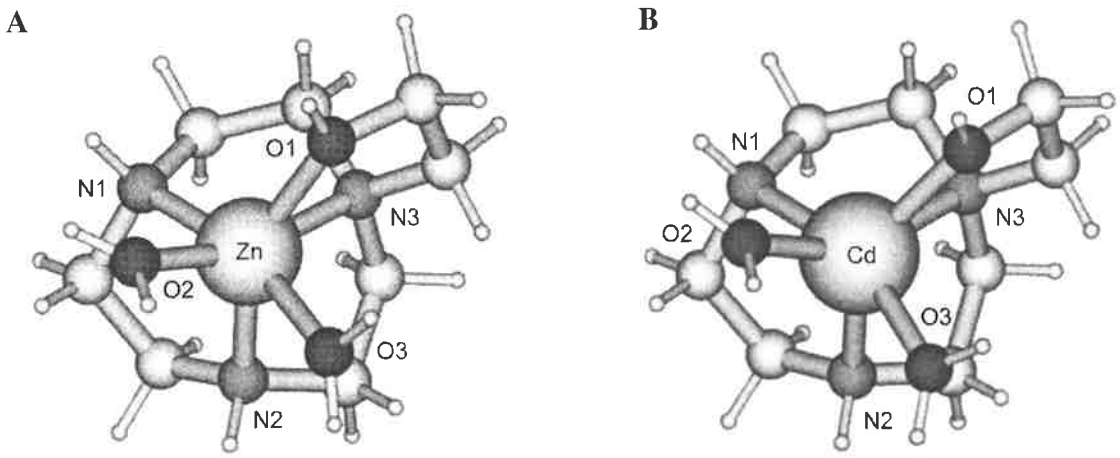

Figure 43. Global energy-minimised structures of [$Zn^{II}2H_2O$-**17**] (**A**) and [$Cd^{II}2H_2O$-**17**] (**B**) determined by Gaussian 94 using the LanL2DZ basis set.

Table 7. Bond distances and angles for [M^{II}-**17**] complexes with $Zn^{II}2H_2O$ and $Cd^{II}2H_2O$ derived from molecular orbital calculations using the Gaussian 94 LanL2DZ basis set.

Distance (pm)	$Zn^{II}2H_2O$	$Cd^{II}2H_2O$	Δ ($M^{II}2H_2O$)
M^{II}-O1	215.892	232.402	16.51
M^{II}-O2	214.267	232.091	17.824
M^{II}-O3	226.154	238.109	11.955
M^{II}-N1	220.081	238.452	18.371
M^{II}-N2	217.277	236.370	19.093
M^{II}-N3	220.232	239.804	19.572
Angle ϕ (deg)			
Twist angle O1	15.206	12.139	-3.068

The globalised minimum energies for the [M^{II}-**17**] complexes Zn^{II}-$2H_2O$ and Cd^{II}-$2H_2O$ are -767.248259 and -750.256292 Hartrees, respectively (1 Hartree = 2617.13 kJ mol^{-1}).

3.5. Summary

Potentiometry and *ab initio* calculations have been used to provide complementary information on the relative acid/base and metal binding properties of the three pendant arm ligands, hec[9], bhec[9] and thec[9].

The pK_a's of each ligand in aqueous solution were determined by potentiometric titration and appear in Table 1. The pendant arms were found to have both a positive and negative effect on amine basicity depending on the number of attached pendant arms and the level of amine protonation. The electron withdrawing nature of the hydroxyethyl groups serves to lower the basicity of the amine donors, however, the pendant arm may also raise the pK_a value by increasing the electron density within the ring cavity. *Ab initio* calculations of the triply protonated one and two-arm ligands show that the hydroxyethyl arms may also stabilise the protonation process by forming intramolecular hydrogen bonds with ammonium protons.

The stability constants, K, of hec[9] and bhec[9] with Zn^{II} and Cd^{II} were also determined by potentiometric titration and appear in Table 2. Comparison between the stability constants of [9]aneN_3 and the three functionalised derivatives reveal that the hydroxyethyl pendant arms may either lower or raise the overall complex stability. The one-arm ligand complexes were found to be less stable than complexes of [9]aneN_3 which is probably due to the combined effects of steric strain caused by the formation of a five-membered chelate and the inductive withdrawing nature of the pendant arm. When a second and third pendant arm was attached to [9]aneN_3 a step-wise increase in stability was observed.

Each ligand was found to bind Zn^{II} ion with greater affinity than Cd^{II} ion. Complementary *ab initio* calculations showed the smaller Zn^{II} ion to be better accommodated in the binding cavity of each functionalised ligand. Metal-ligand bond distances were consistently shorter in the Zn^{II} models and the Zn^{II} ion was shown to sit deeper in the donor cavity. Depending on the number of pendant arms and degree of solvation, the metal ions were found to exist in either distorted tetrahedral, trigonal bipyramidal or trigonal prismatic environments.

Chapter 4. Kinetic Studies of 4-Nitrophenyl Acetate Hydrolysis

4.1. Introduction

Transition metal complexes are widely used in the design of bioinorganic enzyme models, particularly in relation to mimicking the catalytic activity of metalloproteinases and metallophosphoesterases. Kimura's [Zn^{II}-**15**] complex is considered a model for alkaline phosphatase, AP, as the Zn^{II}-RO^- alkoxide has a pK_a of 7.1, which is almost identical to the serine alkoxide anion in AP, Scheme 12, page 20. The [Zn^{II}-**15**] complex catalyses 4-nitrophenyl acetate hydrolysis in a mechanism that is thought to mirror the hydrolysis of phosphomonoesters by AP where the Zn^{II}-RO^- species acts as a direct nucleophile towards the ester substrate, Scheme 13, page 20.

Kimura's mechanism for the hydrolysis of 4-nitrophenyl acetate by [Zn^{II}-**15**] remains questionable. A recent study on the Zn^{II} complex of [12]aneN_3 challenges the role of the Zn^{II}-bound alkoxide or water molecule in the hydrolysis reaction.[178] The cleavage mechanism may proceed through two kinetically equivalent pathways. One possibility is that a Zn^{II} bound water molecule acts as a direct nucleophile towards the ester carbonyl group in a mechanism similar to that proposed by Kimura, pathway **A**, Figure 44. Alternatively, the ester carbonyl group first coordinates the Zn^{II} centre before it is attacked by a hydroxide ion, pathway **B**.

A **B**

Figure 44

A rigorous mechanistic analysis, recently published by Suh, using the Zn^{II} complex of [12]aneN_3 suggests that pathway **B** is the most likely.[178] There are in fact three possible mechanisms for ester cleavage based on pathways **A** and **B** shown in Figure 44. The first mechanism, **1**, in Figure 45 is identical to Kimura's and involves a direct nucleophilic attack by the Zn^{II}-bound water molecule to the carbonyl centre of the ester group. The second and third mechanisms, **2** and **3**, are based on pathway **B** where the carbonyl oxygen group first binds to the coordinated Zn^{II} ion. The Zn^{II} acts as a Lewis acid and polarises the carbonyl

bond, making it more susceptible to nucleophilic attack. In mechanism **2**, the activated ester is then hydrolysed by a Zn^{II}-bound water molecule and in mechanism **3** it is hydrolysed by a free water or hydroxide ion in solution, Figure 45.

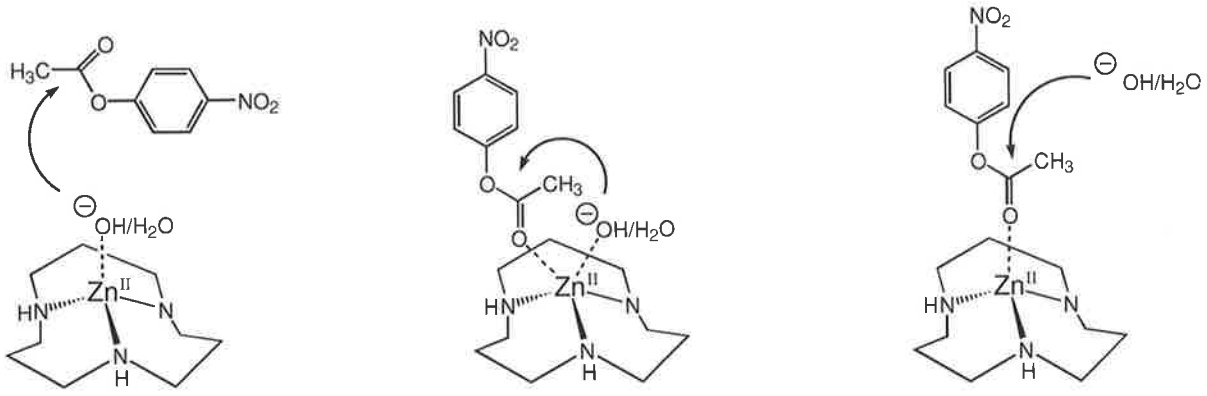

1 **2** **3**

Figure 45

The kinetic data obtained by Suh[178] was incompatible with a mechanism where Zn^{II}-bound water or hydroxide ion acts as a nucleophile towards the ester carbonyl group. The nucleophilicity of oxygen bases is directly related to their basicity and the Zn^{II} bound water and hydroxide ion differ markedly in basicity. The [Zn^{II}-**L**]-OH^- species of the [12]aneN$_3$ (= **L**) complex was 10^9-fold more basic than water, which in turn is more basic than the [Zn^{II}-**L**]-H_2O species. Mechanisms **1** and **2** assume comparable reactivities between the Zn^{II} bound water and hydroxide ion species towards the ester carbonyl so that the rate constants k_1 and k_2 would be equal, Scheme 30.

Mechanism 1

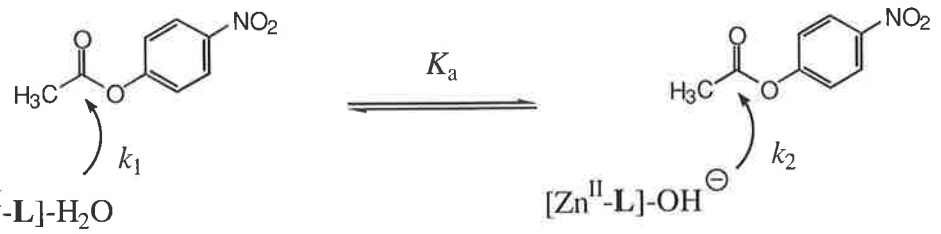

Mechanism 2

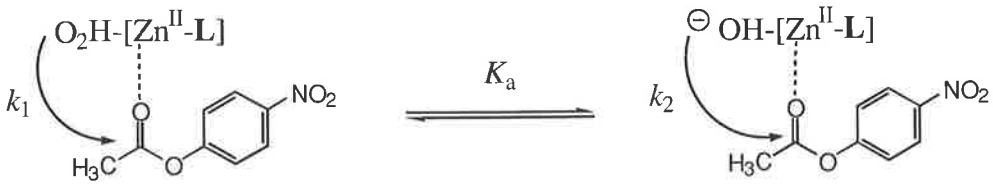

Scheme 30

The large difference in basicity between the [Zn^{II}-**L**]-OH^- and [Zn^{II}-**L**]-H_2O species, however, suggests that k_2 should be approximately 10^7 times greater then k_1, which is inconsistent with either mechanism **1** or **2**. Mechanism **3**, where a nucleophilic water molecule or hydroxide ion from solution attacks the activated ester carbonyl group, as shown in Figure 45, remains the most feasible alternative. This mechanism directly opposes Kimura's idea that the Zn^{II}-bound hydroxyl or alkoxide ion is responsible for the ester hydrolysis. It appears that the catalytic activity of the Zn^{II} complexes is related to their ability to coordinate the ester molecule rather than the nucleophilicity of the bound water molecule.

It was initially the intention of this work to further investigate the importance of ester coordination in the hydrolysis reaction by measuring the catalytic activity of the Zn^{II} complexes of hec[9], **17**, bhec[9], **18** and thec[9], **19**. The three ligands surround the Zn^{II} ion in unique coordination environments where the degree of chelation increases with each additional pendant arm. As the extent of pendant arm chelation increases, the probability of 4-nitrophenyl acetate coordinating the Zn^{II} centre in each complex is expected to decrease. The probability of nucleophilic attack by the carbonyl oxygen of 4-nitrophenyl acetate towards the Zn^{II} centre is statistically greater in the hec[9], **17**, complex, and subsequently, the incidence of hydrolysis would also be greater. Thec[9], **19**, surrounds the Zn^{II} ion in a six-coordinate environment that discourages 4-nitrophenyl acetate coordination and a significantly lower rate constant would be expected if ester coordination was the criteria for hydrolysis.

4.2. Measuring Reaction Rates

The first ligand system studied was hec[9], **17**, as it was anticipated that [Zn^{II}-**17**] would display the largest rate constant of the three ligand-metal complexes.

In order to establish the rate constant of 4-nitrophenyl acetate hydrolysis by [Zn^{II}-**17**], it was important to choose an appropriate pH buffer system that would provide a relatively high concentration of the desired [Zn^{II}-**17**] alkoxide species whilst maintaining a relatively low level of spontaneous 4-nitrophenyl acetate hydrolysis. A borate buffer (0.1 mol dm^{-3}, pH 9.2) was chosen to coincide with the pH conditions used by Kimura for studying [Zn^{II}-**15**]. However, due to the difference in acidity between [Zn^{II}-**17**] (pK_a = 8.5) and [Zn^{II}-**15**] (pK_a =

7.4), the deprotonated alkoxide species of [Zn^{II}-**17**] exists in a relative concentration of only 68% compared with 100% for [Zn^{II}-**15**]. A higher pH solution could not be used as it would substantially increase the rate of the spontaneous reaction and cause precipitation of zinc hydroxide from the solution.

Hydrolysis reactions are generally followed by a change in the optical properties of the substrate such as increased light absorption, fluorescence or rotation. Although [Zn^{II}-**15**] is a potential alkaline phosphatase model, phosphomonoesters such as 4-nitrophenyl phosphate are seldom used for kinetic studies as they undergo extremely slow hydrolysis. A more commonly used ester is 4-nitrophenyl acetate, which gives a large absorbance change upon hydrolysis. Cleavage of 4-nitrophenyl acetate produces 4-nitrophenol that deprotonates under basic conditions to give a bright yellow 4-nitrophenolate anion that absorbs strongly at 400 nm, Scheme 31. All hydrolysis reactions were followed spectrophotometrically by the appearance of 4-nitrophenolate between 350 and 450 nm at 2 nm increments over time.

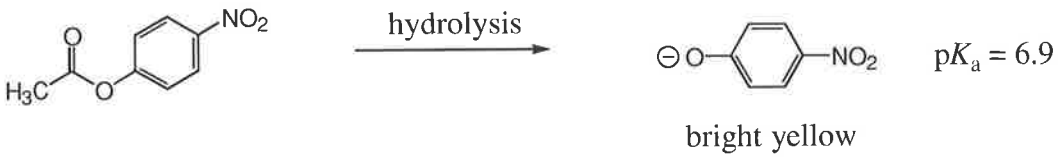

Scheme 31

During the course of reaction between [Zn^{II}-**17**] and 4-nitrophenyl acetate, the concentration of 4-nitrophenyl acetate decreased exponentially with time whilst that of 4-nitrophenolate increased, Figure 46**A**. The observed hydrolysis rate constant, k_{obs}, was obtained by fitting the first order rate equation, $A_\infty - A_t = A_\infty . e^{-kt}$ to the variation of absorbance with time, A_t, where A_∞ is the absorbance at infinite time. A plot of $\ln(A_\infty - A_t)$ against time gave a straight line with the slope equal to the observed rate, k_{obs}, Figure 46**B**.

The corrected rate constant, k_{obs}-k_o, was then obtained by subtracting the rate of the spontaneous reaction, k_o, of 4-nitrophenyl acetate in solution from the observed rate, k_{obs}, where the [Zn^{II}-**17**] complex was present.

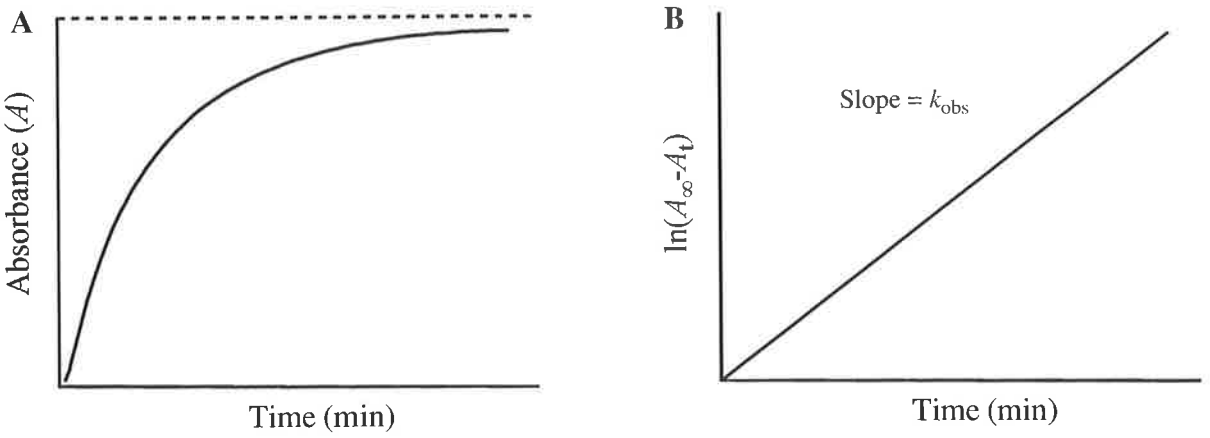

Figure 46

In all cases, the concentration of [Zn^{II}-**17**] was at least 50 fold greater than that of 4-nitrophenyl acetate. The variation of k_{obs}-k_o with [Zn^{II}-**17**] concentration was found to be linear where the coefficient (k_{obs}-k_o)/[[Zn^{II}-**17**]] was equal to the specific rate constant, k_{NA}, for the hydrolysis of 4-nitrophenyl acetate in the presence of [Zn^{II}-**17**], Figure 47**A**.

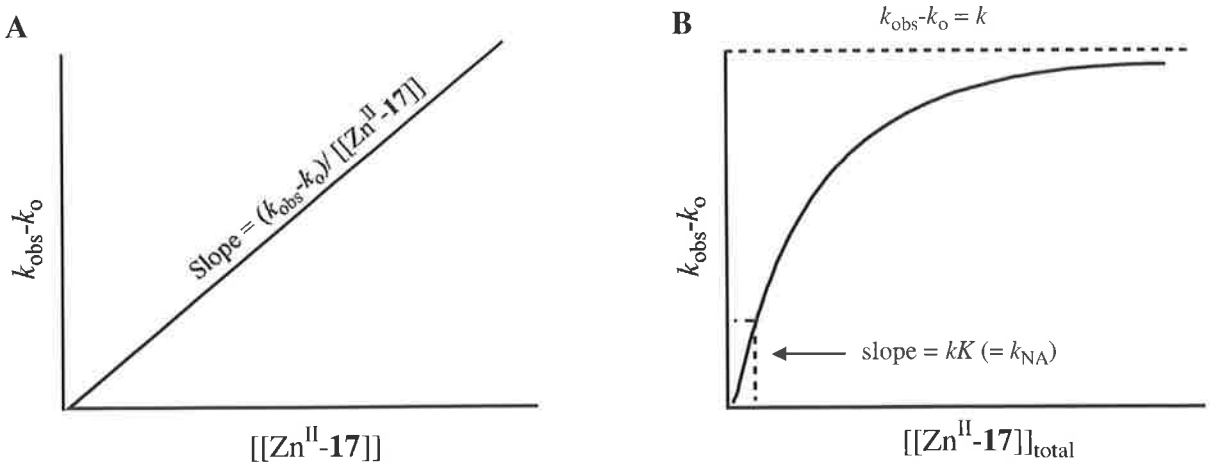

Figure 47

If the hydrolysis process occurs through a Michaelis-Menten mechanism as depicted in equation 4.4, the variation of k_{obs}-k_o with [Zn^{II}-**17**] concentration would resemble Figure 47**B**.

$$[Zn^{II}\text{-}17] + \text{4-nitrophenyl acetate} \underset{\text{fast}}{\overset{K}{\rightleftharpoons}} \underset{\textbf{Michaelis-Menten complex}}{([Zn^{II}\text{-}17]\text{-4-nitrophenyl acetate})} \xrightarrow[\text{slow}]{k} [Zn^{II}\text{-}17] + \text{4-nitrophenolate} + \text{acetate} + H^+ \quad (4.4)$$

Under a Michaelis-Menten mechanism, the rate equation 4.5 would apply,

$$k_{obs}\text{-}k_o = \frac{kK[[Zn^{II}\text{-}\mathbf{17}]]}{1+K[[Zn^{II}\text{-}\mathbf{17}]]} \qquad (4.5)$$

where $[[Zn^{II}\text{-}\mathbf{17}]]$ is in excess over [4-nitrophenyl acetate] and is equal to $[[Zn^{II}\text{-}\mathbf{17}]]_{total}$.

As only a linear variation of $k_{obs}\text{-}k_o$ with $[[Zn^{II}\text{-}\mathbf{17}]]_{total}$ was observed, the hydrolysis reaction occurs either under the limiting conditions, $K[[Zn^{II}\text{-}\mathbf{17}]] << 1$, of a Michaelis-Menten mechanism where the concentration of the Michaelis-Menten complex is extremely low such that $k_{obs}\text{-}k_o = kK[[Zn^{II}\text{-}\mathbf{17}]] \approx k_{NA}[[Zn^{II}\text{-}\mathbf{17}]]_{total}$, or by a simple bimolecular mechanism as depicted in equation 4.6,

$$[Zn^{II}\text{-}\mathbf{17}] + \text{4-nitrophenyl acetate} \xrightarrow{k'} [Zn^{II}\text{-}\mathbf{17}] + \text{4-nitrophenolate} + \text{acetate} + H^+ \qquad (4.6)$$

where k' is the second order rate constant.

It was not possible to distinguish between these mechanisms in the studies that follow, and k_{NA} is used to indicate the slope $(k_{obs}\text{-}k_o)/[\mathbf{17}]$ or $(k_{obs}\text{-}k_o)/[Zn^{II}\text{-}\mathbf{17}]$ throughout.

4.3. Determination of the Rate Constant for 4-Nitrophenyl Acetate Hydrolysis by Hec[9]

Before investigating the catalytic activity of $[Zn^{II}\text{-}\mathbf{17}]$, the reaction between hec[9], **17**, and 4-nitrophenyl acetate was examined to establish the effect of the amine nitrogens on the rate of 4-nitrophenyl acetate hydrolysis. The reaction between uncomplexed Zn^{II} and 4-nitrophenyl acetate could not be examined due to the immediate precipitation of Zn^{II} hydroxide in the pH 9.2 buffer.

Solutions containing hec[9] were prepared by dissolving the appropriate weight of hec[9].2HBr in buffer (I = 0.1 mol dm^{-3}). Reactions were carried out by pipetting 2.0 cm^3 aliquots of the appropriate solution into a quartz cell (1 cm path length) placed in a thermostated cell block of a Diode Array spectrophotometer and the solutions were allowed to equilibrate to 298.2 ± 0.1 K for five minutes. The reaction was initiated by adding 0.02 cm^3 of

4-nitrophenyl acetate in acetonitrile (10^{-3} mol dm^{-3}) to the quartz cell with immediate mixing and the increase in absorbance between 350-450 nm against time was recorded. Each reaction was performed at least three times with the rate constants from each run varying by less than 4% and the results were averaged. The yellow 4-nitrophenolate produced in the hydrolysis reaction was found to absorb most strongly at 400 nm over the 350-450 nm range and the rate constants obtained at 400 nm were chosen for analysis, Figure 48.

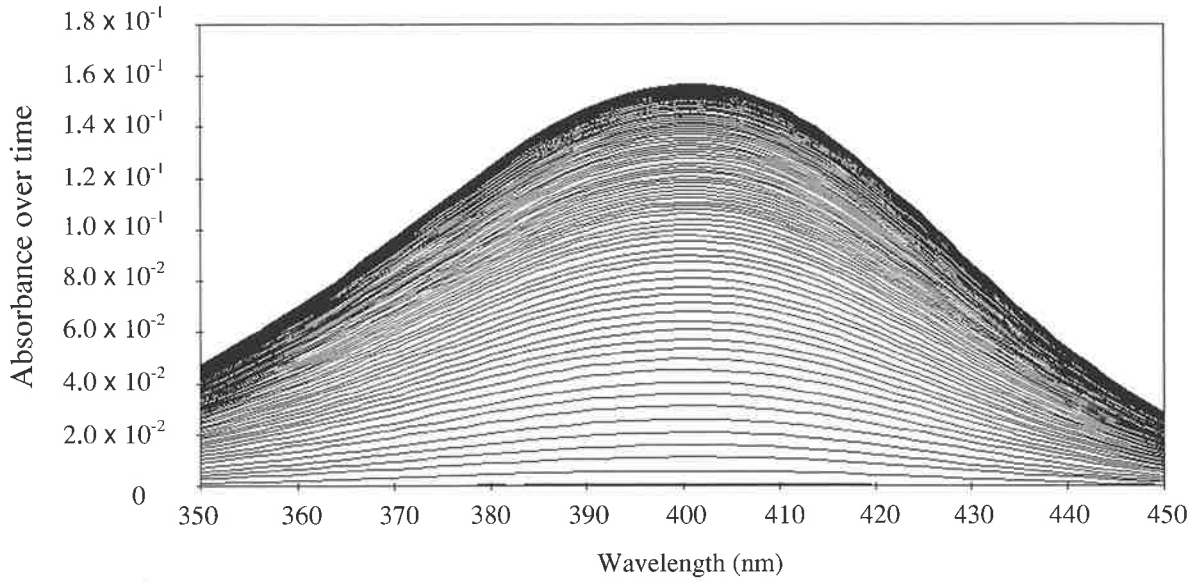

Figure 48. The increase in absorbance of 4-nitrophenolate between 350 and 450 nm over time at 30 second interval scans.

Each reaction exhibited pseudo-first order kinetics when monitored through at least seven half-lives as determined by the variation in absorbance as a function of time, Figure 49. The rate of spontaneous reaction, k_o, of 4-nitrophenyl acetate by the buffer was determined by performing the reaction in the absence of hec[9] and was found to be (5.2 ± 0.19) x 10^{-6} s^{-1} at 400 nm. The rate constants, k_{obs}-k_o, for each hec[9] solution were obtained by subtracting the spontaneous rate, k_o, from the observed rates, k_{obs}.

The rate constant, k_{NA}, for hec[9] in buffer was determined by following the rate of hydrolysis of 4-nitrophenyl acetate (10^{-5} mol dm^{-3}) at varying concentrations of hec[9] [(0.5 - 5) x 10^{-3} mol dm^{-3}] at 298.2 ± 0.1 K. k_{obs}-k_o was found to vary linearly with the concentration of hec[9]. The rate constant, k_{NA}, was obtained from the slope of the line of k_{obs}-k_o against varying concentration and was found to be (6.64 ± 0.16) x 10^{-3} s^{-1} mol^{-1} dm^3 at 400 nm, Figure 50.

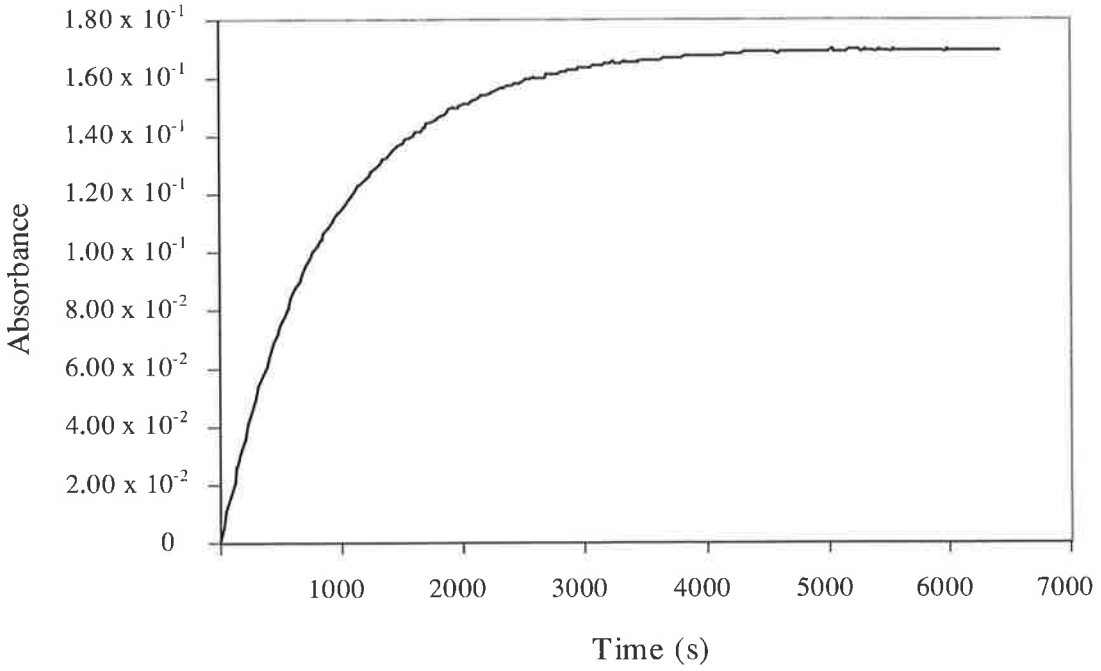

Figure 49. A typical plot of absorbance versus time for the hydrolysis of 4-nitrophenyl acetate in borate buffer (0.1 mol dm^{-3}, I = 0.10, pH 9.2) at 400 nm and 298.2 ± 0.1 K.

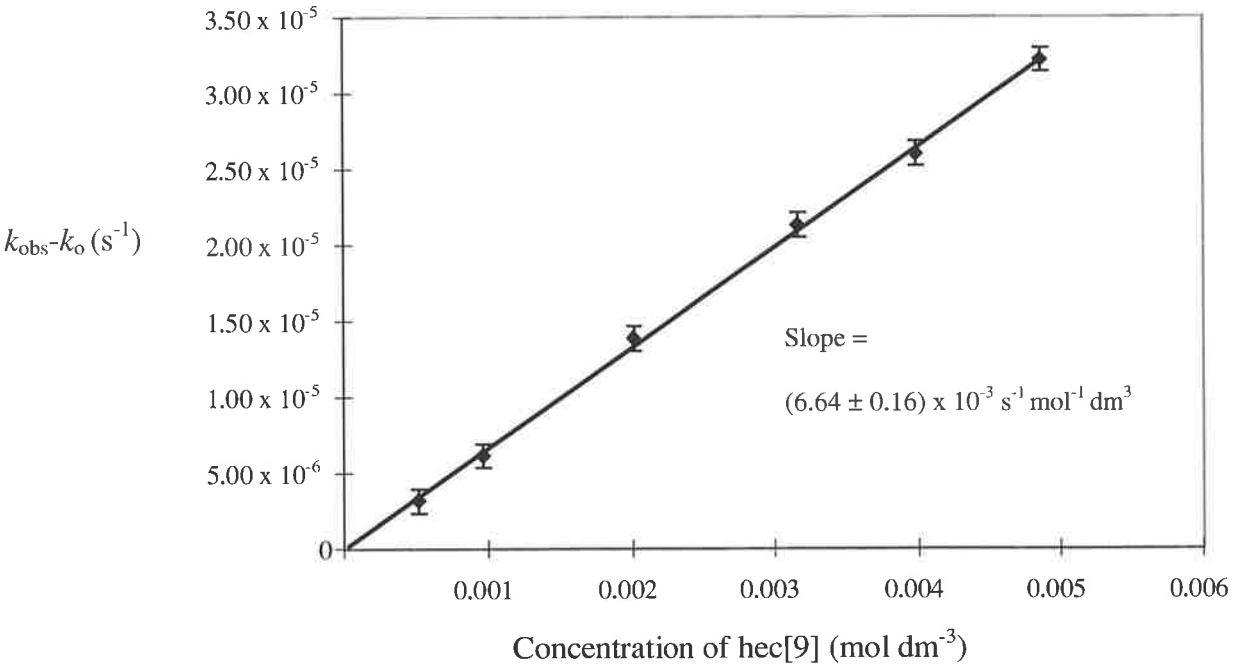

Figure 50. Dependence of k_{obs}-k_o on the concentration of hec[9] **17** at 400 nm in borate buffer (0.1 mol dm^{-3}, I = 0.10, pH 9.2) at 298.2 ± 0.1 K.

Apart from the three nucleophilic nitrogen groups in hec[9], it is conceivable that the pendant arm oxygen could attack 4-nitrophenyl acetate. To establish the identity of the product from the hydrolysis reaction, hec[9] **17** was reacted with 4-nitrophenyl acetate in dichloromethane for one hour. This produced a bright yellow solution that was chromatographed on silica gel to give a yellow oil in 49% yield, Scheme 32. NMR analysis of the product revealed an extremely complex spectra exhibiting 20 carbon resonances (16 alkyl, two methyl and two carbonyl) in the ^{13}C NMR spectrum and 18 proton resonances in the ^{1}H NMR spectrum not including amine or hydroxyl resonances. Identification of each NMR resonance was achieved by a combination of COSY, HSQC and HMBC spectral analyses and the product was identified as the amide species **45**.

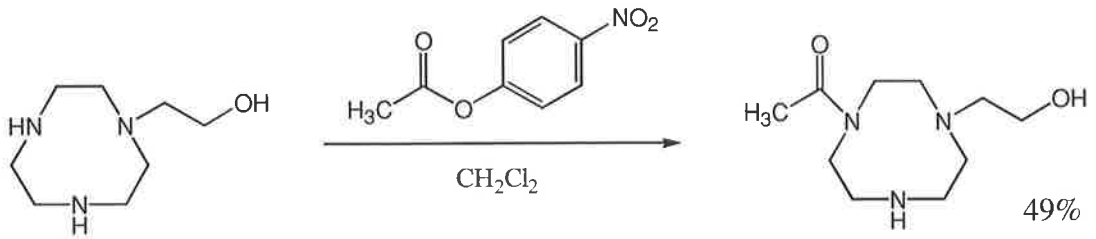

Scheme 32

The number of observed resonances in the NMR spectra is consistent with **45** existing in two unique isomeric forms due to restricted rotation about the C-N amide bond on the NMR time scale, Figure 51.

Although the reaction was performed under different conditions to the buffered aqueous reaction of hec[9] and 4-nitrophenyl acetate, the products from each reaction are expected to be the same, whereby a secondary ring nitrogen attacks the ester carbonyl group and releases 4-nitrophenolate. It is possible, however, that the primary pendant arm oxygen may compete for the ester carbonyl and form a methyl ester group. This product is susceptible to further intramolecular reaction such that the acetyl group may then be transferred from the pendant arm to the secondary ring nitrogen to give species **45**.

Whilst the identity of the reaction product was established, it remained unclear as to whether it was produced through a bimolecular mechanism or a Michaelis-Menten mechanism where the release of the acetate group from **45** is slow.

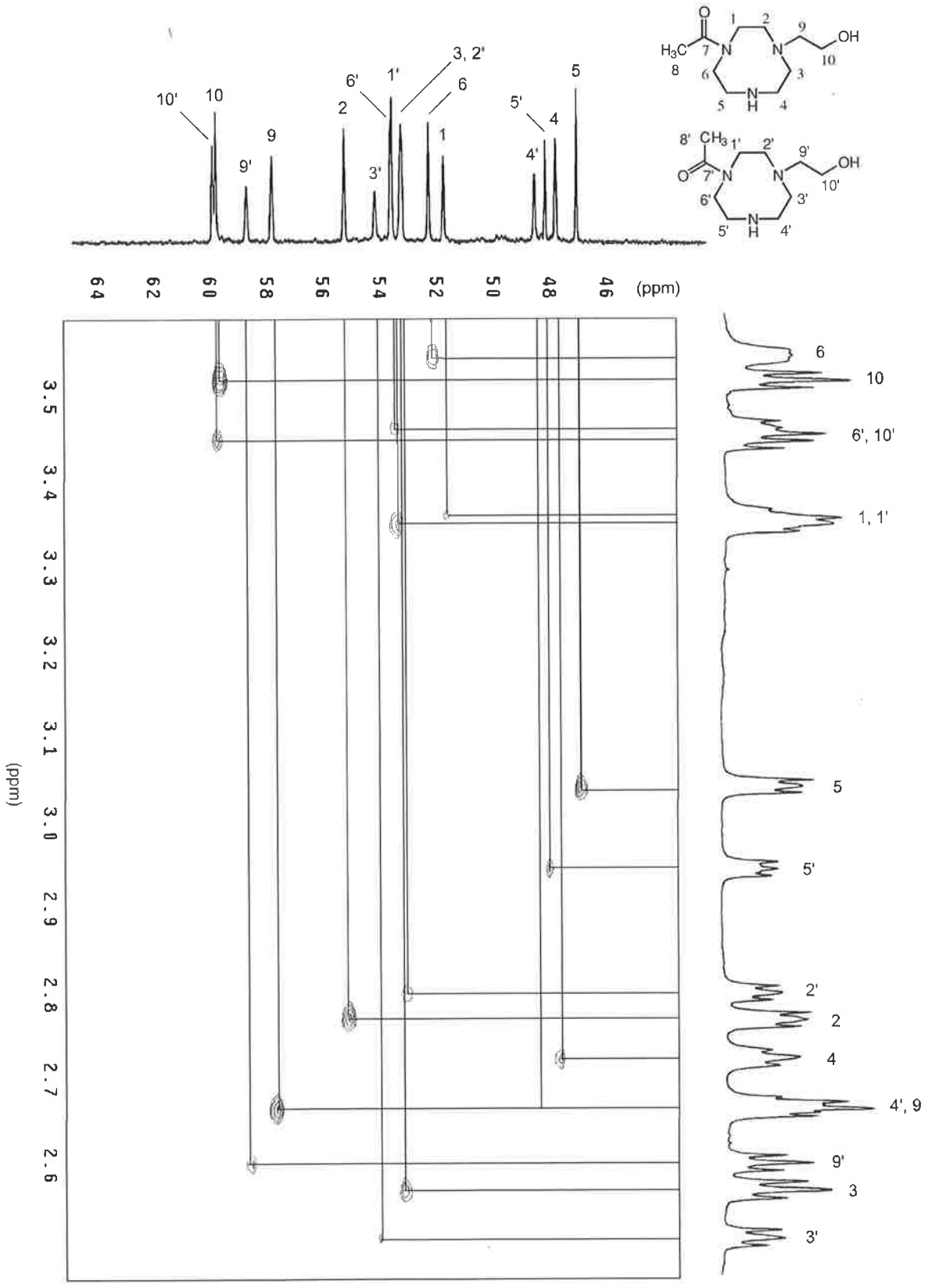

Figure 51. The 600 MHz heteronuclear single quantum coherence (HSQC) spectrum of **45** in $CDCl_3$ showing the ethylene resonances.

4.4. Determination of the Rate Constant for 4-Nitrophenyl Acetate Hydrolysis by [Zn^{II}-17]

Solutions containing [Zn^{II}-**17**] were prepared by dissolving the appropriate weight of complex in the borate buffer. The [Zn^{II}-**17**] complex was generated from an ethanolic solution containing equimolar amounts of $Zn(ClO_4)_2$ and free hec[9] and was isolated as colourless crystals. Attempts to generate the [Zn^{II}-**17**] complex in the borate buffer using $Zn(ClO_4)_2$ and free hec[9] were unsuccessful and on each occasion a white precipitate was produced. Since the [Zn^{II}-**17**] crystals freely dissolved in the buffer solution without producing a precipitate, it was assumed that the white solid formed from the addition of $Zn(ClO_4)_2$ to the hec[9]-buffer solution represented zinc hydroxide which would easily form at pH 9.2 if the rate of hec[9] complexation was appreciably slow.

The rate constant, k_{NA}, for [Zn^{II}-**17**] was determined by following the rate of hydrolysis of 4-nitrophenyl acetate (10^{-5} mol dm^{-3}) in the presence of varying concentrations of complex [(1.4 - 4.3) x 10^{-3} mol dm^{-3}] under identical conditions to the free hec[9] reaction. The rate constants, k_{obs}-k_o, were found to vary linearly with the concentration of [Zn^{II}-**17**] and appear in Figure 52 with the k_{obs}-k_o values of the hec[9] reaction for comparison.

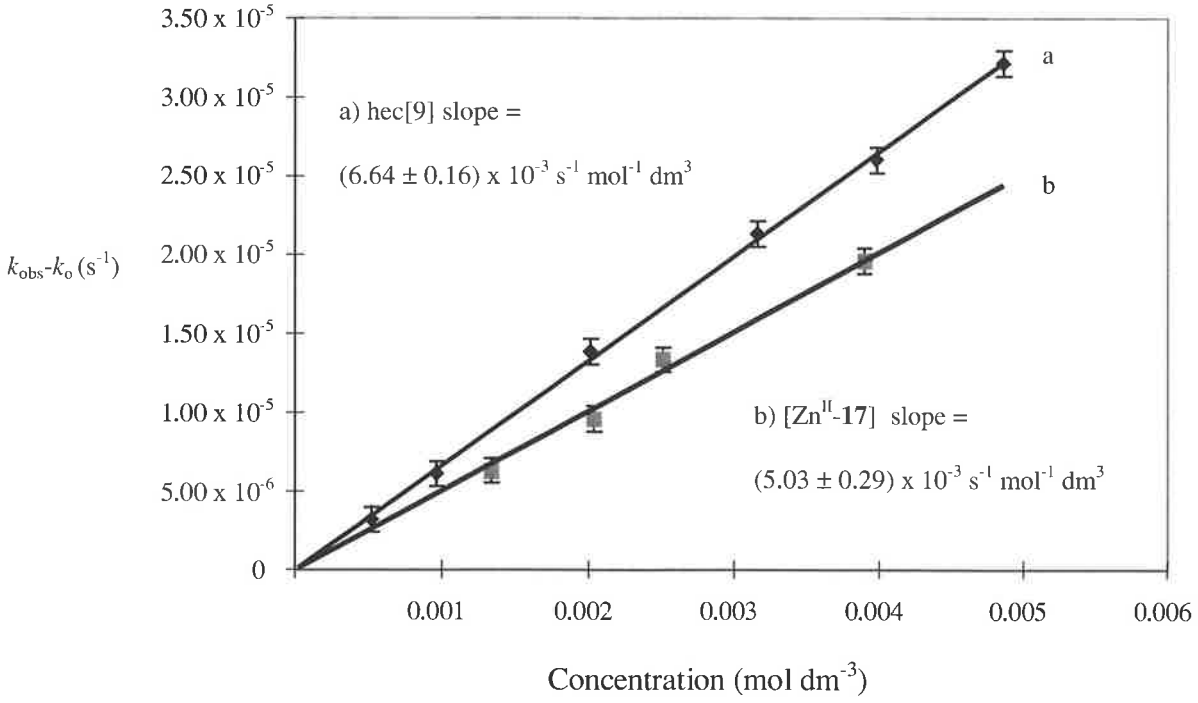

Figure 52. Dependence of k_{obs}-k_o on the concentration of hec[9] **17** and [Zn^{II}-**17**] at 400 nm in borate buffer (0.1 mol dm^{-3}, I = 0.10, pH 9.2) at 400 nm and 298.2 ± 0.1 K.

The rate constant, k_{NA}, of 4-nitrophenyl acetate hydrolysis by [Zn^{II}-**17**] was obtained from the slope of the line of k_{obs}-k_o against varying concentration and found to be (5.03 ± 0.29) x 10^{-3} s^{-1} mol^{-1} dm^3 at 400 nm. The result is quite unexpected as the rate constant of [Zn^{II}-**17**] is 32% smaller than that of hec[9]. The Zn^{II} complexes of [12]aneN$_3$ and **15** are significantly more reactive with rate constants, k_{NA}, of (2.6 ± 0.29) x 10^{-2} and (1.4 ± 0.1) x 10^{-1} s^{-1} mol^{-1} dm^3, respectively. The low rate constant of [Zn^{II}-**17**] suggests that it is a poor catalyst and is unsuitable for modelling alkaline phosphatase.

The reason for the low rate constant is unclear, although it may be a consequence of poor complexation of 4-nitrophenyl acetate to the Zn^{II} centre of [Zn^{II}-**17**]. The pK_a value of the Zn^{II}-bound alcohol or water molecule of [Zn^{II}-**17**] (pK_a = 8.5) is considerably larger than that of [Zn^{II}-**15**] (pK_a = 7.4), suggesting the Zn^{II} ion in the hec[9] complex is appreciably less acidic. Assuming a mechanism whereby 4-nitrophenyl acetate must first coordinate to the Zn^{II} centre to become activated, the rate of hydrolysis would be greater in a system where 4-nitrophenyl acetate has strong affinity for the metal ion. A weakly acidic Zn^{II} ion is soft in nature and does not favour ionic interactions with a carbonyl oxygen. An aquated Zn^{II} ion (pK_a = 9) shows no enhancement in the rate of hydrolysis in the buffered solution over the spontaneous reaction.[178]

The low rate constant observed for [Zn^{II}-**17**] suggests 4-nitrophenyl acetate has little to no affinity for the metal ion and probably represents a bimolecular reaction between the complexed ring amines and 4-nitrophenyl acetate. The lower rate constant of [Zn^{II}-**17**] compared with the free ligand reaction may be due to the reduced nucleophilicity of the complexed amine donors. Hydrolytic analyses of the Zn^{II} complexes of bhec[9] and thec[9] against 4-nitrophenyl acetate were not attempted.

4.5. Summary

The smaller ring size of [9]aneN$_3$ does not render the Zn^{II} ion of [Zn^{II}-**17**] as acidic as that of Kimura's [Zn^{II}-**15**] complex and as a consequence [Zn^{II}-**17**] is less likely to coordinate 4-nitrophenyl acetate. Although the low rate constant of [Zn^{II}-**17**] was disappointing, the result

does support Suh's mechanism which suggests that initial Zn^{II}-ester coordination is necessary for metal-ligand mediated catalysis.

Many new enzyme mimics are becoming increasingly more sophisticated than Kimura's [Zn^{II}-**15**] model. A good model should not only display comparable esterase activity to the enzyme of interest but also pay considerable attention to the microstructural environment within the active site. Many subtle steric and electronic interactions within the active centre are responsible for maintaining substrate selectivity, metal acidity and controlled inhibition.

Attention is now shifting to the design of more realistic models that not only attempt to mimic the restricted environment of an active site but can also operate under physiological conditions rather than in artificial buffered solutions. Valeur and Bardez[94] have developed a new carbonic anhydrase model using reverse micelles. By attaching three imidazole moieties to anionic surfactants through a Zn^{II} counter ion, a micellar core similar to the active site of carbonic anhydrase is produced. In apolar solvents, the amphipathic surfactant molecules form reverse micelles were the polar heads form a central core containing the Zn^{II}-imidazole complex **46** and several water molecules, Figure 53. Analysis by absorbance and fluorescence spectroscopy shows the micelle aggregate has strong hydrolytic activity towards esters in the restricted core space and represents a new direction in the design of enzyme models.

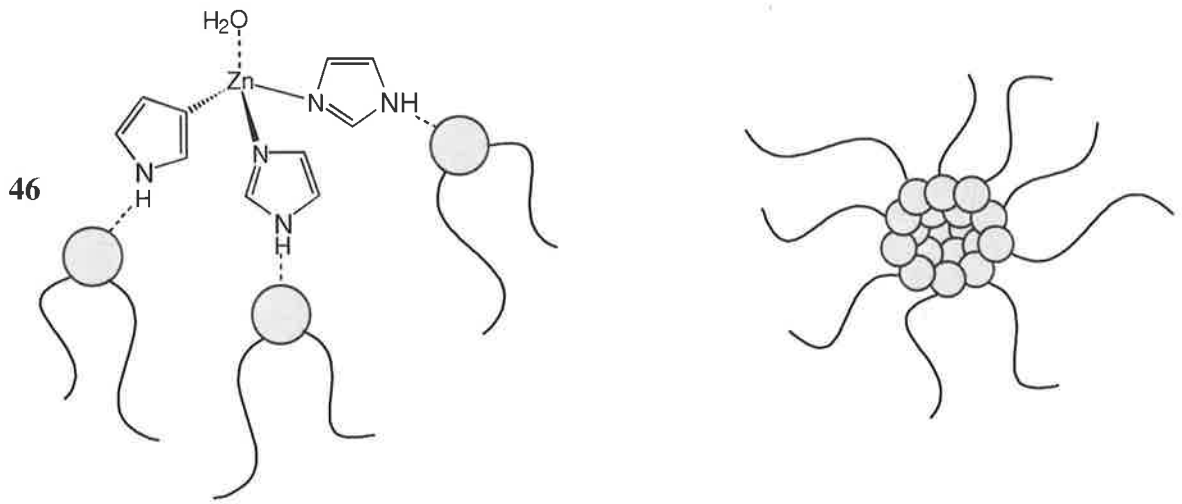

Figure 53. A model for carbonic anhydrase using reverse micelles.

Chapter 5. Syntheses Towards the Isolation of a Zinc Finger Model.

5.1. Introduction

The fifth chapter of this thesis is concerned with the design of a preliminary synthetic strategy for the isolation of a novel zinc finger model. As part of an ongoing project, some initial groundwork has been performed to help identify the most effective synthetic method for attaching a single long pendant arm on [9]aneN$_3$ and to eliminate other unsuccessful methods.

A Class 1 zinc finger contains two histidine and two cysteine residues separated by a polypeptide chain that fold back on one another to coordinate a single Zn^{II} ion, Figure 54A. The intention of this ongoing project is to create a simplified model of the zinc finger loop structure using a [9]aneN$_3$ macrocycle substituted with a single, long pendant arm containing an amino acid functional group. When a Zn^{II} ion is coordinated in the macrocyclic cavity it is anticipated that the pendant arm will fold back and become coordinated to the metal centre through the primary amino acid group, Figure 54B.

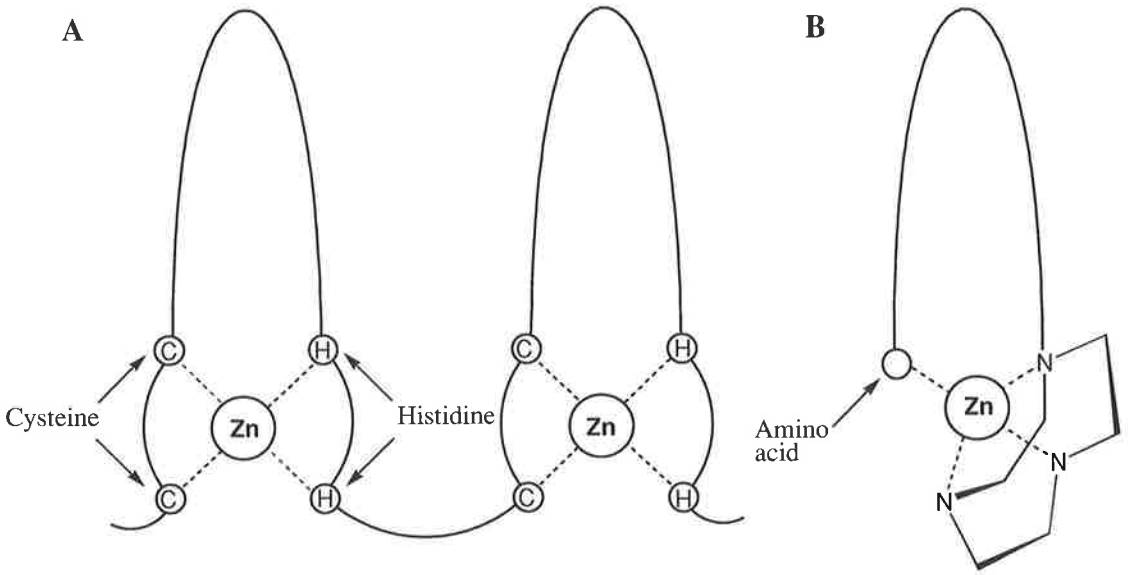

Figure 54. A basic zinc finger model based on a Class 1 zinc finger mini-domain.

The size of the chelate ring that is formed by the coordinating pendant arm is an important consideration in the design of the model and will contribute to the overall stability of the complex. A five-membered chelate ring represents the most stable ring system as it imposes the least amount of steric strain. As the atom number of the chelate ring increases to a six- and seven-membered ring, however, the amount of strain increases and the stability of

the overall complex decreases. An eight- and nine-membered chelate ring is unlikely to form at all and the pendant arm will prefer to remain uncoordinated. However, as the length of the pendant arm continues to grow, it becomes increasingly more floppy and the chance of it folding back towards the metal centre increases. It is envisaged that an amino acid pendant arm of appropriate length will fold back and coordinate the Zn^{II} centre of the [9]aneN_3 complex and mimic the loop structure seen in a Class 1 zinc finger.

5.2. Zinc Finger Design

The most important consideration in reproducing the zinc finger loop is the length of the pendant arm. In the first instance, the synthesis of a relatively small model containing a five-carbon alkyl chain substituted with a single amino acid (e.g. histidine) was attempted. Once an effective synthetic procedure has been established it is hoped that other larger and more complex systems can be built. The predominant aim is to isolate more sophisticated models that contain polypeptide moieties in the pendant arm with various coordinating groups to surround the Zn^{II} ion in different coordination environments, Figure 55.

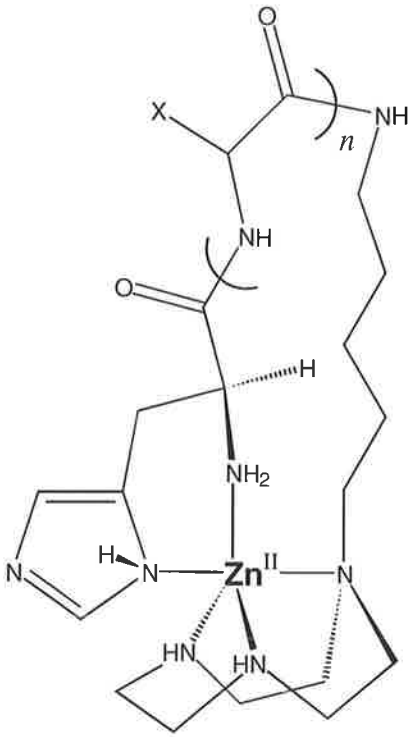

x = unspecified amino acid functional groups(s)

n = 0, 1, 2, 3, etc

Figure 55

Formation of a basic model containing a single primary amino acid requires two major synthetic steps. With regard to the retrosynthetic pathway shown in Scheme 33, the initial concern is the attachment of a single alkyl linker arm to the [9]aneN_3 macrocycle. The alkyl pendant arm should posses an appropriate functional group, such as a primary amine, to allow the attachment of the amino acid group. 5-Aminopentanol, **47**, was chosen as a potential linker arm over a simpler two-carbon arm to avoid problems of pendant arm chelation with the Zn^{II} centre. Although the mono-acid **31** (Scheme 21, page 45) described in Chapter 2 may represent a possible starting point for the attachment of amino acids, the carbonyl group is expected to coordinate the Zn^{II} ion in a five-membered chelate ring that would hinder the coordination of the primary amino acid at the end of the linker arm. By including a five-carbon alkyl chain in the linker arm, the coordination of functional groups in the linker region to the Zn^{II} centre is less favourable, as this would give an unstable eight or nine-membered chelate ring. The second step in the zinc finger synthesis involves the attachment of a primary amino acid group to the single pendant arm ligand **48**. This may be achieved by 1,3-dicyclohexylcarbodiimide (DCC) coupling of the linker arm to an appropriately protected amino acid group, Scheme 33.

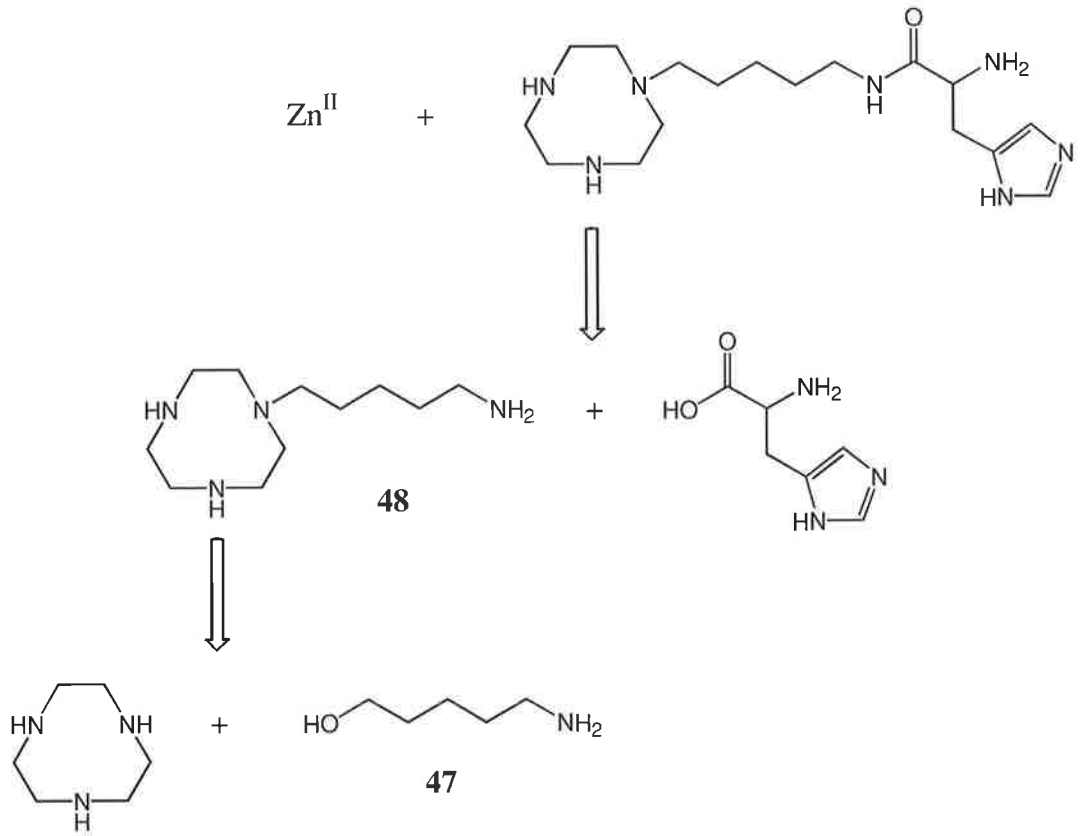

Scheme 33. Retrosynthetic analysis of the simple zinc finger model.

5.3. Syntheses Towards the Attachment of a Single Linker Arm to [9]aneN$_3$

The attachment of a single linker arm to [9]aneN$_3$ raises the immediate problem of selective alkylation. Both the bridged macrocycle **6** and novel di-protected species **37** are possible substrates for achieving mono-alkylation and the application of both compounds was investigated.

In order to achieve alkylation, the first task was to protect the primary amine group of **47** and convert the alcohol to an appropriate leaving group. The initial approach involved protecting the nitrogen with a Boc group and converting the alcohol to a tosylate.

Reaction of **47** with Boc-ON in chloroform for four hours gave a pale yellow oil that was purified by flash column chromatography to give the Boc protected species **49** in 88% yield, Scheme 34a. The product was easily identified by the presence of the *t*butyl group in the ^{1}H NMR spectrum giving a large singlet at δ 1.44 ppm and a carbonyl absorbance at 1693 cm^{-1} in the infrared spectrum.

The alcohol group of **49** was then converted to a tosyl leaving group by treatment with tosyl chloride in dichloromethane over three days. Following purification by flash column chromatography, the Boc protected tosylate **50** was isolated as a viscous oil, Scheme 34b. The product was characterised by the appearance of an aromatic methyl and benzyl resonances in the ^{13}C NMR spectrum and a base peak at *m/z* 358 in the FAB mass spectrum.

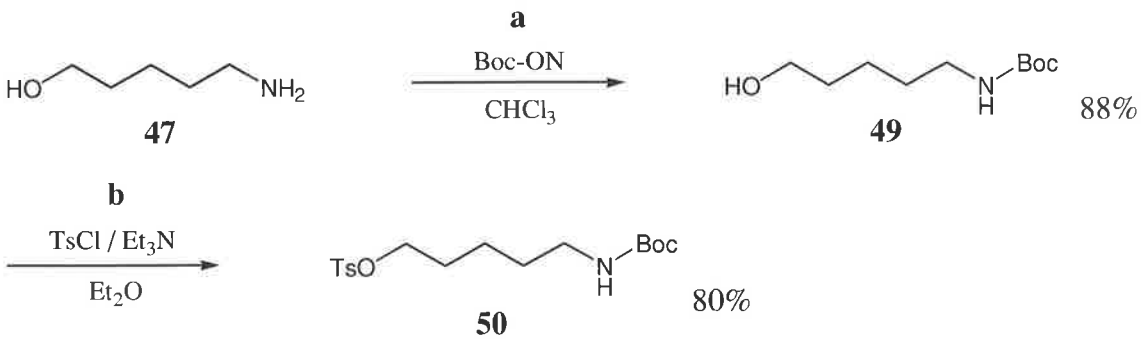

Scheme 34

The attachment of **50** to [9]aneN$_3$ was initially attempted using the bridged macrocycle **6**. It was envisaged that a mono-alkylated intermediate could be generated that would lead to the single arm macrocycle **48** upon hydrolytic cleavage of the bridging ring and removal of the Boc protecting group.

The tosylate **50** and bridged macrocycle **6** were mixed in ether and allowed to stir for three days at room temperature. At the end of this time, however, no precipitate had formed and TLC analysis revealed only starting material, Scheme 35.

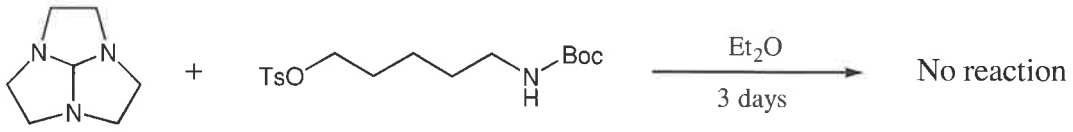

6 **50**

Scheme 35

The tosyl group was clearly unsuitable for reaction with **6** and attention was then directed towards attaching a halide leaving group, which is more commonly used in reactions with **6**. Generally, alkylation reactions with **6** are performed with highly active α-bromo carbonyl or aryl-bromo alkylating agents, however, there are examples of successful alkylation reactions with non-activated alkyl bromides.[81,82] It was hoped that a suitably protected bromide linker arm would react with the bridged macrocycle **6** to give a charged intermediate that, following acid hydrolysis, would lead to the mono-alkylated amine **48**, Scheme 36.

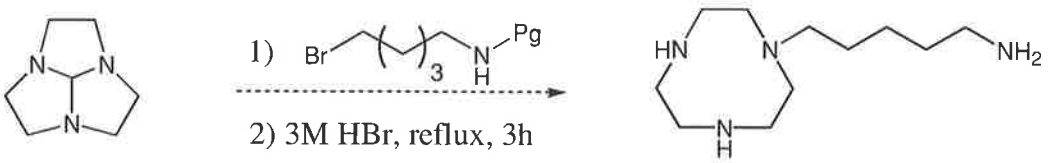

6 **48**

Scheme 36

In the first instance, bromination of the Boc protected alcohol **49** was attempted using lithium bromide and trimethyl silylchloride under refluxing conditions. The Boc protecting group, however, was unstable in the presence of trimethyl silylchloride and after aqueous work-up no product was obtained.

An alternative method for brominating alcohol groups involves the use of 1,2-bis(diphenylphosphino)ethane (DIPHOS) with bromine. Treatment of **49** with DIPHOS/Br_2 at room temperature followed by squat column chromatography gave a white crystalline solid with a melting point of 99-101°C. Analysis of the product by mass spectrometry and ^{13}C

NMR spectroscopy suggested a high molecular weight compound that had lost the Boc protecting group. The mass spectrum confirmed the presence of a bromine compound showing two molecular ion peaks at *m/z* 359 and 357 although the ^{13}C NMR revealed only five ethylene resonances and a single carbonyl resonance at δ 156 ppm. The spectral data was consistent with the formation of the bromo urea **51** where a free amine has coupled with a partially degraded Boc group from another molecule, Scheme 37. Although DIPHOS/Br_2 had replaced the hydroxyl group with a bromine group, the Boc group was unstable under the reaction conditions and an alternative protecting group was needed.

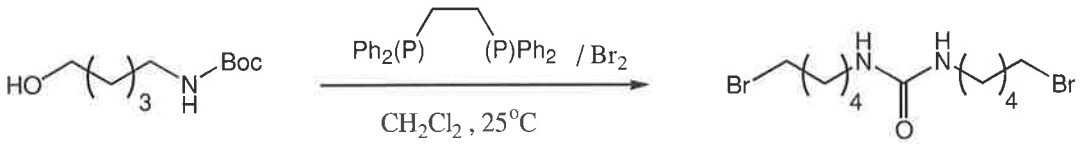

49 **51**

Scheme 37

The suitability of *N*-benzylcarbonyl and *N*-trityl protecting groups in the bromination reaction was then investigated. The addition of a *N*-benzylcarbonyl protecting group was achieved by reacting **47** with 2-(benzyloxycarbonyloxyimino)-2-phenylacetonitrile (Z-ON) in chloroform for four hours. Purification by flash column chromatography gave the Z-protected alcohol **52** in 90% as a clear colourless oil, Scheme 38a. The product was identified by the appearance of a carbonyl absorbance at 1683 cm^{-1} in the infrared spectrum a base peak at *m/z* 236 in the mass spectrum.

Bromination of the alcohol group was attempted by treating **52** with DIPHOS/Br_2 under standard conditions. Subsequent purification of the product by flash column chromatography then gave the Z-protected bromine species **53** as a colourless oil in a low 16% yield, Scheme 38b. The brominated product was distinguished from **52** by two molecular ion peaks at *m/z* 301 and 299 in the mass spectrum and a substantial increase in the R_f value by TLC analysis. The major product in the bromination reaction was benzyl bromide, which was isolated as a non-polar liquid that displayed two molecular ion peaks at *m/z* 171 and 169 in the mass spectrum. The *N*-benzylcarbonyl group proved unstable under the bromination conditions forming benzyl bromide through the nucleophilic attack of bromide anion.

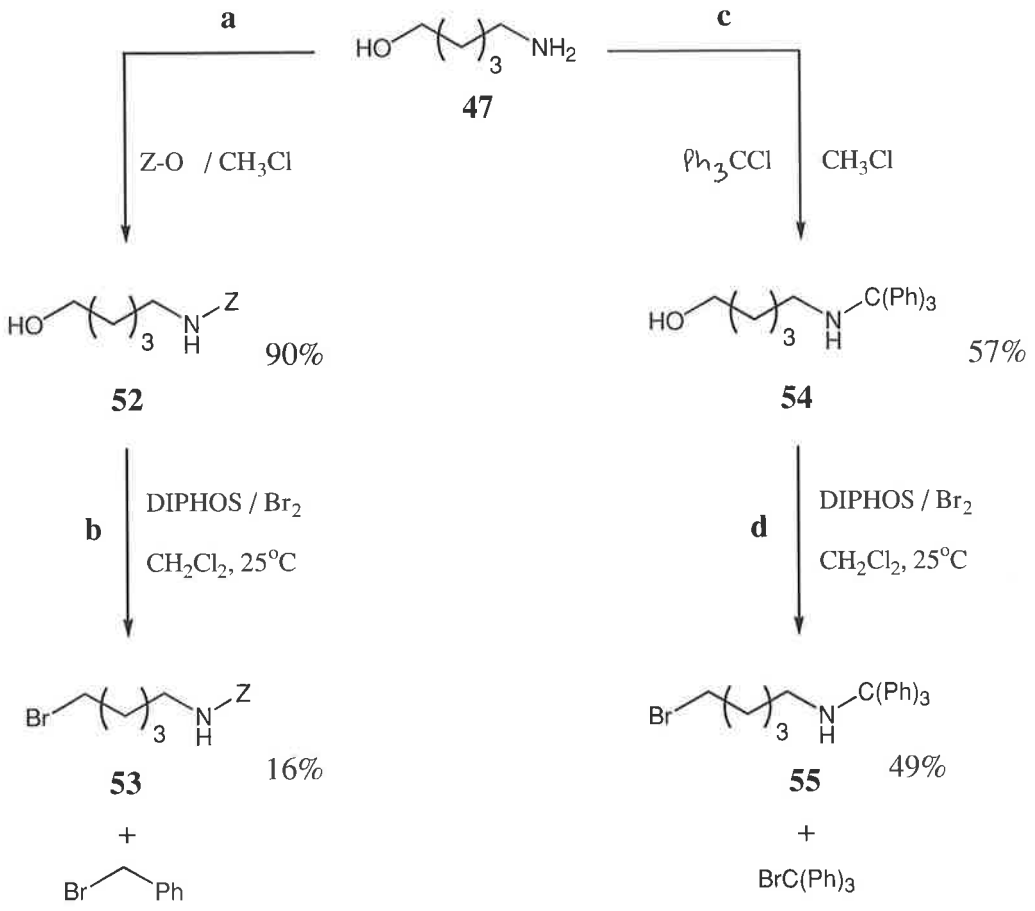

Scheme 38

The *N*-trityl group was then investigated as a suitable amine protecting group. Reaction of **47** with trityl chloride in chloroform for three hours followed by purification by flash column chromatography gave the *N*-trityl species **54** as a colourless oil in 57%, Scheme 38c. The structure of **54** was confirmed by the ^{13}C NMR analysis that showed four high intensity aromatic resonances between δ 126-146 ppm and a single quaternary resonance at δ 71.3 ppm in addition to the ethylene resonances.

Bromination of **54** with DIPHOS/Br_2 at room temperature gave a mixture of products that were identified as the desired bromide species **55** and trityl bromide. Purification of the reaction mixture by flash column chromatography gave **55** as a white solid in 49% yield, Scheme 38d. The bromide derivative was again distinguished from the alcohol by a higher R_f value and the appearance of bromine isotopes in the mass spectrum showing two molecular ions at *m/z* 406 and 408. Despite having isolated **55** in moderate yield, the trityl bromide species proved to be rather unstable. ^{13}C NMR analysis showed **55** to decompose to a mixture of products over time. The addition of **55** to ether or THF also gradually gave a white

precipitate, making it unsuitable for reaction with the bridged macrocycle **6**. The *N*-trityl group is predominantly a steric protecting group and the nitrogen atom is not deactivated to the same extent as in Boc or *N*-benzylcarbonyl derivatives. Gradual intramolecular elimination of HBr by the basic trityl nitrogen will give a six membered ring, which may account for the gradual decomposition of **55**.

The suitability of the *N*-(9-fluorenylmethoxycarbonyl)- (*N*-Fmoc) protecting group was then investigated. The Fmoc protecting group is commonly used in polypeptide synthesis and is stable under acidic conditions while cleaving rapidly under mild basic conditions at room temperature. Nitrogen protection was achieved by reacting **47** and 9-fluorenylmethyl chloroformate (Fmoc-Cl) in aqueous 10% sodium carbonate and dioxane for eight hours at room temperature. Recrystallisation of the product from ethyl acetate/hexane gave **56** as white needles in 79% yield, Scheme 39a. The product was characterised by a strong carbonyl absorbance at 1690 cm^{-1} in the infrared spectrum and additional aromatic resonances in the NMR spectra.

The alcohol group of **56** was then converted to an iodide leaving group using DIPHOS/I_2 under similar conditions to the bromination reaction, Scheme 39b. The iodide group was chosen as a more reactive alternative to bromine in the hope that it might enhance the alkylation reaction with **6**. The iodinated species **57** was isolated as a pale yellow solid after silica gel chromatography in 58% and was distinguished from **56** by the upfield shift of the iodo-carbon at δ 6.5 ppm compared with the alcohol-carbon of **56** at δ 62.2 ppm in the ^{13}C NMR spectrum.

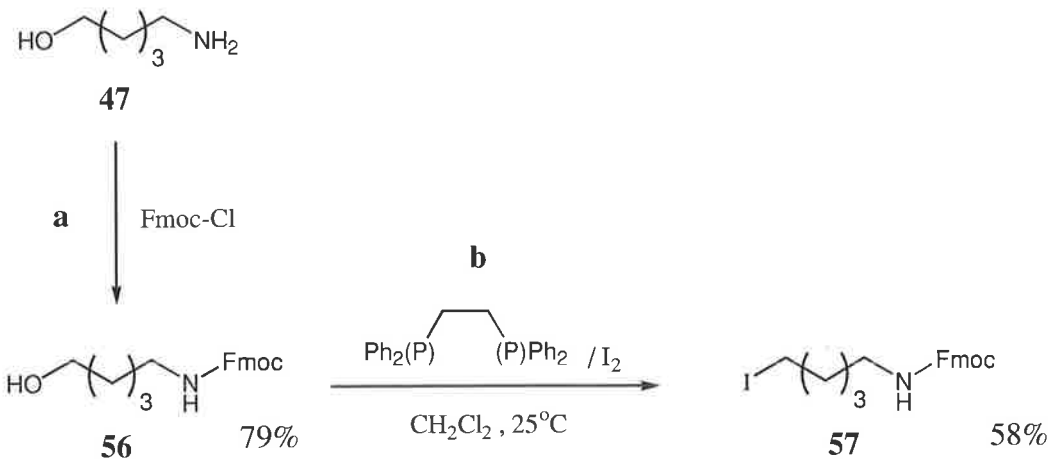

Scheme 39

Alkylation of the bridged macrocycle **6** with the iodo species **57** was attempted in THF and the reaction mixture was allowed to stir for one week. After this time, however, only a minimal amount of precipitate had formed, suggesting minimal reaction between the two compounds. The solvent was then reduced under vacuum to give a viscous residue that was treated with 3M hydrobromic acid under refluxing condition to hydrolyse the bridging ring, Scheme 40. Analysis of the reaction product by ^{13}C NMR spectroscopy revealed a complex mixture of unidentifiable products.

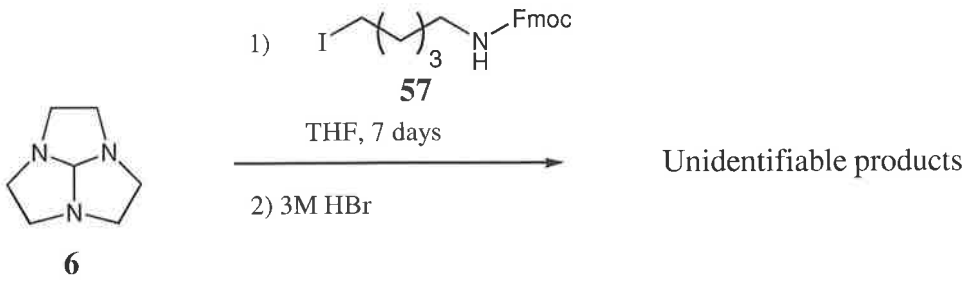

Scheme 40

Having failed to attach the linker arm to [9]aneN_3 using the bridged macrocycle **6**, attention was then shifted to the use of the novel di-protected species **37** (Scheme 29, page 59) in the hope that the secondary nitrogen group of **37** would be more reactive towards alkylation. Again, several alkylating agents with different protecting groups were tested with the di-protected derivative in an attempted to establish the best method of attaching the single linker arm. In addition to the Boc and Fmoc derivatives, another linker arm derivative with an amide protecting group was prepared. Introduction of an amide functional group was achieved by reacting **47** with acetic anhydride in DMF at room temperature. Purification of the product by flash column chromatography gave the amide species **58** as a colourless oil in 97% yield, Scheme 41a. Introduction of the amide group was confirmed by a carbonyl absorbance at 1650 cm^{-1} in the infrared spectrum and a carbonyl resonance at δ 170 ppm in the ^{13}C NMR spectrum. The alcohol group of **58** was then converted to a tosyl leaving group by reaction with tosyl chloride to give the tosylate **59** in 82% yield, Scheme 41b.

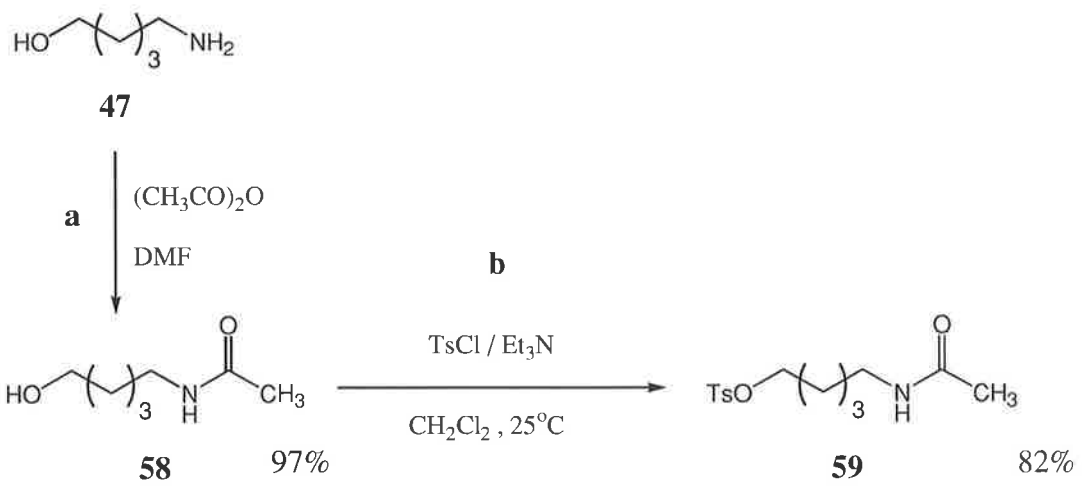

Scheme 41

To determine the most effective method of alkylation, the di-protected species **37** was treated with the Boc-tosylate **50**, Fmoc-iodide **57** and amide-tosylate **59** in DMF under various reaction conditions. Structural analysis of the reaction products by NMR spectroscopy was extremely difficult due to conformational isomerism of the ring system caused by the slow rotation of the ring amide groups on the NMR time scale. To facilitate product analysis, each reaction mixture was further treated with refluxing aqueous hydrobromic acid for three hours to cleave the amide functional groups. The reaction conditions and products are listed in Table 8.

The Boc-tosylate **50** was tested first. Initially, the di-protected species **37** and **50** were reacted in DMF at 110°C using K_2CO_3 as a Lewis acid and KI as a catalyst to convert the tosyl group to the iodo species *in situ*, Table 8 (exp. 1-2). After acid hydrolysis, however, a white solid representing a complex mixture of products was isolated. The Boc and ring amide resonances were absent in the ^{13}C NMR spectrum although a large number of alkyl resonances were observed. When the reaction was repeated using $CsCO_3$ instead of K_2CO_3, similar results were obtained, Table 8 (exp. 3-4). The absence of a large [9]aneN_3 resonance in the ^{13}C NMR spectrum suggested that **37** had been fully consumed by **50**, however, the large number of resonances indicated that further substitution had also occurred, possibly through the linker arm nitrogen from loss of the Boc group in the alkylation step.

Table 8. Attempted alkylation of **37** under various reaction conditions using alternative alkylating agents.

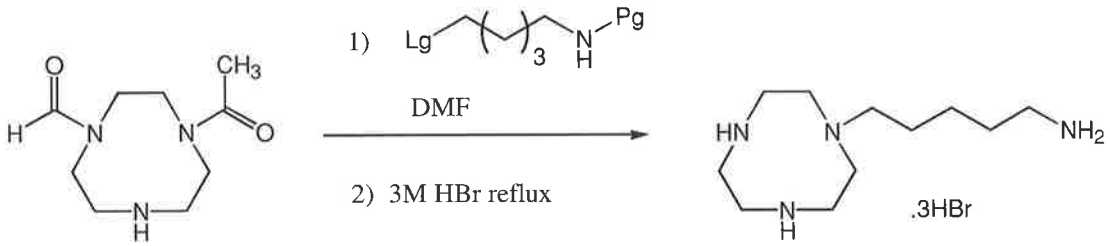

37 **48**

Exp.	Reactant	Molar Equivalents	Lewis base	Catalyst	Alkylation Conditions	Product after HBr reflux
1	**50**	1.5	K_2CO_3	KI	110°C, 16h	Unidentifiable products
2	**50**	1.0	K_2CO_3	KI	110°C, 16h	Unidentifiable products
3	**50**	1.5	$CsCO_3$	KI	110°C, 16h	Unidentifiable products
4	**50**	1.0	$CsCO_3$	KI	110°C, 4h	Unidentifiable products
5	**57**	1.0	$CsCO_3$	-	100°C, 16h	[9]aneN_3.3HBr
6	**57**	1.5	$CsCO_3$	-	100°C, 16 h	[9]aneN_3.3HBr
7	**59**	1.5	$CsCO_3$	KI	120°C / 4h	Unidentifiable products
8	**59**	1.0	$CsCO_3$	-	120°C /4h	Unidentifiable products
9	**59**	0.9	$CsCO_3$	-	55°C / 16 h	Unidentifiable products
10	**59**	1.5	Et_3N	-	55°C / 16 h	[9]aneN_3.3HBr
11	**59**	0.9	Et_3N	-	70°C / 16 h	[9]aneN_3.3HBr
12	**59**	1.5	-	-	70°C / 4 d	Mixture
13	**59**	0.9	-	-	70°C / 4 d	[9]aneN_3.3HBr and **48**

The alkylation of **37** with the Fmoc-iodide species **57** also proved disappointing. Reaction of **37** with 1 and 1.5 equivalents of **57** with $CsCO_3$ followed by acid hydrolysis gave [9]aneN_3.3HBr as the major product. The large amount of [9]aneN_3 suggested that **37** had reacted poorly with the iodide alkylating agent, Table 8 (exp. 5-6).

Attention was then shifted to the amide tosylate **59**. The amide protecting group is more stable than the Boc group and fewer problems associated with decomposition were expected. However, reaction of the amide **59** and **37** with $CsCO_3$ and KI, followed by acid hydrolysis gave a similar mixture of products to those obtained in experiments 1-4. When the reaction was repeated without the KI catalyst at different temperatures a complex mixture of products was again obtained, Table 8 (exp.7-9). All attempts to separate the products by fractional recrystallisation from ethanol were unsuccessful.

The $CsCO_3$ Lewis base was then replaced with triethylamine to see what effect the amine base would have on the alkylation reaction. Unfortunately, the triethylamine appeared to react with **59** with the result that a large amount of [9]aneN_3.3HBr was isolated following acid hydrolysis, Table 8 (exp.10-11).

Finally the reaction was performed in the absence of Lewis base. Without a Lewis base present the di-protected species **37** would become protonated and less reactive. To compensate for the reduced reactivity of protonated **37** the reactions were run for four days. When **37** was reacted with 1.5 equivalents of the amide **59** in DMF at 70°C, a mixture of products was obtained including [9]aneN_3.3HBr, the amine alcohol **47** and the desired product **48** which were distinguishable in the ^{13}C NMR spectrum, Table 8 (exp. 12). The reaction was then repeated using less than one equivalent of **59** to minimise the amount of **47** produced in the final product. Following acid hydrolysis, the reaction gave a 1:1 mixture of [9]aneN_3.3HBr and the mono-alkylated species **48**. The two products were separated by fractional recrystallisation in ethanol and **48** was obtained as a white solid in 17% yield. The product was instantly recognisable by its two-fold symmetry displaying three ring carbon resonances and five smaller intensity pendant arm resonances in the ^{13}C NMR spectrum. Elemental analysis identified **48** as the trihydrobromide salt.

5.4. *Ab Initio* Calculations of Three Potential Zinc Finger Models

Three potential zinc finger models were investigated using *ab initio* calculations. Structural minimisations using the Gaussian 94 LanL2MB basis set were performed on three systems with different amino acid functional groups to establish the feasibility of producing a loop structure. Three amino acids with different donor atoms were chosen to determine which amino acid functional groups would provide the most suitable coordination environments for loop formation. Several input structures were tested for each model to establish the lowest energy conformation. This involved rotating the donor atoms into different spatial locations around the Zn^{II} ion to determine the most energetically favourable conformation around the Zn^{II} centre. Other local minima are also possible through rotation of individual atoms in the loop structure, however, these were not investigated due to the immense number of possible conformations and the extremely small energy differences involved.

The first model tested was [Zn^{II}-**L**Glu], which contains a deprotonated glutamic acid moiety at the *N*-terminal of the linker arm, Figure 56A. This model possesses an amine-carboxylate donor set that is able to form a 13- and 14-membered chelate ring system. The central Zn^{II} is surrounded in a distorted trigonal bipyramidal environment where a carboxylate oxygen atom and an unsubstituted ring nitrogen atom define the axis. The amine and oxygen donors of the amino acid functional group form a five-membered chelate ring with the Zn^{II} ion so that the immediate environment around the metal ion comprises four five-membered chelate rings.

The second model contains a cysteine amino acid moiety attached to the linker arm, Figure 56B. The cysteine amino acid contains a sulfur and nitrogen donor set which may potentially form an 11- and a 12-membered chelate ring with the Zn^{II} ion. The minimised structure of [Zn^{II}-**L**Cys], however, shows the carbonyl oxygen of the amide linkage preferentially binding to the Zn^{II} ion while the cysteine sulfur atom is directed away from the metal centre. This arrangement produces a smaller 10- and 11-membered chelate ring system where the Zn^{II} is surrounded in a trigonal bipyramidal structure by four nitrogen atoms and one oxygen atom. The poor affinity of the sulfur atom for the Zn^{II} ion precludes cysteine as a possible primary amino acid for the zinc finger model.

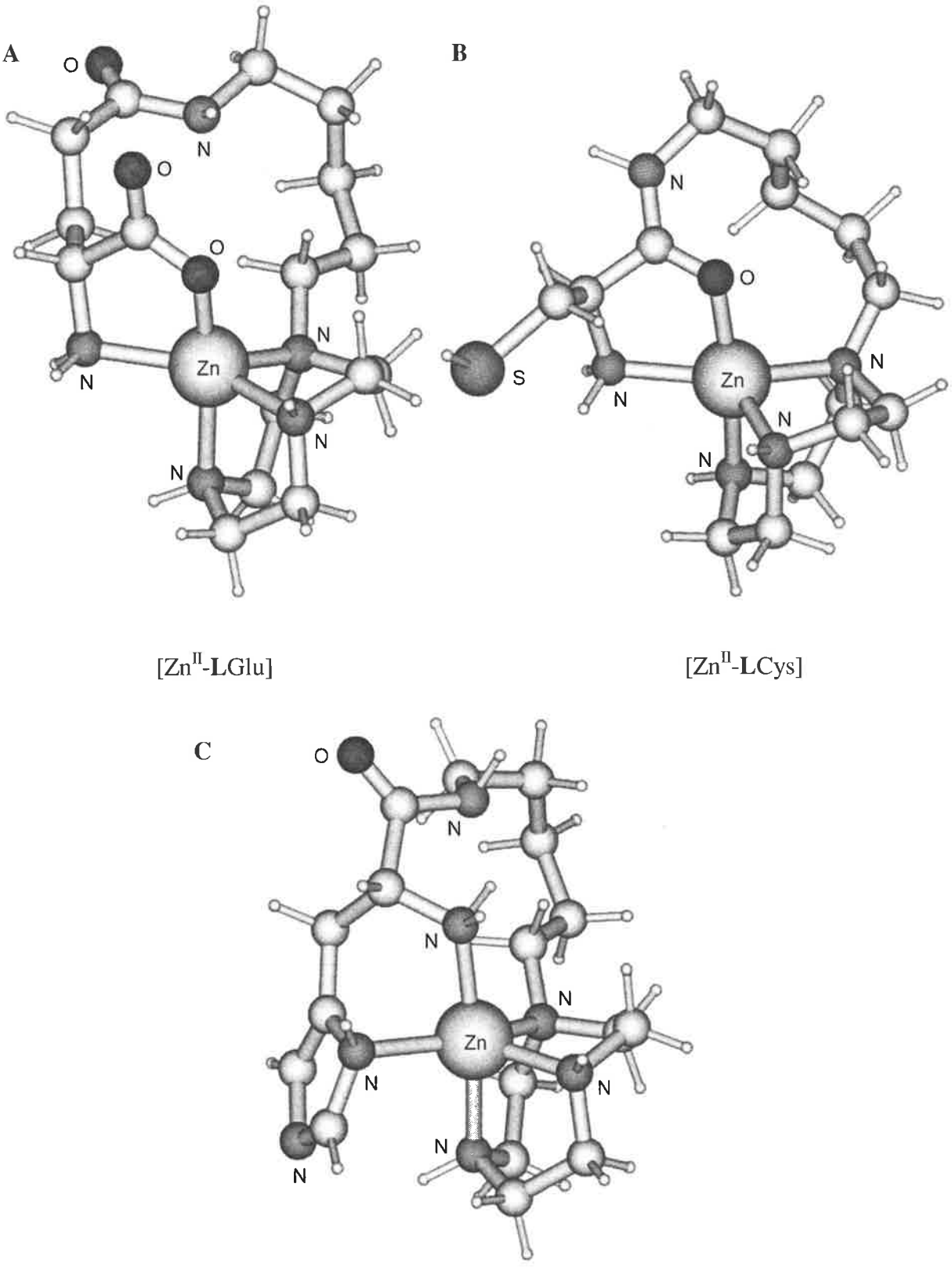

[Zn^{II}-**L**Glu] [Zn^{II}-**L**Cys]

[Zn^{II}-**L**His]

Figure 56. Energy minimised structures of three potential zinc finger models generated with the Gaussian 94 LanL2MB basis set. The minimised energies for [Zn^{II}-LGlu], [Zn^{II}-LCys] and [Zn^{II}-LHis] are –1170.952173, -957.550999 and –1168.493390 Hartrees, respectively.

The third model tested contains a histidine amino acid functional group, Figure 56C. This produced an 11- and a 13-membered chelate ring system whereby the histidine amine atom and the sp^3 imidazole nitrogen atom coordinate the Zn^{II} ion to form an overall five-coordinate distorted trigonal bipyramidal structure. In this model, the Zn^{II} ion is coordinated exclusively by nitrogen donors. Of the two imidazole nitrogen atoms, the sp^2 nitrogen is the more basic but is unable to coordinate the metal centre because of its distant location from the Zn^{II} ion. The two amino acid nitrogen atoms form a six-membered chelate ring with the Zn^{II} ion so that the immediate environment around the metal ion comprises three five-membered and one six-membered chelate ring.

Both the histidine and glutamic acid moieties represent suitable N-terminal ligating groups to encourage loop formation with the coordinated Zn^{II} ion and it is hoped that substantial progress will soon be made towards the isolation of a simple zinc finger model.

5.5. Summary and Future Work

The single pendant arm ligand **48** has been isolated in low yield and represents the starting point to a series of potential zinc finger models of varying size and complexity. The direct alkylation of the di-protected species **37**, as a route to **48** is, however, inefficient and low yielding and a more effective method is needed if large and complex zinc finger models are to be made. An alternative method of attaching the linker arm may involve direct amide bond formation between a [9]aneN_3 nitrogen atom and a carboxylic acid group, Figure 42a. Amide bond formation by DCC coupling is appreciably more facile than direct amine alkylation and it is anticipated that this method might afford more promising results. If both the linker arm and ring amines are protected with Boc groups, the protecting groups could easily be removed using trifluoroacetic acid (TFA) at room temperature to give **60** without cleaving the amide bond, Scheme 42b.

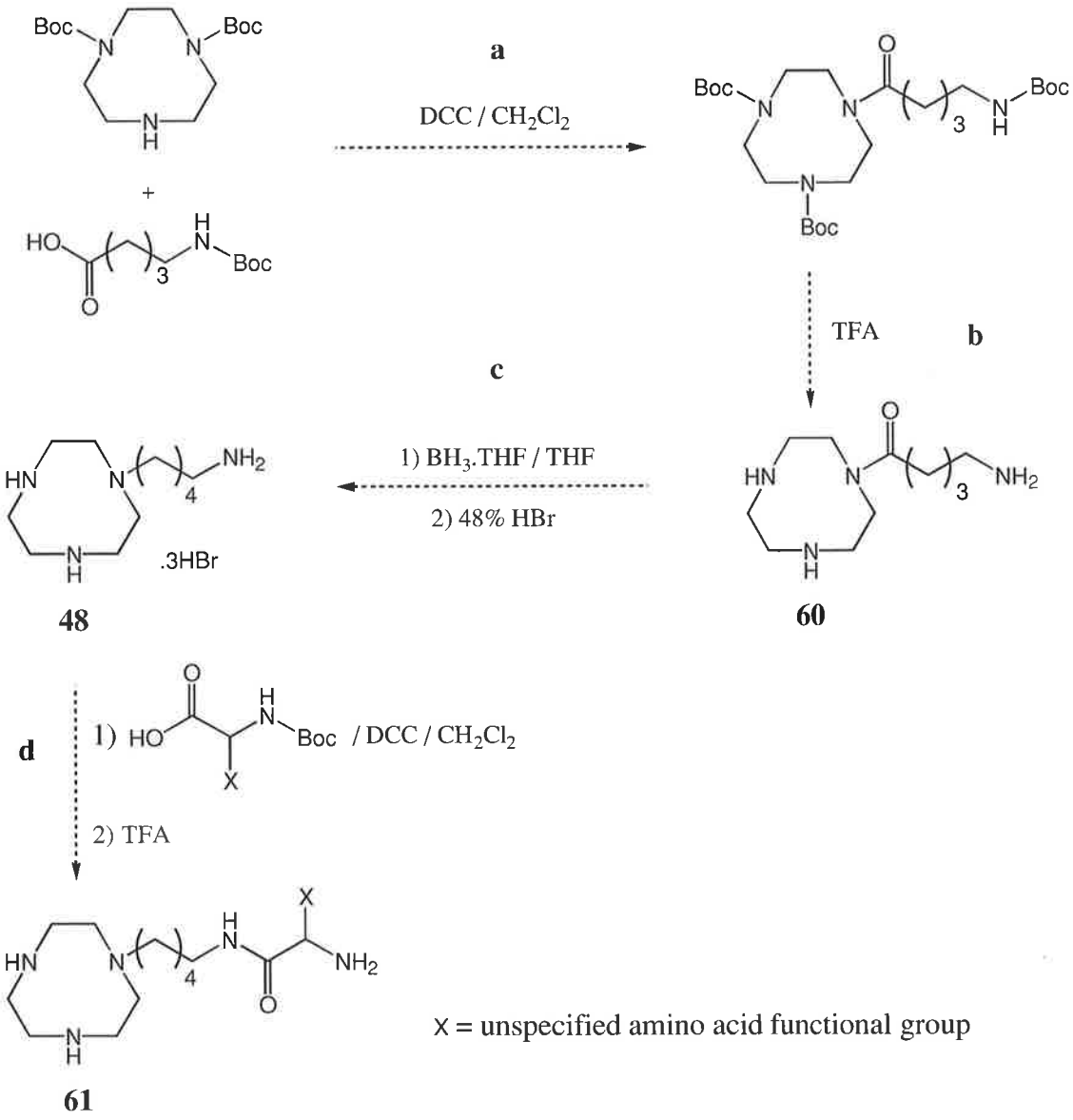

Scheme 42

The single pendant arm ligand **48** may then be obtained by reducing the amide functionality of **60** with borane, Scheme 42c. Finally, an amino acid functional group could be attached by DCC coupling of a suitably protected amino acid to the linker arm amine to give the simple zinc finger model **61**, Scheme 42d. It is anticipated that protection of the secondary ring nitrogen atoms might not be necessary, as the primary linker arm nitrogen would display greater affinity for the carboxylic acid group of the amino acid.

Chapter 6. Experimental

6.1. General

6.1.1. Methods and Materials

Melting points were determined on a Kofler hot-stage apparatus equipped with a Reichart microscope and are uncorrected. Infrared spectra were recorded on a Mattson 270-30 FT spectrometer as nujol mulls or liquid films between sodium chloride plates.

^{1}H and ^{13}C NMR spectra were recorded on either a Varian Gemini-200 (200.13 and 50.32 MHz, respectively) spectrometer or a Varian Gemini-2000 (300.13 and 74.47 MHz, respectively) spectrometer or a Varian Inova (599.95 and 150.87 MHz, respectively) spectrometer. Spectra were obtained for solutions in $CDCl_3$ [tetramethylsilane (δ_H 0.0 for $SiMe_4$) and $CDCl_3$ (δ_C 77.0) as internal standards] at 25°C, or in D_2O [sodium 3-(trimethylsilyl)propanesulfonate (δ_H 0.0 for $SiMe_3$) and *t*-butyl alcohol (δ_C 31.6 for CH_3) as external standards] at 25°C. *J* Values are given in Hz. Chemical shifts are quoted on the δ-scale in parts per million (ppm), followed by multiplicity, coupling constant(s) and assignment. In reporting spectral data the following abbreviations have been used: s, singlet; d, doublet; t, triplet; m, multiplet; br, broad; quart, quartet; quint, quintet. Where the extremities of a multiplet are well defined, a range is given, otherwise a value approaching the centre of the signal is recorded.

Electron impact (EI) mass spectra were recorded on a ZAB 2HF mass spectrometer. The masses of relevant ions are given followed by relative intensity. Liquid spray ionisation (LSI) mass spectra were performed by the Central Science Laboratory, Tasmania.

Flash chromatography was performed on Silica Gel 60, 230-400 mesh (Merck). Thin layer chromatography (TLC) was performed on either aluminium backed Silica Gel 60 plates (Merck) or Aluminium oxide 150 plates (Merck) and were visualised by UV light (254 nm) or by staining in a potassium permanganate dip prepared from potassium permanganate (3 g) and potassium carbonate (20 g) dissolved in aqueous sodium hydroxide solution (5%, 5 cm^3) and water (300 cm^3).

All solvents were distilled and dried before use. Dry THF was freshly prepared by distilling over benzophenone and sodium under nitrogen. DMF was distilled *in vacuo* over anhydrous CaO and stored over 4Å molecular sieves. Organic extracts were dried over anhydrous magnesium sulfate. Elemental analyses were performed at the University of Otago, New Zealand.

6.1.2. Aqueous Potentiometric Titrations

The reagents $NaNO_3$ (Fluka), $ZnSO_4$ (Fluka), $CdSO_4$ (Fluka) and potassium hydrogen phthalate (KHphthalate, BDH) were of analytical grade (purity >99%) and were dried *in vacuo* over P_2O_5. Aqueous perchloric acid [$HClO_4$ (70%), Ajax] was used as received.

Potentiometric titrations were performed using an Orion Ross Sureflow 8172 BN combination pH electrode (0.1 mol dm^{-3} $NaNO_3$) connected to an Orion SA720 potentiometer using a Metrohm E665 Dosimat titrimator with a 5 cm^3 autoburette which was interfaced with a Laser XT/3-8086 IBM compatible personal computer. The titration and data collection was controlled by the programme Autotit7[179] that allowed a maximum 300-second delay time between titrant additions. For each test solution, at least three independent titrations were always made using a literature method.[180,181]

6.1.3. Kinetic Measurements

Kinetic reaction rates were measured spectrophotometrically with a Hewlett Packard Diode Array spectrophotometer equipped with a temperature controlled cell block thermostated at 298.2 ± 0.1 K and interfaced to a Laser XT/3-8086 IBM compatible personal computer. 4-nitrophenyl acetate (NA) hydrolysis was followed at a wavelength range of 350-450 nm at 2 nm increments. The solutions used in the kinetic measurements contained 0.1 mol dm^{-3} boric acid/NaOH buffer (pH 9.2), I = 0.1 ($NaClO_4$) and the pH of each solution was measured with an Orion SA 720 potentiometer and an Orion 8172 Ross Sureflow combination pH electrode filled with $NaClO_4$ (0.10 mol dm^{-3}). The borate buffer was prepared according to Perrin and

Boyd.[182] Boric acid and sodium perchlorate used to make the buffer was obtained from BDH and sodium perchlorate was dried under vacuum over P_2O_5 prior to use.

6.1.4. Molecular Modelling

Ab initio molecular orbital calculations were carried out using the Gaussian 94[125] programme suite using a Silicon Graphics Indigo^2 xZ workstation linked to a Silicon Graphics Power Challenge supercomputer. Geometries were fully optimised at the Hartree-Fock (HF) level of theory using either the 6-31G(*), LanL2DZ or LanL2MB basis sets. Molecular geometries were visualised using the Molden (V3.0) software.

6.2. Synthesis

6.2.1. Syntheses Towards 1,4,7-Triazacyclononane, [9]aneN$_3$

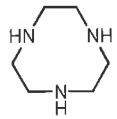

1,2-Di(*p*-toluenesulfonyloxy)ethane, TsOCH$_2$CH$_2$OTs, 21[144]

Triethylamine (53.80 g, 532 mmol) was added drop-wise to a stirred solution of ethylene glycol (15.09 g, 243 mmol) in dichloromethane (100 cm^3) at 0°C. A solution of *p*-toluenesulfonyl chloride (96.75 g, 507 mmol) in dichloromethane (300 cm^3) was then added to the reaction mixture in a drop-wise manner to maintain the low temperature. The reaction mixture was left to stir for two hours at room temperature. The solid triethylamine hydrochloride was filtered off and the filtrate reduced *in vacuo* to give a white precipitous slurry. The precipitate was washed in diethyl ether (500 cm^3) and collected by vacuum filtration. Recrystallisation from ethanol afforded the title compound as white crystals (81.88 g, 91%), mp 121-126°C (Lit.[145] mp 123-125°C); δ_H(200.13 MHz, $CDCl_3$) 2.46 (6H, s, 2 x $ArCH_3$), 4.19 (4H, s, 2 x CH_2O), 7.34 (2H, AA′ portion of AA′XX′, ArH), 7.74 (2H, XX′ portion of AA′XX′, ArH); δ_C(50.32 MHz) 21.66 (2 x CH_3Ar), 66.66 (2 x CH_2O), 127.95 (2 x ArCH), 129.94 (2 x ArCH), 132.41 (ArC), 145.26 (ArC); *m/z* (FAB) 371 [$(M + H)^+$, 14 %], 301 (11), 277 (8), 255 (13), 196 (52), 153 (53), 136 (61), 109 (41), 95 (59), 67 (100), 49 (22). Physical and spectral data were consistent with literature values.[144,145]

1,4,7-Tris(*p*-toluenesulfonyl)diethylenetriamine, TsN(CH$_2$CH$_2$NHTs)$_2$, 20

Triethylamine (152.0 g, 1.51 mol) was added drop-wise to a stirred solution of diethylenetriamine (50.01 g, 485 mmol) in dichloromethane (500 cm^3) at 0°C. A solution of *p*-toluenesulfonyl chloride (276.5 g, 1.45 mol) in dichloromethane (300 cm^3) was then added to the stirred reaction mixture in a drop-wise manner to maintain the low temperature and the reaction mixture was left to stir at room temperature for 12 hours. The white precipitate was

filtered off and retained while the filtrate was reduced *in vacuo* to afford a white solid. Both solids were combined and recrystallised from methanol to give **20** as small white needles (248 g, 90%), mp 174-175°C (Lit.[145] mp 173-175°C); δ_H(200.13 MHz, $CDCl_3$) 2.42 (9H, s, 3 x $ArCH_3$), 3.17 (8H, m, 2 x CH_2NH, 2 x CH_2N), 5.18 (2H, bs, 2 x NH), 7.31 (2H, AA′ portion of AA′XX′, ArH), 7.32 (4H, BB′ portion of BB′YY′, 2 x ArH), 7.61 (2H, XX′ portion of AA′XX′, ArH), 7.76 (4H, YY′ portion of BB′YY′, ArH); δ_C(50.32 MHz) 21.5 (3 x $ArCH_3$), 42.6 (2 x CH_2NH), 50.5 (2 x $TsN\underline{C}H_2$), 127.2 (4 x ArCH), 127.3 (2 x ArCH), 129.8 (4 x ArCH), 130.0 (2 x ArCH), 134.9, 136.9, 143.7, 144.2 (six quaternary ArC); *m/z* (FAB) 566 [$(M + H)^+$, 75 %], 550 (2), 500 (1), 458 (1), 412 (22), 381 (14), 369 (2), 308 (8), 290 (8), 228 (58), 198 (17), 154 (98), 136 (94), 91 (100), 51 (39). Physical and spectral data were consistent with literature values.[145]

1,4,7-Tris(*p*-toluenesulfonyl)diethylenetriamine-1,7-disodium salt, 22[144]

To a rapidly stirred suspension of **20** (248 g, 438 mmol) in absolute ethanol at 0°C was added sodium metal (28.35 g, 1.23 mol) in small portions to maintain the low temperature. The milky solution was then allowed to stir for 12 hours under nitrogen at room temperature. The precipitate was collected by vacuum filtration under flowing nitrogen and the white product washed with absolute ethanol (200 cm^3). The solid was dried under high vacuum at approximately 80°C for several days to give **22** as a white hygroscopic powder (247.45 g, 93%), mp 294-295°C.

1,4,7-Tris(*p*-toluenesulfonyl)-1,4,7-triazacyclononane, 23[2,144]

To a stirred solution of **22** (82.66 g, 136 mmol) in dry *N,N*-dimethylformamide (DMF) (400 cm^3) at 70°C was added a solution of 1,2-Di(*p*-toluenesulfonyloxy)ethane (50.32 g, 136 mmol) in dry DMF (200 cm^3). The reaction mixture was left to stir at 110°C for 12 hours under nitrogen. Removal of the solvent by reduced pressure distillation gave a thick slurry that was suspended with rapid stirring in ice cold water (2.4 dm^3). The mixture was stirred for

30 minutes and the white precipitate was filtered off and washed successively with water, ethanol, and ether. The product was dried under high vacuum and recrystallised from acetone/water to afford **23** as small white needles (49.03 g, 61%), mp 213-215°C (Lit.[145] mp 218-220°C); δ_H(200.13 MHz, $CDCl_3$) 2.44 (9H, s, 3 x $ArCH_3$), 3.42 (12H, s, 6 x CH_2N), 7.33 (6H, AA′ portion of AA′XX′, ArH), 7.70 (6H, XX′ portion of AA′XX′, ArH); δ_C(50.32 MHz) 21.5 (3 x $ArCH_3$), 51.9 [3 x $N(CH_2)_2N$ ring], 127.5 (6 x ArCH), 129.9 (6 x ArCH), 134.7 (3 x ArC), 143.9 (3 x ArC); *m/z* (FAB) 592 [$(M + H)^+$, 100 %], 566 (2), 484 (1), 438 (14), 436 (45), 381 (2), 308 (9), 281 (22), 254 (16), 186 (2), 154 (82), 91 (68), 77 (32). Physical and spectral data were consistent with literature values.[28,144,145]

1,4,7-Triazacyclononane Trihydrobromide, [9]aneN$_3$.3HBr, 24

1,4,7-Tris(*p*-toluenesulfonyl)-1,4,7-triazacyclononane **23** (40.0, 67.7 mmol) was dissolved in sulfuric acid [100 cm^3 (98%)] and the mixture stirred at 110°C for three days. Upon cooling to room temperature, the brown mixture was added slowly to a stirred solution of absolute ethanol (350 cm^3) and ether (100 cm^3) at 0°C. The resulting grey/white precipitate of [9]aneN$_3$.$\frac{1}{2}$ H_2SO_4 was filtered off under nitrogen and dried *in vacuo*. The solid was dissolved in hot water (18 cm^3) and aqueous hydrobromic acid (HBr) (25 cm^3, 48%) was added drop-wise to the solution creating a white precipitate. The mixture was cooled to 0°C and the precipitate was collected by filtration under flowing nitrogen to give **24** as a pale grey powder (21.90 g, 88%), mp 269-277°C (Lit.[28] mp 277-278°C); δ_H(200.13 MHz, D_2O) 4.1 [12H, s, 3 x $N(CH_2)_2N$ ring]; δ_C (50.32 MHz) 44.5 [3 x $N(CH_2)_2N$ ring]; *m/z* (FAB) 130 [$(M + H)^+$, 100%], 114 (3), 102 (1), 94 (26), 86 (7), 76 (16), 63 (6), 59 (27), 46 (27), 33 (30). Physical and spectral data were consistent with literature values.[28]

1,4,7-Triazacyclononane, [9]aneN$_3$

[9]aneN$_3$.3HBr **24** (25.5 g, 68.4 mmol) was dissolved in a solution of NaOH (8.76 g, 219 mmol) in water (25 cm^3) giving a clear brown solution. Benzene (150 cm^3) was added

and the reaction mixture was refluxed at 100°C for two days using a Dean-Stark apparatus to remove the water. The benzene solution was filtered and the solid sodium bromide washed with warm benzene. The filtrate was then reduced *in vacuo* to give a clear oil which formed an amorphous solid upon standing at 0°C (6.57 g, 74%), mp 42-46°C; ν_{max}(neat)/cm^{-1} 3357 (br NH); δ_H(200.13 MHz, $CDCl_3$) 1.94 (3H, bs, 3 x NH), 2.74 [12H, s, 3 x N(CH_2)$_2$N ring]; δ_C(50.32 MHz) 47.5 [6 x N(CH_2)$_2$N ring]; *m/z* (EI) 129 (M^+, 13%), 114 (18), 104 (17), 88 (78), 75 (25), 56 (68), 44 (100), 42 (54), 31 (4).

6.2.2. Syntheses Towards Three- and Four-Pendant Arm Ligands

1,4,7-Tris(2-hydroxyethyl)-1,4,7-triazacyclononane, Thec[9], 19

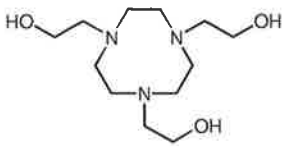

Method 1

Ethylene oxide (0.45 cm^3, 9.04 mmol) in chilled ethanol (3 cm^3) was poured into a solution of [9]aneN_3 (0.37 g, 2.89 mmol) in ethanol (15 cm^3) at 0°C and left to stir for three days in a stoppered flask at room temperature. Removal of the solvent *in vacuo* gave **19** as a viscous oil which was dried under high vacuum at 80°C for six hours (0.76 g, quantitative); ν_{max}(neat)/cm^{-1} 3334 (OH); δ_H(300.13 MHz, $CDCl_3$) 2.64 [12H, s, 3 x N(CH_2)$_2$N ring], 2.75 (6H, t, *J* 5, 3 x NC$\underline{H}_2$$CH_2$OH arm), 3.58 (6H, t, *J* 5, 3 x $NCH_2C\underline{H}_2$OH arm); δ_C(74.47 MHz) 53.07 [3 x N(CH_2)$_2$N ring], 59.30 (3 x N$\underline{C}H_2CH_2$OH arm), 59.96 (3 x $NCH_2\underline{C}H_2$OH arm); *m/z* (EI) 261 (M^+, 5%), 230 (4), 215 (2), 187 (24), 161 (100), 143 (27), 129 (21), 88 (94), 70 (41), 44 (59), 42 (76). Spectral data were consistent with literature values. [45]

Method 2

[9]aneN_3.3HBr, **24**, (4.00 g, 10.75 mmol) was added to a solution of sodium metal (0.517 g, 22.5 mmol) in dry ethanol (300 cm^3) and allowed to stir for 12 hours. The solution was then suction filtered through a pad of Celite, reduced *in vacuo* to approximately 80 cm^3 and cooled to 0°C. Ethylene oxide (1.67 cm^3, 33.4 mmol) in chilled ethanol (6 cm^3) was poured into the solution and the mixture was allowed to stir for four days in a stoppered flask at room temperature. The solvent was removed *in vacuo* to give a white solid, which was dissolved in isopropanol and again filtered. Removal of the solvent *in vacuo* gave a white solid which was recrystallised from isopropanol to afford the sodium bromide complex **26** of thec[9] as white crystals (2.33 g, 63%), mp 154-156°C (Found : C, 39.67; H, 7.60; N, 11.72; $C_{12}H_{27}BrO_3N_3Na$ requires C, 39.57; H, 7.42; N, 11.54%). δ_H(300.13 MHz, D_2O) 2.84 (6H, t, *J* 5.7, 3 x $NC\underline{H}_2CH_2OH$ arm), 2.86 [12H, s, 3 x $N(CH_2)_2N$ ring], 3.72 (6H, t, *J* 5.7, 3 x $NCH_2C\underline{H}_2OH$ arm); δ_C(74.47 MHz) 54.61 [3 x $N(CH_2)_2N$ ring], 60.69 (3 x $N\underline{C}H_2CH_2OH$ arm), 60.86 (3 x $NCH_2\underline{C}H_2OH$ arm). Spectral data were consistent with literature values.[45]

1,1,4,7-Tetrakis(2-hydroxyethyl)-1,4,7-triazacyclononane bromide salt, 27

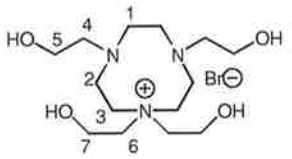

When Method 2 for the synthesis of thec[9] **19** was performed with an excess amount of ethylene oxide, an additional impurity was observed by ^{13}C NMR (D_2O). Separation of thec[9].NaBr **26** from the impurity was achieved by fractional recrystallisation from isopropanol. Upon cooling to 0°C, thec[9].NaBr **26** remained dissolved in the isopropanol while the tetrakis salt **27** crystallised as white prisms, mp 120-121°C (Found : C, 43.58; H, 8.62; N, 10.86. $C_{14}H_{32}BrO_4N_3$ requires C, 43.53; H, 8.35; N, 10.88%); δ_H(300.13 MHz, D_2O) 2.76 [4H, s, 2 x $C(1)H_2$], 2.85 [4H, t, *J* 5.5, 2 x $C(4)H_2$], 3.12 [4H, m, 2 x $C(2)H_2$], 3.70 [4H, t, *J* 5.2, 2 x $C(6)H_2$] 3.75 [4H, t, *J* 5.7, 2 x $C(5)H_2$], 4.08 [4H, t, *J* 5.1, 2 x $C(7)H_2$] 4.27 [4H, br s, 2 x $C(3)H_2$]; δ_C(74.47 MHz) 54.80 [2 x C(2)], 56.69 [2 x C(7)], 59.73 [2 x C(1)], 61.73

[2 x C(3)], 61.81 [2 x C(5)], 61.87 [2 x C(6)], 62.45 [2 x C(4)]. Analytical data were consistent with literature values.[45]

6.2.3. Syntheses Towards Two-Pendant Arm Ligands

1,4,7-Triazatricyclo[5.2.1.0$^{4.10}$]decane, 6[76]

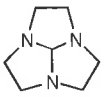

[9]aneN_3 (4.49 g, 34.8 mmol) was added to *N,N*-dimethylformamide dimethyl acetal [4.46 g (94%), 35.2 mmol] and refluxed at 85°C for three hours under nitrogen. Methanol formed in the reaction was removed *in vacuo* and an amber coloured oil was obtained. Kugelrohr distillation of the residue (60°C at 0.023 mm Hg) gave **6** as a colourless oil, (4.58 g, 95%), ν_{max}(neat)/cm^{-1} 3357, 3257 (N), 1678; δ_H(200.13 MHz, $CDCl_3$) 2.81 (6H, AA′ of AA′BB′, 3 x NCH_2 ring), 3.09 (6H, BB′ of AA′BB′, 3 x NCH_2 ring), 5.04 (1H, s, $CH(N)_3$ bridge); δ_C(50.32 MHz) 51.83 [3 x $N(CH_2)_2N$ ring], 104 [$CH(N)_3$ bridge]; *m/z* (EI) 139 (M^+, 100%), 97 (27), 83 (14), 70 (34), 56 (30), 42 (25), 31 (12). Spectral data were consistent with literature values.[75,183]

1-Formyl-1,4,7-triazacyclononane, 28

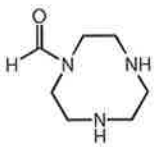

Aqueous hydrochloric acid (HCl) (4.5 cm^3, 2.8 mol dm^{-3}) was added to 1,4,7-triazatricyclo[5.2.1.0$^{4.10}$]decane **6** (1.12 g, 8.06 mmol) at 0°C and stirred at room temperature for 16 hours. The solution was cooled to 0°C and treated with NaOH (5 mol dm^{-3}) until pH 11. The aqueous solution was then saturated with sodium chloride and extracted with dichloromethane (4 x 40 cm^3). The combined organic extracts were dried and the solvent removed *in vacuo* to give a clear oil which was chromatographed on silica gel (NH_4OH-

$H_2O/MeOH/CH_2Cl_2$ 1:59:40, R_f = 0.23) to give **28** as a viscous oil that solidified on standing (0.39 g, 31%), ν_{max}(neat)/cm^{-1} 3383 (NH), 1654 (C=O); δ_H(300.13 MHz, $CDCl_3$) 2.14 (2H, s, NH), 2.77 (4H, m, 2 x CH_2), 2.91 (2H, m, CH_2), 3.12 (2H, m, CH_2), 3.38 (2H, m, CH_2), 3.47 (2H, m, CH_2), 8.15 (1H, s, NCHO); δ_C(74.47 MHz) 46.76, 48.36, 48.70, 49.35, 49.93, 52.64 (NCH_2 ring), 163.88 (NCHO); *m/z* (EI) 157 (M^+, 100%), 155 (1), 141 (11), 128 (18), 114 (31), 101 (44), 98 (13), 85 (83), 71 (33), 56 (77), 44 (84), 42 (61), 31 (2). Spectral data were consistent with literature values.[149]

1-Formyl-4,7-bis(2-hydroxyethyl)-1,4,7-triazacyclononane, 29

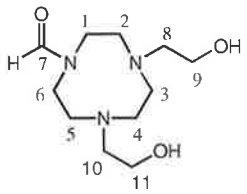

Ethylene oxide (0.40 cm^3, 8.01 mmol) in chilled ethanol (2.5 cm^3) was poured into a solution of 1-formyl-1,4,7-triazacyclononane **28** (0.21 g, 1.36 mmol) in ethanol (15 cm^3) at 0°C and left to stir for three days in a stoppered flask at room temperature. Removal of the solvent *in vacuo* gave **29** as a viscous oil that was dried under high vacuum at 80°C for six hours (0.33 g, quantitative), ν_{max}(neat)/cm^{-1} 3396 (OH), 1655 (C=O); δ_H(600 MHz, $CDCl_3$) 2.59 [2H, m, C(3)H_2], 2.64 [2H, m, C(4)H_2], 2.74 [2H, t, *J* 5.1, C(8)H_2], 2.78 [2H, t, *J* 5.4, C(10)H_2] , 2.92 [2H, m, C(5)H_2], 2.94 [2H, m, C(2)H_2], 3.40 [2H, m, C(6)H_2], 3.47 [2H, m, C(1)H_2], 3.56 [2H, t, *J* 5.4, C(9)H_2], 3.63 [2H, t, *J* 5.4, C(11)H_2], 4.49 (2H, br s, 2 x OH), 8.15 [1H, s, HC(7)O]; δ_C(300 MHz) 47.94 (C1), 51.30 (C6), 52.96 (C2), 54.31 (C4), 54.90 (C3), 55.44 (C5), 59.01 (C10), 59.20 (C11), 59.47 (C9), 59.82 (C8), 163.88 [HC(7)O]; *m/z* (LSI) 246.1808 $(M + H)^+$. $C_{11}H_{24}N_3O_3$ requires 246.1818.

1,4-Bis(2-hydroxyethyl)-1,4,7-triazacyclononane, bhec[9], 18

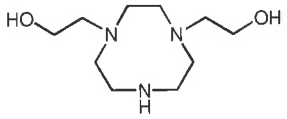

Method 1

1-Formyl-4,7-bis(2-hydroxyethyl)-1,4,7-triazacyclononane **29** (0.394 g, 161 mmol) was refluxed in aqueous HBr (25 cm^3, 3 mol dm^{-3}) at 110°C for 2.5 hours. Removal of the solvent *in vacuo* gave a brittle yellow/white solid that was recrystallised from water/ethanol to give the dihydrobromide salt of **18** as off-white crystals (0.351 g, 58%), mp 155-157°C (Found : C, 31.61; H, 6.85; N, 11.11. $C_{10}H_{25}Br_2O_2N_3$ requires C, 31.68; H, 6.65; N, 11.08%); δ_H(300.13 MHz, D_2O) 3.30 (4H, t, *J* 5.3, 2 x $NC\underline{H}_2CH_2OH$ arm) 3.42 (4H, s, 2 x $NHC\underline{H}_2$ ring), 3.54 [8H, m, 2 x $HNCH_2C\underline{H}_2N$ ring, $(CH_2)_2N$ ring], 3.60 (2H, br s, 2 x OH), 3.98 (4H, t, *J* 5.1, 2 x $NCH_2C\underline{H}_2OH$ arm); δ_C(50.32 MHz) 43.84 (2 x $NHCH_2$ ring), 50.60 (2 x $HNCH_2\underline{C}H_2N$ ring), 51.26 [$(CH_2)_2N$ ring], 58.28 (2 x $N\underline{C}H_2CH_2OH$ arm), 59.28 (2x $NCH_2\underline{C}H_2OH$. arm); *m/z* (LSI) 218.1897 $(M + H)^+$. $C_{10}H_{24}N_3O_2$ requires 218.1868.

Method 2

[9]aneN_3.3HBr **24** (5.08 g, 13.7 mmol) was added to a solution of sodium metal (0.66 g, 28.7 mmol) in dry ethanol (80 cm^3) and allowed to stir for 16 hours. Sodium bromide was removed by gravity filtration and the solution was cooled to 0°C. Ethylene oxide (1.43 cm^3, 28.6 mmol) in chilled ethanol (5 cm^3) was poured into the reaction mixture and the solution was left to stir for four days in a stoppered flask at room temperature. The solvent was removed *in vacuo* to give a viscous oil that was dissolved in water and acidified with aqueous 48% HBr until pH 2. Removal of the solvent *in vacuo* gave a brittle solid that was recrystallised from ethanol to afford the dihydrobromide salt of **18** as small rectangular crystals (2.37 g, 37%). The physical and spectral data were consistent with the values from Method 1. The free ligand was obtained by passing the dihydrobromide salt through an anion exchange column of Amberlite IRA-400 generated with 0.5 mol dm^{-3} NaOH. Removal of water under high vacuum afforded the free ligand as an amorphous solid, ν_{max}(neat)/cm^{-1} 3338 (OH); δ_H(200.13 MHz, $CDCl_3$) 2.67 (4H, t, *J* 5, 2 x $NC\underline{H}_2CH_2OH$ arm), 2.68 (4H, s, 2 x

$NHC\underline{H}_2$ ring), 2.77 [8H, m, 2 x $HNCH_2C\underline{H}_2N$ ring, $(CH_2)_2N$ ring], 3.48 (2H, br s, 2 x OH), 3.61 (4H, t, *J* 5.1, 2 x $NCH_2\underline{C}H_2OH$ arm); δ_C(50.32 MHz) 47.74 (2 x $NHCH_2$ ring), 53.42 (2 x $HNCH_2\underline{C}H_2N$ ring), 53.99 [$(CH_2)_2N$ ring], 59.54 (2 x $N\underline{C}H_2CH_2OH$ arm), 59.75 (2 x $NCH_2\underline{C}H_2OH$ arm); *m/z* (EI) 218 (M^+, 100%), 187 (16), 129 (77), 88 (71), 58 (37), 44 (18).

6.2.4. Syntheses Towards Single Pendant Arm Ligands

1,4-Bis(*tert*-butyloxycarbonyl)-1,4,7-triazacyclononane, 2[68]

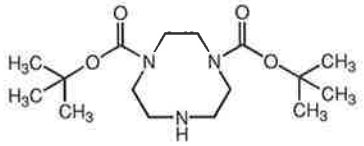

To a stirred solution of [9]aneN_3 (0.99 g, 7.74 mmol) in chloroform (25 cm^3) at 0°C was added 2-(*tert*-butoxycarbonyloxyimino)-2-phenylacetonitrile (Boc-ON) (3.81 g, 15.5 mmol) in chloroform (25 cm^3). The reaction mixture was allowed to reach room temperature and was stirred for approximately four hours or until the disappearance of [9]aneN_3 as detected by TLC analysis. Removal of the solvent *in vacuo* gave a pale yellow oil consisting of **2** and oximinyl phenylacetonitrile. The two products were separated using silica gel chromatography. Initial elution [CH_2Cl_2 (100%)] gave oximinyl phenylacetonitrile as a white solid [mp 126-128°C, R_f = 0.35 (CH_2Cl_2)]. Further elution [MeOH/CH_2Cl_2 (1:19)] gave **2** as a viscous yellow oil (2.02 g, 79%), R_f = 0.23 (MeOH/CH_2Cl_2, 1:19); ν_{max}(neat)/cm^{-1} 3373 (NH), 1693 (C=O); δ_H(300.13 MHz, $CDCl_3$) 1.48 (18H, s, 6 x CH_3), 1.77 (1H, br s, NH), 2.94 (4H, m, NCH_2 ring), 3.24 (2H, m, NCH_2 ring), 3.30 (2H, m, NCH_2 ring), 3.44 (2H, m, NCH_2 ring), 3.49 (2H, m, NCH_2 ring); δ_C(74.47 MHz) 28.4 (6 x CH_3), 47.2, 47.6, 48.0, 48.1, 49.5, 49.7, 50.4, 51.4, 52.2, 52.3, 52.9 (ring carbons), 79.7, 79.8 (C_q), 155.9, 156.2 (C=O); *m/z* (EI) 329 (M^+, 31%), 274 (12), 230 (22), 199 (18), 173 (61), 117 (47), 85 (100), 57 (52), 30 (10). Spectral data were consistent with literature values.[68]

Attempted Alkylation of 1,4-Bis(*tert*-butyloxycarbonyl)-1,4,7-triazacyclononane, 2

Method 1

Ethylene oxide (0.2 cm^3, 4.00 mmol) in chilled ethanol (2 cm^3) was poured into a stirred solution of 1,4-bis(*tert*-butyloxycarbonyl)-1,4,7-triazacyclononane **2** (0.62 g, 1.87 mmol) in ethanol (15 cm^3) at 0°C and left to stir for three days in a stoppered flask at room temperature. Removal of the solvent *in vacuo* gave an oil that was identified as unreacted starting material by TLC and ^{13}C NMR analyses. When the reaction was repeated using DMF instead of ethanol no reaction was observed.

Method 2

N,N-Diisopropylethylamine (0.09 g, 0.68 mmol) was added drop-wise to a stirred solution of 1,4-bis(*tert*-butyloxycarbonyl)-1,4,7-triazacyclononane **2** (0.218 g, 0.66 mmol) in chloroform (20 cm^3). A solution of 2-bromoethanol [0.098 g (97%), 0.76 mmol] in chloroform (5 cm^3) was then added and the reaction mixture heated at reflux for 24 hours under nitrogen. The solvent was removed *in vacuo* to give an oil that was identified as unreacted starting material by TLC and ^{13}C NMR analyses.

1,4,7-Triazabicyclo[4.3.0]non-6-ene-5-one, 35

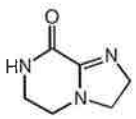

Method 1

Diethylenetriamine (10.0 g, 96.9 mmol) and oxalyl chloride (12.2 g, 96.2 mmol) were each diluted with dichloromethane to 50 cm^3 and the two solutions added simultaneously to a rapidly stirred solution of triethylamine (9.83 g, 97.1 mmol) in dichloromethane (1.75 dm^3) at a rate of 0.8 cm^3/hour using a syringe pump. The addition of the two reactants created an instant white precipitate of polymeric material and the reaction was discontinued.

Method 2

Diethylenetriamine (10.0 g, 96.9 mmol) and diethyl oxalate (14.2 g, 97.2 mmol) were each diluted with absolute ethanol to 50 cm^3 and the two solutions added simultaneously to rapidly stirred refluxing ethanol (1.75 dm^3) at a rate of 0.8 cm^3/hour using a syringe pump. Once addition was complete the stirred reaction mixture was left to reflux for a further five days. The solution was concentrated to approximately 200 cm^3 by distilling off the ethanol and the cloudy solution was cooled to room temperature and filtered. The filtrate was concentrated *in vacuo* to give a viscous orange oil that was chromatographed on silica gel (NH_4OH-H_2O/MeOH/CH_2Cl_2 1:59:40, R_f = 0.5) to give **35** as a pale yellow solid (5.90 g, 44%), mp 172-173°C (Found: C, 51.4; H, 6.29; N, 29.9. $C_6H_9N_3O$ requires C, 51.8; H, 6.52; N, 30.2%); ν_{max}(nujol mull)/cm^{-1} 3479, 3360, 1680, 1620; δ_H(600 MHz, D_2O) 2.99 (2H, t, *J* 6.6, C=NCH_2), 3.62 (2H, m, NHC$\underline{H}_2$), 3.64 (2H, t, *J* 6.6, C=NCH$_2$C$\underline{H}_2$), 3.74 (2H, m, NHCH$_2$C$\underline{H}_2$); δ_C(74.47 MHz) 39.88 (C=N$\underline{C}H_2$), 40.05 (NH$\underline{C}H_2$), 47.59 (NHCH$_2\underline{C}H_2$), 51.88 (C=NCH$_2\underline{C}H_2$), 161.56 (C=N), 161.77 (C=O); *m/z* (EI) 139 (M^+, 100%), 111 (5), 99 (51), 84 (26), 70 (20), 56 (49), 42 (32). This compound has been previously reported in the patent literature.[150]

1-Acetyl-4-formyl-1,4,7-triazacyclononane, 37

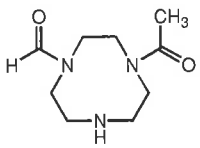

Acetyl bromide (2.62 g, 21.3 mmol) in dry tetrahydrofuran (THF) (10 cm^3) was added drop-wise to a rapidly stirred solution of 1,4,7-triazatricyclo[5.2.1.$0^{4,10}$]decane **6** (2.68 g, 19.3 mmol) in dry THF (200 cm^3) to give an instant white precipitate. After stirring for three hours the solid was vacuum filtered, dissolved in water (50 cm^3) and then heated at reflux for 24 hours. Removal of the solvent *in vacuo* gave an oil which was passed through an anion exchange column of Amberlite IRA-400 generated with 0.1 mol dm^{-3} NaOH. The product was extracted into benzene using a Dean-Stark apparatus. Removal of the solvent *in vacuo* gave **37** as a thick colourless oil that crystallised on standing at 0°C (3.43 g, 89%), mp 79-

81°C (Found: C, 53.3; H, 8.82; N, 20.6. $C_9H_{17}N_3O_2.¼H_2O$ requires C, 53.1; H, 8.66; N, 20.6%); R_f = 0.83 (MeOH/CH_2Cl_2 5:95 on alumina); ν_{max}(neat)/cm^{-1} 3460, 3357 (NH), 1664, 1635 (C=O); δ_H(300.13 MHz, D_2O) 2.07, 2.10, 2.13 (minor) and 2.17 [4 x (3H, s, CH_3)], 2.96 (4H, m, CH_2N ring), 3.31 (4H, m, CH_2N ring), 3.72 (4H, m, CH_2N ring), 8.01, 8.11, 8.13 and 8.16 (minor) [4 x (1H, s, HCO)]; δ_C(74.47 MHz) 22.03, 22.11 and 22.23 [3 x (CH_3)], 44.99, 46.19, 46.39 (coincident double), 47.28, 47.51, 48.32, 48.92 49.45, 49.79, 50.30, 50.57, 51.00, 51.81, 52.15, 53.32, 53.91 and 54.37 (ring carbons), 164.05, 164.13 and 164.15 [3 x (HCO)], 171.29, 171.56 and 171.64 [3 x (CH_3CO)]; *m/z* (LSI) 200.1392 $(M + H)^+$. $C_9H_{18}N_3O_2$ requires 200.1399.

1-Formyl-4,7-(2-hydroxyethyl)-1,4,7-triazacyclononane, 33

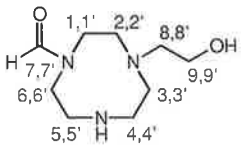

2-Bromoethanol [0.607 g (97%), 4.86 mmol] in dry THF (1 cm^3) was added drop-wise to a rapidly stirred solution of 1,4,7-triazatricyclo[5.2.1.$0^{4.10}$]decane **6** (0.614 g, 4.42 mmol) in dry THF (20 cm^3) and allowed to stir for seven days. The solvent was decanted and the pale yellow residue was washed with dry THF (2 x 2 cm^3) and again decanted. The residue was dissolved in water (10 cm^3) and refluxed for 12 hours. The solvent was then removed *in vacuo* and the residue was passed through an anion exchange column of Amberlite IRA-400 generated with 0.1 mol dm^{-3} NaOH. Removal of the solvent *in vacuo* gave **33** as a pale yellow oil that was dried under high vacuum (0.504 g, 57%), R_f = 0.20 (NH_4OH-H_2O/MeOH 1:99); ν_{max}(neat)/cm^{-1} 3365 (OH), 1660 (C=O); δ_H(600 MHz, $CDCl_3$) 2.60 [2H, t, C(3)H_2], 2.62 [2H, t, C(3′)H_2], 2.73 [4H, m, C(4′)H_2 and C(8′)H_2], 2.77 [4H, m, C(8)H_2 and C(4)H_2], 2.93 [2H, t, *J* 5.1, C(2′)H_2], 2.95 [2H, t, *J* 4.8, C(2)H_2], 3.05 [2H, t, *J* 4.8, C(5′)H_2], 3.07 [2H, t, *J* 4.8, C(5)H_2], 3.35 [2H, t, *J* 5.1, C(1)H_2], 3.43 [2H, m, C(1′)H_2], 3.44 [2H, m, C(6′)H_2], 3.51 [2H, t, *J* 4.8, C(6)H_2], 3.58 [2H, t, *J* 5.4, C(9′)H_2], 3.63 [2H, t, *J* 5.4, C(9)H_2], 8.13 [1H, s, HC(7)O], 8.18 [1H, s, HC(7′)O]; δ_C(600 MHz) 47.19 (C5), 47.36 (C1′), 48.68 (C4′), 49.00 (C4), 49.11 (C5′), 49.36 (C6), 51.21 (C1), 52.30 (6′), 52.84 (C2′), 54.42 (C3), 55.06 (C3′),

55.57 (C2), 57.86 (C8), 58.68 (C8′), 59.77 (C9), 59.95 (C9′), 163.89 [(C7) and (C7′)]; *m/z* (LSI) 202.1557 $(M + H)^+$. $C_9H_{20}N_3O_2$ requires 202.1555.

1-(2-Hydroxyethyl)-1,4,7-triazacyclononane, hec[9], 17

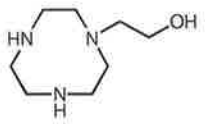

Method 1

Ethylene oxide (0.17 cm^3, 3.52 mmol) in chilled ethanol (4 cm^3) was poured into a solution of 1,4,7-triazatricyclo[5.2.1.$0^{4,10}$]decane **6** (0.163, 1.17 mmol) in ethanol (15 cm^3) at 0°C and left to stir for three days in a stoppered flask at room temperature. Removal of the solvent *in vacuo* gave a complex mixture of unidentifiable products by TLC and ^{13}C NMR ($CDCl_3$) analyses. The mixture was treated with aqueous HBr (20 cm^3, 3 mol dm^{-3}) at 110°C for eight hours. The solvent was again removed and a solid was obtained which also represented a mixture of products by ^{13}C NMR (D_2O) analysis. When the initial reaction was repeated using dry THF instead of ethanol, a complex mixture of products was again obtained.

Method 2

1-Formyl-4,7-(2-hydroxyethyl)-1,4,7-triazacyclononane **33** (0.83 g, 4.12 mmol) was refluxed in aqueous HBr (25 cm^3, 3 mol dm^{-3}) at 110°C for 2.5 hours. Removal of the solvent *in vacuo* gave a brittle yellow/white solid which was recrystallised from water/ethanol to give the dihydrobromide salt of **17** as light brown crystals (0.638 g, 46%), mp 203-206°C (Found: C, 28.7; H, 6.59; N, 12.3. $C_8H_{21}Br_2N_3O$ requires C, 28.7; H, 6.32; N, 12.5%); δ_H(300.13 MHz, D_2O) 2.88 (2H, m, NCH_2 arm), 3.05 (4H, m, 2 x NCH_2 ring), 3.33 (4H, m, 2 x NCH_2 ring), 3.61 [4H, br s, $N(CH_2)_2N$ ring], 3.77 (2H, m, $C\underline{H}_2OH$); δ_C(74.47 MHz) 44.93, 46.46, 50.85 (ring carbons), 58.68 (NCH_2 arm), 60.58 (CH_2OH arm); *m/z* (LSI) 174.1614 $(M + H)^+$. $C_8H_{20}N_3O$ requires 174.1606.

Method 3

Ethylene oxide (0.70 cm^3, 14.0 mmol) in chilled ethanol (4 cm^3) was poured into a solution of 1-acetyl-4-formyl-1,4,7-triazacyclononane **37** (1.20 g, 6.03 mmol) in ethanol at 0°C and left to stir for three days in a stoppered flask at room temperature. The solvent was removed *in vacuo* and the residue refluxed in aqueous HBr (25 cm^3, 3 mol dm^{-3}) at 110°C for 2.5 hours. Removal of the solvent *in vacuo* gave a brittle yellow/white solid that was recrystallised from water/ethanol to give the dihydrobromide salt of **17** as white crystals (1.51 g, 75%). The physical and spectral data were consistent with the values from Method 2.

The free ligand was obtained by passage through an anion exchange column of Amberlite IRA-400 generated with 0.1 mol dm^{-3} NaOH. Removal of water under high vacuum afforded the free ligand as a pale yellow oil. δ_H(300.13 MHz, $CDCl_3$) 2.69 (4H, m, NCH_2 ring), 2.75 (10H, m, NCH_2 arm, 4 x NCH_2 ring), 3.60 (2H, t, *J* 5.3, CH_2OH); δ_C(74.47 MHz) 46.39, 46.85, 52.60 (ring carbons), 58.25 (NCH_2 arm), 59.90 (CH_2OH arm); *m/z* (FAB) 174 [$(M + H)^+$, 100%], 158 (4), 147 (3), 129 (6), 117 (6), 93 (16), 75 (10), 70 (11), 45 (31), 42 (16). Spectral data were consistent with literature values.[82]

1-[2-(*S*)-2-Hydroxypropyl]-1,4,7-triazacyclononane, 38

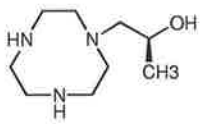

(*S*)-(-)-Propylene oxide (0.947 g, 16.3 mmol) was added to a solution of 1-acetyl-4-formyl-1,4,7-triazacyclononane **37** (0.992 g, 4.98 mmol) in ethanol at 0°C and left to stir for three days in a stoppered flask at room temperature. The solvent was removed *in vacuo* and the residue was refluxed in aqueous HBr (25 cm^3, 3 mol dm^{-3}) at 110°C for 2.5 hours. Removal of the solvent *in vacuo* gave a brittle yellow/white solid which was precipitated from methanol/dichloromethane to give the dihydrobromide salt of **38** as a white solid (1.29 g, 74%); δ_H(300.13 MHz, D_2O) 1.14 (3H, d, *J* 6.0, CH_3), 2.59 (1H, dd, *J* 10.5, 13.8, NCH_2 arm), 2.80 (1H, dd, *J* 2.7, 13.8, NCH_2 arm), 3.06 (4H, m, 2 x NCH_2 ring), 3.32 (4H, m, 2 x NCH_2 ring), 3.60 (4H, m, 2 x NCH_2 ring), 4.07 (1H, ddq, *J* 2.7, 6.0, 10.5, 13.8, C<u>H</u>OH arm);

δ_C(74.47 MHz) 22.46 (CH_3), 44.30, 45.92, 50.38 (ring carbons), 63.62 (NCH_2 arm), 66.92 (CHOH arm); *m/z* (LSI) 188.1767 $(M + H)^+$. $C_9H_{22}N_3O$ requires 188.1762.

The free ligand was obtained by passage through an anion exchange column of Amberlite IRA-400 generated with 0.1 mol dm^{-3} NaOH. Removal of water under high vacuum afforded the free ligand as a pale yellow oil that was dried under high vacuum. δ_H(300.13 MHz, $CDCl_3$) 1.11 (3H, d, *J* 6.0, CH_3), 2.32 (1H, dd, *J* 10.5, 12.7, NCH_2 arm), 2.64-2.83 (13H, m, NCH_2), 3.25 (3H, br s, NH, OH), 3.81 (1H, ddq, *J* 2.9, 6.0, 10.5, 12.7, CHOH arm); δ_C(74.47 MHz) 19.73 (CH_3), 46.78, 47.39, 53.36 (ring carbons), 64.86 (NCH_2 arm), 65.20 (CHOH arm); *m/z* (FAB) 188 [$(M + H)^+$, 100%], 170 (1), 157 (1), 143 (1), 131 (2), 113 (2), 102 (8), 84 (4), 70 (8), 45 (25), 43 (11).

1-[2-(*R*)-2,3-Dihydroxypropyl]-1,4,7-triazacyclononane, 39

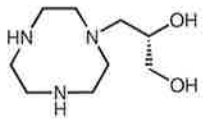

(*R*)-(+)-Glycidol (1.00 g, 13.5 mmol) was added to a solution of 1-acetyl-4-formyl-1,4,7-triazacyclononane **37** (1.09 g, 5.47 mmol) in ethanol at 0°C and left to stir for three days in a stoppered flask at room temperature. The solvent was removed *in vacuo* and the residue was refluxed in aqueous HBr (25 cm^3, 3 mol dm^{-3}) at 110°C for 2.5 hours. Removal of the solvent *in vacuo* gave a brittle light yellow solid that was recrystallised from water/ethanol to give the dihydrobromide salt of **39** as white crystals (1.62 g, 82%), mp 186-188°C (Found: C, 29.4; H, 6.34; N, 11.3. $C_9H_{23}Br_2N_3O_2$ requires C, 29.6; H, 6.35; N, 11.5%); δ_H(599.95 MHz, D_2O) 2.76 (1H, dd, *J* 9.4, 13.9, NCH_2 arm), 2.86 (1H, dd, *J* 3.3, 13.9, NCH_2 arm), 3.04 (2H, m, NCH_2 ring), 3.11 (2H, m, NCH_2 ring), 3.34 (4H, m, 2 x NCH_2 ring), 3.53 (1H, dd, *J* 5.3, 11.9, CH_2OH arm), 3.63 (1H, dd, *J* 4.4, 11.9, CH_2OH arm), 3.64 (4H, m, 2 x NCH_2 ring), 3.97 (1H, dddd, *J* 3.3, 4.4, 5.3, 9.4, CHOH arm); δ_C(74.47 MHz) 44.26, 45.97, 50.56 (ring carbons), 59.26 (NCH_2 arm), 66.18 (CH_2OH arm), 70.93 (CHOH arm); *m/z* (LSI) 204.1701 $(M + H)^+$. $C_9H_{22}N_3O_2$ requires 204.1711.

The free ligand was obtained by passage through an anion exchange column of Amberlite IRA-400 generated with 0.1 mol dm^{-3} NaOH. Removal of water under high

vacuum afforded the free ligand as a pale yellow oil. δ_H(599.95 MHz, $CDCl_3$) 2.63 (1H, dd, *J* 9.3, 12.9, NCH_2 arm), 2.64-2.77 (13H, m, NCH_2), 3.47 (1H, dd, *J* 5.1, 11.5, CH_2OH arm), 3.65 (1H, dd, *J* 3.9, 11.5, CH_2OH arm), 3.75 (1H, dddd, *J* 3.9, 4.2, 5.1, 9.0, CHOH arm); δ_C(74.47 MHz) 45.64, 45.94, 52.53 (ring carbons), 59.76 (NCH_2 arm), 64.61 (CH_2OH arm), 69.81 (CHOH arm); *m/z* (FAB) 204 [$(M + H)^+$, 100%], 185 (4), 171 (2), 159 (4), 140 (3), 118 (16), 111 (10), 93 (14), 85 (16), 70 (20), 56 (33), 43 (23).

2-(1,4,7-Triazacyclononan-1-yl)acetic acid, 31 [149a]

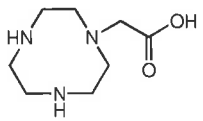

Ethyl bromoacetate (4.28 g, 25.6 mmol) in dry THF (10 cm^3) was added in a drop-wise manner to a rapidly stirred solution of 1,4,7-triazatricyclo[5.2.1.$0^{4,10}$]decane **6** (3.24 g, 23.3 mmol) in dry THF (200 cm^3) to gradually form a white precipitate. The reaction mixture was stirred for four hours and the white solid was collected by vacuum filtration under flowing nitrogen. The solid was then dissolved in aqueous HBr (60 cm^3, 3 mol dm^{-3}) and heated at 110°C for 12 hours. The solvent was removed *in vacuo* to give an off-white solid that was recrystallised from water/ethanol to afford the dihydrobromide salt of **31** as off-white crystals (5.29 g, 65%), mp 264-266°C (Found: C, 27.8 H, 5.42; N, 11.9 %. $C_8H_{19}Br_2N_3O_2$ requires C, 27.5; H, 5.49; N, 12.0 %); ν_{max}(nujol mull)/cm^{-1} 3100-2400 (br OH), 1718 (C=O); δ_H(300.13 MHz, D_2O) 3.13 (4H, m, 2 x NCH_2 ring), 3.36 (4H, m, 2 x NCH_2 ring), 3.65 (2H, s, NCH_2 arm), 3.70 [4H, br s, $N(CH_2)_2N$ ring]; δ_C(74.47 MHz) 44.98, 46.34, 50.82 (ring carbons), 57.32 (NCH_2 arm), 171.94 (CO_2H); *m/z* (FAB) 188 [$(M + H)^+$, 100 %], 170 (1), 159 (1), 144 (2), 142 (3), 130 (9), 115 (1), 100 (3), 94 (42), 76 (16), 74 (5), 59 (17), 47 (16), 33 (15), 31 (4).

4-(2-Hydroxyethyl)-1,4,7-triazonane-1-acetylamide, 45

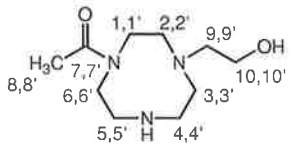

4-Nitrophenyl acetate (0.175 g, 0.966 mmol) in dichloromethane (8 cm^3) was added in a drop-wise manner to a stirred solution of 1-(2-hydroxyethyl)-1,4,7-triazacyclononane **17** (0.173 g, 1.00 mmol) in dichloromethane (20 cm^3) giving the solution a bright yellow colour. Upon stirring for one hour, the solvent was removed *in vacuo* to give an orange oil that was chromatographed on silica gel [NH_4OH-H_2O/MeOH (1:99)] to give **45** as a yellow oil (0.102 g, 49%); R_f = 0.22 (NH_4OH-H_2O/MeOH 1:99); ν_{max}(neat)/cm^{-1} 3401 (OH), 1623 (C=O); δ_H(200.13 MHz, $CDCl_3$) 1.99 [3H, s, (C8′)H_3], 2.01 [3H, s, (C8)H_3], 2.52 [2H, t, *J* 5.4, (C3′)H_2], 2.58 [2H, t, *J* 5.7, (C3)H_2)] 2.61 [2H, t, *J* 5.4, N(C9′)H_2], 2.67 [2H, t, *J* 5.4, N(C9)H_2], 2.68 [2H, t *J* 5.4, (C4′)H_2], 2.74 [2H, t, *J* 5.7, (C4)H_2], 2.78 [2H, t, *J* 5.1, (C2)H_2], 2.81 [2H, t, *J* 4.8, (C2′)H_2], 2.95 [2H, t, *J* 4.8, (C5′)H_2], 3.05 [2H, t, *J* 4.5, (C5)H_2], 3.37 [4H, m, (C1)H_2, (C1′)H_2], 3.46 [2H, t, *J* 5.1, (C10′)$\underline{H}_2$OH], 3.47 [2H, t, *J* 4.8, (C6′)H_2], 3.53 [2H, t, *J* 5.4, (C10)$\underline{H}_2$OH], 3.56 [2H, br t, (C6)H_2], 4.75 [2H, br s, (C10)OH, (C10′)OH]; δ_C(150.87 MHz) 21.96, 22.03 [(C8), (C8′)], 47.03 (C5), 47.78 (C4), 48.14 (C5′), 48.53 (C4′), 51.76 (C1′), 52.27 (C6), 53.24 [(C2′), (C3)], 53.56 (C1), 53.60 (C6′), 54.17 (C3′), 55.24 (C2), 57.81 (C9), 58.70 (C9′), 59.79 (C10), 59.90 (C10′), 171.19, 171.39 [(C7), (C7′)]; *m/z* (LSI) 216.1705 $(M + H)^+$. $C_{10}H_{21}N_3O_2$ requires 216.1712.

6.2.5. Syntheses Towards a Macrocycle Linker Arm

***N*-*tert*-Butoxycarbonyl-5-amino-1-pentanol, 49**

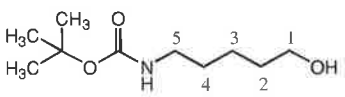

Boc-ON (2.68 g, 10.9 mmol) in chloroform (5 cm^3) was added to a stirred solution of 5-amino-pentanol [1.02 g (95%), 9.39 mmol] in chloroform (25 cm^3) and was stirred for four hours. Removal of the solvent *in vacuo* gave a pale yellow oil consisting of **49** and oximinyl

phenylacetonitrile. The two products were separated using silica gel chromatography. Initial elution with dichloromethane gave oximinyl phenylacetonitrile as a white solid [mp 126-128°C, R_f = 0.35 (CH_2Cl_2)]. Further elution with MeOH/CH_2Cl_2 (5/95%) gave **49** as a clear oil (1.68 g, 88%); R_f = 0.33 (MeOH/CH_2Cl_2, 5:95); ν_{max}(neat)/cm^{-1} 3351 (OH), 1693 (C=O); δ_H(200.13 MHz, $CDCl_3$) 1.44 [9H, s, $(CH_3)_3$], 1.52 (6H, m, 3 x CH_2), 3.13 (2H, quart, *J* 6.2, NCH_2), 3.65 (2H, t, *J* 6.4, CH_2O), 4.57 (1H, br s, OH, NH); δ_C(50.32 MHz) 22.69 (C3), 28.11 [$(CH_3)_3$], 29.46 (C4), 31.86 (C2), 40.15 (C5), 61.85 (C1), 78.75 [$\underline{C}H(CH_3)_3$], 156.11 (C=O); *m/z* (FAB) 204 [$(M + H)^+$, 19%], 147 (61), 107 (77), 67 (100). Spectral data were consistent with literature values.[184,185,186]

N-tert-Butoxycarbonyl-5-amino-1-(*p*-toluenesulfonyloxy)pentane, 50[187]

Triethylamine (2.93 g, 26.9 mmol) was added drop-wise to a stirred solution of *N-tert*-butoxycarbonyl-5-amino-1-pentanol **49** [1.64 g (95%), 8.08 mmol] in dry ether (20 cm^3). A solution of *p*-toluenesulfonyl chloride (1.99 g, 10.4 mmol) in dry ether (10 cm^3) was then added to the reaction mixture in a drop-wise manner and the solution was allowed to stir for three days at room temperature under nitrogen. The solid triethylamine hydrochloride was filtered off under flowing nitrogen and the filtrate reduced *in vacuo* to give a viscous yellow oil. The residue was dissolved in dichloromethane and washed sequentially with aqueous HCl (1 mol dm^{-3}), 5% aqueous $NaHCO_3$ and water. The organic layer was dried and reduced *in vacuo* to give a yellow oil that was chromatographed on silica gel [EtOAc/hexane (1:9) then (1:4)] to give **50** as a clear colourless oil (2.31 g, 80%); R_f = 0.22 (EtOAc/hexane, 1:4); ν_{max}(neat)/cm^{-1} 3382 (NH), 1679 (C=O); δ_H(200.13 MHz, $CDCl_3$) 1.38 (4H, m, 2 x CH_2), 1.44 [9H, s, $(CH_3)_3$], 1.66 (2H, quint, *J* 6.8, CH_2), 2.45 (3H, s, $ArCH_3$), 3.06 (2H, quart, *J* 6.4, NCH_2), 4.02 (2H, t, *J* 6.3, CH_2O), 4.51 (1H, br s, NH), 7.35 (2H, AA′ portion of AA′XX′, ArH), 7.79 (XX′ portion of AA′XX′, ArH); δ_C(50.32 MHz) 21.47 ($ArCH_3$), 22.53 (C3), 28.29 (3 x CH_3), 28.34 (C2), 29.32 (C4), 40.15 (C5), 70.26 (C1), 79.11 [$C(CH_3)_3$], 127.86 (ArCH), 129.84 (ArCH), 133.21 (ArC), 144.74 (ArC), 155.99 (C=O); *m/z* (FAB) 358 [$(M + H)^+$, 3 %], 301 (33), 256 (62), 171 (6), 130 (18), 114 (31), 81 (31), 67 (100), 49 (3).

Attempted Bromination of *N-tert*-Butoxycarbonyl-5-amino-1-pentanol, 49

Method 1

To a solution of *N-tert*-butoxycarbonyl-5-amino-1-pentanol **49** (0.367 g, 1.81 mmol) and lithium bromide (0.343 g, 3.95 mmol) in acetonitrile (15 cm^3) was added chlorotrimethylsilane (0.522 g, 5.08 mmol) in acetonitrile (4 cm^3). The reaction mixture was allowed to reflux for 16 hours under nitrogen. The solvent was removed *in vacuo* and the residue was taken up in ether (25 cm^3). The organic phase was then washed with water (2 x 15 cm^3) and dried. The solvent was then removed *in vacuo* but no product was obtained.

Method 2

To a stirred solution of 1,2-bis(diphenylphosphino)-ethane (DIPHOS) (1.17 g, 2.93 mmol) in dichloromethane (10 cm^3) at 0°C under nitrogen was slowly added Br_2 (0.950 g, 5.94 mmol) in dichloromethane (2 cm^3) in a drop-wise manner. *N-tert*-butoxycarbonyl-5-amino-1-pentanol **49** (0.474 g, 2.33 mmol) in dichloromethane (3 cm^3) was then added and the reaction mixture was allowed to stir at room temperature for two hours. The mixture was added to a solution of pentane/ether (2:1) creating a white precipitate. The entire mixture was passed through a squat column of silica gel [pentane/Et_2O (2:1)] to give a white solid that was recrystallised from isopropanol to afford the bromo-urea **51** as white crystals, mp 99-101°C; ν_{max}(neat)/cm^{-1} 3334, 3338 (NH), 1608 (C=O); δ_H(300.13 MHz, $CDCl_3$) 1.51 (4H, m, 2 x CH_2), 1.63 (1H, br s, OH), 1.88 (2H, quint, *J* 6.9, CH_2), 3.19 (2H, quart, *J* 6.4, NCH_2), 3.41 (2H, t, *J* 6.6, CH_2Br), 4.29 (1H, br m, NH); δ_C(50.32 MHz) 25.39 (2 x CH_2), 29.44 (2 x CH_2), 32.31 (2 x CH_2), 33.61 (2 x NCH_2), 40.36 (2 x CH_2Br), 156.06 (C=O); *m/z* (EI) 359, 357 (M^+, 18%), 279, 277 (47), 249 (4), 197 (24), 166 (6), 142 (8), 112 (59), 84 (72), 69 (39), 30 (100).

Benzyl *N*-(5-hydroxypentyl)carbamate, 52

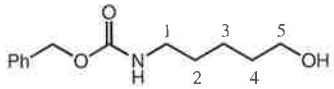

N-(Benzyloxycarbonyloxy)succinimide (Z-ON) (2.58 g, 10.4 mmol) in chloroform (5 cm^3) was added to a stirred solution of 5-amino-pentanol [0.973 g (95%), 9.43 mmol] in chloroform (25 cm^3) and the reaction mixture was allowed to stir for four hours. The organic layer was washed with water (20 cm^3) and dried. Removal of the solvent *in vacuo* gave a pale yellow oil that was chromatographed on silica gel [MeOH/CH_2Cl_2 (1:19)] to give **52** as a clear colourless oil (2.01 g, 90%); R_f = 0.38 (MeOH/CH_2Cl_2, 1:19); ν_{max}(neat)/cm^{-1} 3334 (OH), 1683 (C=O); δ_H(300.13 MHz, $CDCl_3$) 1.40 (2H, m, CH_2), 1.55 (4H, m, 2 x CH_2), 3.20 (2H, quart, *J* 6.4, NCH_2), 3.64 (2H, t, *J* 6.3, CH_2O), 4.89 (1H, br s, OH, NH), 5.09 (2H, s, $PhCH_2$), 7.34 (5H, m, ArH); δ_C(74.47 MHz) 22.80 (C3), 29.63 (C2), 32.10 (C4), 40.86 (C1), 62.39 ($PhCH_2$), 66.51 (C5), 127.97 (2 x ArCH, ArC), 128.40 (2 x ArCH), 136.58 (ArC), 156.50 (C=O); *m/z* (EI) 237 (M^+, 36 %), 194 (64), 181 (18), 108 (36), 91 (100), 85 (11), 65 (13), 41 (6), 31 (12).

Benzyl *N*-(5-bromopentyl)carbamate, 53

To a stirred solution of DIPHOS (0.869 g, 2.18 mmol) in dichloromethane (10 cm^3) at 0°C under nitrogen was slowly added Br_2 (0.703 g, 4.39 mmol) in dichloromethane (2 cm^3) in a drop-wise manner. Benzyl *N*-(5-hydroxypentyl)carbamate **52** (0.414 g, 1.75 mmol) in dichloromethane (3 cm^3) was then added and the reaction mixture was allowed to stir at room temperature for two hours. The reaction mixture was reduced *in vacuo* and chromatographed on silica gel [CH_2Cl_2 (100%)]. Removal of the solvent *in vacuo* gave a viscous oil that consisted of benzyl bromide and **53** in 6:1 ratio. The residue was further purified by silica gel chromatography [hexane (100%)] to give benzyl bromide, R_f = 0.38 (hexane); δ_H(300.13 MHz, $CDCl_3$) 4.47 (2H, s, $PhCH_2$), 7.30 (5H, m, ArH); δ_C(74.47 MHz) 33.48 (CH_2Br), 128.35 (ArCH), 128.74 (2 x ArCH), 128.98 (2 x ArCH), 137.76 (ArC); *m/z* (EI) 171, 169 (M^+, 28%), 91 (100), 81, 79 (7), 65 (25), 62 (9), 51 (13), 39 (23). Further elution [EtOAc/hexane (1:4)] gave **53** as a colourless oil (0.086 g, 16%); R_f = 0.33 (EtOAc/hexane,

1:4); ν_{max}(neat)/cm^{-1} 3419, 3338 (NH), 1697 (C=O); δ_H(300.13 MHz, $CDCl_3$) 1.48 (4H, m, 2 x CH_2), 1.85 (2H, quint, *J* 6.4, CH_2), 3.18 (2H, quart, *J* 6, NCH_2), 3.38 (2H, t, *J* 6.6, CH_2Br), 4.91 (1H, br s, NH), 5.08 (2H, s, $PhCH_2$), 7.32 (5H, m, ArH); δ_C(74.47 MHz) 22.04 (C3), 28.90 (C2), 32.06 (C4), 33.34 (C5), 40.58 (C1), 66.33 ($PhCH_2$), 127.83 (2 x ArCH, ArC), 128.27 (2 x ArCH), 136.48 (ArC), 156.27 (C=O); *m/z* (FAB) 301, 299 [$(M + H)^+$, 15%], 256 (2), 210 (3), 181 (22), 164 (3), 131 (4), 108 (53), 91 (100), 65 (8), 55 (3), 41 (4).

5-(Triphenylmethylamino)-1-pentanol, 54

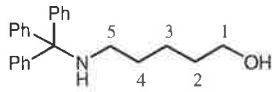

Triethylamine (3.40 g, 31.3 mmol) was added drop-wise to a stirred solution of 5-amino-pentanol [1.84 g (95%), 17.9 mmol] in dichloromethane (20 cm^3). Triphenylmethyl chloride (4.96 g, 17.8 mmol) in dichloromethane (20 cm^3) was then added drop-wise to the rapidly stirred solution and the mixture was allowed to stir for three hours at room temperature. The organic solution was washed with water (2 x 15 cm^3) and dried. Removal of the solvent *in vacuo* gave a pale yellow oil that was chromatographed on silica gel [EtOAc/hexane (1:9), (1:4) and then (2:3)] to give **54** as a viscous oil that crystallised to an amorphous solid on standing (3.49 g, 57%); R_f = 0.48 [EtOAc/hexane, (2:3)]; ν_{max}(neat)/cm^{-1} 3330 (OH); δ_H(300.13 MHz, $CDCl_3$) 1.37 (2H, m, CH_2), 1.50 (4H, m, 2 x CH_2), 2.19 (2H, t, *J* 6.7, NCH_2), 3.03 (1H, br s, OH, NH), 3.58 (2H, t, *J* 6.4, CH_2O), 7.19 (3H, m, ArH), 7.27 (6H, m, ArH), 7.45 (6H, m, ArH); δ_C(74.47 MHz) 23.50 (C3), 30.21 (C4), 32.55 (C2), 43.72 (C5), 62.73 (C1), 71.26 [$(Ph)_3CN$], 126.33 (3 x ArCH), 127.79 (6 x ArCH), 128.64 (6 x ArCH), 145.71 (3 x ArC); *m/z* (EI) 345 (M^+, 8 %), 304 (31), 269 (100), 244 (82), 228 (3), 194 (3), 165 (23), 149 (2), 137 (2), 104 (8), 81 (5), 69 (13), 43 (14).

***N*-(5-Bromopentyl)-*N*- triphenylmethylamine, 55**

To a stirred solution of DIPHOS (1.74 g, 4.36 mmol) in dichloromethane (20 cm^3) at 0°C under nitrogen was slowly added Br_2 (1.39 g, 8.69 mmol) in dichloromethane (4 cm^3) in a

drop-wise manner. 5-(Triphenylmethylamino)-1-pentanol **54** (1.20 g, 3.48 mmol) in dichloromethane (3 cm^3) was added and the reaction mixture was allowed to stir at 0°C for two hours. The organic solution was then washed with 10% aqueous Na_2CO_3 (2 x 15 cm^3), dried and the solvent removed *in vacuo*. The resulting white precipitate was chromatographed on a squat column of silica gel [CH_2Cl_2 (100%)] to give an impure solid that was further purified by silica gel chromatography, [hexane (100%)] and [EtOAc/hexane (1:9)], to give **55** as a white solid (0.699 g, 49%); R_f = 0.68 (EtOAc/hexane, 1:9); δ_H(300.13 MHz, $CDCl_3$) 1.13 (2H, m, CH_2), 1.55 (2H, quint, *J* 6.6, CH_2), 1.69 (2H, m, CH_2), 2.08 (1H, br s, NH), 3.04 (2H, m, NCH_2), 3.19 (2H, t, *J* 6.4, CH_2Br), 7.35 (9H, m, ArH), 7.70 (6H, m, ArH); δ_C(74.47 MHz) 25.93 (C3), 29.93 (C4), 32.68 (C2), 33.72 (C1), 43.34 (C5), 70.96 [$(Ph)_3CN$], 126.20 (3 x ArCH), 127.74 (6 x ArCH), 128.61 (6 x ArCH), 146.10 (3 x ArC); *m/z* (EI) 408, 406 (M^+, 13 %), 331, 329 (30), 244 (100), 229 (6), 194 (3), 165 (54), 115 (3), 84 (28), 77 (6), 41 (9).

9-Fluorenylmethyl *N*-(5-hydroxypentyl)carbamate, 56

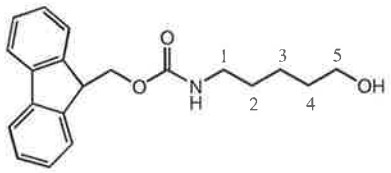

To a stirred solution of 5-amino-pentanol [0.895 g (95%), 8.68 mmol] in aqueous 10% Na_2CO_3 (20 cm^3) and 1,4-dioxane (10 cm^3) at 0°C was added 9-fluorenylmethyl chloroformate (Fmoc-Cl) in 1,4-dioxane (20 cm^3) in a drop-wise manner. The reaction mixture was stirred for six hours at room temperature and extracted with dichloromethane (2 x 30 cm^3). The solvent was dried and removed *in vacuo* to give a white solid that was recrystallised from EtOAc/hexane to afford **56** as fine white needles (2.23 g, 79%), mp 110-112°C; R_f = 0.51 ($MeOH/CH_2Cl_2$, 1:9); ν_{max}(neat)/cm^{-1} 3324 NH, 1693, 1672 C=O; δ_H(300.13 MHz, $CDCl_3$) 1.37 (2H, m, CH_2), 1.53 (4H, m, CH_2), 1.82 (1H, br s, OH), 3.17 (2II, quart, *J* 6.2, NCH_2), 3.61 (2H, t, *J* 6.3, CH_2OH), 4.19 (1H, t, *J* 6.5, ArCH), 4.39 (2H, d, *J* 6.6, CH_2OC=O), 4.90 (1H, br s, NH), 7.29 (2H, m, ArH), 7.38 (2H, m, ArH), 7.57 (2H, m, ArH), 7.74 (2H, m, ArH); δ_C(74.47 MHz) 22.78 (C3), 29.50 (C2), 31.99 (C4), 40.73 (C1), 47.11 (ArCH), 62.22 (C5), 66.30 ($\underline{C}H_2OC$=O), 119.79, 124.85, 126.86, 127.49 (ArCH),

141.12, 143.83 (ArC), 156.47 (C=O); *m/z* (EI) 325 (M^+, 3%), 284 (2), 264 (2), 236 (3), 222 (2), 179 (100), 153 (2), 139 (1), 112 (1), 87 (2), 69 (6), 30 (6). Spectral data were consistent with literature values.[188]

9-Fluorenylmethyl *N*-(5-iodopentyl)carbamate, 57

To a stirred solution of DIPHOS (0.683 g, 1.71 mmol) in dichloromethane (20 cm^3) at 0°C under nitrogen was slowly added I_2 (0.869, 3.42 mmol) in dichloromethane (50 cm^3). 9-Fluorenylmethyl *N*-(5-hydroxypentyl)carbamate, **56**, (0.446 g, 1.37 mmol) in dichloromethane (15 cm^3) was then added and the reaction mixture was allowed to stir at 0°C for two hours. The organic solution was washed with 10% aqueous Na_2CO_3 (2 x 15 cm^3), dried and the solvent removed *in vacuo*. The resulting white precipitate was purified by silica gel chromatography [CH_2Cl_2 (100%)] to give **57** as a white solid (0.346 g, 58%), mp 112-115°C; R_f = 0.40 (CH_2Cl_2); ν_{max}(neat)/cm^{-1} 3335 NH, 1687 C=O; δ_H(300.13 MHz, $CDCl_3$) 1.38 (4H, m, 2 x CH_2), 1.74 (2H, m, CH_2), 3.09 (4H, m, NCH_2, CH_2I), 4.13 (1H, t, *J* 6.6, ArCH), 4.32 (2H, d, *J* 6.3, CH_2OC=O), 4.73 (1H, br s, NH), 7.23 (2H, m, ArH), 7.32 (2H, m, ArH), 7.51 (2H, m, ArH), 7.68 (2H, m, ArH); δ_C(74.47 MHz) 6.53 (C5), 27.43 (C3), 28.76 (C2), 32.83 (C4), 40.63 (C1), 47.20 (ArCH), 66.37 ($\underline{C}H_2OC$=O), 119.84, 124.88, 126.90, 127.53 (ArCH), 141.19, 143.86 (ArC), 156.29 (C=O).

5-Amido-1-pentanol, 58

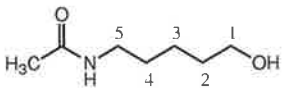

To a stirred solution of acetic anhydride (7.98 g, 78.2 mmol) in DMF (25 cm^3) at 0°C was added 5-amino-pentanol [2.50 g (95%), 24.3 mmol] in a drop-wise manner. The mixture was stirred at room temperature for 1.5 hours whereupon the solvent was removed by reduced pressure distillation. The resulting residue was dried under high vacuum at 80°C and then chromatographed on silica gel [MeOH/CH_2Cl_2 (1:9)] to give **58** as a clear colourless oil (3.66, 97%); R_f = 0.32 (MeOH/CH_2Cl_2, 1:9); ν_{max}(neat)/cm^{-1} 3293 (OH), 3095 (NH), 1650 (C=O);

δ_H(300.13 MHz, $CDCl_3$) 1.41 (2H, m, CH_2), 1.55 (4H, m, 2 x CH_2), 1.97 (3H, s, CH_3), 3.22 (2H, quart, *J* 6.4, NCH_2), 3.35 (1H, br s, OH, NH), 3.61 (2H, t, *J* 6.3, CH_2OH); δ_C(74.47 MHz) 22.99 (C3), 23.01 ($\underline{C}H_3C{=}O$), 29.09 (C4), 32.04 (C2), 39.41 (C5), 62.08 (C1), 170.54 (C=O); *m/z* (EI) 145 (M^+, 37 %), 115 (7), 102 (13), 100 (16), 86 (28), 85 (11), 72 (62), 68 (7), 60 (34), 45(12), 43 (100), 31 (50).

5-Amido-1-(*p*-toluenesulfonyloxy)pentane, 59

Triethylamine (5.14 g, 50.8 mmol) was added in a drop-wise manner to a stirred solution of 5-amido-1-pentanol **58** (3.68 g, 25.4 mmol) in dichloromethane (40 cm^3) at 0°C. A solution of *p*-toluenesulfonyl chloride (5.43 g, 28.5 mmol) in dichloromethane (40 cm^3) was then added to the reaction mixture in a drop-wise manner to maintain the low temperature. The reaction mixture was left to stir for three days at room temperature. The residue was dissolved in dichloromethane and washed sequentially with aqueous HCl (1 mol dm^{-3}), 5% aqueous $NaHCO_3$ and water. The organic layer was dried and then reduced *in vacuo* to give a yellow oil which was chromatographed on silica gel [$MeOH/CH_2Cl_2$ (1:19)] to give **59** as a clear colourless oil (6.22 g, 82%); R_f = 0.30 ($MeOH/CH_2Cl_2$, 1:19); ν_{max}(neat)/cm^{-1} 3294, 2938 (NH), 1652 (C=O); δ_H(300.13 MHz, $CDCl_3$) 1.37 (2H, m, CH_2), 1.45 (2H, m, CH_2), 1.67 (2H, quint, *J* 6.3, CH_2), 1.96 (3H, s, CH_3), 2.46 (3H, s, $ArCH_3$), 3.19 (2H, quart, *J* 6.3, NCH_2), 4.02 (2H, t, *J* 6.3, CH_2O), 5.86 (1H, br s, OH), 7.36 (2H, AA′ portion of AA′XX′, ArH), 7.78 (2H, XX′ portion of AA′XX′, ArH); δ_C(74.47 MHz) 21.53 ($ArCH_3$), 22.66 (C3), 23.15 ($\underline{C}H_3C{=}O$), 28.37 (C4), 28.78 (C2), 39.14 (C5), 70.29 (C1), 127.74 (ArCH), 129.81 (ArCH), 132.99 (ArC), 144.76 (ArC), 170.10 (C=O); *m/z* (EI) 299 (M^+, 24 %), 256 (9), 236 (1), 188 (3), 173 (17), 144 (42), 128 (31), 105 (8), 91 (61), 72 (58), 43 (100), 30 (91).

6.2.6. Attachment of Linker Arm to [9]aneN$_3$

1-(5-Aminopentyl)-1,4,7-triazacyclononane, 48

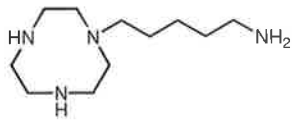

Method 1

To a solution of 1,4,7-triazatricyclo[5.2.1.0^{4,10}]decane **6** (0.159 g, 1.15 mmol) in dry THF (20 cm^3) was added *N-tert*-butoxycarbonyl-5-amino-1-(*p*-toluenesulfonyloxy)pentane **50** (0.410 g, 1.15 mmol) in dry THF (5 cm^3). The reaction mixture was refluxed overnight under nitrogen. Analysis by TLC revealed only starting material.

Method 2

To a solution of 1,4,7-triazatricyclo[5.2.1.0^{4,10}]decane **6** (0.146 g, 1.05 mmol) in dry THF (20 cm^3) was added 9-fluorenylmethyl *N*-(5-iodopentyl)carbamate **57** (0.457 g, 1.05 mmol) in dry THF (5 cm^3) and the reaction mixture was stirred for seven days. The solvent was removed *in vacuo* and the residue was refluxed in aqueous HBr (25 cm^3, 3 mol dm^{-3}) at 110°C for 2.5 hours. Removal of the solvent *in vacuo* gave a yellow/white solid consisting of unidentifiable products by ^{13}C NMR analysis.

General Procedure for Methods 3-6

To a solution of 1-acetyl-4-formyl-1,4,7-triazacyclononane **37** (one mol equivalent) and *N-tert*-butoxycarbonyl-5-amino-1-(*p*-toluenesulfonyloxy)pentane **50** (one or 1.5 mol equivalents) in dry DMF (10 cm^3/1.0 mmol) was added K_2CO_3 or $CsCO_3$ (three mol equivalents) and a catalytic amount of KI and the solution was stirred at 110°C for a defined period of time. The solvent was removed *in vacuo* and the residue partitioned between dichloromethane (25 cm^3) and water (10 cm^3). The organic layer was separated and the aqueous layer was extracted with two further amounts of dichloromethane (2 x 20 cm^3). The combined organic extracts were reduced *in vacuo* to give pale yellow oils that were refluxed

in aqueous HBr (25 cm^3, 3 mol dm^{-3}) at 110°C for 2.5 hours. Removal of the solvent *in vacuo* gave light yellow solids that consisted of unidentifiable products when analysed by ^{13}C NMR spectroscopy.

Method 3

1-Acetyl-4-formyl-1,4,7-triazacyclononane **37** (one mol equivalent) was treated with *N-tert*-butoxycarbonyl-5-amino-1-(*p*-toluenesulfonyloxy)pentane **50** (1.5 mol equivalents) and K_2CO_3 at 110°C for 16 hours.

Method 4

1-Acetyl-4-formyl-1,4,7-triazacyclononane **37** (one mol equivalent) was treated with *N-tert*-butoxycarbonyl-5-amino-1-(*p*-toluenesulfonyloxy)pentane **50** (one mol equivalent) and K_2CO_3 at 110°C for 16 hours.

Method 5

1-Acetyl-4-formyl-1,4,7-triazacyclononane **37** (one mol equivalent) was treated with *N-tert*-butoxycarbonyl-5-amino-1-(*p*-toluenesulfonyloxy)pentane **50** (1.5 mol equivalents) and $CsCO_3$ at 110°C for 16 hours.

Method 6

1-Acetyl-4-formyl-1,4,7-triazacyclononane **37** (one mol equivalent) was treated with *N-tert*-butoxycarbonyl-5-amino-1-(*p*-toluenesulfonyloxy)pentane **50** (one mol equivalent) and $CsCO_3$ at 110°C for four hours.

General Procedure for Methods 7-8

To a solution of 1-acetyl-4-formyl-1,4,7-triazacyclononane **37** (one mol equivalent) and 9-fluorenylmethyl *N*-(5-iodopentyl)carbamate **57** (one or 1.5 mol equivalents) in dry

DMF (10 cm^3/1.0 mmol) was added $CsCO_3$ (three mol equivalents) and the solution was stirred at 110°C for 16 hours. The solvent was removed *in vacuo* and the residue partitioned between dichloromethane (25 cm^3) and water (10 cm^3). The organic layer was separated and the aqueous layer was extracted with two further amounts of dichloromethane (2 x 20 cm^3). The combined organic extracts were reduced *in vacuo* to give pale yellow oils that were refluxed in aqueous HBr (25 cm^3, 3 mol dm^{-3}) at 110°C for 2.5 hours. Removal of the solvent *in vacuo* gave a light yellow solid that consisted predominantly of [9]aneN_3.3HBr **24** when analysed by ^{13}C NMR spectroscopy.

Method 7

1-Acetyl-4-formyl-1,4,7-triazacyclononane **37** (one mol equivalent) was treated with 9-fluorenylmethyl *N*-(5-iodopentyl)carbamate **57** (one mol equivalent).

Method 8

1-Acetyl-4-formyl-1,4,7-triazacyclononane **37** (one mol equivalent) was treated with 9-fluorenylmethyl *N*-(5-iodopentyl)carbamate **57** (1.5 mol equivalents).

General Procedure for Methods 9-14

To a solution of 1-acetyl-4-formyl-1,4,7-triazacyclononane **37** (one mol equivalent) in dry DMF (10 cm^3/1.0 mmol) with or without $CsCO_3$ (three mol equivalents) or triethylamine (1.5 mol equivalents) was added 5-amido-1-(*p*-toluenesulfonyloxy)pentane **59** (one or 1.5 mol equivalents) and the solution was stirred at a defined temperature for a defined period of time. The solvent was removed *in vacuo* and the residue partitioned between dichloromethane (25 cm^3) and water (10 cm^3). The organic layer was separated and the aqueous layer was extracted with two further amounts of dichloromethane (2 x 20 cm^3). The combined organic extracts were reduced *in vacuo* to give pale yellow oils that were refluxed in aqueous HBr (25 cm^3, 3 mol dm^{-3}) at 110°C for 2.5 hours. Removal of the solvent *in vacuo* gave light yellow solids.

Method 9

1-Acetyl-4-formyl-1,4,7-triazacyclononane **37** (one mol equivalent) was treated with 5-amido-1-(*p*-toluenesulfonyloxy)pentane **59** (1.5 mol equivalents) in the presence of $CsCO_3$ and a catalytic amount of KI at 120°C for four hours. Analysis of by ^{13}C NMR spectroscopy revealed a mixture of unidentifiable products.

Method 10

1-Acetyl-4-formyl-1,4,7-triazacyclononane **37** (one mol equivalent) was treated with 5-amido-1-(*p*-toluenesulfonyloxy)pentane **59** (one mol equivalent) in the presence of $CsCO_3$ at 120°C for four hours. Analysis of by ^{13}C NMR spectroscopy revealed a mixture of unidentifiable products.

Method 11

1-Acetyl-4-formyl-1,4,7-triazacyclononane **37** (one mol equivalent) was treated with 5-amido-1-(*p*-toluenesulfonyloxy)pentane **59** (0.9 mol equivalents) in the presence of $CsCO_3$ at 55°C for 16 hours. Analysis of by ^{13}C NMR spectroscopy revealed a mixture of unidentifiable products.

Method 12

1-Acetyl-4-formyl-1,4,7-triazacyclononane **37** (one mol equivalent) was treated with 5-amido-1-(*p*-toluenesulfonyloxy)pentane **59** (1.5 mol equivalents) in the presence of triethylamine at 55°C for 16 hours. Analysis of by ^{13}C NMR spectroscopy revealed mainly [9]aneN_3.3HBr **24**.

Method 13

1-Acetyl-4-formyl-1,4,7-triazacyclononane **37** (one mol equivalent) was treated with 5-amido-1-(*p*-toluenesulfonyloxy)pentane **59** (1.5 mol equivalents) in the presence of

triethylamine at 70°C for 16 hours. Analysis of by ^{13}C NMR spectroscopy revealed mainly [9]aneN_3.3HBr **24**.

Method 14

1-Acetyl-4-formyl-1,4,7-triazacyclononane **37** (one mol equivalent) was treated with 5-amido-1-(*p*-toluenesulfonyloxy)pentane **59** (1.5 mol equivalents) at 70°C for four days. Analysis of by ^{13}C NMR spectroscopy revealed a mixture of products.

Method 15

To a solution of 1-acetyl-4-formyl-1,4,7-triazacyclononane **37** (0.338 g, 1.69 mmol) in dry DMF (15 cm^3) was added 5-amido-1-(*p*-toluenesulfonyloxy)pentane **59** (0.451 g, 1.51 mmol) and the solution was stirred at 70°C for four days. The solvent was removed *in vacuo* and the residue partitioned between dichloromethane (25 cm^3) and water (10 cm^3). The organic layer was separated and the aqueous layer was extracted with two further amounts of dichloromethane (2 x 20 cm^3). The combined organic extracts were reduced *in vacuo* to give a pale yellow oil that was refluxed in aqueous HBr (25 cm^3, 3 mol dm^{-3}) at 110°C for 2.5 hours. Removal of the solvent *in vacuo* gave a light yellow solid consisting of a mixture of [9]aneN_3.3HBr **24** and **48**. Repeated fractional recrystallisation from ethanol afforded [9]aneN_3.3HBr **24** followed by the trihydrobromide salt of **48** as a white solid (0.131 g, 17%), mp 207-208°C (Found: C, 28.90 H, 6.60; N, 12.01 %. $C_{11}H_{29}Br_3N_4$ requires C, 28.91; H, 6.39; N, 12.26 %); δ_H(300.13 MHz, D_2O) 1.37 (2H, m, CH_2), 1.66 (4H, m, 2 x CH_2), 2.90 (2H, t, *J* 8.1, $C\underline{H}_2NH_2$ arm), 2.98 (2H, t, *J* 7.5, NCH_2 arm), 3.15 (4H, m, 2 x NCH_2 ring), 3.32 (4H, m, 2 x NCH_2 ring), 3.47 (4H, m, 2 x NCH_2); δ_C(74.47 MHz) 25.43 (CH_2), 25.55 (CH_2), 28.62 (CH_2), 41.49 (CH_2NH_2 arm), 44.19, 45.03, 50.29 (ring carbons), 57.37 (NCH_2 arm); *m/z* (LSI) 215.2227 $(M + H)^+$. $C_{11}H_{27}N_4$ requires 215.2236.

6.3. Aqueous Potentiometric Titrations

6.3.1. Preparation of Solutions

All solutions were prepared using ultra purified deionised water prepared with a MilliQ-Reagent system giving water with a specific resistance greater than 15 MΩ cm. This water was then refluxed for five hours under nitrogen to remove CO_2 gas.

6.3.1.1. Metal Ion Solutions

Aqueous solutions of $ZnSO_4$ (0.155 mol dm^{-3}) and $CdSO_4$ (0.0113 mol dm^{-3}) were prepared from the appropriate sulfate salts that had been stored under vacuum over P_2O_5. The metal solutions were standardised in triplicate by passage of 2 cm^3 aliquots through a cation exchange column of Dowex AG 50W-X2 generated with HCl (0.1 mol dm^{-3}) followed by manual titration against NaOH (0.100 mol dm^{-3}) using a bromothymol blue indicator.

6.3.1.2. Ligand Solutions

Ligand solutions (0.001 mol dm^{-3}) were made by dissolving the appropriate weight of ligand hydrobromide salt into an aqueous stock solution of $HClO_4$ (0.003 mol dm^{-3}) and $NaNO_3$ (0.097 mol dm^{-3}). The metal-ligand solutions were prepared by adding an equimolar amount of the metal ion solution directly to the aliquot of titrant ligand solution (10 cm^3) immediately before titration.

6.3.1.3. Aqueous NaOH Solution

Aqueous NaOH (0.100 mol dm^{-3}) was prepared from a convol (BDH) and was stored in a bottle vented with a drying tube containing self indicating "Carbosorb" soda lime (10-16 mesh, BDH) to prevent CO_2 absorption. This was standardised on a weekly basis by titration against aqueous potassium hydrogen phthalate solution (0.01 mol dm^{-3}).

6.3.2. Titration Procedure

Titrations were carried out at [total ligand] = 0.001 mol dm^{-3} in the presence or absence of equimolar $ZnSO_4$ or $CdSO_4$ at an ionic strength maintained at 0.1 mol dm^{-3} with $NaNO_3$ and at least three independent titrations were always made. All titrations were performed on 10 cm^3 aliquots of test solution in a three-necked 20 cm^3 water-jacketed titration vessel at 298.2 ± 0.1 K. The titration temperature was controlled using a thermostated water bath fitted with a Isotherm Circulator.

The titrant solution was stirred with a magnetic stirring bar and the three-necked vessel was fitted with an electrode, a NaOH dispenser hose and a gas line that bubbled a fine stream of nitrogen gas, filtered through $NaNO_3$ (0.1 mol dm^{-3}), into the solution throughout the titration. The titration solution remained closed to the atmosphere except for a small exit for excess nitrogen gas. Each sample was allowed to stir with streaming nitrogen for 15 minutes prior to commencing the titration.

The electrode was calibrated each day to determine the E_o and pK_w values of the system. This was achieved by titrating the aqueous stock solution of $HClO_4$ (0.003 mol dm^{-3}) and $NaNO_3$ (0.097 mol dm^{-3}) against the standardised NaOH solution and fitting the data to the Nernst equation (6.1).

$$E = E_o + \frac{RT}{F} \ln[H^+] \qquad (6.1)$$

where

E is the observed potential (mV)

E_o is the standard potential for the electrode (mV)

R is the gas constant, 8.314 (J K^{-1} mol^{-1})

T is the temperature (K)

F is Faraday's constant, 9.6487 x 10^4 (C mol^{-1})

$[H^+]$ is the proton concentration

At a fixed temperature (298.2 K) the Nernst equation (6.1) becomes,

$$\mathrm{pH} = \frac{(E_o - E)}{59.15} \qquad (6.2)$$

where pH = -log[H^+].

When considering pK_w = pH + pOH and pOH = -log[OH^-], equation (6.2) becomes

$$pK_w = \frac{(E_o - E)}{59.15} + \mathrm{pOH} \qquad (6.3)$$

The calibration parameters E_o and pK_w were obtained from equations 6.2 and 6.3, respectively, using the MacCalib[189] programme with literature[190] diffusion correction terms, E_o = 2.463 and pK_w = 1.057, for aqueous $NaNO_3$ (0.1 mol dm^{-3}). Under these conditions the average pK_w was 13.7.

At least three titrations were performed for each system. The pK_a's and stability constants were determined using the Fortran programme Superquad.[172] The final constants represent an average from at least two calculated titrations where the χ^2 of each run was less than 12.6 at the 95% confidence level. Averaging was performed using the Matlab programme Errors.[191]

6.4. Kinetic Measurements of the Hydrolysis of 4-Nitrophenyl Acetate

6.4.1. Preparation of Solutions

All solutions were prepared using ultra purified deionised water prepared with a MilliQ-Reagent system giving water with a specific resistance greater than 15 MΩ cm. Aqueous NaOH (0.1 mol dm^{-3}) solution was prepared from a convol (BDH).

6.4.1.1. Borate Buffer, pH 9.2

A boric acid/NaOH buffer (0.1 mol dm^{-3}, I = 0.10, pH 9.20) was prepared from boric acid (3.094 g) and $NaClO_4$ (3.23 g) dissolved in NaOH (264 cm^3, 0.1 mol dm^{-3}) and the solution was made up to 0.5 litres using ultra purified water.

6.4.1.2. 4-Nitrophenyl Acetate in Acetonitrile

4-Nitrophenyl acetate (0.0184 g) was dissolved in dry acetonitrile and made up to 10 cm^{-3} to give a 0.01 mol dm^{-3} solution that was stored in darkness. 1cm^3 of this solution was diluted daily in dry acetonitrile to 10cm^3 to give a fresh 0.001 mol dm^{-3} solution.

6.4.1.3. Hec[9] Solutions in Borate Buffer

Hec[9] solutions [(1 - 5) x 10^{-3} mol dm^{-3}] were prepared by dissolving the appropriate weight of hec[9].2HBr in aqueous borate buffer (0.1 mol dm^{-3}, I = 0.10, pH 9.20). The pH of each solution was measured with a pH electrode and fine adjustments of 0.1 - 0.2 pH units were made with microlitre amounts of NaOH (10 mol dm^{-3}).

6.4.1.4. [Zn^{II}-17] Solutions in Borate Buffer

[Zn^{II}-**17**] solutions [(1.4 - 4.3) x 10^{-3} mol dm^{-3}] were prepared by dissolving the appropriate weight of [Zn^{II}-**17**] complex in aqueous borate buffer (0.1 mol dm^{-3}, I = 0.10, pH 9.20). The [Zn^{II}-**17**] complex was generated from an ethanolic solution containing equimolar

amounts of $Zn(ClO_4)_2$ and free hec[9] **17** and was isolated as colourless crystals; *m/z* (LSI) 236.0730 $[C_8H_{18}N_3OZn]^+$.

6.4.2. Reaction Procedure

Reactions were carried out by pipetting 2.0 cm^3 aliquots of the appropriate solution into a quartz cell (1 cm path length) placed in the water-jacketed cell block of the Diode Array spectrophotometer. The cell block was maintained at 298.2 ± 0.1 K with circulating water from a thermostated water bath fitted with a Isotherm Circulator. The solutions were allowed to equilibrate for five minutes. The reaction was initiated by adding 0.02 cm^3 of ester in acetonitrile (0.001 mol dm^{-3}) to the quartz cell with immediate mixing. A blank reference scan was taken and data collection was started immediately after. The reaction was followed by the increase in absorbance of 4-nitrophenolate between 350-450 nm at 2 nm increments.

Each reaction was followed by pseudo-first order kinetics and monitored through at least seven half-lives. Each reaction was performed at least three times with the rate constants from each run varying by less than 4% and the results were averaged.

The rate constant, k_o, for the spontaneous hydrolysis of 4-nitrophenyl acetate in buffer and the observed rate constants, k_{obs}, for the reaction between 4-nitrophenyl acetate and hec[9] or [Zn^{II}-**17**] in buffer were obtained from the slope of the straight line formed by plotting $\ln(A_\infty - A_t)$ against time and the corrected rate constants, $k_{obs}-k_o$, were obtained by subtracting the spontaneous rate constant from the observed rate constants. Rate constants, $k_{obs}-k_o$, for 4-nitrophenyl acetate hydrolysis in the presence of hec[9] or [Zn^{II}-**17**] were determined at varying concentrations [(1 - 5) x 10^{-3} mol dm^{-3}]. The specific rate constant, k_{NA}, was taken as the coefficient $(k_{obs}-k_o)$/[[hec[9]] or $(k_{obs}-k_o)$/[[Zn^{II}-**17**]]. Errors were calculated from the standard deviation of rate constants from each run.

APPENDIX A. X-ray Crystallographic Data

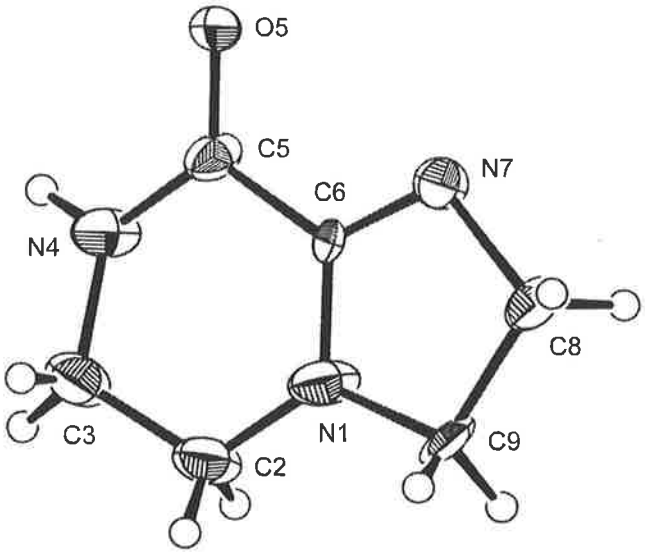

Figure A1. X-ray crystal structure of 1,4,7-triazabicyclo[4.3.0]non-6-ene-5-one, **35**.

Intramolecular Distances (Å)

atom	atom	distance	atom	atom	distance
O(5)	C(5)	1.209(7)	N(8)	H(10)	0.944
N(1)	N(8)	1.431(8)	C(3)	H(3a)	0.958
N(1)	C(6)	1.354(8)	C(3)	H(3b)	0.993
N(1)	C(9)	1.458(8)	C(5)	C(6)	1.509(9)
N(4)	C(3)	1.47(1)	C(8)	C(9)	1.555(9)
N(4)	C(5)	.328(8)	C(8)	H(8b)	0.961
N(4)	H(4)	0.963	C(8)	H(8a)	0.976
N(7)	C(6)	1.282(7)	C(9)	H(9b)	1.006
N(7)	C(8)	1.502(8)	C(9)	H(9a)	0.943
N(8)	C(3)	1.47(1)			

Intramolecular Bond Angles (deg.)

atom	atom	atom	angle	atom	atom	atom	angle
N(8)	N(1)	C(6)	123.5(7)	O(5)	C(5)	C(6)	119.3(6)
N(8)	N(1)	C(9)	125.8(6)	N(4)	C(5)	C(6)	115.6(6)
C(6)	N(1)	C(9)	110.1(6)	N(1)	C(6)	N(7)	116.8(7)
C(3)	N(4)	C(5)	123.6(7)	N(1)	C(6)	C(5)	119.5(6)
C(3)	N(4)	H(4)	118.18	N(7)	C(6)	C(5)	123.6(7)
C(5)	N(4)	H(4)	118.21	N(7)	C(8)	C(9)	106.3(5)
C(6)	N(7)	C(8)	105.9(6)	N(7)	C(8)	H(8b)	110.43
N(1)	N(8)	C(3)	114.7(8)	N(7)	C(8)	H(8a)	109.98
N(1)	N(8)	H(10)	122.49	C(9)	C(8)	H(8b)	109.41
C(3)	N(8)	H(10)	122.59	C(9)	C(8)	H(8a)	111.01
N(4)	C(3)	N(8)	113.2(9)	H(8b)	C(8)	H(8a)	109.71
N(4)	C(3)	H(3a)	109.75	N(1)	C(9)	C(8)	100.5(5)
N(4)	C(3)	H(3b)	108.82	N(1)	C(9)	H(9b)	111.84
N(8)	C(3)	H(3a	107.35	N(1)	C(9)	H(9a)	112.33
N(8)	C(3)	H(3b)	109.05	C(8)	C(9)	H(9b)	109.98
H(3a)	C(3)	H(3b)	108.53	C(8)	C(9)	H(9a)	113.32
O(5)	C(5)	N(4)	123.8(7)	H(9b)	C(9)	H(9a)	108.71

APPENDIX B. Experimental Data for the Hydrolysis of 4-Nitrophenyl Acetate in the Absence and Presence of Hec[9]

Table B1. The rate constants, k_o, for the spontaneous hydrolysis of 4-nitrophenyl acetate (**A**), and the observed rate constants, k_{obs}, (**B**) and the corrected rate constants, k_{obs}-k_o, (**C**) for the reaction of 4-nitrophenyl acetate and hec[9] in borate buffer (0.1 mol dm^{-3}, I = 0.1, pH 9.2) at 400 nm and 298.2 ± 0.1 K. Errors in parentheses represent the standard deviation between each run.

A

Experiment no.	k_o (1) (10^{-6} s^{-1})	k_o (2) (10^{-6} s^{-1})	k_o (3) (10^{-6} s^{-1})	k_o (4) (10^{-6} s^{-1})	k_o (avg) (10^{-6} s^{-1})
1	5.169	5.265	5.470	5.019	5.231 (± 0.1889)

B

Conc. (10^{-3} mol dm^{-3})	k_{obs} (1) (10^{-5} s^{-1})	k_{obs} (2) (10^{-5} s^{-1})	k_{obs} (3) (10^{-5} s^{-1})	k_{obs} (4) (10^{-5} s^{-1})
0.5	0.839	0.8378	0.839	-
1.0	1.124	1.147	1.136	-
2.0	1.914	1.912	1.896	1.912
3.0	2.642	2.651	2.661	2.631
4.0	3.523	3.107	3.075	3.186
5.0	3.842	3.791	3.812	3.826

C

Conc. (10^{-3} mol dm^{-3})	k_{obs} -k_o (1) (10^{-5} s^{-1})	k_{obs} -k_o (2) (10^{-5} s^{-1})	k_{obs} -k_o (3) (10^{-5} s^{-1})	k_{obs} -k_o (4) (10^{-5} s^{-1})	k_{obs} -k_o (avg) (10^{-5} s^{-1})
0.5	0.3069	0.30568	0.3069	-	0.3065 (± 0.001)
1.0	0.5919	0.6149	0.6039	-	0.6036 (± 0.011)
2.0	1.3819	1.3799	1.3639	1.3799	1.3764 (± 0.008)
3.0	2.1099	2.1189	2.1289	2.0989	2.1141 (± 0.013)
4.0	2.5749	2.5429	2.6539	-	2.5906 (± 0.057)
5.0	3.3099	3.2589	3.2799	3.2939	3.2857 (± 0.022)

APPENDIX C. Experimental Data for the Hydrolysis of 4-Nitrophenyl Acetate in the Absence and Presence of [Zn^{II}-17]

Table C1. The rate constants, k_o, for the spontaneous hydrolysis of 4-nitrophenyl acetate (**A**), and the observed rate constants, k_{obs}, (**B**) and the corrected rate constants, k_{obs}-k_o, (**C**) for the reaction of 4-nitrophenyl acetate and [Zn^{II}-**17**] in borate buffer (0.1 mol dm^{-3}, I = 0.1, pH 9.2) at 400 nm and 298.2 ± 0.1 K. Errors in parentheses represent the standard deviation between each run.

A

Experiment no.	k_o (1) (10^{-6} s^{-1})	k_o (2) (10^{-6} s^{-1})	k_o (3) (10^{-6} s^{-1})	k_o (4) (10^{-6} s^{-1})	k_o (avg) (10^{-6} s^{-1})
2	5.260	5.258	5.372	-	5.297 (± 0.065)

B

Conc. (10^{-3} mol dm^{-3})	k_{obs} (1) (10^{-5} s^{-1})	k_{obs} (2) (10^{-5} s^{-1})	k_{obs} (3) (10^{-5} s^{-1})	k_{obs} (4) (10^{-5} s^{-1})
1.30	1.140	1.160	1.154	1.168
2.03	1.490	1.533	1.481	-
2.35	1.870	1.870	1.788	1.831
3.90	2.470	2.500	2.441	2.418

C

Conc. (10^{-3} mol dm^{-3})	k_{obs} -k_o (1) (10^{-5} s^{-1})	k_{obs} -k_o (2) (10^{-5} s^{-1})	k_{obs} -k_o (3) (10^{-5} s^{-1})	k_{obs} -k_o (4) (10^{-5} s^{-1})	k_{obs} -k_o (avg) (10^{-5} s^{-1})
1.30	0.6103	0.6303	0.6243	0.6383	0.6258 (± 0.012)
2.03	0.9603	1.0033	0.9513	-	0.9716 (± 0.028)
2.35	1.3403	1.3403	1.2583	1.3012	1.3100 (± 0.039)
3.90	1.9403	1.9703	1.9113	1.8883	1.9275 (± 0.036)

APPENDIX D. Publications and Presentations arising from this Thesis

"A general method for the preparation of single pendant arm 2-hydroxyalkyl-1,4,7-triazacyclononane macrocycles", S. P. Creaser, S. F. Lincoln and S. M. Pyke, *J. Chem. Soc., Perkin Trans. 1*, 1999, 1211-1213.

"Crystal structure of 1,4,7-triazabicyclo[4.3.0]non-6-ene-5-one, $C_6H_9N_3O$", S. P. Creaser, S. F. Lincoln, S. M. Pyke and E. R. T. Tiekink, *Z. Kristallogr.*, 1998, **213**, 41.

"Syntheses and coordination studies of [9]aneN_3 derivatives with increasing numbers of hydroxyethyl pendant arms", S. P. Creaser, Adelaide Organic Chemistry Symposium, Adelaide Chemistry Department, S.A., 6th December, 1999.

"Syntheses and coordination studies of [9]aneN_3 derivatives with increasing numbers of hydroxyethyl pendant arms", S. P. Creaser, S. F. Lincoln and S. M. Pyke, 16th National Organic Conference, Leura, N.S.W., 12th-17th July, 1998.

A general method for the preparation of single pendant arm 2-hydroxyalkyl-1,4,7-triazacyclononane macrocycles

Steffen P. Creaser, Stephen F. Lincoln * and Simon M. Pyke *

Department of Chemistry, University of Adelaide, S.A. 5005, Australia.
E-mail: spyke@chemistry.adelaide.edu.au

Received (in Cambridge) 23rd December 1998, Accepted 11th March 1999

The facile synthesis of a di-protected 1,4,7-triazacyclononane derivative that provides a simple route to single pendant arm 2-hydroxyalkyl triaza-macrocycles through reaction with epoxides is described.

Introduction

The *N*-functionalisation of aza-macrocycles by reaction with substituted epoxides is an area of considerable synthetic activity as such macrocycles yield an impressive array of metal complexes.[1] Although the selective functionalisation of less than the total number of nitrogens of aza-macrocycles is more challenging, it offers the enticing opportunity to produce coordinately unsaturated metal complexes.[2] Recently, a general synthesis of 1,4,7-triazacyclononane, [9]aneN$_3$, substituted by pendant arms at two of the nitrogens was published.[3] We require [9]aneN$_3$ and similar macrocycles substituted with only a single hydroxyalkyl pendant arm for biomimetic studies. Although there are isolated examples of such mono-substituted macrocycles,[4,5] there remains no general synthetic method for attaching a range of single hydroxyalkyl pendant arms to [9]aneN$_3$, the key to which lies in the generation of a suitable di-protected [9]aneN$_3$ intermediate. Existing protection methods involve either selective detosylation[6] or the use of bulky carbamate groups[7] which decrease the reactivity of the third amine donor toward ordinary alkylating agents. Such di-protected species are usually unsuitable for reaction with epoxides and generally require activated alkylating agents such as organo-triflates or acyl-bromide compounds. A more reactive di-protected intermediate, which can react readily with a range of epoxides, is needed.

Discussion

In order to maintain an adequate reactivity of the di-protected [9]aneN$_3$ intermediate, we sought to incorporate smaller protecting groups which might impose less steric influence over the third amine donor. We initially attempted to isolate the dioxoamine **1** where two of the amine donors are protected as internal amide groups, however, the high dilution reaction between diethylenetriamine and diethyl oxalate preferentially gave the bicyclic compound **2** (Scheme 1), the structure of which was confirmed by X-ray crystallography.[8]

Our attention then shifted to the introduction of external amide functional groups and we now report the synthesis of a reactive di-protected [9]aneN$_3$ intermediate, **5**, which offers a general route to single pendant arm aza-macrocycles (Scheme 2). The macrocycle [9]aneN$_3$ **3** was first converted to the orthoamide **4** which was then treated with one equivalent of acetyl bromide. Subsequent aqueous hydrolysis followed by anion exchange chromatography gave **5** as a white solid in 89% yield.

Although high resolution mass spectrometry of **5** and a single spot observed by TLC infers a single compound, the NMR spectra reveal a mixture of isomeric forms. The ^{13}C NMR spectrum of **5** in $CDCl_3$ shows 21 aliphatic resonances

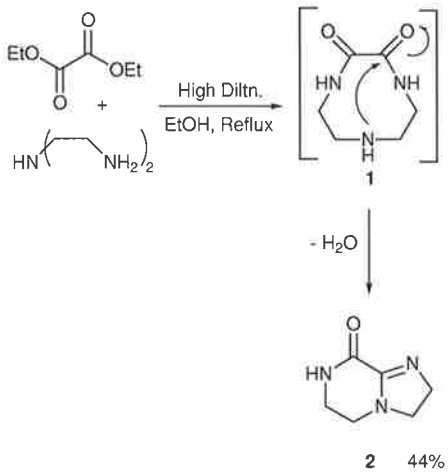

Scheme 1

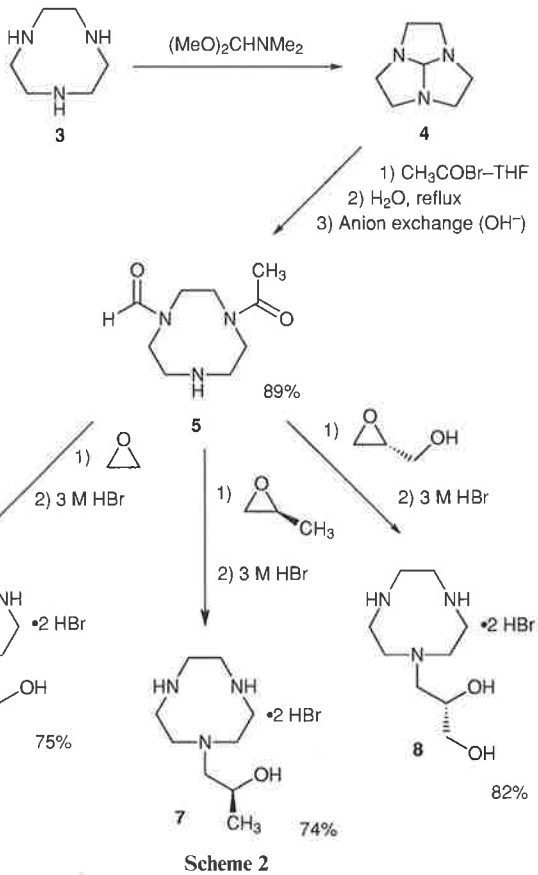

Scheme 2

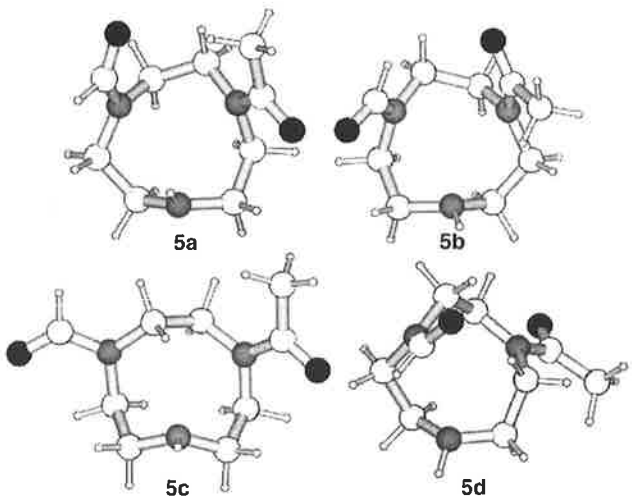

Fig. 1 The four most stable isomers obtained from *ab initio* calculations. The oxygen atoms are represented by black spheres, the nitrogen atoms by grey spheres and the carbon and hydrogen atoms by white spheres.

(three methyl, 18 ring), three formyl C=O resonances and three acetamide C=O resonances as the major spectral components.

Similarly, the ^{1}H NMR spectrum reveals three major methyl singlets and three major formyl singlets. An additional fourth methyl and fourth formyl singlet are also observable but are considerably lower in intensity suggesting a fourth less stable isomer. This number of observed resonances is consistent with **5** existing in three major and one minor isomeric forms which interconvert slowly on the NMR timescale due to restricted rotation about the C–N amide bonds.[9,10] Rotation about each amide group of **5** allows the possibility of four configurational isomers which would each give unique resonances in the ^{13}C NMR spectrum.

Ab initio calculations suggest the lowest energy conformations of each isomer to be those shown in Fig. 1, where the energies of **5a**, **5b**, **5c** and **5d** are −663.783743, −663.783645, −663.779449 and −663.775964 Hartrees respectively in the gas phase (1 Hartree = 2625.5 kJ mol^{-1}). The isomers **5a** and **5b**, where the amide dipoles are directly aligned, represent the most stable configurations. The least stable isomer is **5d** where the oxygen atoms of each amide group are orientated toward each other. While these calculations generate the probable isomeric structures in the gas phase they are not necessarily a guide to the relative stabilities in solution. It is known that tertiary amides form intermolecular dipole–dipole aggregates in solution which may account for the qualitatively similar populations of the three dominant isomers in the NMR spectra.[9]

The reaction of epoxide and orthoamide **4**, as a pathway to mono-alkylated [9]aneN$_3$, was found to be inappropriate, with the reaction in ethanol giving a mixture of products by TLC and NMR. The reaction of **5** with the epoxides, however, followed by acid hydrolysis of the protecting groups, gave the three single pendant arm macrocycles **6**, **7** and **8** as recrystallisable HBr salts in good yield (Scheme 2). The macrocycles were stored as HBr salts until needed. The free ligands can be obtained by anion exchange chromatography in virtually quantitative yield if required. This represents an improved method for producing mono-functionalised [9]aneN$_3$ derivatives with small hydroxyalkyl pendant arms.

Experimental

Materials and methods

Melting points were determined on a Kofler hot-stage apparatus equipped with a Reichert microscope and are uncorrected. Infrared spectra were recorded on a Mattson 270-30 FT spectrometer as Nujol mulls or liquid films between sodium chloride plates. ^{1}H and ^{13}C NMR spectra were recorded on a Varian Gemini-2000 (300 and 74.47 MHz respectively) spectrometer or a Varian Inova (600 MHz) spectrometer. Spectra were obtained for solutions in $CDCl_3$ [tetramethylsilane (δ_H 0.0) and $CDCl_3$ (δ_C 77.0) as internal standards] at 25 °C, or in D_2O [sodium 3-(trimethylsilyl)propanesulfonate (δ_H 0.0 for $SiMe_3$) and *tert*-butyl alcohol (δ_C 31.6 for CH_3) as external standards] at 25 °C. *J* Values are given in Hz. Electron impact (EI) mass spectra were recorded on a ZAB 2HF mass spectrometer while liquid spray ionisation (LSI) mass spectra were performed by the Central Science Laboratory, Tasmania. Flash chromatography was performed on Silica Gel 60, 230–400 mesh (Merck). Thin layer chromatography (TLC) was performed on either aluminium backed silica gel 60 plates (Merck) or aluminium oxide 150 plates (Merck) and were visualised by UV light (254 nm) or by potassium permanganate dip. All solvents were distilled and dried before use. Dry THF was freshly prepared by distilling over benzophenone and sodium under nitrogen. Ultrapurified deionised water was used for anion exchange chromatography. Elemental analyses were performed by the University of Otago, New Zealand. 1,4,7-Triazacyclononane **3**[11] and its orthoamide derivative, 1,4,7-triazatricyclo-[5.2.1.0^{4,10}]decane **4**,[12] were prepared according to published procedures.

1,4,7-Triazabicyclo[4.3.0]non-6-en-5-one 2

Diethylenetriamine (10.0 g, 96.9 mmol) and diethyl oxalate (14.2 g, 97.2 mmol) were each diluted in absolute ethanol to 50 cm^3 and the two solutions added simultaneously to rapidly stirred refluxing ethanol (1.75 dm^3) at a rate of 0.8 cm^3 h^{-1} using a syringe pump. Once addition was complete the stirred reaction mixture was left to reflux for a further 5 days. The solution was then concentrated to *ca.* 200 cm^3 by distillation of the ethanol and the cloudy solution was cooled to room temperature and filtered. The filtrate was concentrated *in vacuo* to give a viscous orange oil which was chromatographed on silica gel [(NH_4OH–H_2O)–MeOH–CH_2Cl_2 1:59:40, R_f = 0.5] to yield **2** as a pale yellow solid (5.90 g, 44%), mp 172–173 °C (Found: C, 51.4; H, 6.29; N, 29.9. $C_6H_9N_3O$ requires C, 51.8; H, 6.52; N, 30.2%); ν_{max}(Nujol mull)/cm^{-1} 3479, 3360, 1680, 1620; δ_H(600 MHz, D_2O) 2.99 (2H, t, *J* 6.6, C=NCH_2), 3.62 (2H, m, NHCH_2), 3.64 (2H, t, *J* 6.6, C=NCH$_2$CH_2), 3.74 (2H, m, NHCH$_2$CH_2); δ_C(74.47 MHz) 39.88 (C=NCH_2), 40.05 (NHCH_2), 47.59 (NHCH$_2$CH_2), 51.88 (C=NCH$_2$CH_2), 161.56 (C=N), 161.77 (C=O); *m/z* (EI) 139 (M$^+$, 100%), 111 (5), 99 (51), 84 (26), 70 (20), 56 (49), 42 (32). This compound has been previously reported in the patent literature.[13]

1-Acetyl-4-formyl-1,4,7-triazacyclononane 5

Acetyl bromide (2.62 g, 21.3 mmol) in dry THF (10 cm^3) was added dropwise to a rapidly stirred solution of orthoamide **4** (2.68 g, 19.3 mmol) in dry THF (200 cm^3) to give an instant white precipitate. After stirring for 3 h the solid was vacuum filtered, dissolved in H_2O (50 cm^3) and then heated at reflux for 24 h. Removal of the solvent *in vacuo* gave an oil which was passed through an anion exchange column of Amberlite IRA-400 generated with 0.1 mol dm^{-3} NaOH. The product was then extracted into C_6H_6 using a Dean–Stark apparatus. Removal of the solvent *in vacuo* gave **5** as a thick colourless oil which crystallised on standing at 0 °C (3.43 g, 89%), mp 79–81 °C (Found: C, 53.3; H, 8.82; N, 20.6. $C_9H_{17}N_3O_2 \cdot \frac{1}{4}H_2O$ requires C, 53.1; H, 8.66; N, 20.6%); R_f = 0.83 (MeOH–CH_2Cl_2 5:95 on alumina); ν_{max}(neat)/cm^{-1} 3460, 3357, 1664, 1635; δ_H(300 MHz, D_2O) 2.07, 2.10, 2.13 (minor) and 2.17 [4 × (3H, s, CH_3)], 2.96 (4H, m, CH_2N ring), 3.31 (4H, m, CH_2N ring), 3.72 (4H, m, CH_2N ring), 8.01, 8.11, 8.13 and 8.16 (minor) [4 × (1H, s, HCO)]; δ_C(74.47 MHz) 22.03, 22.11 and 22.23 [3 × (CH_3)], 44.99, 46.19, 46.39 (coincident double), 47.28, 47.51, 48.32, 48.92 49.45, 49.79, 50.30, 50.57, 51.00, 51.81, 52.15, 53.32, 53.91 and 54.37

(ring carbons), 164.05, 164.13 and 164.15 [3 × (HCO)], 171.29, 171.56 and 171.64 [3 × (CH_3CO)]; *m/z* (LSI) 200.1392 $(M + H)^+$, $C_9H_{18}N_3O_2$ requires 200.1399.

General procedure for alkylation and hydrolysis

Epoxide (3 mol equiv.) was added to a solution of **5** in ethanol at 0 °C and then stirred at 25 °C for 3–4 days. The solvent was removed *in vacuo* and the product was refluxed in 3 mol dm^{-3} HBr at 110 °C for 2.5 h. Removal of the solvent *in vacuo* gave each product as a brittle yellow–white solid. Products **6** and **8** were recrystallised from H_2O–EtOH while product **7** was precipitated from MeOH–CH_2Cl_2. If required, the free ligands may be obtained by passage through an anion exchange column of Amberlite IRA-400 generated with 0.1 mol dm^{-3} NaOH followed by *in vacuo* removal of H_2O.

1-(2-Hydroxyethyl)-1,4,7-triazacyclononane dihydrobromide 6

White crystals (75%), mp 203–206 °C (Found: C, 28.7; H, 6.59; N, 12.3. $C_8H_{21}Br_2N_3O$ requires C, 28.7; H, 6.32; N, 12.5%); δ_H(300 MHz, D_2O) 2.88 (2H, m, NCH_2 arm), 3.05 (4H, m, NCH_2 ring), 3.33 (4H, m, NCH_2 ring), 3.61 (4H, br s, NCH_2 ring), 3.77 (2H, m, CH_2OH); δ_C(74.47 MHz) 44.93, 46.46, 50.85 (ring carbons), 58.68 (NCH_2 arm), 60.58 (CH_2OH arm); *m/z* (LSI) 174.1614 $(M + H)^+$, $C_8H_{20}N_3O$ requires 174.1606. Spectral data is consistent with the literature values for the free ligand.[4]

1-[(2*S*)-2-Hydroxypropyl]-1,4,7-triazacyclononane dihydrobromide 7

White solid (74%); δ_H(300 MHz, D_2O) 1.14 (3H, d, *J* 6.0, CH_3), 2.59 (1H, dd, *J* 10.5, 13.8, NCH_2 arm), 2.80 (1H, dd, *J* 2.7, 13.8, NCH_2 arm), 3.06 (4H, m, NCH_2 ring), 3.32 (4H, m, NCH_2 ring), 3.60 (4H, m, NCH_2 ring), 4.07 (1H, ddq, *J* 2.7, 6.0, 10.5, 13.8, CHOH arm); δ_C(74.47 MHz) 22.46 (CH_3), 44.30, 45.92, 50.38 (ring carbons), 63.62 (NCH_2 arm), 66.92 (CHOH arm); *m/z* (LSI) 188.1767 $(M + H)^+$, $C_9H_{22}N_3O$ requires 188.1762.

1-[(2*R*)-2,3-Dihydroxypropyl]-1,4,7-triazacyclononane dihydrobromide 8

White crystals (82%), mp 186–188 °C (Found: C, 29.4; H, 6.34; N, 11.3. $C_9H_{23}Br_2N_3O_2$ requires C, 29.6; H, 6.35; N, 11.5%); δ_H(600 MHz, D_2O) 2.76 (1H, dd, *J* 9.4, 13.9, NCH_2 arm), 2.86 (1H, dd, *J* 3.3, 13.9, NCH_2 arm), 3.04 (2H, m, NCH_2 ring), 3.11 (2H, m, NCH_2 ring), 3.34 (4H, m, NCH_2 ring), 3.53 (1H, dd, *J* 5.3, 11.9, CH_2OH arm), 3.63 (1H, dd, *J* 4.4, 11.9, CH_2OH arm), 3.64 (4H, m, NCH_2 ring), 3.97 (1H, dddd, *J* 3.3, 4.4, 5.3, 9.4, CHOH arm); δ_C(74.47 MHz) 44.26, 45.97, 50.56 (ring carbons), 59.26 (NCH_2 arm), 66.18 (CH_2OH arm), 70.93 (CHOH arm); *m/z* (LSI) 204.1701 $(M + H)^+$, $C_9H_{22}N_3O_2$ requires 204.1711.

Molecular modelling

Geometries for each isomer of **5** were fully optimised at the Hartree–Fock (HF) level of theory using the 6-31G* basis set. All calculations were carried out using the Gaussian 94 program suite.[14] In addition to configurational isomerism, the conformation of the nine membered ring may also vary by rotation of individual ring atoms. The combination of these effects produced a range of isomers corresponding to 18 local energy minima. The four lowest energy isomers are shown in Fig. 1.

Acknowledgements

We thank the Australian Research Council for an Australian Postgraduate Award for S. P. Creaser. We also thank Dr M. A. Buntine for advice on *ab initio* calculations.

References

1 I. A. Fallis, L. J. Farrugia, N. M. Macdonald and R. D. Peacock, *J. Chem. Soc., Dalton Trans.*, 1993, 2759; R. Luckay, R. D. Hancock, I. Cukrowski and J. H. Reibenspies, *Inorg. Chim. Acta*, 1996, **246**, 159; J. Huskens and A. D. Sherry, *Chem. Commun.*, 1997, 845; S. F. Lincoln, *Coord. Chem. Rev.*, 1997, **166**, 255; S. L. Whitbread, J. Weeks, P. Valente, M. A. Buntine, S. F. Lincoln and K. P. Wainwright, *Aust. J. Chem.*, 1997, **50**, 853; R. S. Dhillon, S. E. Madbak, F. G. Ciccone, M. A. Buntine, S. F. Lincoln and K. P. Wainwright, *J. Am. Chem. Soc.*, 1997, **119**, 6126; S. L. Whitbread, P. Valente, M. A. Buntine, P. Clements, S. F. Lincoln and K. P. Wainwright, *J. Am. Chem. Soc*, 1998, **120**, 2862.
2 E. Kimura, I. Nakamura, T. Koike, M. Shionoya, Y. Kodama, T. Ikeda and M. Shiro, *J. Am. Chem. Soc.*, 1994, **116**, 4764; M. L. Turonek, P. Moore, H. J. Classe and N. W. Alcock, *J. Chem. Soc., Dalton Trans.*, 1995, 3659; L. Spiccia, G. D. Fallon, M. J. Grannas, P. J. Nichols and E. R. T. Tiekink, *Inorg. Chim. Acta*, 1998, **279**, 192; D. Parker, P. K. Senanayake and J. A. G. Williams, *J. Chem. Soc., Perkin Trans. 2*, 1998, 2129.
3 A. J. Blake, I. A. Fallis, R. O. Gould, S. Parsons, S. A. Ross and M. Schröder, *J. Chem. Soc., Chem. Commun.*, 1994, 2467.
4 A. J. Blake, I. A. Fallis, R. O. Gould, S. Parsons, S. A. Ross and M. Schröder, *J. Chem. Soc., Dalton Trans.*, 1996, 4379.
5 I. A. Fallis, P. C. Griffiths, P. M. Griffiths, D. E. Hibbs, M. B. Hursthouse and A. L. Winnington, *Chem. Commun.*, 1998, 665.
6 J. L. Sessler, J. W. Sibert and V. Lynch, *Inorg. Chem.*, 1990, **29**, 4143.
7 Z. Kovacs and A. D. Sherry, *Tetrahedron Lett.*, 1995, **36**, 9269.
8 S. P. Creaser, S. F. Lincoln, S. M. Pyke and E. R. T. Tiekink, *Z. Kristallogr.*, 1998, **213**, 41.
9 B. C. Challis and J. A. Challis, in *Comprehensive Organic Chemistry*, ed. I. O. Sutherland, Pergamon, Oxford, 1979, ch. 9.9.2, pp. 986–1002.
10 A. J. Blake, I. A. Fallis, A. Heppeler, S. Parsons, S. A. Ross and M. Schröder, *J. Chem. Soc., Dalton Trans.*, 1996, 31.
11 A. McAuley, P. R. Norman and O. Olubuyide, *Inorg. Chem.*, 1984, **23**, 1938.
12 G. R. Weisman, D. J. Vachon, V. B. Johnson and D. A. Gronbeck, *J. Chem. Soc., Chem. Commun.*, 1987, 886.
13 G. P. Speranza and M. L. Plishka, US Patent 5,324,838, 1994.
14 Gaussian 94, Revision D.3, M. J. Frisch, G. W. Trucks, H. B. Schlegel, P. M. W. Gill, B. G. Johnson, M. A. Robb, J. R. Cheeseman, T. Keith, G. A. Petersson, J. A. Montgomery, K. Raghavachari, M. A. Al-Laham, V. G. Zakrzewski, J. V. Ortiz, J. B. Foresman, J. Cioslowski, B. B. Stefanov, A. Nanayakkara, M. Challacombe, C. Y. Peng, P. Y. Ayala, W. Chen, M. W. Wong, J. L. Andres, E. S. Replogle, R. Gomperts, R. L. Martin, D. J. Fox, J. S. Binkley, D. J. Defrees, J. Baker, J. P. Stewart, M. Head-Gordon, C. Gonzalez and J. A. Pople, Gaussian Inc., Pittsburgh, PA, 1995.

Paper 8/09981B

Crystal structure of 1,4,7-triazabicyclo[4.3.0]non-6-ene-5-one, $C_6H_9N_3O$

S. P. Creaser, S. F. Lincoln, S. M. Pyke and E. R. T. Tiekink

The University of Adelaide, Department of Chemistry, Australia 5005

Received March 21, 1997, CSD-No. 402968

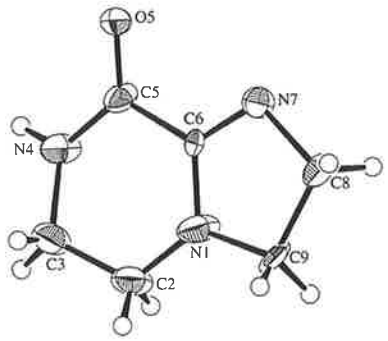

Source of material: Diethylene triamine (10 g, 96.9 mmol) and diethyl oxalate (14.17 g, 97 mmol) were each diluted in absolute alcohol to 50 ml and the two solutions added simultaneously to rapidly stirred refluxing ethanol (1.75 l) at a rate of 0.8 ml/h. Once addition was complete, the stirred reaction mixture was heated at reflux for further 5 days. The solution was then concentrated to ca 200 ml by distillation of the ethanol. The cloudy solution was cooled to room temperature and filtered. The filtrate was concentrated in vacuo to give a viscous orange oil. The crude material was chromatographed on silica gel (NH_4OH-H_2O 1%, MeOH 59%, CH_2Cl_2 40%) to yield a pale yellow solid (5.9 g, 44%); mp 445 K – 446 K. Crystals for the X-ray study were grown by the vapour diffusion of ether into a methanol solution of the compound. The title compound has been reported previously in the patent literature (see ref. 1). The structure shows the presence of a lactam chromophore and a C6=N7 double bond as seen in *d*(N4–C5), *d*(C5–O) and *d*(C6–N7) of 1.327(7) Å, 1.200(6) Å and 1.283(6) Å, respectively. A close intramolecular contact of 2.50 Å between the O5 and H4 atoms is noted. In the lattice the molecules stack ca parallel to the *c*-direction and align in a zip-like fashion so that the five-membered rings are, on average, separated by 3.51 Å. This arrangement has the consequence that the carbonyl O atom is situated in a region of the lattice defined by the methylene H atoms (range of O···H 2.5 Å – 3.0 Å) as well as H4 (2.85 Å).

$C_6H_9N_3O$, orthorhombic, $Pna2_1$ (No. 33), a =10.344(2) Å, b =9.470(2) Å, c =6.984(3) Å, V =684.1 Å^3, Z =4, $R(F)$ =0.055, $R_w(F)$ =0.034.

Table 1. Parameters used for the X-ray data collection

Crystal:	colorless block, size 0.13 x 0.16 x 0.24 mm
Wavelength:	Mo K_α radiation (0.7107 Å)
μ:	0.96 cm^{-1}
Diffractometer:	Rigaku AFC6R
Scan mode:	ω/2θ
$T_{measurement}$:	293 K
$2\theta_{max}$:	55°
N(hkl)$_{unique}$:	432
Criterion for F_o:	$F_o > 3\,\sigma(F_o)$
N($param$)$_{refined}$:	90
Program:	TEXSAN

Table 2. Final atomic coordinates and displacement parameters (in Å^2)

Atom	Site	x	y	z	U_{iso}
H(2a)	4*a*	–0.2832	0.1607	–0.0946	0.0677
H(2b)	4*a*	–0.2991	0.1162	0.1228	0.0677
H(3a)	4*a*	–0.4354	–0.0217	–0.0051	0.0735
H(3b)	4*a*	–0.3564	–0.0340	–0.1986	0.0735
H(4)	4*a*	–0.3582	–0.2446	0.0411	0.0568
H(8a)	4*a*	0.1450	0.0850	–0.0940	0.0501
H(8b)	4*a*	0.1344	0.0858	0.1323	0.0501
H(9a)	4*a*	–0.0376	0.2300	0.1078	0.0562
H(9b)	4*a*	–0.0350	0.2174	–0.1183	0.0562

Acknowledgment. The Australian Research Council is thanked for support.

References

1. Speranza, G. P.; Plishka, M. L.: Bicyclo[4.3.0]1,4,7-triazanon-4-ene-one useful in the extraction of precious metals. US Patent 5,324,838, USA 1994.

Table 3. Final atomic coordinates and displacement parameters (in Å^2)

Atom	Site	x	y	z	U_{11}	U_{22}	U_{33}	U_{12}	U_{13}	U_{23}
O(5)	4*a*	–0.1269(2)	–0.3158(2)	0.0	0.041(2)	0.029(1)	0.158(4)	0.005(1)	–0.037(4)	–0.013(5)
N(1)	4*a*	–0.1359(3)	0.0589(3)	0.009(2)	0.037(2)	0.026(1)	0.113(3)	0.000(1)	0.022(6)	–0.002(6)
N(4)	4*a*	–0.2979(2)	–0.1714(2)	0.003(2)	0.033(1)	0.033(1)	0.076(3)	0.000(1)	0.023(4)	0.009(4)
N(7)	4*a*	0.0392(3)	–0.0813(3)	0.010(2)	0.030(1)	0.032(1)	0.064(2)	–0.005(1)	0.003(5)	0.006(5)
C(2)	4*a*	–0.2701(4)	0.0854(4)	–0.002(2)	0.041(2)	0.032(2)	0.095(5)	0.006(2)	0.005(6)	0.015(6)
C(3)	4*a*	–0.3500(4)	–0.0336(4)	–0.060(1)	0.033(2)	0.040(2)	0.112(7)	0.002(2)	–0.005(3)	0.016(3)
C(5)	4*a*	–0.1723(3)	–0.1995(3)	0.009(2)	0.032(1)	0.031(1)	0.062(3)	–0.001(1)	0.013(6)	–0.015(5)
C(6)	4*a*	–0.0844(3)	–0.0720(3)	0.003(2)	0.033(1)	0.028(1)	0.048(3)	0.002(1)	–0.023(4)	–0.016(4)
C(8)	4*a*	0.0881(3)	0.0680(4)	0.014(2)	0.043(2)	0.034(1)	0.048(3)	–0.009(1)	0.006(5)	–0.014(6)
C(9)	4*a*	–0.0330(3)	0.1648(3)	0.001(2)	0.050(2)	0.024(2)	0.067(3)	–0.009(1)	0.001(7)	–0.025(5)

REFERENCES

1. T. J. Atkins, J. E. Richman and W. F. Oettie, *Org. Synth.*, 1978, **58**, 86-98.
2. J. E. Richman and T. J. Atkins, *J. Am. Chem. Soc.*, 1974, **96**, 2268-2270.
3. D. K. Cabbiness and D. W. Margerum, *J. Am. Chem. Soc.*, 1969, **91**, 6540-6541.
4. D. Munro, *Chem. in Britain*, 1977, **13**, 100-105.
5. M. Kodama and E. Kimura, *J. Chem. Soc., Chem. Commun.*, 1975, 326-327.
6. L. Fabbrizzi, P. Paoletti and A. B. P. Lever, *Inorg. Chem.*, 1976, **15**, 1502-1506.
7. M. Kodama and E. Kimura, *J. Chem. Soc., Chem. Commun.*, 1975, 891-892.
8. M. Kodama and E. Kimura, *J. Chem. Soc., Dalton Trans.*, 1976, 116-121.
9. M. Kodama and E. Kimura, *J. Chem. Soc., Dalton Trans.*, 1976, 1720-1724.
10. M. Kodama and E. Kimura, *J. Chem. Soc., Dalton Trans.*, 1976, 2341-2345.
11. M. Kodama and E. Kimura, *J. Chem. Soc., Dalton Trans.*, 1977, 2269-2276.
12. F. P. Hinz and D. W. Margerum, *Inorg. Chem.*, 1974, **13**, 2941-2949.
13. F. P. Hinz and D. W. Margerum, *J. Am. Chem. Soc.*, 1974, **96**, 4993-4994.
14. M. Micheloni and P. Paoletti, *Inorg. Chim. Acta*, 1980, **43**, 109-112.
15. A. Dei and R. Gori, *Inorg. Chim. Acta*, 1975, **14**, 157-160.
16. A. Anichini, L. Fabbrizzi and P. Paoletti, *J. Chem. Soc., Chem. Commun.*, 1977, 244-245.
17. R. M. Clay, M. Micheloni and P. Paoletti, W. V. Steele, *J. Am. Chem. Soc.*, 1979, **101**, 4119-4122.
18. P. Paoletti, L. Fabbrizzi and R. Barbucci, *Inorg. Chim. Acta Rev.*, 1973, **7**, 43-68.
19. P. Paoletti. L. Fabbrizzi and R. Barbucci, *Inorg. Chem.*, 1973, **12**, 1961-1962.
20. A. Anichini, L. Fabbrizzi, P. Paoletti and R. M. Clay, *Inorg. Chim. Acta*, 1977, **22**, L25-L27.
21. L. Fabbrizzi, P. Paoletti and R. M. Clay, *Inorg. Chem.*, 1978, **17**, 1042-1046.

22. A. Anichini, L. Fabbrizzi, P. Paoletti and R. M. Clay, *J. Chem. Soc., Dalton Trans.*, 1978, 577-583.

23. R. I. Izatt, K. Pawlak and J. S. Bradshaw, *Chem. Rev.*, 1991, **91**, 1721-2085.

24. P. Comba, *Coord. Chem. Rev.*, 1999, **182**, 343-371.

25. "Coordination Chemistry of Macrocyclic Compounds", edited by G. A. Melson, Plenum Press, New York, 1979.

26. D. H. Busch, K. Farmery, V. Goedken, V. Kalovic, A. C. Melnyk, C. R. Sperati and N. Tokel, in "Bioinorganic Chemistry", edited by R. F. Gould, A. C. S., Washington, D. C., 1971.

27. A. Bianchi, M. Micheloni and P. Paoletti, *Coord. Chem. Rev.*, 1991, **110**, 17-113.

28. R. Yang and L. J. Zompa, *Inorg. Chem.*, 1976, **15**, 1499-1502.

29. G. Schwarzenbach and J. E. Prue, *Helv. Chim. Acta*, 1950, **33**, 985-995.

30. M. Ciampolini and P. Paoletti, *J. Phys. Chem.*, 1961, **65**, 1224-1226.

31. T. Arishima, K. Hamada and S. Takamoto, *Nippon Kagaku Kaishi*, 1973, 1119-1121.

32. P. Chaudhuri and K. Wieghardt, *Prog. Inorg. Chem.*, 1987, **35**, 329-436.

33. K. Wieghardt, U. Bossek, P. Chaudhuri, W. Herrmann, B. C. Menke and J. Weiss, *Inorg. Chem.*, 1982, **21**, 4308-4314.

34. F. McLaren, P. Moore and A. M. Wynn, *J. Chem. Soc., Chem. Commun.*, 1989, 789-800.

35. C. M. Madeyski, J. P. Michael and R. D. Hancock, *Inorg. Chem.*, 1984, **23**, 1487-1489.

36. S. P. Kasprzyk and R. G. Wilkins, *Inorg. Chem.*, 1982, **21**, 3349-3352.

37. R. W. Hay, M. P. Pujari, W. T. Moodie, S. Craig, D. T. Richens, A. Perotti and L. Ungaretti, *J. Chem. Soc., Dalton Trans.*, 1987, 2605-2613.

38. T. A. Kaden, *Helv. Chim. Acta*, 1970, **53**, 617-622; T. A. Kaden, *ibid.*, 1971, **54**, 2307-2312; R. Buxtorf and T. A. Kaden, *ibid.*, 1974, **57**, 1035-1042; L. Hertli and T. A. Kaden, *ibid.*, 1974, **57**, 1328-1333; L. Hertli and T. A. Kaden, *ibid.*, 1981, **64**, 33-37;

W. Steinman and T. A. Kaden, *ibid.*, 1975, **58**, 1358-1366; P. S. Grunow and T. A. Kaden, *ibid.*, 1978, **61**, 2291-2296; A. P. Leugger, L. Hertli and T. A. Kaden, *ibid.*, 1978, **61**, 2296-2306; T. J. Rideo and T. A. Kaden, *ibid.*, 1979, **62**, 1089-1096; C. S. Kallianou and T. A. Kaden, *ibid.*, 1979, **62**, 2562-2568.

39. L. Fabrizzi, T. A. Kaden, A. Perotti, B. Seghi and L. Siegfried, *Inorg. Chem.*, 1986, **25**, 321-327.

40. S. F. Lincoln, J. H. Coates, D. A. Hadi and D. L. Pisaniello, *Inorg. Chim. Acta*, 1984, **81**, L9-L10.

41. K. Wieghardt, P. Chaudhuri, B. Nuber and J. Weiss, *Inorg. Chem.*, 1982, **21**, 3086-3090.

42. M. Takahasi and S. Takamoto, *Bull. Chem. Soc. Jpn.*, 1977, **50**, 3413-3414.

43. T. Weyhermüller, K. Weighardt and P. Chaudhuri, *J. Chem. Soc., Dalton Trans.*, 1998, 3805-3813.

44. B. A. Sayer, J. P. Michael and R. D. Handcock, *Inorg. Chim. Acta*, 1983, **77**, L63-L64.

45. R. Luckay, R. D. Hancock, I. Cukrowski and J. H. Reibenspies, *Inorg. Chim. Acta*, 1996, **246**, 159-169.

46. D. A. Moore, P. E. Fanwick and M. J. Welch, *Inorg. Chem.*, 1990, **29**, 672-676.

47. L. R. Gahan, G. A. Lawrance and A. M. Sargeson, *Aust. J. Chem.*, 1982, **35**, 1119-1131.

48. I. A. Fallis, L. J. Farrugia, N. M. Macdonald and R. D. Peacock, *J. Chem. Soc., Dalton Trans*, 1993, 2759-2763.

49. J. Huskens and A. D. Sherry, *Chem. Commun.*, 1997, 845-846.

50. S. L. Whitbread, J. Weeks, P. Valente, M. A. Buntine, S. F. Lincoln and K. P. Wainwright, *J. Aust .Chem.*, 1997, **50**, 853-856; S. L. Whitbread, J. Weeks, P. Valente, M. A. Buntine, S. F. Lincoln and K. P. Wainwright, *ibid.*, 1999, **52**, 82.

51. S. F. Lincoln, *Coord. Chem. Rev.*, 1997, **166**, 255-289.

52. R. S. Dhillon, S. E. Madbak, F. G. Ciccone, M. A. Buntine, S. F. Lincoln and K. P. Wainwright, *J. Am. Chem. Soc.*, 1997, **119**, 6126-6134.

53. S. L. Whitbread, P. Valente, M. A. Buntine, P. Clements, S. F. Lincoln and K. P. Wainwright, *J. Am. Chem. Soc.*, 1998, **120**, 2862-2869.

54. C. J. Broan, E. Cole, K. J. Jankowski, D. Parker, K. Pulukkody, B. A. Boyce, N. R. A. Beeley, K. Millar and A. T. Millican, *Synthesis*, 1992, 63-68.

55. R. Ziessel and J. -M. Lehn, *Helv. Chim. Acta*, 1990, **73**, 1149-1162.

56. M. Di Vaira, F. Manni and P. Stoppioni, *J. Chem. Soc., Chem. Commun.*, 1989, 126-127.

57. G. A. McLachlan, G. D. Fallon, R. L. Martin, B. Moubaraki, K. S. Murray and L. Spiccia, *Inorg. Chem.*, 1994, **33**, 4663-4668.

58. H. Chen, M. M. Olmstead, R. L. Albright, J. Devenyi and R. H. Fish, *Angew. Chem. Int. Ed. Engl.*, 1997, **36**, 642-644.

59. C. Stockheim, L. Hoster, T. Weyhermüller, K. Wieghardt and B. Nuber, *J. Chem. Soc., Dalton Trans.*, 1996, 4409-4416.

60. M. Di Vaira, F. Mani and P. Stoppioni, *Inorg. Chim. Acta*, 1998, **273**, 151-159.

61. I. A. Fallis, P. C. Griffiths, P. M. Griffiths, D. E. Hibbs, M. B. Hursthouse and A. L. Winnington, *Chem. Commun.*, 1998, 665-666.

62. M. Studer, A. Riesen and T. A. Kaden, *Helv. Chim. Acta*, 1989, **72**, 307-312.

63. J. Huskens and A. D. Sherry, *J. Am. Chem. Soc.*, 1996, **118**, 4396-4404.

64. D. G. Fortier and A. McAuley, *J. Chem. Soc., Dalton Trans.*, 1991, 101-109.

65. N. J. Sessler, J. W. Silbert and V. Lynch, *Inorg. Chem.*, 1990, **29**, 4143-4146.

66. K. Wieghardt, I. Tolksdorf and W. Herrmann, *Inorg. Chem.*, 1985, **24**, 1230-1235.

67. A. E. Martin, T. M. Ford and J. E. Bulkowski, *J. Org. Chem.*, 1982, **47**, 412-415.

68. Z. Kovacs and D. Sherry, *Tetrahedron Lett.*, 1995, **36**, 9269-9272.

69. I. M. Helps, D. Parker, K. J. Jankowski, J. Chapman and P. E. Nicholson, *J. Chem. Soc., Perkin Trans. 1*, 1989, 2079-2082.

70. "Macrocycle Synthesis; A Practical Approach", edited by D. Parker, Oxford University Press, Oxford, 1996.

71. E. Kimura, I. Nakamura, T. Koike, M. Shionoya, Y. Kodama, T. Ikeda and M. Shiro, *J. Am. Chem. Soc.*, 1994, **116**, 4764-4771.

72. E. Kimura, Y. Kuramoto, T. Koike, H. Fujioka, M. Kodama, *J. Org. Chem.*, 1990, **55**, 42-46; T. Koike, S. Kajitani, I. Nakamura, E. Kimura and M. Shiro, *J. Am. Chem. Soc.*, 1995, **117**, 1210-1219.

73. M. A. Santos, M. Gaspar, M. L. S. S. Goncalves and M. T. Amorim, *Inorg. Chim. Acta*, 1998, **278**, 51-60.

74. T. J. Atkins, U.S. Patent 4085106, 1978; T. J. Atkins, *Chem. Abstr.*, 1978, **89**, P129553Z.

75. G. R. Weisman, V. Johnson and R. E. Fiala, *Tetrahedron Lett.*, 1980, **21**, 3635-3638.

76. G. R. Weisman, D. J. Vachon, V. B. Johnson and D. A. Gronbeck, *J. Chem. Soc., Chem. Commun.*, 1987, 886-887.

77. A. J. Blake, I. A. Fallis, R. O. Gould, S. G. Harris, S. Parsons, S. A. Ross and M. Schröder, *Acta Cryst., Sect. C*, 1995, **51**, 738-741.

78. L. J. Farrugia, P. A. Lovett and R. D. Peacock, *Acta Cryst., Sect. C*, 1993, **49**, 2164-2165.

79. A. J. Blake, I. A. Fallis, R. O. Gould, S. Parsons, S. A. Ross and M. Schröder, *J. Chem. Soc., Chem. Commun.*, 1994, 2467-2469.

80. D. Schulz, T. Weyhermüller, K. Wieghardt and B. Nuber, *Inorg. Chim. Acta*, 1995, **240**, 217-229.

81. L. Farrugia, P. A. Lovatt and R. D. Peacock, *Inorg. Chim. Acta*, 1996, **246**, 343-348.

82. A. J. Blake, I. A. Fallis, R. O. Gould, S. Parsons, S. A. Ross and M. Schröder, *J. Chem. Soc., Dalton Trans.*, 1996, 4379-4387.

83. D. Ellis, L. J. Farrugia, D. T. Hickman, P. A. Lovatt and R. D. Peacock, *Chem. Commun.*, 1996, 1817-1818.

84. B. Graham, G. D. Fallon, M. T. W. Hearn, D. C. R. Hockless, G. Lazarev and L. Spiccia, *Inorg. Chem.*, 1997, **36**, 6366-6373.

85. P. Hubsch-Weber and M-T. Youinou, *Tetrahedron Lett.*, 1997, **38**, 1911-1914.

86. S. J. Brudnell, L. Spiccia, A. M. Bond, P. Comba and D. C. R. Hockless, *Inorg. Chem.*, 1998, **37**, 3705-3713.

87. H. Weller, L. Siegfried, M. Neuburger, M. Zehnder and T. A. Kaden, *Helv. Chim. Acta*, 1997, **80**, 2315-2328.

88. F. H. Fry, B. Graham, L. Spiccia, D. C. R. Hockless and E. R. T. Tiekink, *J. Chem. Soc., Dalton Trans.*, 827-831.

89. H. Rasmussen and P. Q. Barrett, *Physiol. Rev.*, 1984, **64**, 938-984.

90. J. Huskens and A. D. Sherry, *J. Chem. Soc., Dalton Trans.*, 1998, 177-184.

91. D. De Vos and T. Bein, *J. Chem. Soc., Chem. Commun.*, 1996, 917-918.

92. D. E. De Vos and T. Bein, *J. Organometallic Chem.*, 1996, **520**, 195-200.

93. M. J. Young and J. Chin, *J. Am. Chem. Soc.*, 1995, **117**, 10577-10578.

94. B. Valeur and E. Bardez, *Chem. in Britain*, 1995, **31**, 216-220.

95. A. J. Bryan, A. P. de Silva, S. A. de Silva, R. A. D. D. Rupasinghe and K. R. A. S. Sandanayake, *Biosensors*, 1989, **4**, 169.

96. R. A. Bissell, A.P. de Silva, H. Q. N. Gunaratne, P. L. M. Lynch, G. E. M. Maguire and K. R. A. S. Sandanayake, *Chem. Soc. Rev.*, 1992, 187-195.

97. B. Konig, M. Pelka, H. Zieg, T. Ritter, H. Bouas-Laurent, R. Bonneau and J-P. Desvergne, *J. Am. Chem. Soc.*, 1999, **121**, 1681-1687.

98. D. Parker and J. A. G. Williams, *J. Chem. Soc., Dalton Trans.*, 1996, 3613-3628.

99. D. Parker, P. K. Senanayake and J. A. G. Williams, *J. Chem. Soc., Perkin Trans. 2*, 1998, 2129-2139.

100. R. B. Lauffer, *Chem. Rev.*, 1987, **87**, 901-927.

101. A. S. Craig, I. M. Helps, K.J. Jankowski, D. Parker, N. R. A. Beeley, B. A. Boyce, M. A. W. Eaton, A. T. Millican, K. Millar, A. Phipps, S. K. Rhind, A. Harrison and C. Walker, *J. Chem. Soc., Chem. Commun.*, 1989, 794-796.

102. J. R. Morphy, D. Parker, R. Kataky, A. Harrison, M. A. W. Eaton, A. Millican, A. Phipps and C. Walker, *J. Chem. Soc., Chem. Commun.*, 1989, 792-794.

103. J. P. L. Cox, K. J. Lankowski, R. Kataky, D. Parker, N. R. A. Beeley, B. A. Boyce, M. A. W. Eaton, K. Millar, A. T. Millican, A. Harrison and C. Walker, *J. Chem. Soc., Chem. Commun.*, 1989, 797-798.

104. M. K. Moi and S. J. DeNardo, *J. Am. Chem. Soc.*, 1988, **110**, 6266-6267.

105. E. Lopez, C. Chypre, B. Alpha and G. Mathis, *Clin. Chem.*, 1993, **39**, 196-201.

106. E. Kimura and M. Shionoya, in "Transition Metals in Supramolecular Chemistry", edited by L. Fabbrizzi and A. Poggi, Kluwer Academic Publishers, Netherlands, 1994, p. 245-259.

107. R. Krämer, *Coord. Chem. Rev.*, 1999, **182**, 243-261.

108. E. Kimura and T. Koike, *Comments Inorg. Chem.*, 1991, **11**, 285-301.

109. E. Kimura, *Prog. Inorg. Chem.*, 1994, **41**, 443-491.

110. J. Suh, *Acc. Chem. Res.*, 1992, **25**, 273-279.

111. K. D. Karlin, *Science*, 1993, **261**, 701-708.

112. A. E. Brown, T. A. Jones and A. Liljas, *Proteins*, 1988, **4**, 274-282.

113. D. N. Silverman and S. Lindskog, *Acc. Chem. Res.*, 1988, **21**, 30-36.

114. E. E. Kim and H. W. Wyckoff, *J. Mol. Biol.*, 1991, **218**, 449-464.

115. J. E. Butler-Ransohoff, D. A. Kendall and E. T. Kaiser, in "Metal ions in biological systems", Vol. 25, Marcel Deckker, New York, 1989, p. 395.

116. D. W. Christianson and W. N. Lipscomb, *Acc. Chem. Res.*, 1989, **22**, 62-69.

117. D. S. Auld, J. F. Riordan and B. L. Vallee, in "Metal ions in biological systems", Vol. 25, Marcel Deckker, New York, 1989, p. 359.

118. S. Mangani and P. Orioli, *Inorg. Chem.*, 1992, **31**, 365-368.

119. Y. Pocker, in "Metal ions in biological systems", Vol. 25, Marcel Deckker, New York, 1989, p. 335.

120. H. Eklund, A. Jones and G. Schneider, in "Zinc Enzymes", Birkhäuser, Boston, 1986, p. 377.

121. F. Y. -H. Wu, in "Zinc Enzymes", edited by I. Bertini, C. Luchinat, M. Maret and M. Zeppezauer, Birkhäuser, Boston, MA, 1986, p. 533.

122. C. F. Springgate, A. S. Mildvan, R. Arbrahamson and J. L. Engle, *J. Biol. Chem.*, 1973, **248**, 5987-5993.

123. E. Kimura, T. Shiota, T. Koike, M. Shiro and M. Kodama, *J. Am. Chem. Soc.*, 1990, **112**, 5805-5811.

124. J. B. Foresman and Æ. Frisch, "Exploring Chemistry with Electronic Structure Methods: A Guide to Using Gaussian", 2nd Edition, Gaussian Inc., Pittsburgh, 1993.

125. Gaussian 94, Revision C. 3, M. J. Frisch, G. W. Trucks, H. B Schlegel, P. M. W. Gill, B. G. Johnson, M. A. Robb, J. R. Cheeseman, T. Keith, G. A. Petersson, J. A. Montgomery, K. Raghavachari, M. A. Al-Laham, V. G. Zakrzewski, J. V. Ortiz, J. B. Foresman, J. Cioslowski, B. B. Stefanov, A. Nanayakkara, M. Challacombe, C. Y. Peng, P. Y. Ayala, W. Chen, M. W. Wong, J. L. Andres, E. S. Replogle, R. Gomperts, R. L. Martin, D. J. Fox, J. S. Binkley, D. J. Defrees, J. Baker, J. P. Stewart, M. Head-Gordon, C. Gonzalez and J. A. Pople, Gaussian Inc., Pittsburgh, PA, 1995.

126. M. J. Frisch, Æ Frisch and J. B. Foresman, "Gaussian 94 User's Guide", Gaussian Inc., Pittsburgh, 1994.

127. D. Rhodes and A. Klug. *Sci. Am.*, 1993, 56-65.

128. J. M. Berg, *Nature Biotechnology*, 1997, **15**, 323.

129. A. Klug and D. Rhodes, *TIBS*, 1987, **12**, 464-469.

130. J. W. R. Schwabe and A. Klug, *Nat. Struct. Biol.*, 1994, **1**, 345-349.

131. J. Miller, A. D. McLachlan and A. Klug, *EMBO J.*, 1985, **4**, 1609-1614.

132. M. Lee, G. P. Gippert, K. Soman, D. A. Case and P. E. Wright, *Science*, 1989, **245**, 635-637.

133. P. F. G. Sims, *Lecture Notes*, UMIST, UK.

134. N. Pavletich and C. O. Pabo, *Science*, 1991, **252**, 809-817.

135. B. F. Luisi, W. X. Xu, Z. Otwinowski, L. P. Freedman, K. R. Yamamoto and P. B. Sigler, *Nature*, 1991, **352**, 497-505.

136. S. C. Harrison, *Nature*, 1991, **353**, 715-719.

137. J. W. R. Scwabe and D. Rhodes, *TIBS*, 1991, **16**, 291-296.

138. J. M. Berg, *Acc. Chem. Res.*, 1995, **28**, 14-19.

139. Y-G. Kim, J. Cha and S. Chandrasegaran, *Proc. Natl. Acad. Sci. USA*, 1996, **93**, 1156-1160.

140. C. A. Kim and J. M. Berg, *Nat. Struct. Biol.*, 1996, **3**, 940-945.

141. Y. Choo, I. Sanchez-Garcia and A. Klug, *Nature*, 1994, **372**, 642-645.

142. B. I. Dahiyat and S. L. Mayo, *Science*, 1997, **278**, 82-87.

143. E-I. Ochiai, *J. Chem. Educ.*, 1988, **65**, 943-946.

144. A. McAuley, P. R. Norman and O. Olubuyide, *Inorg. Chem.*, 1984, **23**, 1938-1943.

145. G.H. Searle and R.J. Geue, *Aust. J. Chem.*, 1984, **37**, 959-970.

146. R. G. Pearson, *J. Am. Chem. Soc.*, 1963, **85**, 3533-3539.

147. R. G. Pearson, *Coord. Chem. Rev.*, 1990, **100**, 403-425.

149a: See also: M. Studer and T. A. Kaden, Helv. Chim. Acta, 1986, 69, 217; D. Schulz, T. Weyhermueller, K. Wieghardt and B. Nuber, Inorg. Chim. Acta, 1995, 240, 217.

148. R. G. Pearson, "Hard and Soft Acids and Bases", John Wiley, New York, 1973.

149. A. J. Blake, I. A. Fallis, A. Heppeler, S. Parsons, S. A. Ross and M. Schröder, *J. Chem. Soc., Dalton Trans.*, 1996, 31-43.

150. G. P. Speranza and M. L. Plishka, US Patent 5,324,838, 1994.

151. B. C. Challis and J. A. Challis, in "Comprehensive Organic Chemistry", edited by. I. O. Sutherland, Pergamon, Oxford, 1979, ch. 9.9.2, p.986.

152. A. E. Martell and R. J. Montekaitis, "Determination and Use of Stability Constants", VCH Publications, New York, 1988.

153. M. Kodama and E. Kimura, *J. Chem. Soc., Dalton. Trans.*, 1978, 1081-1085.

154. E. Kimura and T. Yatsunami, *Chem. Pharm. Bull. Jpn.*, 1980, **28**, 994-997.

155. L. Fabbrizzi and L. J. Zompa, *Inorg. Nucl. Chem. Lett.*, 1977, **13**, 287-290.

156. B. S. Nakani, J. J. B. Welsh and R. D. Hancock, *Inorg. Chem.*, 1983, **22**, 2956-2958.

157. M. Kodama and E. Kimura, *J. Chem. Soc., Dalton. Trans.*, 1978, 104-110.

158. M. Kodama and E. Kimura, *J. Chem. Soc., Dalton. Trans.*, 1977, 1473-1478.

159. M. Kodama and E. Kimura, *J. Chem. Soc., Dalton. Trans.*, 1976, 2335-2338.

160. C. F. G. C. Geraldes, M. C. Alpoim, M. P. M. Marques, A. D. Sherry and M. Singh, *Inorg. Chem.*, 1985, **24**, 3876-3881.

161. T. J. Reido and T. A. Kaden, *Helv. Chim. Acta*, 1979, **62**, 1089-1096.

162. T. J. Reido and T. A. Kaden, *Chimia*, 1977, **31**, 220-222.

163. R. W. Renfrew, R. S. Jamison and D. C. Weatherburn, *Inorg. Chem.*, 1979, **18**, 1584-1589.

164. V. J. Thöm, G. D. Hosken and R. D. Hancock, *Inorg. Chem.*, 1985, **24**, 3378-3381.

165. F. P. Hinz and D. W. Margerum, *Inorg. Chem.*, 1974, **13**, 2941-2949.

166. H. Häfliger and T. A. Kaden, *Helv. Chim. Acta*, 1979, **62**, 683-688.

167. M. Micheloni, P. Paoletti, S. Bürki and T. A. Kaden, *Helv. Chim. Acta*, 1982, **65**, 587-594.

168. H. Irving and D. H. Mellor, *J. Chem. Soc.*, 1955, 3457-3457.

169. W. R. Harris and A. E. Martell, *Inorg. Chem.*, 1976, **15**, 713-720.

170. G. Schwarzenbach and H. Akermann, *Helv. Chim. Acta*, 1949, **32**, 1543-1554.

171. G. Schwarzenbach and E. Freitag, *Helv. Chim. Acta*, 1951, **34**, 1492-1502.

172. P. Gans, A. Sabatini and A. Vacca, *J. Chem. Soc., Dalton Trans.*, 1985, 1195-1200.

173. R. M. Smith and A. E. Martell, "Critical Stability Constants, Volume 2: Amines", Plenum Press, New York, 1975.

174. R. D. Hancock, *Inorg. Chim. Acta*, 1981, **49**, 145-148.

175. R. D. Hancock, *Pure and Appl. Chem.*, 1986, **58**, 1445-1452.

176. L. J. Zompa, *Inorg. Chem.*, 1978, **17**, 2531-2536.

177. J. Emsley, *Chem. Soc. Rev.*, 1980, 91-124.

178. J. Suh, S. A. Son and M. P. Suh, *Inorg. Chem.*, 1998, **37**, 4872-4877.

179. A. P. Arnold and P. A. Duckworth, University of Adelaide, 1989.

180. B. G. Cox, H. Schneider and J. Stroka, *J. Am. Chem. Soc.*, 1978, **100**, 4746-4749.

181. B. G. Cox, J. Garcia-Rosas and H. Schneider, *J. Am. Chem. Soc.*, 1981, **103**, 1384-1389.

182. D. D. Perrin and B. Dempsey, "Buffers for pH and Metal Ion Control", edited by Chapman and Hall, Wiley, London, New York, 1974.

183. T. J. Atkins, *J. Am. Chem. Soc.*, 1980, **102**, 6364-6365.

184. B. H. Lee and M. J. Miller, *J. Org. Chem.*, 1983, **48**, 24-31.

185. T. Wang, H. An, T. A. Vickers, R. Bharadwaj and P. D. Cook, *Tetrahedron*, 1998, **54**, 7955-7976.

186. P. G. Mattingly, *Synthesis*, 1990, **4**, 366-368.

187. C. Trabaud, J. Dessolin, M. Camplo, O. Hantz, F. Zoulim, C. Borel, M. Meyer, G. Pepe, J-C. Chermann and J-L. Kraus, *Antiviral Chem. Chemother.,* 1998, **9**, 73-84.

188. P. Kong Thoo Lin, V. A. Kuksa and N. M. Maguire, *Synthesis*, 1998, 859-866.

189. A. Sabatini, A. Vacca and P. Gans, *Talanta*, 1974, **21**, 53-77.

190. P. A. Duckworth, University of Adelaide, private communication, 1991.

191. K. M. Hendrickson, Ph.D. Thesis, University of Adelaide, 1999.